MEROCYANINE DYES FOR SOLUTION-PROCESSED ORGANIC BULK HETEROJUNCTION SOLAR CELLS

Dissertation zur Erlangung des
naturwissenschaftlichen Doktorgrades
der Julius-Maximilians-Universität Würzburg

vorgelegt von
Hannah Bürckstümmer
aus Regensburg

Würzburg 2011

Eingereicht am 31.10.2011
Bei der Fakultät für Chemie und Pharmazie

Gutachter der schriftlichen Arbeit:
1. Gutachter: Prof. Dr. Frank Würthner
2. Gutachter: Prof Dr. Klaus Meerholz

Prüfer des öffentlichen Promotionskolloquiums
1. Prüfer: Prof. Dr. Frank Würthner
2. Prüfer: Prof. Dr. Klaus Meerholz
3. Prüfer:

Datum des öffentlichen Promotionskolloquiums:

Doktorurkunde ausgehändigt am:

List of abbreviations:

AFM	atomic force microscopy
BHJ	bulk heterojunction
t-Boc	*tert*-butoxycarbonyl
BODIPY	borondipyrromethene
CV	cyclic voltammetry
DCM	dichloromethane
DMF	*N*,*N*-dimethylformamide
DMSO	dimethylsulfoxide
DOS	density of states
DPP	diketopyrrolopyrrole
Fc	ferrocen
FF	fill factor
$E_{1/2}$	half-wave potential of a reversible redox process
E_p	peak potential of an irreversible redox process
EI	electron ionization
ESI	electrospray ionization
EQE	external quantum efficiency
GPC	gel permeation chromatography
h	hour(s)
HBC	hexabenzocoronene
HOMO	highest occupied molecular orbital
HPLC	high pressure liquid chromatography
HRMS	high resolution mass spectrometry
ICT	intramolecular charge transfer
ITO	indium tin oxide
J_{SC}	short-circuit current density
LiF	lithium fluoride
LUMO	lowest unoccupied molecular orbital
MALDI	matrix-assisted laser desorption injection
MC	merocyanine
min	minute(s)
MoO_3	Molybdenum Oxide
Mp	melting point
MPP	maximum power point
MS	mass spectrometry
NIR	near-infrared
NMR	nuclear magnetic resonance
ODCB	*ortho*-dichlorobenzene

OFET	organic field effect transistor
OLED	organic light emitting device
P3HT	poly(3-hexylthiophene)
PAH	polycyclic aromatic hydrocarbon
PCBM	[6,6]-phenyl-butyric-acid methyl ester
PCE	power conversion efficiency
PPV	polyphenylenevinylene
rt	room temperature
SCE	standard calomel electrode
THF	tetrahydrofuran
TPA	triphenylamine
UV-vis	ultaviolett-visible
V_{OC}	open circuit voltage
WAXS	wide angle X-ray scattering
XRD	X-ray diffraction

Table of Contents

Aim of the thesis

Looking at the progress of economy starting from the 18th century a period of constant growth was always followed by a deep depression, which is summarized in Kondratieff's theory about the long cycles of prosperity (Figure 1).[1] Today, one can consider the current financial crisis as the beginning of the 6th Kondratieff wave bringing us back to a period of sustainable growth. According to experts, environmental technology, including renewable energy sources such as solar cell technology could be a major driving force in the forthcoming Kondratieff cycle.

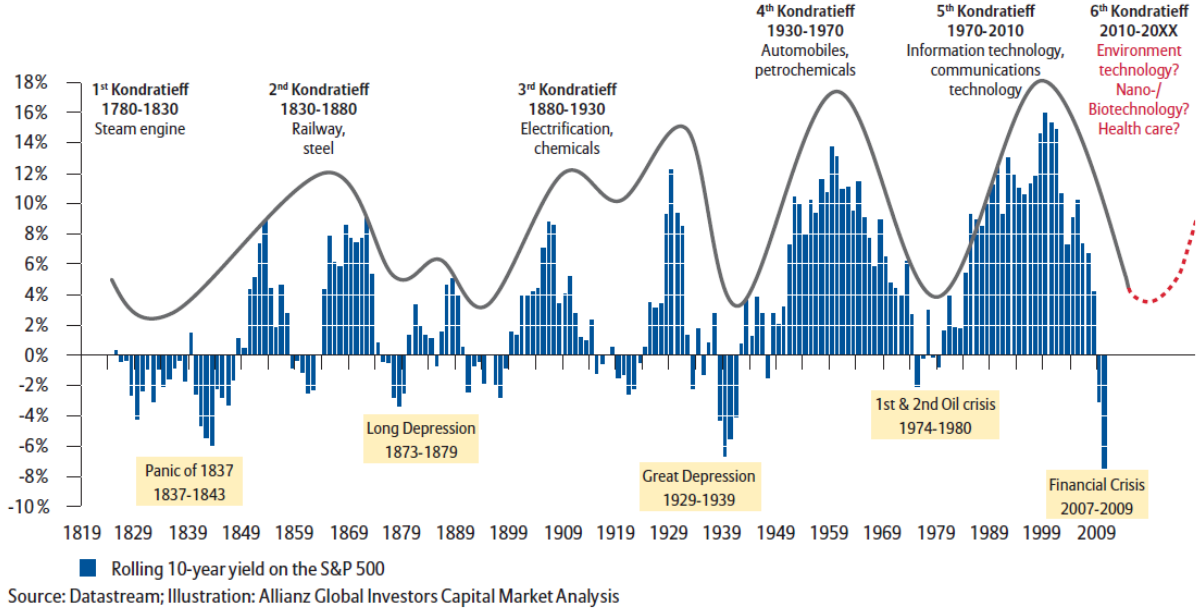

Figure 1. Illustration of the (Kondratieff) waves of prosperity.

Even without regard to the commercial aspect, power produced by photovoltaic devices is highly attractive due to the CO_2-neutral energy production, which does not contribute to the critical greenhouse effect. Additionally, energy by solar irradiation is provided to the earth every day in huge amounts, so no limitation problems occur like in the case of today's main resources of power such as oil, coal or uranium.

Besides the classical silicon technology, reaching module efficiencies of 23%,[2] the so-called third generation of photovoltaic cells including organic solar cells is gaining rapidly in interest as they offer advantages such as thin films and flexible substrates. Organic solar cells can be fabricated either by evaporation of small molecules or by solution-processing of small molecules or polymeric semiconductors.[3] Record efficiencies of 8.3% are reported for

polymeric organic solar cells as well as for vacuum-deposited organic devices based on small molecules.[2]

The groups of Würthner and Meerholz reported in 2008 for the first time the successful application of dipolar merocyanine dyes in bulk heterojunction (BHJ) organic solar cells with power conversion efficiencies up to 1.7%.[4] Benefits of these small molecular materials are their simple synthesis and purification processes, monodispersity and consequently well-defined material properties. Furthermore, the electronic character of the chromophores and consequently their properties can be adjusted by carefully choosing the used donor and acceptor moieties to meet the requirements for organic solar cells. Solution-processing was selected as the method of cell fabrication as this simple method is well-suited for material screening. Based on this knowledge, it was the aim of this work to explore the suitability of this class of dyes and develop new generations of chromophores with improved properties relating to BHJ organic solar cells. First, the synthesis of a library of dyes was envisaged to screen broadly different donor and acceptor groups. The characterization of the resulting dyes mainly by means of UV-vis spectroscopy and cyclic voltammetry should result in a data set suitable to estimate the performance of the chromophores in the solar devices. After testing the materials in photovoltaic cells, structure-property relationships between molecular and solar cell characteristics are to be derived. Additionally, single crystal analysis of selected chromophores was aimed to gain insight into the arrangement of the dyes in the solid state and possible correlations of the packing motif and the performance in the solar cells.

Chapter 1 introduces the relevant physical basics necessary to understand the general processes in organic solar cells and to characterize them. Moreover, its historic development starting from the first attempts to today's state of the art is sketched and a comprehensive overview of small organic molecules applied in solution-processed bulk heterojunction solar cells is given.

Chapter 2 describes a series of merocyanine dyes having an indolenine donor unit in common, but different electron-accepting moieties. The synthesis, optical and electrochemical investigations are reported and discussed, followed by the description of crystal structures derived from single crystal analysis. The suitability of these highly dipolar dyes as electron-donors in organic solar cells is explained by their antiparallel arrangement in the solid state, resulting in the annihilation of the large ground state dipole moments. Furthermore, by modification of the periphery of a chromophore a distinctly improved photovoltaic device with 2.6% efficiency was obtained.

Chapter 3 is based on a series of dyes with an aminothiophene donor. By varying the acceptor strength, chromophore **EL86** with well adapted optical and electronic properties was generated. Single crystal analysis showed again the formation of centrosymmetric dimers, leading to an extinct dipole moment on the supramolecular level. All dyes were analyzed in a standard cell set-up, whereas the cell design of the best performing dye, **EL86**, was optimized to achieve an efficiency of 4.0%.

Chapter 4 gives details on the synthesis of novel merocyanine dyes with extended π-system and the strong acceptor moiety 2-oxo-5-dicyanomethylene-pyrrolidine exhibiting absorption in the near-infrared. The chromophores were combined with both $PC_{61}BM$ and $PC_{71}BM$ and resulted in almost colorless, transparent devices.

Chapter 5 summarizes the efforts performed in the thesis by an in-depth analysis concerning the optical and electrochemical properties of a comprehensive series of 90 chromophores. Additionally, the corresponding solar devices are investigated and reported in detail. In order to derive structure-property relationships, the molecular properties were correlated with the characteristics of the respective photovoltaic cells and a set of general design rules was established.

Chapter 6 and *Chapter 7* conclude the thesis with summaries in English and German.

Chapter 1

Introduction

Abstract: This chapter gives a short introduction to the class of merocyanine dyes, followed by a definition of the important physical equations for characterizing organic solar cells. Furthermore, the historic development of organic photovoltaics beginning with the first devices reported in the 1970th until today's state of the art is reviewed shortly. The different cell designs, such as single layer, planar heterojunction and bulk heterojunction and their limitations are illustrated. Finally, a comprehensive overview of solution-processed BHJ organic solar cells based on small molecules is given, which is divided into the several groups according to the structural features of the materials.

1.1 Merocyanine dyes[5]

Merocyanines belong to the class of polymethine dyes, which are characterized by a π-conjugated polymethine chain assembled by an odd number of "–CH=" building blocks and electron-donor or electron-acceptor units as end groups of the chain. Symmetrical dyes display two identical end groups, whereas unsymmetrical dyes such as merocyanines exhibit two different end groups, namely an electron-donor (D) and an electron-acceptor (A) group.

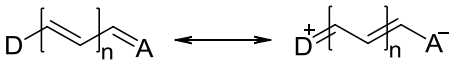

Chart 1. Neutral and zwitterionic resonance structure of merocyanine dyes.

Depending on D and A, the ground state of a merocyanine dye can be described mainly by the neutral resonance structure (polyene-type dye), by the zwitterionic structure (betaine-type dye) or equally by both resonance structures (cyanine-type dye). In the case of weakly electron-donating and electron-withdrawing end groups, the corresponding merocyanine dye is usually polyene-like displaying alternating –C=C– double and –C–C– single bonds within the methine bridge. Strengthening of the end groups increases the electron density transfer from the donor unit to acceptor group and leads to a leveling of the bond lengths and concomitantly a large ground state dipole moment.[6] At the so-called *cyanine limit* the cyanine-type chromophore displays no bond length alternation at all.[7]

The absorption spectra of merocyanine dyes mirror their electronic character and thus allow a first evaluation of their electronic nature. At the *cyanine limit* the excitation energy displays a minimum, resulting in absorption at the longest possible wavelength for the given π-conjugated system. Furthermore, almost no geometric changes accompany the transition, resulting in narrow and intense absorption bands.

By changing the number of "–CH=" units in the methine bridge or the donor and acceptor end groups the electronic characteristics can be tuned at will. Due to their properties and diversity, merocyanine dyes found application as spectral sensitizers in photography, as markers in biology and medicine and in the field of photorefractive materials and non-linear optics.[7,8,] In recent years, they were also applied successfully in dye-sensitized solar cells as potential alternatives to the standard ruthenium sensitizer.[9]

1.2 Organic solar cells

1.2.1 Characterization of organic solar cells

The performance of solar cells is dependent on the power conversion efficiency η, which is described by the ratio of the output power, determined by the number and electrochemical potential of electrons collected in the external electric circuit, to the input power, described by the number and energy of incident photons. The input power is a function of the used light, the output power is correlated to the product of three characteristics J_{SC}, V_{OC} and FF. At the short-circuit current density (J_{SC}) the voltage across the cell is zero, and the open-circuit voltage (V_{OC}) is the maximum voltage available in a cell, occurring at zero current (Figure 2).

$$\eta = \frac{P_{out}}{P_{in}} = \frac{J_{SC} \cdot V_{OC} \cdot FF}{I_0} \cdot 100 \qquad (1)$$

with:

η	=	efficiency [%]
P_{out}	=	output power
P_{in}	=	input power
J_{SC}	=	short-circuit current density [mA cm^{-2}]
V_{OC}	=	open-circuit voltage [V]
I_0	=	light intensity [mW cm^{-2}]
FF	=	fill factor

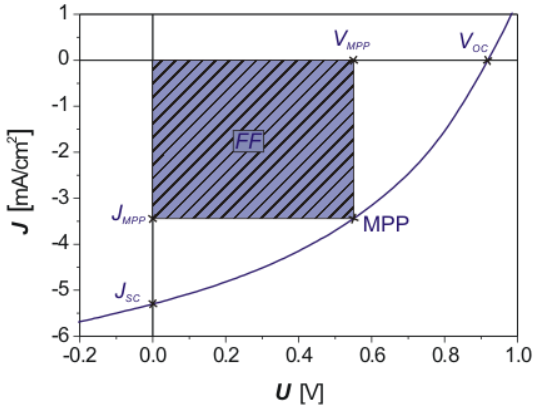

Figure 2. *JV* response of a MC based organic solar cells.

The fill factor (FF) is derived from the shape of the *JV* response and can be calculated according to equation 2. In the ideal, but non-realistic case where no recombination processes occurs, the shape of the *JV* curve would be rectangular and the FF equal to 1.

$$FF = \frac{J_{MPP} \cdot V_{MPP}}{J_{SC} \cdot V_{OC}} \quad (2)$$

with:

J_{MPP} = current density at the maximum power point [mA cm^{-2}]
V_{MPP} = voltage at the maximum power point [V]

A further important characteristic for a solar cell is the EQE spectrum, like depicted in Figure 3. Here the external quantum efficiency is plotted against the wavelength of the used light. Typically, the EQE spectrum follows the UV-vis spectrum of the applied dye and shows the ratio of the sun light, which can be transformed into collected electrons at a certain wavelength. The calculation of the single data points occurs according to equation 3.

$$EQE = \frac{1240 \cdot J_{Ph}}{\lambda \cdot I_0} \cdot 100 \quad (3)$$

with:

EQE = external quantum efficiency [%]
J_{Ph} = short-circuit current density for monochromatic irradiation [mAcm^{-2}]
λ = wavelength [nm]
I_0 = light intensity [mW cm^{-2}]

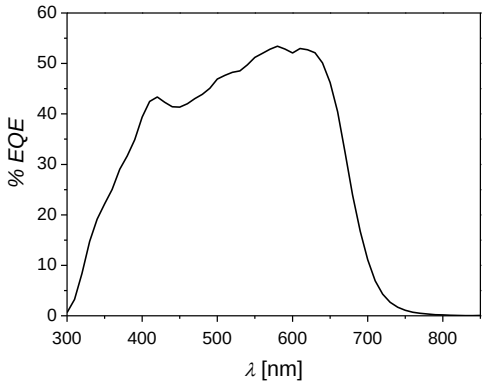

Figure 3. EQE spectrum of a device built with **EL86** (60wt% $PC_{71}BM$).

1.2.2 Historic development and fundamental processes

In the seventies of the last century, the first examples of solar cells (Figure 4, left) based on organic chromophores were reported. These cells were based on single active layers of dye molecules between two electrodes. In 1975, Tang et. al described the fabrication of a solar cell by electrodeposition of a microcrystalline chlorophyll film on top of an semitransparent Cr electrode with an overall efficiency of 0.02%.[10] A few years later, the group of Fishman announced the first merocyanine **MC 1** (Figure 4, right) applied in a 1 cm^2 solar cell by

vacuum-deposition. The cells with active layer thicknesses of 10–500 nm reached remarkably high power conversion efficiency (PCE) up to 0.7% at reduced light intensity of 78 mW cm^{-2}.[11] One reason for the high PCE is the V_{OC} of 1.2 eV, which is directly originated in single layer organic solar cells by the difference in work function of the front electrode and the back electrode. As Al/Al_2O_3 with a transparency of only 50% served as front electrode the J_{SC} of 1.8 mA cm^{-2} is all the more intriguing.

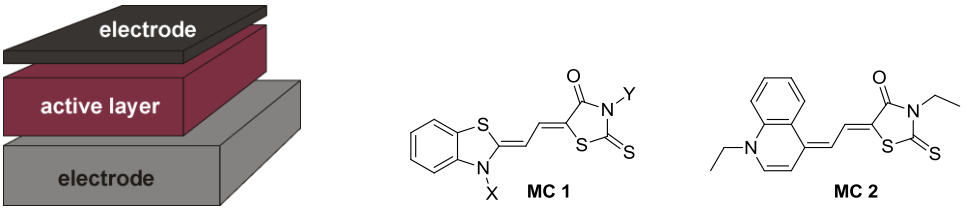

Figure 4. Cell design of a single layer solar device (left) and molecular structures of **MC 1** and **MC 2** (right).

In 1981, Chamberlain *et. al* used **MC 2** (Figure 4) in single layer organic solar cells with Al/Al_2O_3 as front electrode and gold as back contact. The authors described a significant increase in photovoltaic response, when the active layers were doped with iodine by vapour diffusion. With active layer thicknesses of 25 nm and a light intensity of 45 mW cm^{-2} a maximal power conversion efficiency of 0.2% was achieved.[12] The effect of the dopant material was further investigated and the strongest effect found for a Cl_2-doped active layer of **MC 2**.[13] The authors suggested that the excitons generated upon illumination can dissociate into charge carriers at the dopant sites. With an active layer thickness of 30 nm a PCE of 0.3% was determined at 90 mW cm^{-2}.

The cell efficiencies of the early single layer solar cells were limited, which is partly due to the physics of organic semiconductors. In inorganic semiconductors, the absorption of light typically leads to the immediate generation of free charge carriers. By contrast, excitation of organic material generates electron-hole pairs tightly bound together by coulomb attraction, so-called excitons.[14] In order to generate free charge carriers, which can contribute to the external current, the excitons need to dissociate. Generally, this is possible in the presence of an external electric field or at the interface of two different materials with sufficient energy offset of the frontier molecular orbitals (FMO).[15] Thus, the excitons have to reach the interface by diffusion, whereat exciton diffusion lengths of 10–20 nm[16] are the crucial parameter.

In 1986, Tang was the first to discover the advantage of an organic heterojunction by building a planar bilayer solar cell with copper phthalocyanine as electron donor and a perylene

derivative as electron acceptor material.[17] Applying the two-layer design resulted in a solar device with an unprecedented efficiency of ~1%. However, the bilayer is limited by the short exciton diffusion lengths of organic materials (Figure 5a). For this reason, the active layers thicknesses are usually very thin to assure that most of the created excitons can reach the interface. This results in a limited optical density and consequently restricted absorption efficiency of the device.

In 1995, the groups of Heeger and Holmes independently developed the concept of a bulk heterojunction, which circumvents the constraints of short exciton diffusion lengths.[18] Holmes and coworkers applied the BHJ to create an efficient photodiode consisting of two polyphenylenevinylene (PPV) compounds,[18a] while the group of Heeger combined a PPV derivative with [6,6]-phenyl-C_{61}-butyric-acid methyl ester ($PC_{61}BM$) in the active layer of an organic solar cell.[18b]

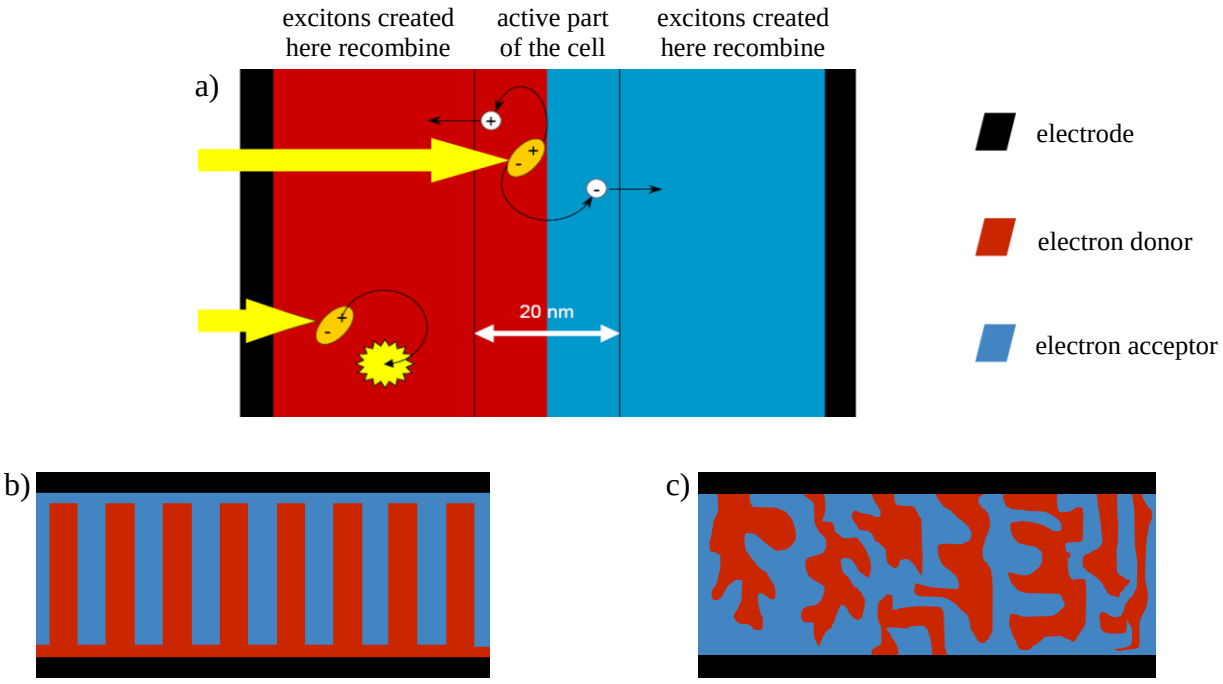

Figure 5. a) Schematic representation of a bilayer solar cell, exciton dissociation and recombination, respectively. b) Ideal bulk heterojunction solar cell. c) Schematic representation of an actual bulk heterojunction solar cell.

The ideal case of a BHJ presents an interpenetrating network with a large interface between electron donor and electron acceptor, where all generated excitons are within short distance to the next interface (Figure 5b). In fact, fabrication of the bulk heterojunction occurs by spin-coating a solution mixture of both components or by co-evaporation in the case of vacuum-deposition. The formation of the distinct domains is effected by phase-separation forces dependent on the used materials and conditions. Here, the possibilities to influence the

morphology, such as controlled evaporation rates, choice of solvent or weight ratios and postproduction treatments like annealing are limited. Hence, an actual bulk heterojunction is thought to look more like depicted in Figure 5c, containing also dead ends and domains too large for all excitons to reach the interface.

Besides an optimized morphology of the active layer, adjustment of the electronic character of the single components in the cell is crucial for its performance. Upon irradiation with light one electron, for example of the donor materials, is excited from the HOMO to the LUMO (process 1, Figure 6). After diffusion of the excited state to the interface between donor and acceptor component, the created exciton can dissociate and one electron can be transferred to the LUMO of the acceptor (process 2), while a hole is left in the donor. The required driving force for exciton splitting is given with an electronic offset of 0.3–0.4 eV between the LUMO levels.[19] Free electrons migrate within the domain of acceptor material to the metal electrode by hopping transport (process 3), while the holes in the electron donor diffuse to the front electrode (process 4). One important characteristic of the solar device, the V_{OC}, can be estimated by the simple FMO picture displayed in Figure 6: the distance between the HOMO of the electron donor and the LUMO of the electron acceptor is the theoretical V_{OC} one would achieved without any loss mechanism. Thus, donor materials exhibiting low-lying HOMO levels are preferable.

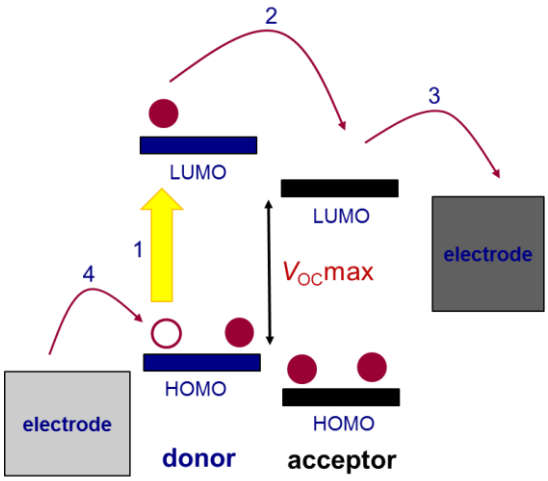

Figure 6. Schematic illustration of the electronic character of the single components and the operation principle of an organic solar cell.

To date, polymeric electron-donating materials dominate the field of solution-processed organic solar cells and score with record PCEs. Hence, a brief outline is given in the following. Starting with first reports in 1995, PPV derivatives were introduced as first polymers in organic solar cells.[18b] In combination with fullerene derivatives, efficiencies of

~3% were achieved in 2001.[20] Later, the thiophene derivative poly-3-hexylthiophene (P3HT) was established as standard material in polymeric organic solar cells due to improved overlap with the solar spectrum compared to PPV and its tendency to self-organize, resulting in improved charge carrier mobilites. The self-ordering process can be supported by heat treatment or solvent vapor annealing, yielding quite efficient solar cells with PCE up to ~5%.[21] One restricting factor of P3HT is the relatively high-lying HOMO of about –5.2 eV and its absorption maximum at ~530 nm in the solid state. Recently, low-band gap copolymers containing electron donating and electron accepting units gained in attention. Here, light harvesting over a broader absorption range is possible while achieving comparable high V_{OC} values. Due to this new concept and the application of $PC_{71}BM$, contributing significantly to the absorption of the solar cell, a boost in efficiency with values >8% was reported.[2,22]

1.2.3 Solution-processed BHJ organic solar cells based on small molecular donors

Unless stated otherwise, all described examples were BHJ solar cells and the results were determined at standard conditions: 1.5 AM and 100 mW cm^{-2} light intensity.

1.2.3.1 Oligothiophene-based donor materials

Thiophene-based materials have been applied for years in organic electronic devices due to their excellent electronic properties and high environmental and thermal stability. With regioregular poly(3-hexylthiophene) very high charge carrier mobilities of up to 0.1 cm^2 V^{-1} s^{-1} were achieved in thin film transistors.[23]

Thus, early in 2006, Roncali and coworkers started to investigate the potential of oligothiophenes in solution processed BHJ solar cells (Table 1).[24] They analyzed several linear, two-dimensional star-shaped compounds and the three-dimensional system **1**. The latter, based on a silicon core with four terthiophene arms, showed the most promising solar cell of this work: despite an absorption onset at 440 nm a short-circuit current density of 1.2 mA cm^{-2} and a high V_{OC} of 0.85 V was achieved. The overall efficiency of 0.3% was far behind the performance of the polymeric solar cells at that time, but these results represented still a starting point for organic solar cells based on small molecular donors.

Shortly after the publication of Roncali's work, Zhu et. al reported the application of x-shaped C_4-substituted thiophene oligomers in solution-processed BHJ solar cells.[25] The x-shaped structure was chosen to create a non-planar geometry, preventing aggregation and

enhancing the solubility of the compounds. By extending the oligothiophene chains, the authors observed a red-shift of the absorption maximum accompanied by an increase of the HOMO energy up to –5.26 eV for compound **2**. Compound **2** with the smallest band gap of the investigated series showed the highest J_{SC} of 3.7 mA cm^{-2} and remarkably also the highest V_{OC} of 0.85 V. This was rationalized by the very different film-forming abilities of the presented materials, affecting the whole performance of the respective device. The corresponding devices displayed a PCE of 0.8%

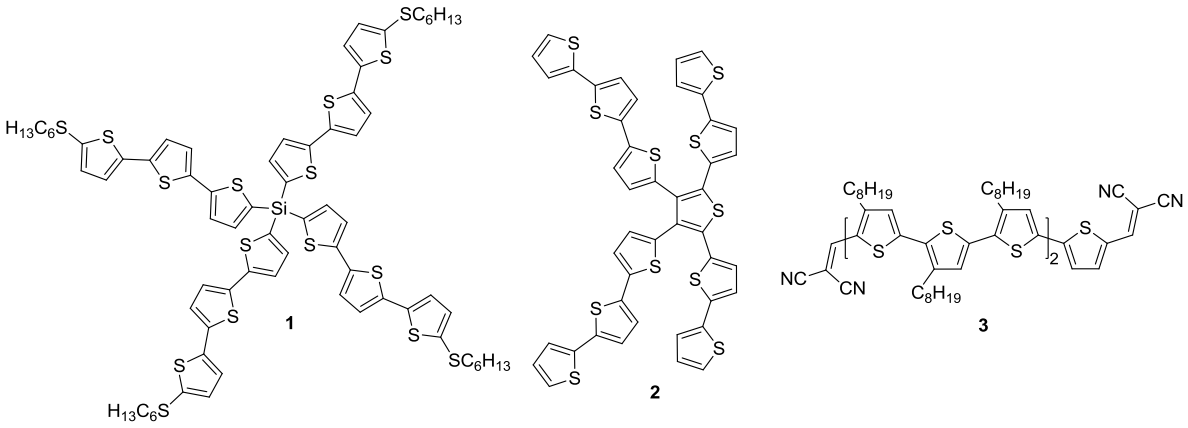

One major drawback of thiophene-based molecules with respect to application in organic solar cells is their absorption at rather short wavelengths (λ_{max} ~ 400 nm). Bäuerle and his group approached this problem by attaching two terminal electron-accpeting units at an oligothiophene for vacuum-deposited organic solar cells, entailing a bathochromic shift of the absorption maximum of ~100 nm.[26] The cooperation of Chen, Yin and their coworkers applied the same concept, but employed additional solubilizing octyl chains in septithiophene **3** for solution-processing.[27] In the thin film, the absorption band is broadened and shifted to longer wavelength by additional 100 nm, resulting in a good overlap of the absorption profile with the solar spectrum. These effects, together with the high hole mobility of pristine compound **3** of ~10^{-4} cm^2 V^{-1} s^{-1}, were explained by the planarity of the chromophore and the consequent $\pi\pi$-stacks of the molecules in the solid state. Applying **3** in a BHJ solar cell in combination with $PC_{61}BM$ yielded a highly efficient solar cell with an exceptionally large J_{SC} of 12.4 mA cm^{-2} and a PCE of 3.7%. Interestingly, no annealing procedures were reported to improve the cell performance. In the case of P3HT, this is a common method to improve the intermolecular packing of the thiophene chains and consequently the cell efficiency. Furthermore, the shape of the presented *JV*-curves and the low fill factor of 0.34 both hint at charge transport problems.

Table 1. Absorption maxima in solution, HOMO energies, hole mobilites and solar cell characteristics of the compounds **1**–**5** in combination with $PC_{61}BM$.

	λ_{max} (nm)[a]	HOMO (eV)	μ ($cm^2\ V^{-1}\ s^{-1}$)	wt% PCBM	V_{OC} (V)	J_{SC} (mA cm^{-2})	FF	η (%)	Ref
1	390	/	/	63	0.85	1.2	0.24	0.3	24[g]
2	390[b]	–5.26[b]	/	55	0.85	3.7	0.26	0.8	25
3	517[c (26)]	–5.13[e]	1.5×10^{-4} [(27a)]	58	0.88	12.4	0.34	3.7	27b
4	450	/	2.3×10^{-4}	80	0.94	3.4	0.40	1.3	29[h]
5	390[d]	–5.28[f]	/	67	0.97	4.2	0.42	1.7	30

[a] Thin film. [b] Solvent/calculation not specified. [c] Chloroform solution. [d] THF solution. [e] $E_{HOMO} = -e(E_{ox}^{onset} + 4.4)$, Redox potential measured versus SCE. [f] $E_{HOMO} = -e(E_{ox}^{onset} + 5.1)$; Redox potential measured versus Fc/Fc^+. [g] 79 mW cm^{-2}. [h] Annealing at 90 °C for 10 min.

Conjugated dendrimers combine the defined structures of small molecules with the advantages of large molecular weights of polymers. Their three-dimensional shape entails usually good solubility, film-forming abilities and an isotropic electronic nature, making them good candidates for application in amorphous optoelectronic devices.[28]

Kopidakis, Shaheen and coworkers combined the dendritic approach with the beneficial charge transport properties of oligothiophenes by synthesizing a series of dendrimers with increasing size.[29] They reported a decrease of the optical band gap related with increasing molecular size of the dendritic compounds. Furthermore, the hole mobility of the pristine material was enhanced from 1.6×10^{-5} $cm^2\ V^{-1}\ s^{-1}$ for a molecule with π-bridge consisting of one thiophene to 2.3×10^{-4} $cm^2\ V^{-1}\ s^{-1}$ for compound **4** with three thiophene units in the bridge. Both effects resulted in a significantly increased J_{SC} and a PCE of 0.5%. Optimization of the $PC_{61}BM$ weight ratio and the layer thickness involved a strongly enhanced fill factor of 0.4, a short-circuit current density of 3.4 mA cm^{-2} and an overall efficiency of 1.3%. Here, all devices were annealed for 10 min at 90 °C.

The most promising results with dendrimers in organic solar cells were reported by Bäuerle and his group. In 2008, they described two series of highly branched oligothiophene-based dendrons and dendrimers with an increasing number of thiophenes starting from 9 to 92 units.[30] The hyperbranched structure led to well soluble macromolecules without the need of solubilizing alkyl-chains. Furthermore, the large size of the higher dendrimers like **5** defines a lower limit for the domain size in the active layer and creates therefore a tool to control the morphology of the respective solar cell. Here again, increasing the number of thiophene units comes along with absorption at longer wavelengths and a shift of the HOMO to higher energies. Nevertheless, very high voltages of ~1 V were obtained for the whole series. Concerning J_{SC}, the authors observed increasing values upon increasing the molecule size,

which can be rationalized by the enhanced absorption. Optimization of the $PC_{61}BM$ weight ratio yielded a solar device based on compound **5** with a J_{SC} of 4.2 mA cm^{-2}, a fill factor of 0.42 and a PCE of 1.7%. Here, temperature annealing did not result in a beneficial change of intermolecular arrangement and consequently no improvement in device efficiency was found.

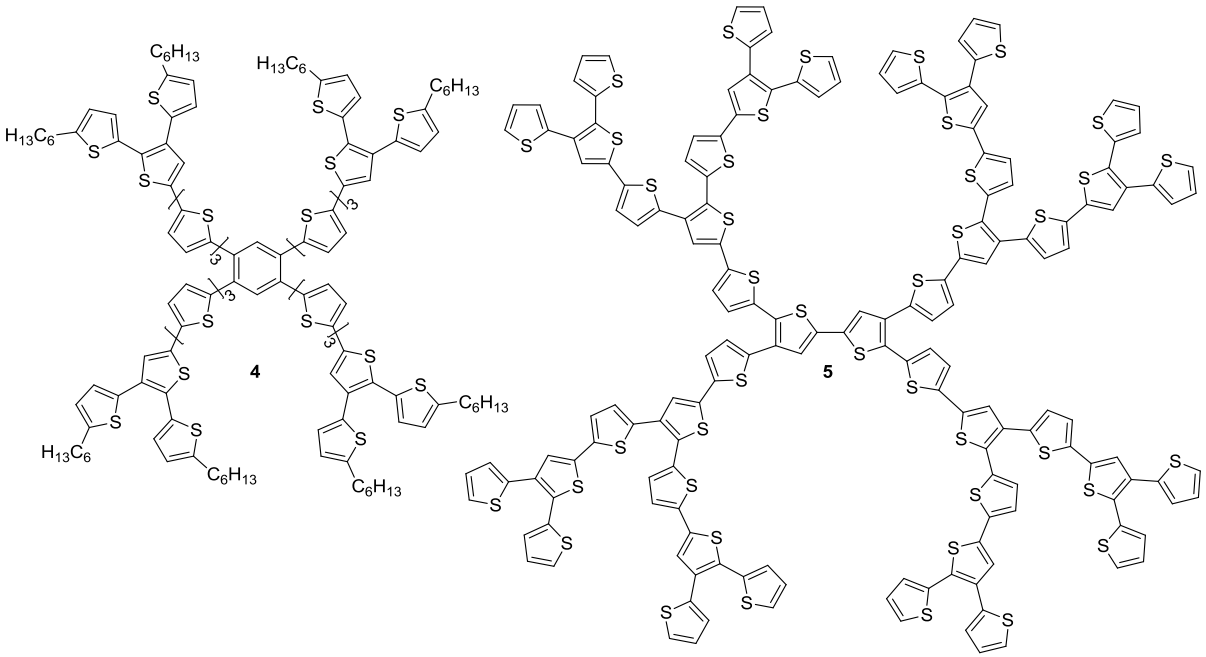

In general, thiophene-based solar cells are hampered by their absorption at rather short wavelengths around 400 nm. Short-circuit current densities higher than ~4 mA cm^{-2} are only possible, when $PC_{71}BM$, which contributes significantly to the absorption in the visible part of the spectrum, is involved. A bathochromic shift of the absorption band and consequently enhanced J_{SC} values are possible by adding electron-acceptors to the thiophene scaffold like in compound **3**. Nevertheless, usually high voltages of up to 1 V are obtained. Furthermore, it seems that the larger the size of the oligothiophenes, the better the respective solar cells performance. One possible explanation could be the lower limit of the domain size set by the mere dimension of a single macromolecule. Interestingly, only in one example (chromophore **4**) annealing was reported to improve the photovoltaic response.

1.2.3.2 Triphenylamine-based star-shaped donor materials

The triphenylamine (TPA) unit exhibits a three-dimensional propeller-like structure endowing TPA derivatives with good solubilities and isotropic optical and charge-transport properties. TPA-based compounds with good hole-transporting or electroluminescent properties have been developed and applied for example in organic light-emitting diodes.[31]

The group of Roncali first evaluated the potential of TPA derivatives in solution processed bulk heterojunction solar cells.[32] The functionalization with dithienylethylene π-conjugated chains and electron acceptors like in compound **7** enlarged the π-system and induced an intramolecular charge transfer (ICT), resulting in absorption at longer wavelengths. Table 2 summarizes the electronic data of the chromophores and the corresponding solar devices. The respective device built with dye **6** suffers from a low fill factor and short-circuit current density. A significant increase in J_{SC} was obtained by employing compound **7**, which absorbs at longer wavelengths than **6** and can consequently absorb larger fraction of the incoming light. Hence, the power conversion efficiency could be raised from 0.4% (**6**) to 0.8% (**7**).

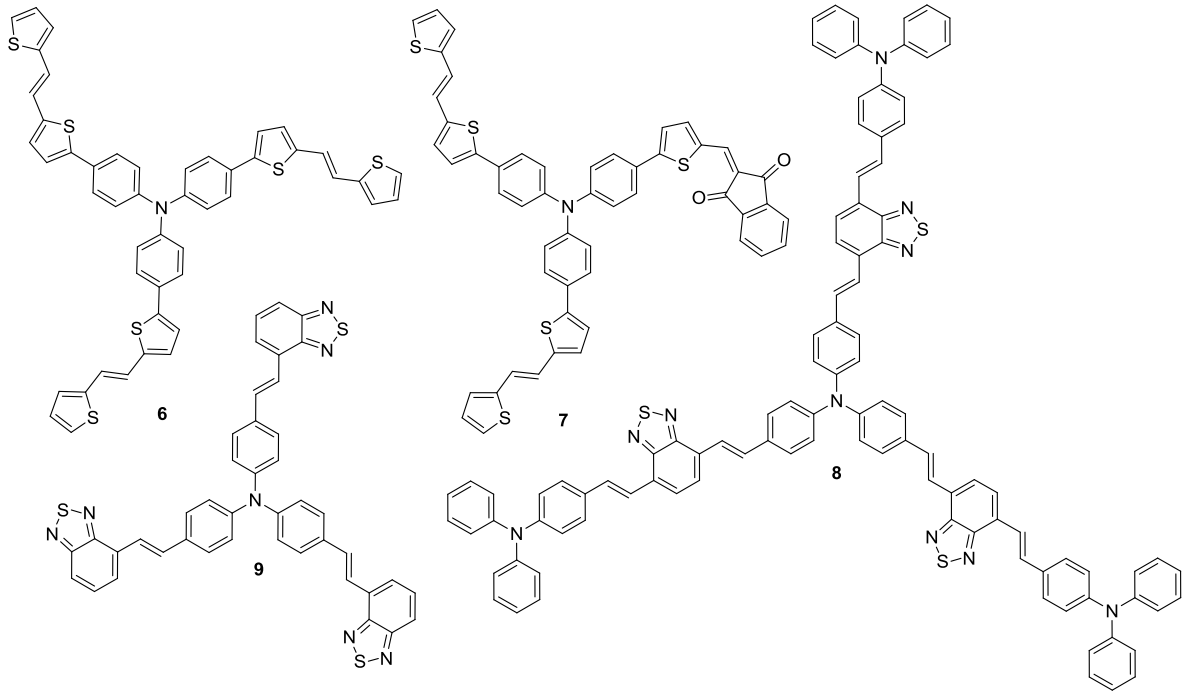

Two years later, Li et al. reported results on star-shaped triphenylamine dyes as donor materials in BHJ solar cells in the first of numerous publications.[33] They compared the performance of molecule **8** using benzothiadiazole as acceptor units with the one of the respective linear compound.[33a] The star-shaped compound **8** revealed higher charge carrier mobility, enhanced absorbance and better film forming properties, resulting in a three times enhanced J_{SC} 4.2 mA cm^{-2} than the linear derivative.[33b] Compared to the device with **7**, the solar cell containing **8** displayed a higher V_{OC} and FF and a PCE of 1.3%.

Chromophore **9** with shorter arms and π-system shows a hypsochromically shifted absorption band, but a lower HOMO energy. The latter entailed a higher value for V_{OC} of 0.93 V after an optimization of the cathode material, but an inferior current density of 1.5 mA cm^{-2} resulted in a low PCE of 0.6%.[33d]

Table 2. Absorption maxima in solution, HOMO energies, hole mobilites and solar cell characteristics of the compounds **6**–**12** in combination with $PC_{61}BM$ or $PC_{71}BM$.

	λ_{max} (nm)[a]	HOMO (eV)[d]	μ ($cm^2\ V^{-1}\ s^{-1}$)	wt% PCBM	V_{OC} (V)	J_{SC} (mA cm^{-2})	FF	η (%)	Ref
6	424	–5.2[e]	/	75	0.60	2.4	0.28	0.4	32
7	536	–5.3[e]	/	75	0.66	4.1	0.30	0.8	32
8	531[b]	–5.30	4.7×10^{-5}	75	0.81	4.2	0.39	1.3	33a
9	460	–5.41	/	75	0.93	1.5	0.43	0.6	33b
10	509[c]	–5.19	/	75[g]	0.85	8.6	0.33	2.4	33d
11	518[c]	–5.06	/	67[g]	0.88	7.8	0.44	3.0	33f
12	512[c]	–5.28[f]	4.9×10^{-4}	67[g]	0.87	9.5	0.52	4.3	33g

[a] CH_2Cl_2 solution. [b] Chlorobenzene solution. [c] Chloroform solution. [d] $E_{HOMO} = -e(E_{ox}^{onset} + 4.71)$, Redox potential measured versus Ag/Ag^+. [e] Value estimated from cyclic voltammogram. [f] $E_{HOMO} = -e(E_{ox}^{onset} + 4.8)$; Redox potential measured versus Fc/Fc^+. [g] $PC_{71}BM$.

The 4-hexyl-thiophene units at the end of each arm in compound **10** extend the π-system compared with **9** and results in good film-forming properties.[33d] Though a similar absorption maximum than in dye **8** was obtained, the resulting J_{SC} was significantly increased to a high value of 8.6 mA cm^{-2} and a PCE of 2.4% was obtained. Partially, this is originated by the use of $PC_{71}BM$, showing enhanced absorption in the visible region. Additionally, variation of the cathode material from Al to Mg/Al led to a further increase in current density.

In chromophore **11**, dicyanovinyl was used instead of benzothiadiazole to obtain ICT absorption bands.[33f] The performance of chromophore **11** was compared with the respective dye without the vinylene linkage within the arms of the molecule. Obviously, the red-shifted absorption of **11** entails a larger current density of 7.8 mA cm^{-2} and subsequently results in a superior solar cell with a high PCE of 3.0%.

Recently, Li, Zhan and coworkers reported an impressive solar cell with 4.3% efficiency achieved by a further structure optimization.[33g] In compound **12** they combined the approach of using oligothiophenes to enable good charge transport with benzothiadiazole units as electron acceptors as well as π-bridge. The high obtained open-circuit voltage of 0.87 V is comparable to the values achieved for the previous TPA derivatives. However, the fill factor of 0.52 is exceptionally high for a BHJ solar device based on a small molecular donor and the J_{SC} of almost 10 mA cm^{-2} is considerable, too. The authors rationalize these results with the strong absorption, high hole mobility and relatively low HOMO level of chromophore **12**.

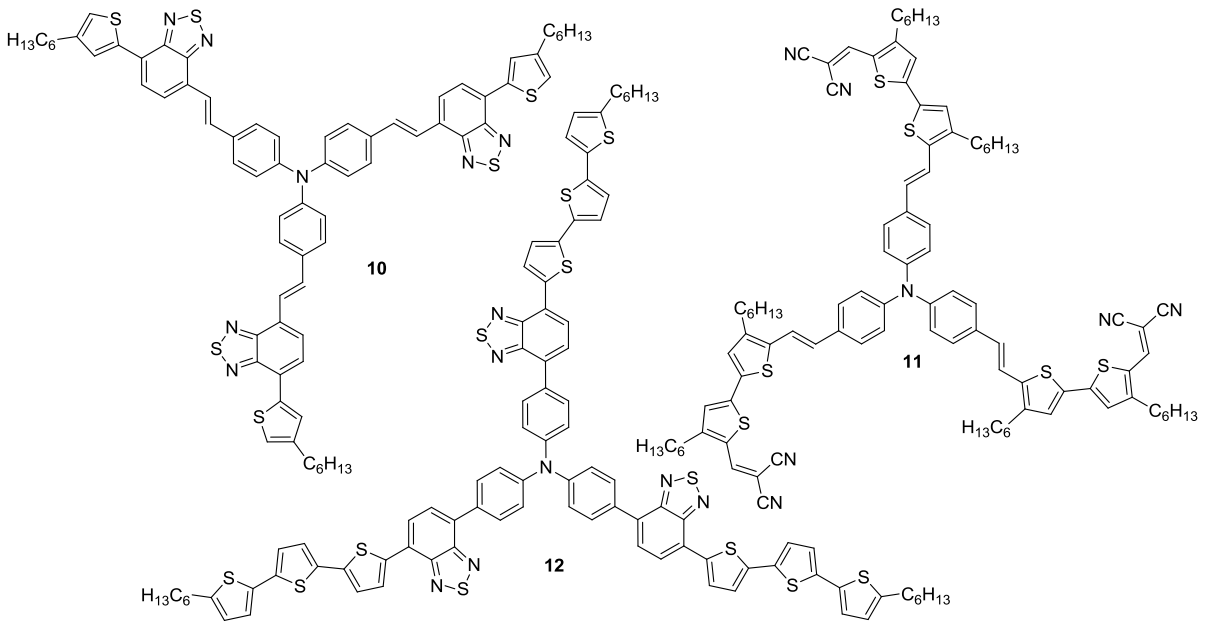

Seemingly, exchanging the flexible vinylene units by more rigid aromatic moieties is beneficial for the charge transport properties. Although the described HOMO energies differ by 0.35 eV, the open circuit voltages of the solar cells reported by Li vary only by 0.1 V. The authors suggest that the morphology of the active layer and also the hole mobility influence strongly the respective V_{OC} of a solar cell. In none of the described examples, annealing or solvent vapor annealing was reported to improve the cell performance. Here, the compound with the highest molecular mass, dye **12**, yielded the most efficient solar device. Interestingly, in the case of the triphenylamine derivatives, usually high amounts of PCBM in the active layer resulted in the best solar cells.

1.2.3.3 PAH derivatives as donor materials

Polycyclic aromatic hydrocarbons and their derivatives are long since known for their excellent charge transport properties. The most prominent candidate of this family is pentacene, with charge carrier mobilities up to 5 $cm^2\ V^{-1}\ s^{-1}$.[34]

The electronic details and solar cells characteristics of the dyes described in this section can be found in Table 3. The first example of an acene derivative applied successfully in organic BHJ solar cells was reported by Malliaras and coworkers in 2007.[35] They found that anthradithiophene **13** forms crystalline spherulites in a blend with $PC_{61}BM$ upon solvent vapor annealing (Figure 7). This was done by transferring the thin films into a sealed sample holder directly after preparation. The residual solvents within the spin-coated active layer, toluene and *o*-dichlorobenzene, induced the restructuring of the donor-acceptor blend. The higher the coverage of the film with the spherulites, the higher the measured J_{SC} values got.

The best device was found to exhibit 82% spherulite coverage, a J_{SC} of 3.0 mA cm^{-2} and a PCE of 1.0%. However, the authors state that the crystallites within the spherulites consisting of dye **13** were too large to allow for efficient charge separation.

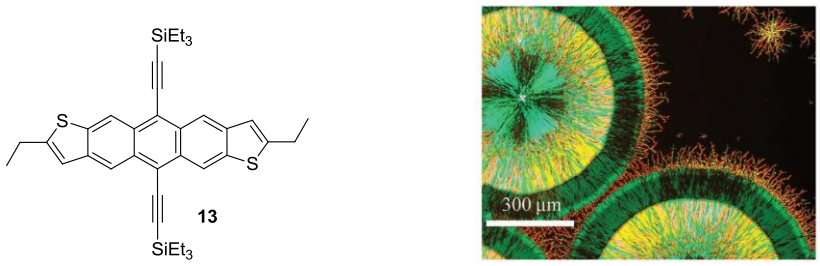

Figure 7. a) Molecular structure of compound **13**. b) Optical micrographs of the spherulites formed by **13** in mixed films with $PC_{61}BM$. Reprinted with permission from ref. 35. Copyright 2007 American Chemical Society.

The groups of Marrocchi, Facchetti and Marks spend efforts to investigate anthracene derivatives with regard to their application in OFETs and organic BHJ solar cells.[36,37] Compound **14** represents the first reported example, a conjugated diarylanthracene derivative with four solubilizing hexyloxy groups. The low HOMO level at –5.51 eV allows for a high V_{OC} of 0.89 V and a relatively high fill factor of 0.45 was obtained after annealing at 60 °C for 1 h. However, the moderate J_{SC} of 3.1 mA cm^{-2} results in an efficiency of only 1.3%. This can be partially explained by the absorption around 450 nm in solution, which covers only a fraction of the incoming light. The enlarged π-system of **15** results in a reduced band gap and a red-shift of the absorption band. Furthermore, the authors built OFETs containing **15** with a quite high hole mobility of 2.0×10^{-2} cm^2 V^{-1} s^{-1}, which are two orders of magnitude higher than that of compound **14**. Nevertheless, almost the same cell characteristics were measured. Though, the device built with compound **15** showed its best performance without annealing procedure. In reference 37b the compounds **14** and **15** were compared to the respective analogous with olefinic spacer units instead acetylene units. Here, the olefinic derivatives showed clearly inferior solar cell performance due to lower V_{OC} and J_{SC} values. The first were attributed to higher HOMO levels, the latter to a lower hole mobility of the materials.

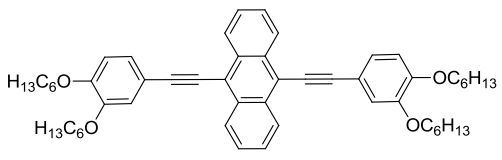

14

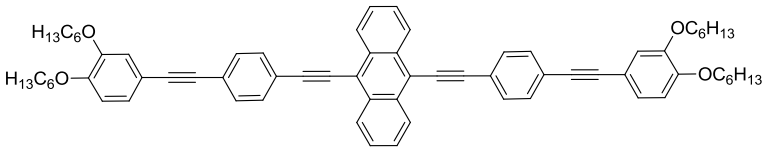

15

Table 3 Absorption maxima in solution, HOMO energies, hole mobilites and solar cell characteristics of the compounds **13**–**18** in combination with $PC_{61}BM$ or $PC_{71}BM$.

	λ_{max} (nm)[a]	HOMO (eV)	μ ($cm^2\ V^{-1}\ s^{-1}$)	wt% PCBM	V_{OC} (V)	J_{SC} (mA cm^{-2})	FF	η (%)	Ref
13	/	–5.15[d]	/	30	0.84	3.0	0.40	1.0	35[i]
14	457	–5.51[e]	3.9×10^{-4}	33	0.89	3.1	0.45	1.3	37b[j]
15	486	–5.44[f]	2.0×10^{-2}	33	0.95	2.6	0.48	1.2	37b
16	550[b]	–5.35[e]	/	50	0.83	6.6	0.41	2.3	38
17	364[c]	–5.03[f]	2.8×10^{-4}	67	0.90	2.7	0.61	1.5	39[k]
18	369[c]	–5.28[g]	/	67[h]	1.00	6.4	0.38	2.5	41

[a] Chloroform solution. [b] Estimated from thin film. [c] CH_2Cl_2 solution. [d] Calculation not specified. [e] $E_{HOMO} = -e(E_{ox}^{1/2} + 4.8)$; Redox potential measured versus Fc/Fc^+. [f] $E_{HOMO} = -e(E_{ox}^{onset} + 4.8)$; Redox potential measured versus Fc/Fc^+. [g] $E_{HOMO} = -e(E_{ox}^{onset} + 5.1)$; Redox potential measured versus Fc/Fc^+. [h] $PC_{71}BM$. [i] Solvent vapor annealing. [j] Annealed at 60 °C for 1 h. [k] Annealing at 150 °C for 15 s.

In 2009, Watkins and coworkers reported the implementation of dibenzo[*b*,*def*]chrysene **16** in bulk heterojunction solar cells.[38] The synthesis of this material is very simple and scalable, as it can be produced in one step starting from a commercial available dye. By changing the spin-coating solvent from chlorobenzene to chloroform, the J_{SC} could be raised from 3×10^{-3} mA cm^{-2} to 6.6 mA cm^{-2}. This was attributed to the phase separation, which occurred in the first case in the micrometer regime, while films processed with chloroform at high concentrations exhibit domains in nanometer regime. With a V_{OC} of 0.83 V and a fill factor of 0.41, a respectable solar cell efficiency of 2.3% was achieved.

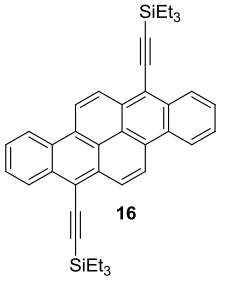

16

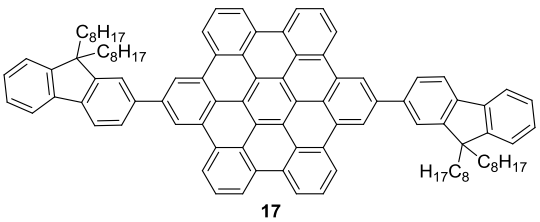

17

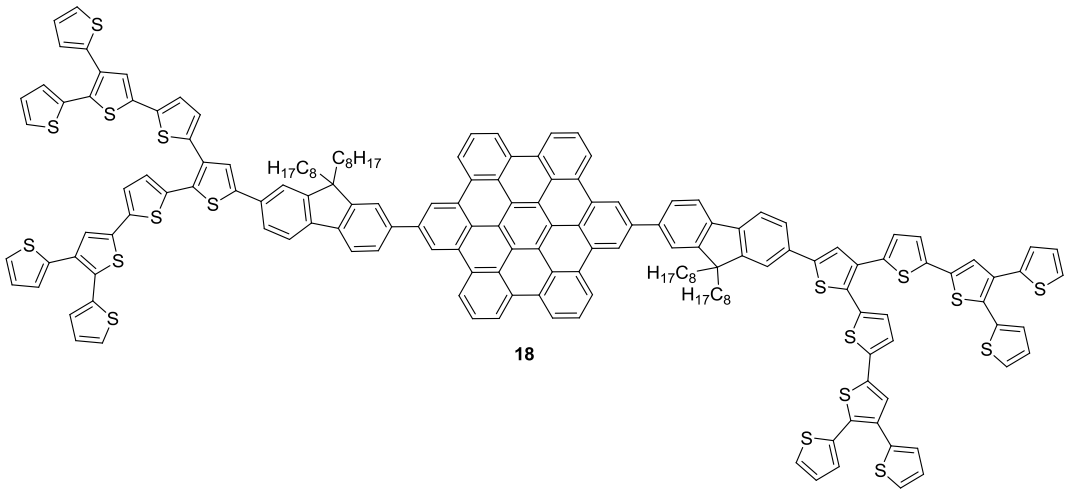

18

As an approach to control the morphology of the active layer Bäuerle and Holmes applied hexa-*peri*-benzocoronones (HBCs) functionalized with solubilizing 9,9-dioctylfluorenyl moieties like the compounds **17** and **18** in BHJ organic solar cells, as HBC derivatives are known to self-organize into columnar stacks.[39] Besides their ability to self-assemble, HBCs have shown high charge transport mobilities up to 5×10^{-3} cm^2 V^{-1} s^{-1} in OFETs.[40] The authors compared the solar cell performance of different derivatives bearing two or six fluorenyl units at the HBC core. Solar cells built with the latter showed moderate V_{OC} and FF, but almost zero short-circuit current density. As the absorption properties of both compounds are very similar, the authors rationalized these results with the observed disordered bulk structure due to the steric hindrance caused by the six bulky fluorenyl units and the resulting low charge carrier mobility of the dye measured in OFETs. By contrast, HBC **17** is still able to form strong $\pi\pi$-contacts in the thin film, leading to highly organized structures observed by wide-angle X-ray scattering (WAXS) experiments. Though the HOMO level is located at rather high energies (–5.03 eV), voltages of ~0.9 V were achieved in the respective solar cells. Furthermore, annealing for 15 s at 150 °C increased both FF and J_{SC} to 0.61 and 2.7 mA cm^{-2}, respectively, indicating a further ordering of the HBC cores. The very high FF points to balanced charge carrier mobilities in the donor and as well in the acceptor domains, which was confirmed by the determination of the charge transport properties in OFETs. In total, a PCE of 1.5% was achieved.

Based on the promising results with HBC derivatives, Bäuerle and Holmes attached thiophene dendrons of different size to compound **17**. Here, the fluorenyl units were used as an easy option for further functionalization in order to improve the absorption properties of the material.[41] All tested compounds showed very high V_{OC} values of 0.9–1.0 V. For J_{SC}, an enhancement with increased dendron size was measured, which is in accordance with the

broadening of the absorption spectra. The compound with least amount of thiophene units showed the highest fill factor of 0.54, while compound **18** showed a fill factor of 0.38. This was attributed to the lower degree of self-organization in active layers comprising compound **18**, determined by two-dimensional WAXS. The respective devices containing **18** and $PC_{61}BM$ showed slightly improved V_{OC} and J_{SC} compared to cells built with **17**, but a lower FF. Hence, a similar PCE was reached. By combining **18** with $PC_{71}BM$, a high short-circuit current density of 6.4 mA cm^{-2} and a PCE of 2.5% was accomplished. In summary, the rational combination of thiophene dendrons and HBC as scaffold for self-assembly produced a promising material with regard to application in organic solar cells.

The presented PAH and acene derivatives, respectively, show absorption maxima in solution between 360 and 490 nm. As the solar flux peaks at ~700 nm, these devices can only absorb a fraction of the incoming light, which is reflected by the usually low J_{SC} values around 3 mA cm^{-2}. Replacing $PC_{61}BM$ by $PC_{71}BM$ can improve the light harvesting abilities of the films, as shown with chromophore **18**. Though several HOMO levels are located at quite high potentials, the reported V_{OC} values are ranging at a remarkable level of 0.8–1.0 V. Most interestingly are the very high fill factors up to 0.6 in the case of compound **17**, which are reached after annealing procedures. This can be rationalized by the tendency of these substances to self-organize into ordered structures in the bulk, a process, which can be enhanced by heating or exposing to solvent vapor. Furthermore, PAH derivatives allow a high dye load in the active layer with PCBM weight percentages down to 30%.

1.2.3.4 Donors based on donor-acceptor-donor (D-A-D) subunits

The presence of electron-deficient and electron-rich moieties (push-pull subunits) within a conjugated molecule reduces the band gap of the material and induces an intramolecular charge transfer. In some examples presented in section 1.2.3.2, electron accepting units in combination with a central triphenylamine were also applied to obtain absorption at longer wavelengths. Besides the conventional triphenylamine, electron-donating units like oligothiophenes, carbazole and other amine derivatives are commonly used. Benzothiadiazole, 2-pyran-4-ylidenemalononitrile (PM) or fluorenone represent traditional electron-accepting groups, but others like diketopyrrolopyrrole or squarylic acids are gaining in attention in the field of organic photovoltaics. Most of the described examples in this section are symmetric donor-acceptor-donor systems connected by thiophene, phenyl or vinylene π-bridges, showing a more or less linear shape. Exceptions are represented by the

molecule **22**, deriving strongly from the linear shape, and chromophore **30**, which is an acceptor-donor-acceptor system.

For clarity, the presented examples are arranged into groups having the same central acceptor unit. The electronic details and solar cell characteristics of all chromophores presented in chapter 1.2.3.4 are compiled in Table 4. Early in 2006, Li and his coworkers reported the application of the first D-A-D chromophore, **19**, in solution processed bulk heterojunction solar cells.[42] The electron-donating triphenylamine units were connected to the electron-deficient benzothiadiazole by thiophene and vinylene spacer units. Upon optimizing the cathode material from Mg/Al via LiF/Al to Ba/Al they could improve the solar cell efficiency. Though the fill factor and open-circuit voltage were moderate, the very low short-circuit current density of 0.9 mA cm^{-2} lead to an overall deficient solar device with a PCE 0.3%.

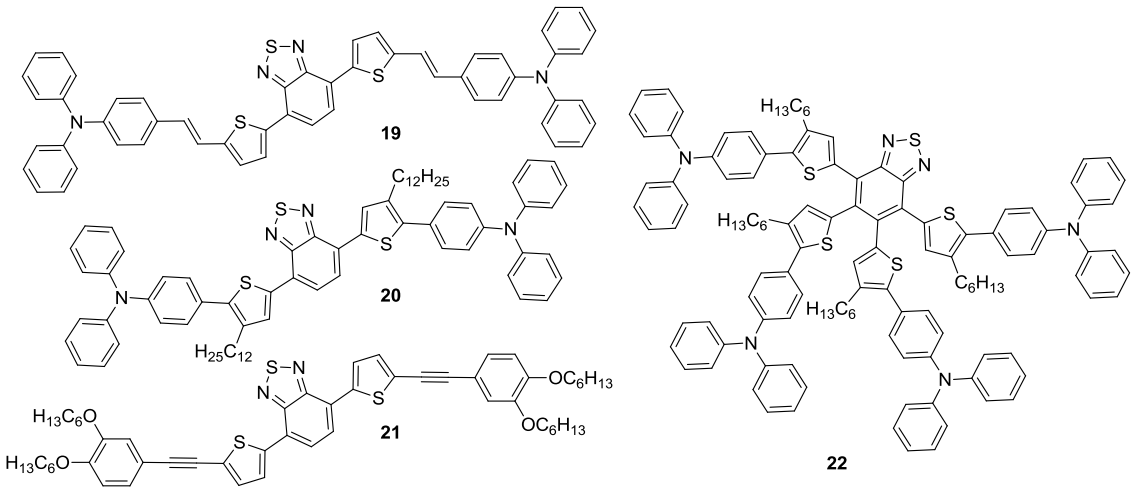

Later, the authors developed the system further by removing the vinylene linker and adding two solubilizing dodecyl groups in chromophore **20**.[43] The lower HOMO level entailed a very high V_{OC} of 0.93 V and higher short-circuit current densities were observed though **20** exhibits a narrower band gap compared to **19**. Partially, this can be ascribed to the use of $PC_{71}BM$, which contributes to the absorbance and generation of excitons. In accordance with standard procedures reported for solar cells containing polymeric electron donors, the influence of additives to the performance of the solar cell was tested. Addition of 1% 1,8-octanedithiol resulted in an increase in J_{SC} from 6.0 mA cm^{-2} to 7.5 mA cm^{-2}, while the V_{OC} and fill factor stayed at high values of 0.93 V and 0.41, respectively. UV-vis experiments showed enhanced absorption upon addition of the additive, which was reflected by significantly higher external quantum efficiency (EQE) values. The authors investigated the active layer by atomic force microscopy (AFM) and found a roughening of the surface when

the additive is present, which was rationalized by an amplified aggregation process. In total, a high PCE of 2.9% was achieved.

Table 4. Absorption maxima in solution, HOMO energies, hole mobilites and solar cell characteristics of the compounds **19**–**36** in combination with $PC_{61}BM$ or $PC_{71}BM$.

	λ_{max} (nm)[a]	HOMO (eV)[f]	μ ($cm^2\ V^{-1}\ s^{-1}$)	wt% PCBM	V_{OC} (V)	J_{SC} (mA cm^{-2})	FF	η (%)	Ref
19	560[b]	–5.1[g]	/	50	0.76	0.9	0.33	0.3	42[r]
20	534[b]	–5.16	3.5×10^{-7}	75[q]	0.93	7.5	0.41	2.9	43
21	503	–5.37[h]	6.6×10^{-5}	50	0.88	2.2	0.34	0.7	45
22	489[c]	–5.4[i]	/	75[q]	0.92	4.9	0.41	1.8	46
23	466[d]	–5.14[j]	1.2×10^{-6}	75	0.90	2.1	0.41	0.8	47
24	480[c]	–5.28[k]	1.4×10^{-5}	67	0.98	4.2	0.37	1.5	48
25	504	–5.44[l]	5.9×10^{-5}	70	0.90	4.3	0.30	1.2	49
26	538	–5.15[h]	/	75[q]	0.78	6.8	0.39	2.1	50[s]
27	616	–5.03[m]	5.0×10^{-7}	30	0.67	8.4	0.45	2.3	51
28	650[b]	–5.2[i]	1.0×10^{-4}	50[q]	0.75	9.2	0.44	3.0	52
29	630	–5.2[i]	3.0×10^{-5}	40[q]	0.92	10.0	0.48	4.4	53[t]
30	624	–5.40[f]	3.3×10^{-3}	40	0.84	11.3	0.42	4.1	54[t]
31	740	–5.0[n]	/	75	0.62	5.7	0.35	1.2	55
32	701[e]	–5.1[o]	1.3×10^{-3}	40	0.31	12.6	0.47	1.8	56[u]
33	729	–5.0[n]	/	75[q]	0.57	9.3	0.37	2.0	57[v]
34	680[b]	–5.1[n]	/	86	0.92	12.0	0.50	5.2	58c[w]
35	580[e]	–5.16	2.0×10^{-8}	67	0.89	4.2	0.46	1.7	59
36	579[c]	–5.5[p]	/	50	0.74	6.3	0.38	1.8	60[x]

[a] Chloroform solution. [b] Estimated from thin film. [c] THF solution. [d] Toluene solution. [e] CH_2Cl_2 solution. [f] $E_{HOMO} = -e(E_{ox}^{1/2} + 4.8)$; Redox potential measured versus Fc/Fc^+. [g] $E_{HOMO} = -e(E_{ox}^{onset} + 4.4)$, Redox potential measured versus SCE. [h] $E_{HOMO} = -e(E_{ox} + 4.71)$, Redox potential measured versus Ag/Ag^+. [i] Determined by UPS. [j] $E_{HOMO} = -e(E_{ox}^{onset} + 4.39)$; Redox potential measured versus Ag wire.[44] [k] $E_{HOMO} = -e(E_{ox}^{onset} + 4.63)$, Redox potential measured versus Ag/Ag^+. [l] $E_{HOMO} = -e(E_{ox}^{onset} + 4.69)$, Redox potential measured versus Ag/Ag^+. [m] $E_{HOMO} = -e(E_{ox}^{onset} + 4.6)$; Redox potential measured versus Fc/Fc^+. [n] Calculation not specified. [o] $E_{HOMO} = -e(E_{ox}^{1/2} + 5.15)$; Redox potential measured versus Fc/Fc^+. [p] $E_{HOMO} = -e(E_{ox} + 5.1)$; Redox potential measured versus Fc/Fc^+. [q] $PC_{71}BM$. [r] 85 mW cm^{-2}. [s] Annealed at 80 °C for 30 min. [t] Annealed at 110 °C for 10 min. [u] Annealed at 110 °C for 15 min. [v] Annealed at 50 °C for 30 min. [w] Solvent vapor annealing for 10 min with CH_2Cl_2. [x] Annealed at 70 °C for 30 min.

Ouyang and coworkers reported the synthesis and application of chromophore **21** in BHJ solar cells, where benzothiadiazole serves again as electron-deficient unit. They chose the acetylenic spacer unit to create a stiff molecular chain, which could facilitate the charge transport and enhance intermolecular interactions.[45] The used donor unit displays weaker electron donating properties than triphenylamine, resulting in a larger band gap, but also lower HOMO energy. Chromophore **21** was compared with the respective molecule bearing additional acetylene-phenylene spacer moieties. Although the charge carrier mobility of a

pure film of the latter was superior to a film of **21**, the mobility of the blend with $PC_{61}BM$ was one order of magnitude lower than the one of blends containing compound **21**. The most efficient solar cells were built with 50% of dye **21** with a moderate efficiency of 0.7%. Annealing procedures at various temperatures were analyzed, but only decreased cell performances were obtained.

The group of Zhang employed the same structural motives like in compound **20**, but applied them to form the star-shaped molecule **22**[46] as well, following the promising examples with three-dimensional triphenylamine chromophores and oligothiophene dendrimers. Comparison of the star-shaped molecule with the respective linear compound revealed a larger band gap, but also a lower HOMO level for the former. In the solar cells, the dyes were combined with $PC_{71}BM$ and considerable J_{SC} up to ~5 mA cm^{-2} and V_{OC} up to 0.92 V were achieved. The star-shaped molecule **22** turned out to result in slightly better devices with a maximal PCE of 1.8% due to the lower HOMO level compared to the linear dye and consequently higher V_{OC}.

Besides benzothiadiazole, the 2-pyran-4-ylidenemalononitrile (PM) unit was also applied frequently as strongly electron-accepting unit in symmetrical donor-acceptor-donor molecules for solution-processed BHJ solar cells. In 2007, the group of Li first synthesized chromophore **23** using this acceptor unit in combination with triphenylamine as electron-donating moieties and phenylene-vinylene π-bridges and investigated its properties in organic solar cells.[47] First experiments with a 1:1 mixture of dye **23** and $PC_{61}BM$ resulted in a solar cell with high V_{OC} (0.9 V), but the low J_{SC} and FF led to a PCE of 0.4%. Optimizing the weight ratio and changing the electrode material from LiF/Al to Ba/Al resulted in an improved cell with an efficiency of 0.8%, belonging to the top values at this time.

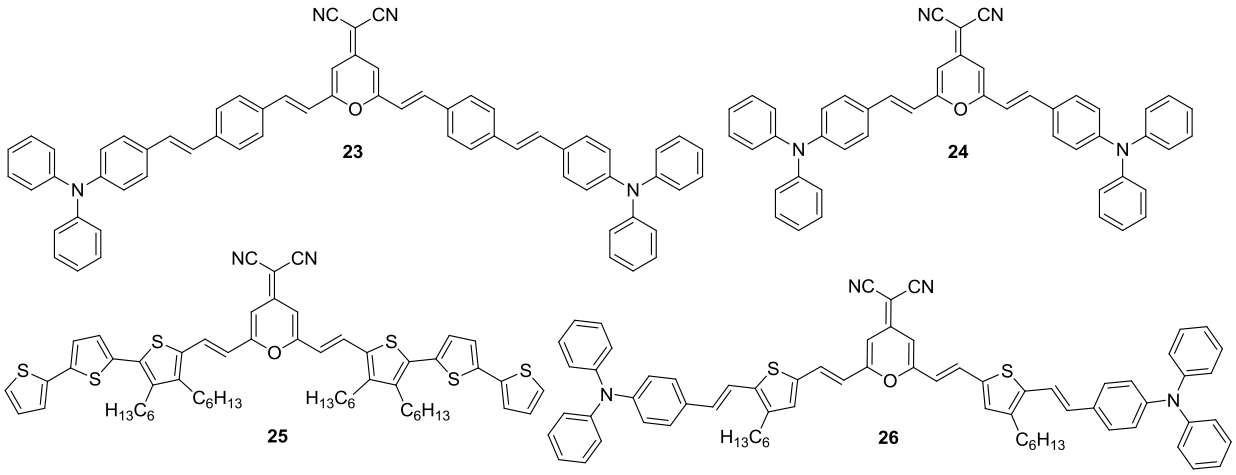

23 **24** **25** **26**

Two years later, Tian and his coworkers used the same structural motif, but synthesized the shorter chromophore **24** for BHJ solar cells.[48] The compound shows absorption at a slightly

longer wavelength, a lower HOMO level and also better charge transport properties. Furthermore, a maximum in solar cell performance was found with a higher dye loading of 33wt% compared to 25wt% (dye **23**). These improvements translate to a solar device with higher V_{OC} of 0.98 V and a doubled J_{SC} (4.2 mA cm^{-2}) as well as PCE (0.8%). The presented chromophores all show absorption at relatively short wavelengths, limiting the light harvesting properties. Thus, the group of Tian replaced the popular electron-donor triphenylamine by an oligothiophene unit in compound **25**.[49] Furthermore, the planar oligothiophenes are known to stack in the solid state and usually display good charge transport properties. Actually, the absorption of chromophore **25** is slightly red-shifted and the measured hole mobility is improved compared to the one of dye **24**. Investigation of the BHJ solar cells containing chromophore **25** revealed a comparable performance like in the case of **24**. In total, a high V_{OC} (0.9 V), moderate short-circuit current density (4.2 mA cm^{-2}) and low fill factor of 0.3 gave a moderate solar cell efficiency of 1.2%.

Just recently, Li and his coworkers presented their further developments with this class of dyes: they substituted the styrene units in **23** by thienylenevinylene in **26** to achieve both higher solubility and improved charge transport properties.[50] Furthermore, this entailed a red-shift of the absorption band by ~70 nm. Due to its better absorption properties, the authors chose $PC_{71}BM$ as acceptor material. Hence, they could improve the PCE of solar cells containing chromophore **23** to 1.4%, mainly originated by a higher J_{SC}. Application of the new dye **26** resulted in even higher J_{SC} of 6.8 mA cm^{-2}, which can be explained by its enhanced absorption at longer wavelength. The overall efficiency of 2.1% is the highest reported for dyes containing the PM acceptor unit.

The presented D-A-D chromophores with conventional acceptor units displayed so far absorption at rather short wavelengths with maxima ranging from 466–538 nm in solution. This limits the harvesting of photons as only a fraction of the incoming light can be utilized and results in relatively low short-circuit current densities. The group of Nguyen made use of the stronger electron-acceptor diketopyrrolopyrrole (DPP), which is applied in large scale as high-performance pigment in paints and inks. Combining the DPP core with oligothiophenes results in symmetric chromophores with broad absorption bands centered at ~620 nm, affording a good overlap with the terrestrial solar spectrum. The first reported compound in 2008 was dye **27**, exhibiting *t*-Boc group at the *N*,*N*-positions of the DPP unit to provide sufficient solubility.[51] Although the determined hole mobility of this chromophore with 5.0×10^{-7} cm^2 V^{-1} s^{-1} in the blend with $PC_{61}BM$ was very low, the respective solar device

displayed a considerable PCE of 2.3% due to the high J_{SC} of 8.4 mA cm^{-2} and fill factor of 0.45. Interestingly, these results were obtained for very high donor concentrations of 70wt%.

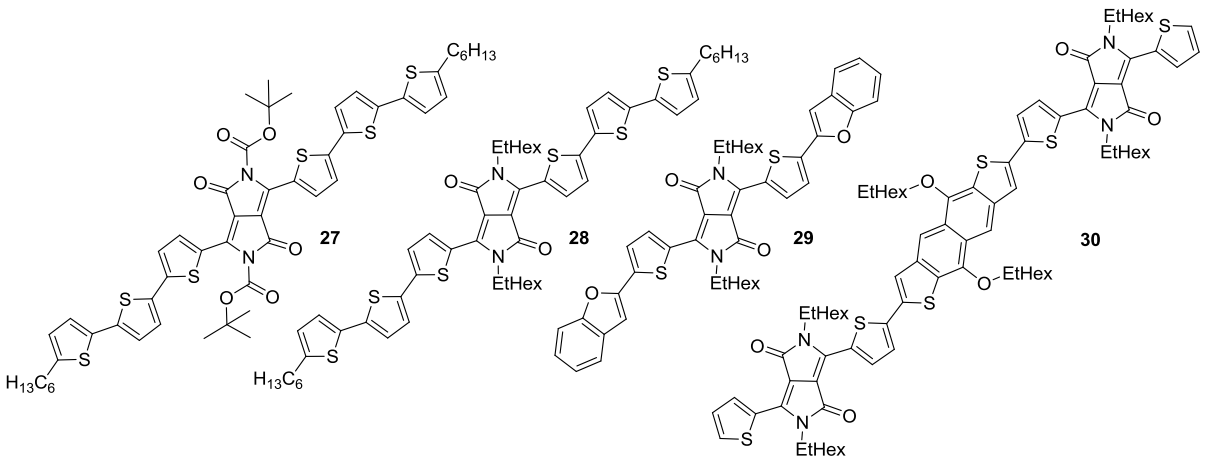

However, the *t*-Boc protecting group is cleaved at elevated temperatures, which hampers the application in outdoors devices and prohibits thermal post-treatment of the device, which could further improve the efficiency of the cells. For these reasons, *t*-Boc was substituted by the thermally stable 2-ethylhexyl group at the *N*,*N*-positions of the DPP core in dye **28**.[52] This compound exhibits not only an enhanced solubility and a significantly improved hole mobility, but also a beneficially lower HOMO level compared with **27**. Thus, the corresponding solar devices displayed an improved V_{OC} of 0.75 V. Furthermore, the application of $PC_{71}BM$ resulted in an improved photocurrent of 9.2 mA cm^{-2} and a remarkable PCE of 3.0%. This is all the more interesting, as these excellent results were obtained with a lower dye loading of 50wt% compared with the previous example of dye **27**.

Further improvements were achieved by replacing the oligothiophenes by benzofuranes in **29** and keeping $PC_{71}BM$ as electron accepting material.[53] Although, the HOMO level of **29** determined by UPS was the same as the one of dye **28**, a distinctly higher V_{OC} of 0.92 V was reached. Additionally, annealing of the solar cells at 110 °C led to a remarkable improvement of J_{SC} from 1.5 mA cm^{-2} to 10 mA cm^{-2}, which was assigned to an improved phase separation providing more percolation pathways for the charge carriers. Both aspects contribute to one of today's best performing solution-processed small molecule solar cells showing a PCE of 4.4%.

Just recently, Marks and Facchetti explored further the potential of DPP based chromophores for organic solar cells. They designed acceptor-donor-acceptor molecule **30** with DPP as the part with high electron affinity and naphtondithiophene as electron donor.[54] The naphtondithiophene unit was introduced to enhance the hole mobility and actually, a high value of 3.3×10^{-3} cm^2 V^{-1} s^{-1} for a blend with $PC_{61}BM$ was found. The absorption

properties with λ_{max} in solution at 624 nm are comparable to the other DPP based chromophores. However, annealing at 110 °C of the blends resulted in extremely high J_{SC} of 11.3 mA cm^{-2}, which could be originated by the good charge transport properties of the dye. As the V_{OC} (0.84 V) and fill factor (0.42) are lower than in the cells containing dye **29**, the overall performance with 4.1% is also slightly behind the record holder. Nevertheless, these results are striking as here the cheaper C_{61} fullerene showing only low absorption in the visible region was employed.

The squarylic acid is a very strong electron-accepting unit, allowing for absorption at long wavelength when combined with electron donors. The first squaraine dye **31**, having also a donor-acceptor-donor structure, investigated in organic solar cells was described by Marks, Pagani and Facchetti in 2008.[55] The solar devices were optimized with regard to the solvent for spin-coating, the dye:$PC_{61}BM$ weight ratio and post-treatments. The best results were obtained for chloroform with 75wt% $PC_{61}BM$ and no annealing of the active layer. Despite the high HOMO level a reasonable V_{OC} of 0.62 was achieved. In combination with the good J_{SC} of almost 6 mA cm^{-2} a PCE of 1.2% was reached for photovoltaic devices with thin active layers of 30 nm.

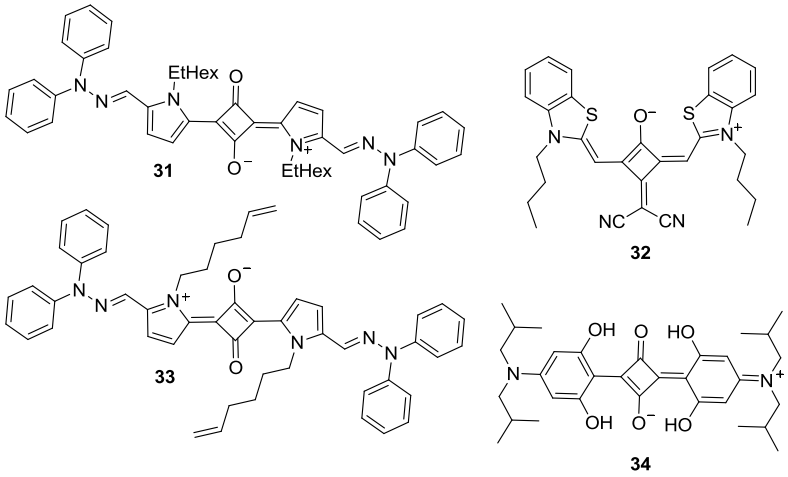

The groups of Würthner and Meerholz modified the squarylic acid by attaching an additional electron acceptor, dicyanovinyl.[56] Two benzothiazole units serve as electron donors to extend the absorption of chromophore **32** in the NIR. This planar compound shows a 2D brickwall packing in the crystalline state, which is considered to be beneficial for charge transport. Actually, OFETs containing **32** displayed quite high hole mobilites of 1.3×10^{-3} cm^2 V^{-1} s^{-1} after annealing. Combined with the electron accepting material $PC_{61}BM$, exceptional high J_{SC} of 12.6 mA cm^{-2} and also good fill factors of 0.47 were obtained. However, the PCE of these cells is limited by the low open-circuit voltage of 0.31 V due to the high HOMO level.

Nevertheless, an efficiency of 1.8% could be achieved after annealing of the devices at 110 °C.

Based on their earlier finding on squaraine dyes, Marks and Facchetti further developed their system.[57] The 2-ethylhexyl chains of **31** were replaced by *n*-hexenyl chains in **33**, which resulted in a more compact packing of the molecules in the crystalline state. This modification did not change the HOMO level and influenced only marginally the absorption maximum, which is located in the case of **33** at 729 nm. Here, the squaraine was joined with $PC_{71}BM$ and the devices were annealed afterwards. As expected, a similar V_{OC} of ~0.6 V like in the case of **31** was determined. The short-circuit current density could be improved to 8.2 mA cm^{-2} for the non-annealed cell and 9.3 mA cm^{-2} after the temperature treatment. In total, a respectable performance of 2.0% could be achieved with the modified chromophore **33**.

Forrest and his coworkers investigated chromophore **34** with an absorption band centered at 680 nm thoroughly in both solution-processed and vapor-deposited organic solar cells.[58] Although the exciton diffusion length of **34** was determined to be very small (1.6 nm), it's very high absorption strength can partially compensate this deficit. For this reason, even blends with only 14% of the chromophore can absorb a substantial amount of light. In combination with $PC_{61}BM$ and MoO_3 as hole transporting layer, high J_{SC} of 9.23 mA cm^{-2} and PCE of 3.0% were achieved. The absorption could be strengthened by using the $PC_{71}BM$ fullerene, but here, the cells suffered from low fill factors due to high series resistances. Therefore, the authors applied just recently solvent vapor annealing to **34**:$PC_{71}BM$ blends, to improve the morphology and create pathways for the charge carriers with low resistivity. Exposing the cell to dichloromethane vapor for 10 min did indeed improve the fill factor to 0.5 by causing the growth of squaraine crystals with a size of ~2.0 nm. This process came along with an increase in absorption intensity and EQE. Further exposure to the solvent vapor led to bigger crystals and reduced cell performance. By this post-treatment, the efficiency of the cell could be improved from 2.4% (as-cast) to the outstanding value of 5.2% for the optimized exposure time of 10 min.

The group of Chu combined the electron-deficient dibenzothienoquinoxaline entity with two peripheral triphenylamine units to create the linear chromophore **35** and one dye with a more bend shape.[59] Solar cells built with **35** and $PC_{61}BM$ showed appreciable high V_{OC} of 0.89 V, moderate J_{SC} (4.2 mA cm^{-2}) and fill factor (0.46), which led to a PCE of 1.7%. The non-

linear dye produced significantly lower J_{SC} in solar cells, which were rationalized by an imbalanced charger carrier transport in the active layer and absorption at shorter wavelengths.

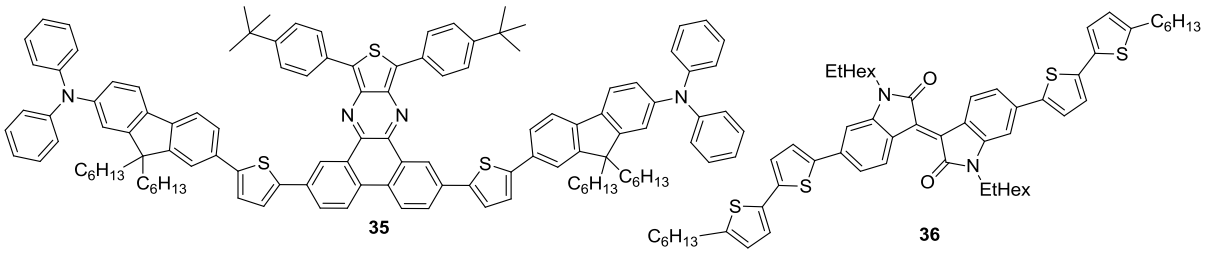

Inspired by the DPP chromophores, Reynolds and his coworkers designed the D-A-D dye **36** employing an isoindigo unit as acceptor for application in organic solar cells.[60] The compound absorbs strongly from 300–600 nm with a maximum at 579 nm and appears almost black in solution. Furthermore, it displays a beneficially low-lying HOMO level of –5.5 eV. In the photovoltaic cells, the donor-acceptor-donor structure achieved a considerable J_{SC} of 6.3 mA cm^{-2} and a PCE of 1.8% after annealing at 100 °C.

The presented D-A-D chromophores display very different physical properties and behavior in solar cells. Nevertheless, one can state, that high J_{SC} are only possible with chromophores exhibiting absorption maxima beyond 600 nm and often in combination with $PC_{71}BM$. Furthermore, high V_{OC} values of >0.8 V are quite usual and can even be reached with dyes having a high HOMO of –5.1 eV (**34**). Most of the photovoltaic devices containing D-A-D structures suffer from low fill factors, which do not exceed 0.5. To obtain highly efficient devices, sophisticated procedures like adding solvent additives (**20**) or post-treatments like annealing (**29**) or solvent-vapor annealing (**34**) proved to be successful.

1.2.3.5 Donors based on donor-acceptor (D-A) subunits

The following section deals with unsymmetrical donor-acceptor chromophores. In 2008, Kronenberg *et al.* described the successful application of two series of donor-acceptor dyes, thus merocyanines in solution-processed BHJ organic solar cells.[4] The most efficient solar cells were built with chromophore **MD304**, showing absorption at the longest wavelength of 625 nm of the series. This enables a good overlap of the absorption spectrum with the solar irradiance and originates a high J_{SC} of 6.3 mA cm^{-2}. In combination with 70wt% $PC_{61}BM$ a PCE of 1.7% was reached, which was at this time a record result.

In 2010, the groups of Tao and Wong took an oligothiophene conjugated π-bridge and attached an electron-donating triphenylamine unit at one end and the electron-deficient dicyanovinyl at the other.[61] The authors compared the performance of unsymmetrical dipolar chromophore **37** with a dye containing a sexithiophene. Both compounds display very similar

optical and electrochemical properties. The potential of both candidates was explored in BHJ solar cell and dye **37** was found to give a superior performance with a moderate PCE of 1.7% at optimized film thicknesses of 150 nm and a $PC_{61}BM$ weight ratio of 80%.

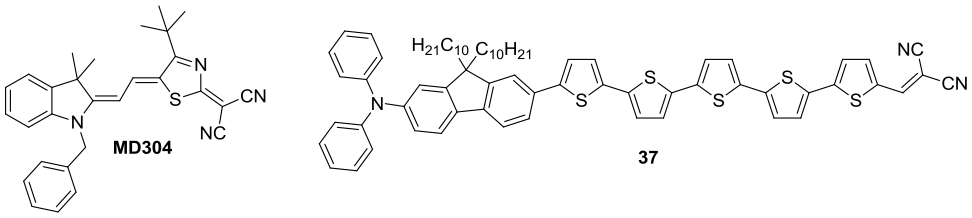

Table 5. Absorption maxima in solution, HOMO energies, hole mobilites and solar cell characteristics of the compounds **MD304** and **34** in combination with $PC_{61}BM$.

	λ_{max} (nm)	HOMO (eV)	wt% PCBM	V_{OC} (V)	J_{SC} (mA cm^{-2})	FF	η (%)	Ref
MD304	625[a]	–5.59[c]	70	0.76	6.3	0.36	1.7	4
37	526[b]	–5.10[d]	80	0.79	5.4	0.40	1.7	61

[a] CH_2Cl_2 solution. [b] Chloroform solution. [c] $E_{HOMO} = -e(E_{ox}^{1/2} + 5.15)$, Redox potential measured versus Fc/Fc^+. [d] $E_{HOMO} = -e(E_{ox} + 4.8)$, Redox potential measured versus Fc/Fc^+.

1.2.3.6 Tetrabenzoporphyrine as donor material[62]

Phthalocyanine and phorphyrine chromophores show absorption at long wavelengths, which makes them interesting for solar cell applications. However, their solubility is usually quite low. Hence, this class of dyes was mostly applied in vacuum-processed BHJ organic solar cells with high PCE of ~5%.[63]

In 2009, Nakamura and Sato presented an innovative and efficient procedure to create organic solar cells with a controlled and structured morphology. They designed the soluble porphyrin compound **CP**, which can be thermally converted to form the insoluble, crystalline tetrabenzoporphyrine **BP** (Figure 8a) exhibiting an absorption maximum at 680 nm and a HOMO level of –5.1 eV. Furthermore, they introduced a new fullerene derivative **SIMEF** (Figure 8b), showing a LUMO level 0.1 eV higher than $PC_{61}BM$. Additionally, the spin-coated amorphous phase of SIMEF converts to a crystalline material at 149 °C.

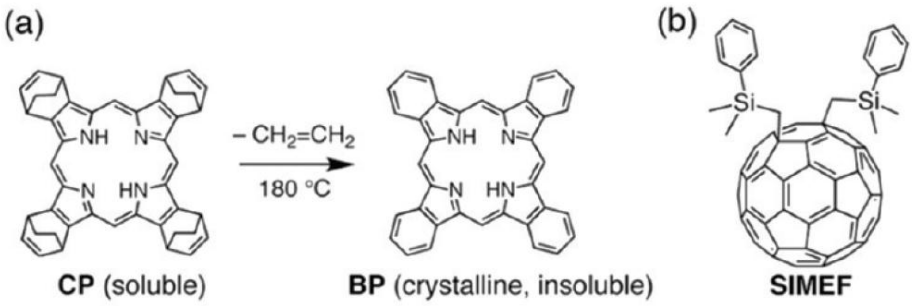

Figure 8. a) Thermal retro-Diels-Alder reaction of donor precursor **CP** to donor **BP**. b) Fullerene derivative **SIMEF**. Reprinted with permission from ref. 62. Copyright 2009 American Chemical Society.

The fabrication of the cells starts with spin-coating of the soluble donor precursor **CP**. Thermal treatment at 180 °C creates a 20 nm crystalline layer of **BP**. Next, a mixture of **CP** (30wt%) and **SIMEF** (70wt%) is spin-coated. Upon thermal annealing at 180 °C crystalline columns are formed by **BP** and enable an almost ideal interdigitated system of electron donor **BP** and the fullerene derivative, which is also crystalline at this temperature (Figure 9). On top of the blend a 20 nm layer of **SIMEF** is applied. The round **BP** columns have a diameter of 20–30 nm, which is in good aggreement with the exciton diffusion lengths of 10–20 nm.[16] Photovoltaic devices with this architecture exhibit exceptionally high fill factors of 0.65 and good V_{OC} of 0.75 V. The highly ordered structure could also be the origin for the very high J_{SC} of 10.5 mA cm^{-2}. With this sophisticated cell design an excellent power conversion efficiency of 5.2% was achieved.

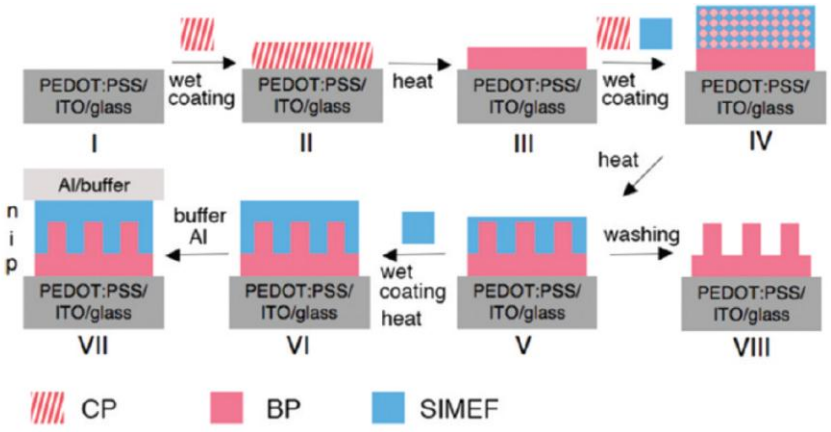

Figure 9. Solution processing of a BHJ organic solar cell with columnar structure. Reprinted with permission from ref. 62. Copyright 2009 American Chemical Society.

1.2.3.7 Miscellaneous donor dye materials

In recent years, several groups introduced new chromophore systems in organic solar cells, which cannot be classified into one of the previously described dye classes. Table 6 and Table 7 summarize the optical and electrochemical properties of the dyes reported in this section and the solar cell characteristics of the respective devices.

Borondipyrromethene (BODIPY) dyes exhibit high absorption strength, good chemical stability and their absorption range can be tuned by means of the substituents, qualifying them as electron donors in organic solar cells. Roncali, Ziessel and coworkers first investigated in 2009 the dyes **40** and **41** in combination with $PC_{61}BM$.[64] The low-lying HOMO levels allow for good V_{OC} of 0.75 V and 0.80 V, respectively. Although dye **40** shows a more extensively conjugated π-system and absorption at longer wavelengths than **41**, the photovoltaic devices built with both displayed similar J_{SC} of 4.1–4.4 mA cm^{-2} and PCE of 1.2–1.3%. One limitation of BODIPY dyes are the narrow absorption bands, preventing high short-circuit current densities. To circumvent this problem, the authors mixed both dyes **40** and **41** with complementary absorption spectra together in a blend with $PC_{61}BM$.[65] Interestingly, this cell did not only display a higher J_{SC} value of 4.7 mA cm^{-2} than the cell with one chromophore, but also a higher V_{OC} of 0.87 V, resulting in an improved PCE of 1.7%.

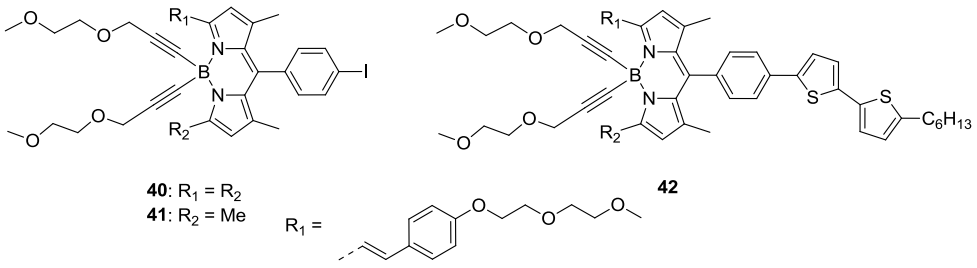

In 2010, the authors described a further development of their BODIPY system: they attached a bithiophene unit to the peripheries of the chromophore to enhance the charge carrier properties.[66] Due to the non-planarity of the system, this modulation in compound **42** did only marginally influence the optical and electrochemical properties compared to dye **40** without the bithiophene unit. As expected, this results in the same V_{OC} of 0.75 V, like measured for a device with **40**. Compared to a device built with compound **40**, J_{SC} is significantly enhanced to 7.0 mA cm^{-2} and a PCE of 2.2% was determined. This improvement could be originated by the higher hole mobility of **421**, which was determined in hole only devices. Here, the mobility found for chromophore **42** was twice as high as the one for devices containing compound **40**.

Table 6. Absorption maxima in solution, HOMO energies, hole mobilites and solar cell characteristics of the electron donors **40**–**47** in combination with $PC_{61}BM$ or $PC_{71}BM$.

	λ_{max} (nm)[a]	HOMO (eV)[d]	μ ($cm^2\ V^{-1}\ s^{-1}$)	wt% PCBM	V_{OC} (V)	J_{SC} (mA cm^{-2})	FF	η (%)	Ref
40	646[b]	–5.56[e]	/	67	0.75	4.1	0.44	1.3	64
41	572[b]	–5.69[e]	/	67	0.80	4.4	0.34	1.2	64
42	649[b]	–5.61[e]	1.0×10^{-4}	67	0.75	7.0	0.38	2.2	66[i]
43	500[c]	–5.55[f]	2.1×10^{-4}	67[h]	0.72	8.9	0.35	2.2	67
44	540[c]	–5.28[g]	1.5×10^{-4}	75[h]	0.82	8.5	0.43	3.0	68[j]
45	648	–5.2	1.9×10^{-4}	50	0.89	7.4	0.58	3.8	69[k]
46	590	–5.2	1.5×10^{-5}	50	0.93	7.1	0.54	3.6	70[k,l]
47	420	–5.10	6.6×10^{-5}	50	0.74	8.2	0.52	3.2	71[m]

[a] THF solution. [b] CH_2Cl_2 solution. [c] Chloroform solution [d] $E_{HOMO} = -e(E_{ox}^{onset} + 4.71)$, Redox potential measured versus Ag/Ag^+. [e] $E_{HOMO} = -e(E_{ox} + 4.95)$, Redox potential measured versus SCE. [f] $E_{HOMO} = -e(E_{ox} + 5.1)$; Redox potential measured versus Fc/Fc^+. [g] $E_{HOMO} = -e(E_{ox}^{onset} + 5.1)$; Redox potential measured versus Fc/Fc^+. [h] $PC_{71}BM$. [i] 90 mW cm^{-2}. [j] Annealed at 70 °C for 30 min. [k] Annealed at 100 °C for 2 min. [l] Solvent vapor annealing with THF. [m] Annealed at 120 °C for 10 min.

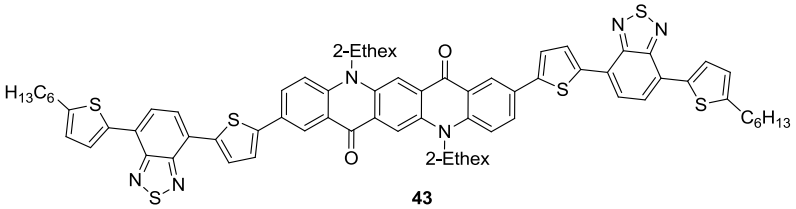

43

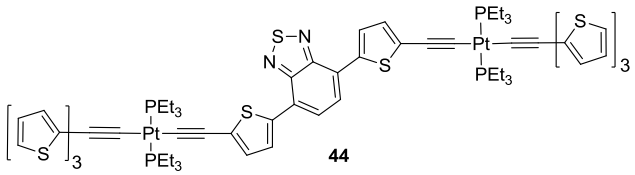

44

The groups of Fréchet and Ma employed the quinacridone chromophore **43** in blends with $PC_{71}BM$ in photovoltaic cells.[67] As quinacridone pigments are known for their exceptional chemical stability, they are interesting candidates for organic electronics. First results with the quinacridone-based materials showed reasonable hole mobilities, which was enhanced significantly when blended with $PC_{71}BM$ to amount to 2.1×10^{-4} $cm^2\ V^{-1}\ s^{-1}$. The solar cells displayed high J_{SC} of 8.9 mA cm^{-2}, which can be attributed to the broad and intense absorption between 350–650 nm with EQE values up to 45%. In combination with the good V_{OC} of 0.72 V an appreciable PCE of 2.2% was reached.

Fréchet and his coworkers also reported the application of a platinum-acetylide chromophore combined with oligothiophene units in organic solar cells with $PC_{71}BM$ as electron acceptor.[68] The first should allow for absorption at long wavelengths due to internal charge transfer, whereas the oligothiophenes should enable high hole mobilities. Besides compound

44, derivatives with two and four thiophene units were analyzed. Obviously, increasing the number of thiophene units does not influence the HOMO and LUMO levels, which are significant for the performance of the corresponding solar cell, but only the HOMO to LUMO+1 transition. This results in a broadening of the absorption band without changing the band gap of the material. In combination with $PC_{61}BM$, dye **44** showed a high V_{OC} (0.78 V), moderate J_{SC} (5.4 mA cm^{-2}) and fill factor (0.39) and a PCE of 1.7% after annealing the cell at 70 °C for 30 min. Blending the chromophore with $PC_{71}BM$ led to an increase in all cell characteristics, especially J_{SC}, and a PCE of 3.0%. The compound with four thiophene units displays a broader absorption band than **44**, but lower solubility, thus showing reduced performance in solar devices.

In 2010, the groups of Sharma and Mikroyannidis reported the application of several new efficient small molecules in organic solar cells. Here, they incorporated units like phenylene vinylene, alkoxy substituted phenyls or benzoselenadiazole commonly employed in small band gap polymers. One interesting example represents the star-shaped triazine compound **45** with three cyano-vinylene 4-nitrophenyl segments, generated by a simple two-step synthesis.[69] In the photovoltaic devices a high dye loading of 50wt% was found to give the best results. As-cast films of **45** and $PC_{61}BM$ already displayed a considerable photovoltaic response with an efficiency of 2.6%. By annealing the cells at 100 °C for 2 min, J_{SC} was improved from 5.1 to 7.4 mA cm^{-2} and pretty high fill factor (0.58) as well as PCE (3.8%) values were achieved. The improved J_{SC} was reflected by the increase in EQE_{max} from 55% to 65% and an increase of the hole mobility by one order of magnitude. The authors rationalized this effect by a ordering of the material and consequently higher crystallinity of the films, monitored by absorption spectroscopy and XRD experiments.

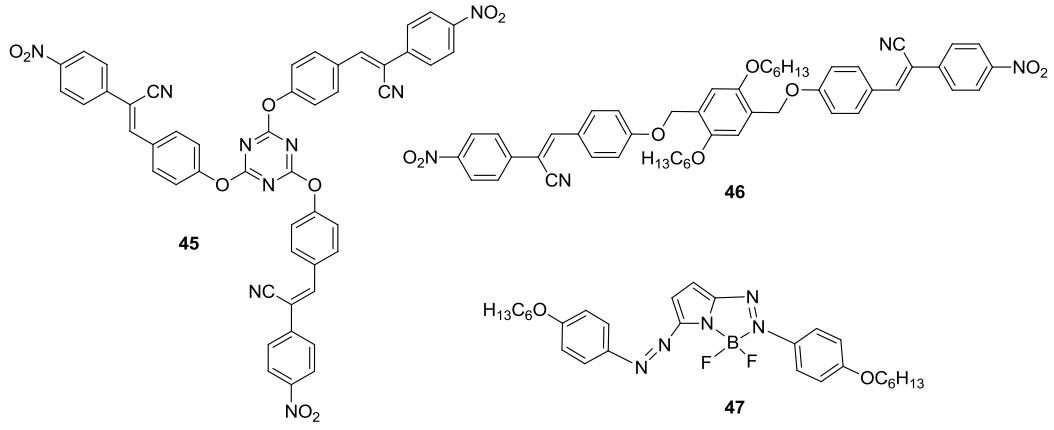

In chromophore **46**, the authors kept the cyano-vinylene 4-nitrophenyl units and combined these with a central alkoxy substituted phenyl moiety.[70] Compound **46** displays a broad

absorption band centered at 590 nm in THF solution, which is red-shifted to 622 nm in the thin film. The as-cast devices built with dye **46** showed high V_{OC} of 0.93 V despite the relatively high-lying HOMO level and good fill factor of 0.48. However, the J_{SC} of 3.8 mA cm^{-2} resulted in a moderate PCE of 1.7%. Solvent vapor annealing with THF of the blends before evaporating the electrode resulted in a strong increase in J_{SC} to 6.4 mA cm^{-2}. Annealing at 100 °C for 2 min did further increase the current density and a PCE of 3.6% was achieved. Like in the example of dye **45**, the improvement due to the post-treatments was explained by an enhanced self-organization and crystallinity of the chromophores. Investigation of the charge carrier properties revealed, that the electron mobility is barely influenced by the post-treatments, but the hole mobility increases by on order of magnitude to give almost balanced charge transport properties in the donor and acceptor domains.

Additionally, Sharma and Mikroyannidis explored the potential of a bisazopyrrole dye and the corresponding fluorine-boron complex **47** in BHJ solar cells.[71] In solution, the dyes showed absorption at rather short wavelength with a maximum for **47** at 420 nm. However, the absorption band displayed a distinct red-shift and broadening in the solid state enabling absorption up to ~800 nm, which is mirrored in the respective EQE spectrum. The corresponding dye without BF_2 exhibit a narrower absorption band with significantly less intensity at longer wavelengths. The first solar cells gave promising results for both chromophores: PCEs of 1.8% for the dye without BF_2 and 2.2% for **47** were measured. Then, the authors examined the effects of annealing before and after deposition of the aluminum electrode. They found higher V_{OC} and FF for the latter case due to decreased dark currents. The increase in J_{SC} was similar for both techniques and was ascribed to a more balanced charge transport. Under optimized conditions an appreciable efficiency of 3.2% was achieved for the bisazopyrrole derivative **47**. The better performance compared to the chromophore without BF_2 (2.7%) is mainly a result of the broader absorption band of **47** and consequently higher J_{SC} values.

Besides the ubiquitous fullerene derivatives, the groups of Sharma and Mikroyannidis are one of the very few, who employ also perylene bisimide compounds such as **49** and **51** as electron accepting materials. These perylenes display higher LUMO levels than $PC_{61}BM$ conferring high V_{OC} and are able to contribute considerable to the light harvesting of the cells. Blending the phenylene vinylene derivative **48** with 78wt% perylene-pyrene bisimide **49** with complementary absorption spectra gave a photovoltaic device with very high V_{OC} of ~1 V, good fill factor of 0.46, moderate J_{SC} of 4.2 mA cm^{-2} and a PCE of 1.9%.[72] For comparison,

the respective cell with $PC_{61}BM$ gave a lower J_{SC} of 3.1 mA cm^{-2} and 1.4% efficiency due to the low absorption of the C_{60}-fullerene in the visible range. The cell with the perylene acceptor was improved by introducing first a thin ZnO layer between the blend and the aluminum electrode and annealing the device at 100 °C for 10 min. Both procedures increased the photocurrent density. The ZnO acts as hole blocking layer, thus enhancing the amount of charges collected at the aluminum electrode, but represents also an optical spacer redistributing non-absorbed photons into the active layer. The heat treatment enhances the crystallinity of the film and consequently its charge transport properties. The optimized cell showed still the high V_{OC} value, but improved J_{SC} of 6.3 mA cm^{-2} and fill factor of 0.53, entailing an overall PCE of 3.2%. As there are only very few reports of perylene dyes as electron acceptors in organic solar cells, these excellent results comparable with the best cell containing PCBM are all the more captivating.

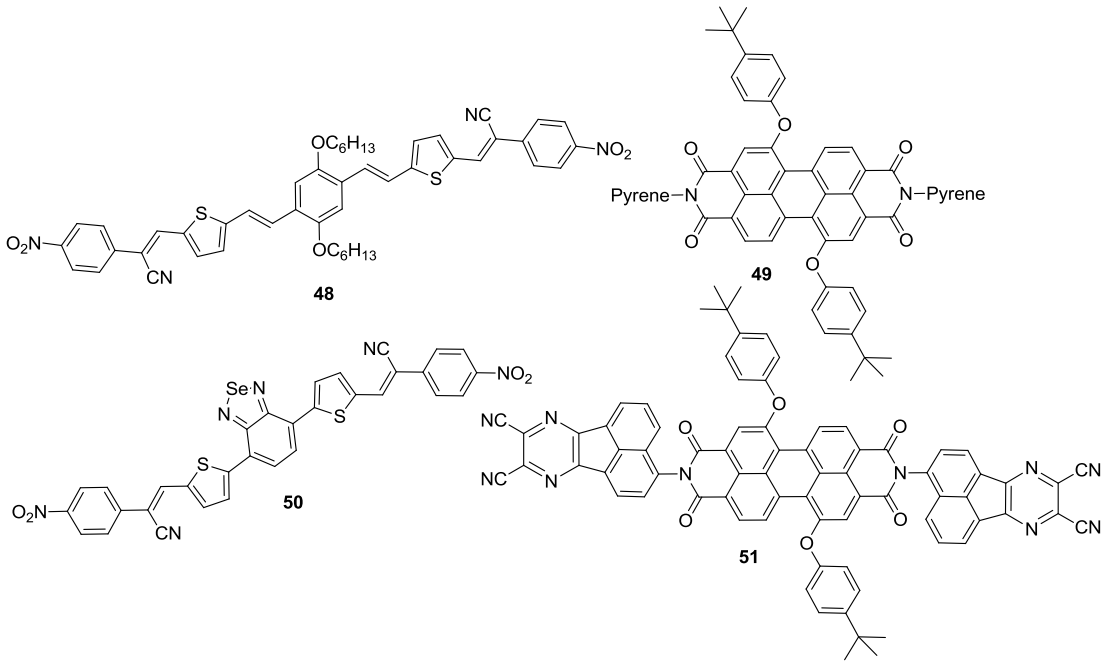

Table 7. Absorption maxima in solution, FMO energies and hole mobilites of the compounds **48**–**51** and solar cell characteristics of cells containing **48**:**49** and **50**:**51** blends.

	λ_{max} (nm) [a]	FMO (eV) [c]	μ (cm^2 V^{-1} s^{-1})	V_{OC} (V)	J_{SC} (mA cm^{-2})	FF	η (%)	Ref
Donor **48**	640	–5.0 [d]	10^{-4}	0.95	6.3	0.53	3.2	72 [f]
Acceptor **49**	450	–3.8 [e]	10^{-3}					
Donor **50**	650 [b]	–5.25 [d]	1.3×10^{-4}	0.90	8.3	0.52	3.9	73 [f]
Acceptor **51**	455 [b]	–3.95 [e]	5.4×10^{-4}					

[a] Estimated from the thin film. [b] THF solution. [c] $E_{HOMO} = -e(E_{ox}^{onset} + 4.71)$, Redox potential measured versus Ag/Ag^+. [d] HOMO. [e] LUMO. [f] Annealed at 100 °C for 10 min.

As an extension to their research, two acetonaphtonpyrazine dicarbonitrile units were attached to the perylene, providing compound **51** with an extended flat surface for improved self-ordering.[73] As electron donor, the benzoselenadiazole derivative **50** with an absorption band centered at 650 nm both in solution and in the thin film was used. In the blend, the combination of both compounds enables intense absorption starting from 350 to 750 nm. The as-cast devices exhibit relatively low J_{SC} values of 2.9 mA cm^{-2} resulting in PCE of 1.3%. Annealing at 100 °C for 10 min did increase the photocurrent to a high level of 8.3 mA cm^{-2} that relates to a 10 times higher hole mobility originated by the enhanced crystallinity of compound **50**. Combined with the V_{OC} of 0.90 V and high fill factor of 0.52 a remarkable performance of 3.9% was accomplished.

The last section illustrates the fast developments in the field of small molecule based solution-processed BHJ solar cell. In the beginning, traditional structures like triphenylamines or oligothiophenes known for their beneficial charge transport properties dominated the research. However, today, highly efficient solar cell can be obtained with chromophore belonging to very different dye classes, be it based on pigments or the monomeric units of small band gap polymers. After the design of an innovative chromophore system, which meets the basic demands concerning the FMO levels and the absorption properties, optimal cell design, processing conditions, post-treatments and latterly the combination with the right electron acceptor are crucial to explore its potential.

Chapter 2

Tailored merocyanine dyes for solution-processed BHJ solar cells*

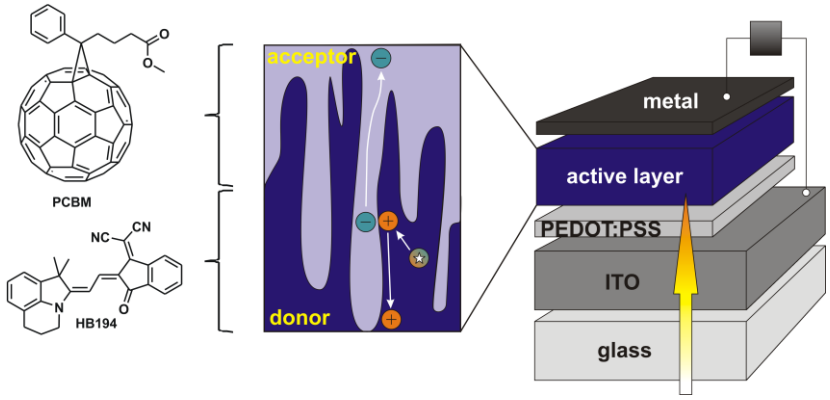

Abstract: A series of merocyanine dye having an indolenine donor in common, but bearing five different acceptor units has been synthesized and characterized by means of UV-vis, EOAM spectroscopy and cyclic voltammetry. Due to varying acceptor strengths, the colors of the dyes in solution range from orange (λ_{max}~500 nm) via magenta (λ_{max}~580 nm) to blue (λ_{max}~630 nm). Single crystal analysis revealed for six chromophores a slipped antiparallel stacking motif, resulting in the annihilation of the dipole moment already in the dimer unit. A modification of the "Fischer base" donor with a bridging propylene spacer yielded good hole conduction properties and a photovoltaic device with a PCE of 2.6% (55wt% $PC_{61}BM$).

* A part of this chapter was communicated in: Bürckstümmer, H.; Kronenberg, M. N.; Gsänger, M.; Stolte, M.; Meerholz, K.; Würthner, F. *J. Mater. Chem* **2010**, *20*, 240. Reproduced in parts by permission of The Royal Society of Chemistry. Copyright (2010)
Solar cell devices were built by N. M. Kronenberg (University of Köln). Single crystal analyses were performed by M. Gsänger (**HB194**, **HB330**, **HB331**, **MD319**, **MD353** and **MD376**) and A. Ojala (**HB364**, BASF SE, Ludwigshafen), electro-optical absorption measurements by Dr. M. Stolte and cyclic voltammetry and DSC by A.-M. Krause; synthetic support was given by M. Kaiser (**MD**) and P. Seufert-Baumbach (University of Würzburg).

2.1 Introduction

Conversion of solar energy into electricity provides a sustainable approach to satisfy the rapidly increasing energy demand worldwide. Photovoltaic devices based on organic semiconductors bear the potential for large-scale and cost-effective power generation. Due to their ease of processing, mechanical flexibility and substantially low material consumption, organic solar cells have evolved as a promising alternative to silicon solar cells.[74] Starting with a power conversion efficiency (PCE) of 1% for a planar heterojunction solar cell in 1986,[17] the introduction of the bulk heterojunction (BHJ) concept in the nineties led to a boost in efficiency.[18] The key component in BHJ solar cells is the photoactive layer composed of an interpenetrating network of an electron donor and an electron acceptor. Upon irradiation of such photoactive layers with sunlight, strongly bound electron-hole pairs (excitons) are generated, which diffuse across the blend. The highly enlarged donor-acceptor interface of the bulk heterojunction is very advantageous since efficient charge separation takes place at the interface.[75] Typically used donor materials for BHJ solar cells are conjugated polymers like poly(3-hexylthiophene) (P3HT),[21] while soluble fullerene derivatives such as [6,6]-phenyl-C_{61}-butyric-acid methyl ester (PCBM) are widely applied as electron acceptor materials. With these materials, PCEs up to 6%, external quantum efficiencies (EQE) exceeding 80% and internal quantum efficiencies (IQE) close to 100% have been achieved.[21,76] Besides the spherical fullerene derivatives, new materials like carbon nanotubes are emerging as candidates for photovoltaic devices.[77]

Most of the photovoltaic p-type semiconducting polymers exhibit good charge carrier mobilities[78] and favorable solution processability. However, they are afflicted with low absorption coefficients and difficult purification procedures. Moreover, their optical and electronic properties and, consequently, the photovoltaic performance depend strongly on specific characteristics such as molecular weight, regioregularity or chain length distribution, which are not easily adjustable. By contrast, small organic molecules are structurally well-defined, monodisperse and easy to purify. Thus, in recent years solution-processed small molecules have emerged for BHJ solar cells, and considerable photovoltaic efficiencies have been achieved by the groups of Nguyen with diketopyrrolopyrrole chromophores (4.4%),[53] Chen and Yin with acceptor substituted oligothiophenes (3.7%),[25b] Lin and Zhan with triphenylamines (4.3%)[33g] and Forrest with squaraine dyes (5.2%).[58c]

Merocyanine (MC) dyes possess high absorption coefficients, dipole moments and polarizabilities, and they were employed in nonlinear optics and as photorefractive

materials.[7,79] Furthermore, such dyes with easily tunable absorption properties have attracted much attention as substitutes for ruthenium dyes applied in dye-sensitized solar cells.[9,80]

In 2008, blends of MC dyes and fullerene derivative $PC_{61}BM$ were successfully applied in solution-processed BHJ solar cells with PCEs of up to 1.7%.[4] The chromophore **MD376** (Chart 2) was identified, possessing an indolenine donor ("Fischer base") with a flexible alkyl chain and a 2-(3-oxo-indan-1-ylidene)-malononitrile acceptor, as a highly promising electron-donor component for PCBM-based BHJ solar cells.[4]

Here a substantially improved solar cell performance of 2.6% for a newly designed MC dye containing a rigid donor unit and optimized morphology is reported. After analysis of the photovoltaic characteristics of devices based on **MD376**:$PC_{61}BM$ blends and the structural features of dye **MD376**, this push-pull dye has been modified by bridging the indolenine donor with an ethylene group in **HB193** and a propylene group in **HB194** to diminish the flexibility of the donor unit and to ensure a more planar geometry. The rigidification of the chromophore should decrease the vibronic degrees of freedom and control the packing of the dyes in the active layer and, consequently, modify the morphology of the BHJ solar cell. Additionally, four new acceptor moieties with varying electron-accpeting strengths were introduced and combined with the three Fischer base donors (Chart 2). The electronic character of the acceptor part has a strong influence on both the absorption properties and the FMO energies, which was employed to tailor the dye according to the requirements for organic solar cells. Thus, chromophores with absorption maxima ranging over the whole visible spectrum were generated, whereas all compounds showed beneficically low HOMO levels. Following the synthesis, analysis of all chromophores in BHJ solar cells in combination with $PC_{61}BM$ was carried out.

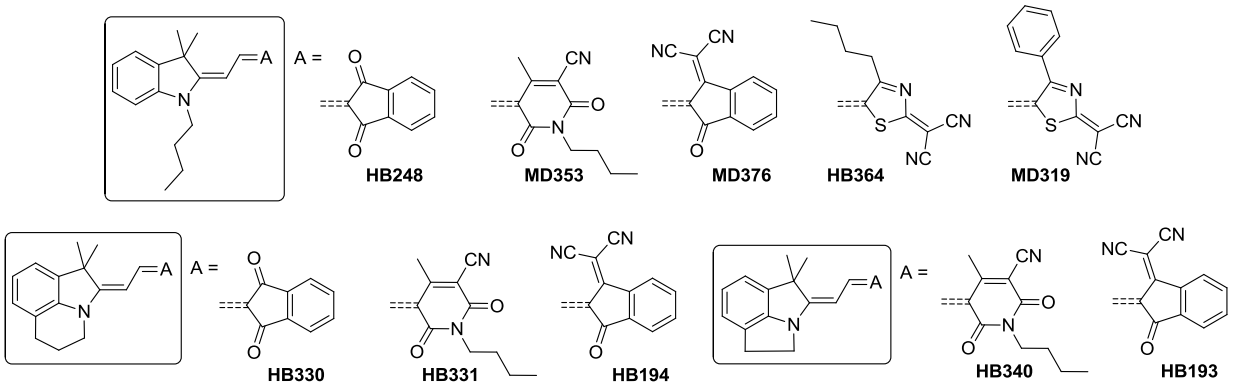

Chart 2. Chemical structures of the investigated merocyanine dyes.

2.2 Results and discussion

2.2.1 Synthesis

Most of the MC dyes presented in Chart 2 were generated according to procedure **A**: in a Knoevenagel reaction, a CH-active acceptor compound **Acc** was reacted with the corresponding indolenine aldehyde to result in the respective chromophore with yields of 42-83% (Scheme 1).[4] The dyes **MD376**, **HB193** and **HB194** were synthesized according to a second route **B** outlined in Scheme 1. In a multistep reaction, including a Fischer indol synthesis, the commercially available precursors **52a**,**b** were converted to the tetrafluoroborate salts **53a**,**b**.[81] The following acid-base reaction resulted in compounds **54a**,**b** with good yields. These precursors were subsequently coupled in a three-component condensation reaction with triethyl orthoformate and the acceptor component **58**[82] to afford the magenta colored MC dyes **MD376**, **HB193** and **HB194** with a yield of 50%, 19% and 60%, respectively.

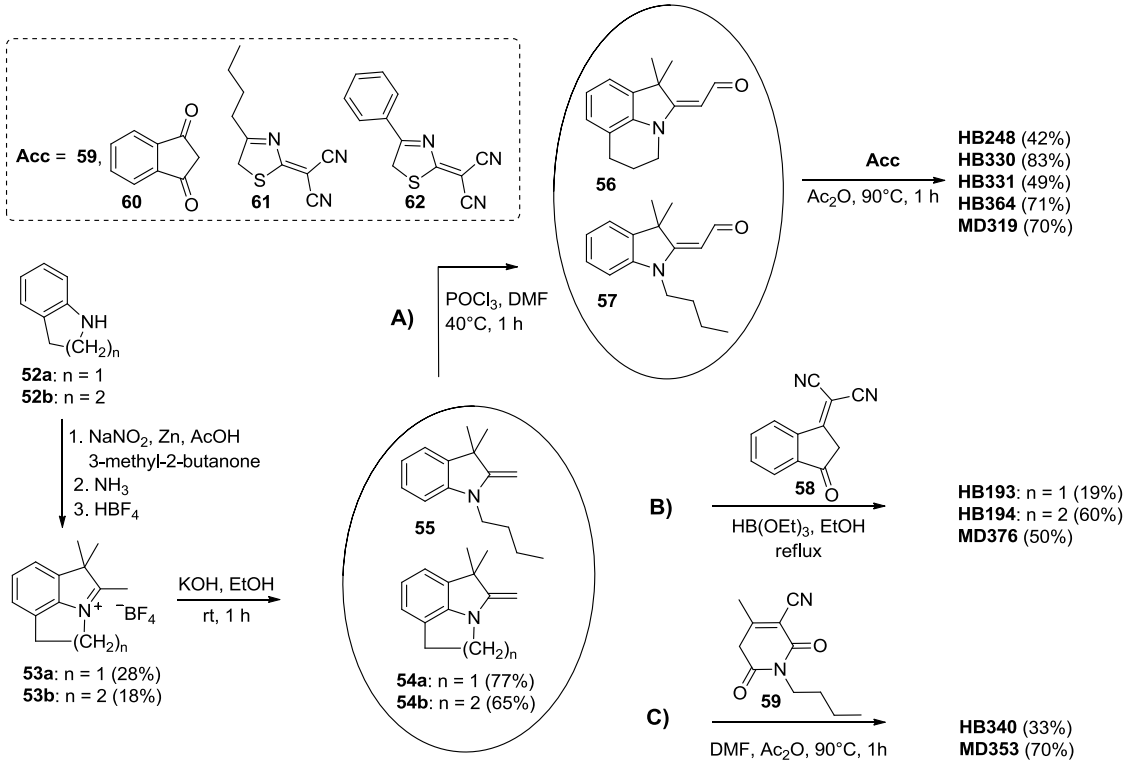

Scheme 1. Synthetic route to presented MC dyes with the respective yield in parantheses.

In a third synthetic strategy **C** the pyridone acceptor **59** was converted in a mixture of Ac_2O and DMF to the enamine before reaction with donor **55**. **MD353** was obtained wirh a yield of 70%.[83] The reaction of the methylene base **54a** bearing an ethylene bridging unit with

pyridine **59** gave compound **HB340** in significantly lower yield of 33%. The details of all new synthetic steps are described in section 2.5.

2.2.2 Absorption and redox properties

The absorption properties of the synthesized dyes were analyzed by means of UV-vis and EOAM spectroscopy,[91] the electrochemical features were investigated by cyclic voltammetry.[103] The absorption bands of the described dyes depend on the reciprocal interaction of the donor and acceptor parts. Chromophores with the weak acceptor indandione (**HB248** and **HB330**) show orange color in dichloromethane solution and absorption maxima around 500 nm, whereas the stronger thiazole unit (**HB364**, **MD319**) results in a deep blue color and absorption bands centered at ~620 nm (Table 8 and Figure 8). The propylene bridging unit has no significant influence on the absorption properties. Regarding the ethylene bridging unit, a bathochromic shift of λ_{max} of 9 nm (**HB340**) and 10 nm (**HB193**) compared to the *n*-butyl derivatives was found.

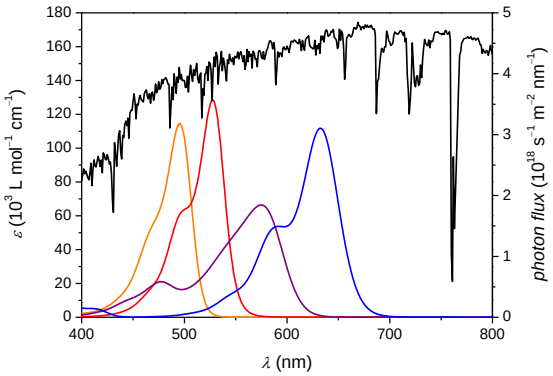

Figure 10. UV-vis spectra of **HB248** (orange line), **MD353** (red line), **MD376** (violet line), **MD319** (blue line) in CH_2Cl_2 ($c_0 \sim 10^{-5}$ mol L^{-1}) at 298 K and photon flux at 1.5 AM conditions (black line)

The exctionction coefficients of most presented chromophores show very high values well above 10^5 L mol^{-1} cm^{-1}. Solely the magenta colored series based on dicycanovinyl indandione acceptor **58** displays lower values of 51100-66400 L mol^{-1} cm^{-1}. As the extinction coefficient at λ_{max} is not sufficient to give a comprehensive description the absorption strength of a chromophore, we determined the transition dipole moment μ^2_{ag} by integration of the absorption bands. Furthermore, we defined the physical parameter $\mu^2_{ag} M^{-1}$ as the absorption density, which includes the molecular weight M of the molecule and is directly correlated to its tinctorial strength. The chromophores of this series show all high transition dipole moments of 93–125 D^2 and absorption strengths $\mu^2_{ag} M^{-1}$ of 0.23–0.29 D^2 mol g^{-1}, beneficial for light harvesting. Here, the correlation between transition dipole

moment μ^2_{ag} and absorption density $\mu^2_{ag}\ M^{-1}$ is almost linear, as the chromophores show similar molecular weights of ~400 g mol^{-1}. The advantage of $\mu^2_{ag}\ M^{-1}$ becomes obvious, when looking at **HB340** and **HB193**, bearing both the ethylene unit. Although ε at λ_{max} is decreased compared to the *n*-butyl derivatives, the absorption density stays the same due to lower molecular weight. According to EOAM spectroscopy, chromophore **HB340** shows a very small change of the dipole moment of 1.6 D upon excitation and a high ground state dipole moment of 11.8 D. The dye series with the indandione acceptor **58** displays lower ground state dipole moments of 6.2–6.7 D and higher, but still small dipole changes of 3.2–4.2 D upon excitation.

All described chromophores display beneficially low-lying HOMO levels located at –5.82 eV to –5.62 eV. As expected, the HOMO energies were influenced only weakly by the variation of the acceptor unit. Interestingly, the propylene bridging unit results in an increase in HOMO energy of 0.06–0.15 eV compared to the respective *n*-butyl compounds. Introduction of the ethylene unit originates a further increase of 0.04–0.05 eV compared to the propylene spacer. The LUMO energies ranging between –3.66 eV and –3.20 eV are influenced strongly by the variation of the acceptor unit. The influence of the bridging units on the LUMOs is less pronounced than on the HOMO energies.

Table 8. Electro-optical and electrochemical properties of the investigated MC dyes

MC dye	λ_{max} (nm)[a]	ε (L mol^{-1} cm^{-1}) [a]	μ^2_{ag} (D^2) [a]	$\mu^2_{ag}\ M^{-1}$ (D^2 mol g^{-1})	μ_g (D)[b]	$\Delta\mu$ (D)[b]	E_{HOMO} (eV)[c]	E_{LUMO} (eV)[d]
HB248	496	114600	94	0.25	/	/	–5.76*	–3.26
HB330	500	111200	95	0.27	/	/	–5.68*	–3.20
MD353	528	129900	106	0.25	/	/	–5.82	–3.47
HB331	529	133500	109	0.26	/	/	–5.76	–3.42
HB340	537	117400	106	0.26	11.8	1.6	–5.71	–3.40
MD376	576	66400	98	0.23	6.2	4.2	–5.80	–3.65
HB194	578	60300	98	0.24	6.7	4.0	–5.75	–3.60
HB193	586	51100	93	0.24	6.3	3.2	–5.71	–3.59
HB364	616	133000	125	0.29	/	/	–5.62	–3.61
MD319	632	112000	110	0.25	/	/	–5.62	–3.66

[a] UV-vis measurements for dilute solution (c_0 ~10^{-5} M) in CH_2Cl_2. [b] 1,4-dioxane (c_0 ~ 10^{-6} M). [c] Calculated from CV measurements ($E_{1/2}^{ox}$/*E_p) in CH_2Cl_2 calibrated against the ferrocene/ferrocenium couple (Fc/Fc^+, –5.15 eV) as internal standard. [d] $E_{LUMO} = E_{HOMO} + (hc/\lambda_{max})$.

2.2.3 Packing in the solid state

To shed light into the packing features of MC dyes, single crystal X-ray analysis was performed for seven dyes presented in this chapter.

The chromophores of **MD319** with a thiazol eacceptor arrange in discrete π-stacks where the chromophores are located in a slipped antiparallel packing motif in planes parallel to each other (Figure 11a,b). Unless stated otherwise all given spacings were determined between these parallel planes comprising the chromophores. The distances between the planes alternate and create one close and one more distant centrosymmetric dimeric unit. Accordingly, the dipolar character of the dye already vanishes upon dimerization wihin the closely packed supramolecular dimer unit.[101b] One of the centrosymmetric dimer units within the stack shows a short distance of 3.52 Å (close dimer), creating a pronounced contact between the π-areas of the molecules, whereas the more distant dimer exhibits a spacing of 3.82 Å (distant dimer). Within each stack, the dyes of **MD319** are shifted longitudinally to each other so that the sulfur atoms rest almost on top of each other with S-S distances of 3.74 Å in the close dimer and 4.21 Å in the distant dimer. The larger spacing of the distant dimer is originated by the steric demand of the two methyl groups at the indolenine donor and the bulky phenyl unit at the acceptor part. **HB364** is equipped with a different thiazole acceptor unit, but shows the same arrangement in the single crystal. Both chromophores are not completely planar. **MD319** shows an angle between donor and acceptor part of 13.6°, whereas the dye with less bulky substituents (**HB364**) displays a distinctly smaller angle of 5.5°. Both in **MD319** and in **HB364**, the C-C bond lengths of the methine bridge are differing only marginally, pointing to systems close to the *cyanine limit* (Figure 11c), which is in accordance to the sharp absorption bands with large exctinction coefficients in the absorption spectrum (Figure 10).[7]

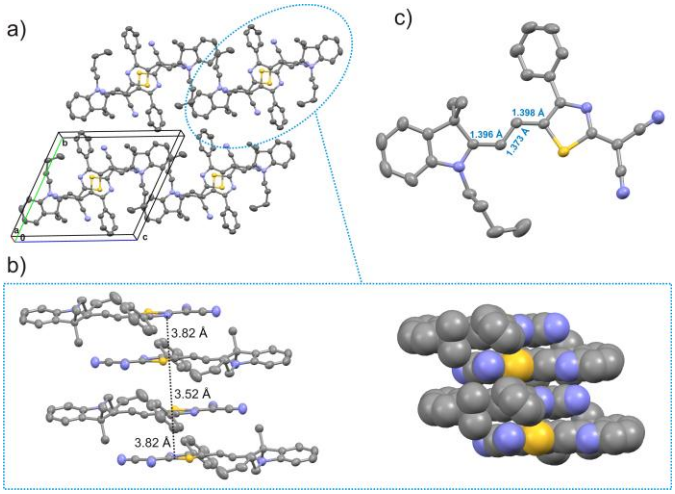

Figure 11. a) Top view on the *b*-*c*-plane of the unit cell of **MD319**. b) π-Stack of **MD319** in the *a*-*c*-plane of the unit cell with antiparallel packing motif and spacefill view of the stack (for clarity, in b) the butyl chains and all protons are omitted). c) Molecular structure of **MD319** in the solid state.

In the solid state, **MD376** also packs in π-stacks seperate from each other, in which the dyes are situated in parallel planes (Figure 12). Furthermore, within the stacks, antiparallel dimeric units with alterating distances were observed. The molecules of **MD376** show a small distortion angle of 5.4° between acceptor and donor unit and solely the donor part of the molecules exhibits a significant steric demand. This enables a close packing of the molecules with a small longitudinally shift within the closer dimeric unit and a small distance of 3.37 Å between the planes comprising the chromophores (Figure 12b). All butyl chains show to the outside of the close dimer, entailing a longitudinally shift of the distant dimer allowing contact only between the π-areas of the acceptor parts of neighboring molecules and creating a distance between the chromophores of 3.55 Å.

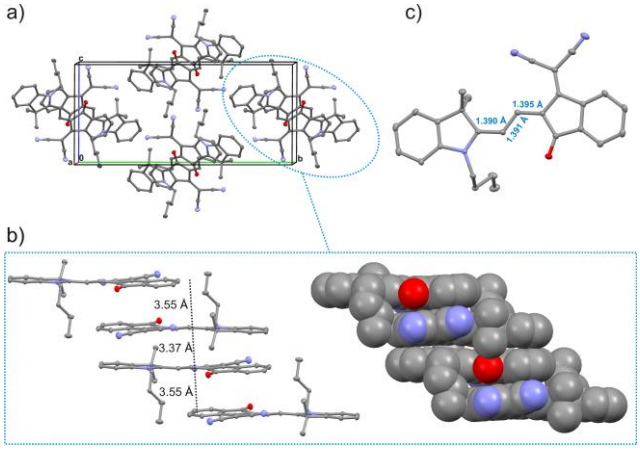

Figure 12. a) Top view on the *b*-*c*-plane of the unit cell of **MD376**. b) π-Stack of **MD376** in the *a*-*c* plane of the unit cell with antiparallel packing motif and spacefill view of the stack. c) Molecular crystal structure of **MD376** in the solid state (for clarity, all protons are omitted).

In the case of **HB194**,[84] two types of π-stacking arrangements are recognized along the *a*-axis of the unit cell (Figure 13b,c). In one case, the dyes are stacked as strongly displaced antiparallel dimers with close van-der-Waals contacts (3.64 Å) between the indolenine donor units (Figure 13b). In the other case, a nearly perpendicular (88.1°) arrangement between neighboring dyes is observed, where the contact is provided between the acceptor units (Figure 13c). Here, the spacings alternate between 3.43 Å and 3.48 Å. The chromophore of **HB194** is nearly planar, showing a distortion angle between donor and acceptor plane of 3.5°. Like in all the other cases, almost no C-C bond length alternation in the methine bridge is observed (Figure 13d), pointing to a π-conjugated system close to the *cyanine limit*. The electro-optical absorption measurements support this finding as a small dipole difference upon excitation of 4.0 D was found for **HB194**.

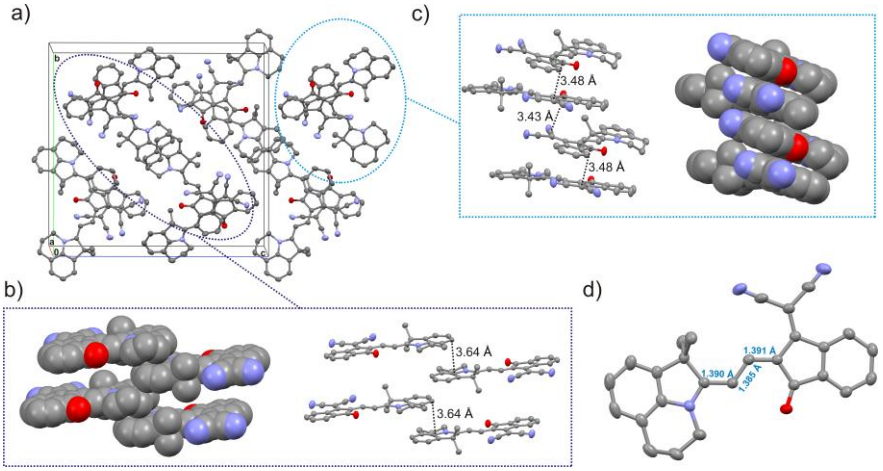

Figure 13. a) Top view on the *b*-*c*-plane of the unit cell of **HB194**. b) Antiparallel donor π-stack. c) Antiparallel acceptor π-stack. d) Molecular structure of **HB194** in the solid state (for clarity, all protons are omitted).

Although **HB331** exhibits a different acceptor unit than **MD376**, it displays nearly the same solid state packing. It differs only by a larger spacing of 3.46 Å (close dimer) and 3.96 Å (distant dimer), respectively, between adjacent molecules planes in one π-stack. Furthermore, the chromophore is more distorted with an angle of 18.7° between donor and acceptor unit.

The chromophores of **MD353** also arrange in stacks built up by close and more distant dimers. Here, the stacks interdigitate with each other, forming a two-dimensional brickwork-like structure depicted in Figure 14. The relatively strong distortion within the chromophore with an angle of 24.3° between donor and acceptor part could be the reason for the relatively long distances between close dimer (3.98 Å) and distant dimer (4.31 Å). The negligible bond length alternation of the methine bridge (1.401 Å, 1.385 Å, 1.410 Å) points to the cyanine-type character of **MD353** as well as the sharp and intense absorption band in the UV-vis spectrum (Figure 10).

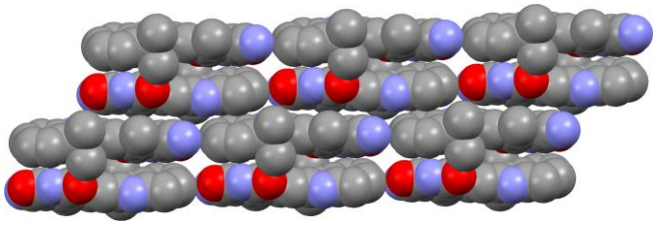

Figure 14. Spacefill view of the brickwork-like packing of **MD353** with slipped antiparallel motif.

The packing behavior of **HB330** in the single crystal differs from the other described examples. Although the chromophores pack again in discrete π-stacks forming single strands with no reciprocal interaction, this is the only example, where the dipole moments are oriented parallel to each other (Figure 15). The chromophores are situated in planes parallel

to each other with constant distance of 3.74 Å. The steric hindrance of the two methyl groups at the Fischer base donor may causes the strong longitudinal shift of the molecules, generating a close contact area only between the π-system of the acceptor unit of one molecule with the donor of the adjacent dye.

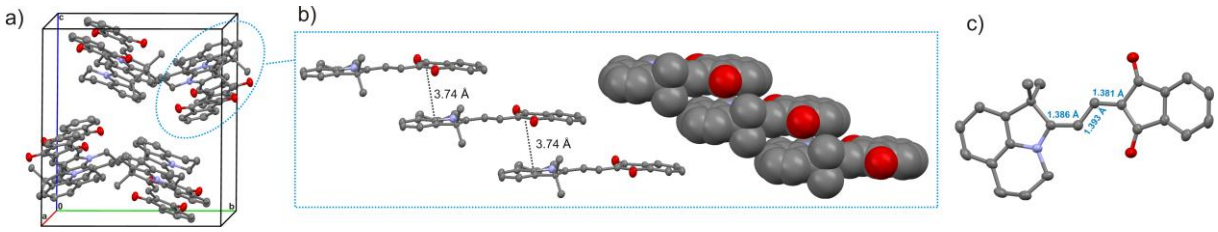

Figure 15. a) Top view on the *b*-*c*-plane of the unit cell of **HB330**. b) π-Stack of **HB330** in *a*-*c*-plane with antiparallel packing motif and spacefill view of the stack. c) Molecular structure of **HB330** in the solid state (for clarity all protons are omitted).

The presented chromophores show several common packing features in the single crystals. In the investigated samples, the molecules arrange in π-stacks with a slipped antiparallel stacking motif, where the dyes are located in parallel planes. The distances between these planes alternate and create one close and one more distant centrosymmetric dimeric unit. In the examples of **MD319**, **HB364**, **MD376**, **HB331** and **HB330** the π-stacks are separate from each other and show no repricporcal interaction. In **MD353**, the stacks interdigitate and form a two-dimensional brickwork-like structure. The π-stacks of chromophore **HB194** overlap, too, thus a zig-zack-like pattern is generated (Figure 13a). The packing motif of **HB330** is the only example, where no antiparallel arrangement of the dyes was found. Here the dipoles align in a parallel fashion. Furthermore, equal distances between all chromophores within a stack were determined. In all investigated examples, the C-C bond lengths of the methine bridge are differing only marginally, pointing to systems close to the *cyanine limit*.[7] This is in agreement with the narrow and intense absorption bands (Figure 10) and the determined small dipole differences upon excitation (Table 8).

The *cyanine limit* provides the highest possible tinctorial strength (absorbance) and longest wavelength absorption band, both are desired properties for photovoltaics. On the other hand, a very high dipolarity is given for such MC dyes in the *cyanine limit* owing to substantial charge transfer from the electron donor to the electron-accepting unit of the molecules. For the presented dyes ground state dipole moments μ_g of 6.2–11.8 D were determined by EOAM spectroscopy, being typically for these MC dyes. According to Bässlers theory such high dipole moments are expected to have a negative impact on the charge carrier mobility of

an organic semiconductor due to a broadening of the density-of-states (DOS) function.[85] However, this model was developed for randomly oriented dipoles, whereas the chromophores presented here are arranged in a slipped antiparallel stacking motif with a canceled dipole moment already on the dimer level.

2.2.4 Photovoltaic devices

Bulk heterojunction solar cells were fabricated in the group of Prof. Meerholz at the University of Cologne with the typical architecture ITO/PEDOT:PSS(40 nm)/MC:$PC_{61}BM$ /Al(120 nm). Thorough studies regarding the layer thickness and donor-to-acceptor ratio resulted in optimized device parameters. The characteristics of the solar cells and OFET devices based on MC dyes are given in Table 9. Unless stated otherwise, the solar devices were fabricated from dye:$P_{61}CBM$ (25:75wt%) solutions of chlorobenzene. In accordance with previous results,[4] the highest short circuit currents (J_{SC}) and, consequently, the highest power conversion efficiencies (η) were achieved for solar cells with an active layer thickness of 50-60 nm.

Table 9. Absorption, hole transport and photovoltaic characteristics of spin-coated thin films of MC dyes and their blends with $PC_{61}BM$ (75wt% $PC_{61}BM$)

MC dye	λ_{max} (nm)[e]	μ_h^{dye} ($cm^2\ V^{-1}\ s^{-1}$)[f]	μ_h^{blend} ($cm^2\ V^{-1}\ s^{-1}$)[f]	V_{OC} (V)	J_{SC} (mA cm^{-2})	FF	η (%)
HB248	508	n. d.		0.68	2.1	0.31	0.4
HB330	513	n. d.		0.68	2.8	0.32	0.6
MD353[a]	545	n. d.		0.67	3.7	0.28	0.7
HB331	549	n. d.		0.76	3.3	0.33	0.8
HB340	557	n. d.		0.79	4.0	0.36	1.1
MD376	605	1×10^{-5}	9×10^{-7}	0.90	5.3	0.32	1.5
HB194[b]	612	5×10^{-5}	2×10^{-5}	0.94	8.2	0.34	2.6
HB193[c]	621	3×10^{-6}	1×10^{-6}	0.84	6.1	0.32	1.6
HB364[d]	650	n. d.		0.60	4.5	0.33	0.9
MD319[d]	659	n. d.		0.65	7.3	0.33	1.6

[a] 70wt% PCBM. [b] 55wt% PCBM. [c] 65wt% PCBM. [d] Spin-coated from chloroform solution. [e] UV-vis maxima of the thin film. [f] μ_h values were determined in OFETs using the pristine MC dye and MC:$PC_{61}BM$ blends, respectively.

The LUMO energies of >(–3.66 eV) and the according donor-acceptor junction provide sufficient driving force to surmount the exciton binding energy.[16a,86] It is an advantageous property of these MC dyes that they possess low-lying HOMO levels despite their absorbance at rather low energy. The open-circuit voltages (V_{OC}) of the presented dyes vary between 0.60 V to 0.94 V. This range is in accordance with the differences in the HOMO energies of the dyes, ranging between –5.62 and –5.82 eV (Table 8). The short-circuit densities display a

significantly broader interval from 2.1 mA cm^{-2} to 8.2 mA cm^{-2} (Figure 16). Here, the dyes with absorption at the shortest wavelengths, i.e. indandione derivatives **HB248** and **HB330**, exhibit the lowest values, whereas the the higher values >5 mA cm^{-2} are all obtained for dyes bearing the thiazol and dicyanovinyl indandione acceptor units that afford absorption maxima between 600 nm and 680 nm in thin films. The best value of 8.2 mA cm^{-2} was obtained with **HB194** exhibiting a propylene bridging unit. The modest fill factors (FF~0.3) of all investigated devices might be ascribed to the relatively low charge carrier mobility of the present MC dyes (Table 9) compared to the electron mobility of 2×10^{-3} cm^2 V^{-1} s^{-1} of $PC_{61}BM$.[87] A difference of more than two orders of magnitude between the hole and electron mobilities suggests the build-up of space charge,[88] limiting the performance of the devices. Generally, the introduction of the bridging units at the indolenine unit result in an improved J_{SC} compared to the derivatives with the *n*-butyl chain, although the absorption properties in solution and in thin films are barely influenced. For the ethylene spacer an improvement of 8% (**HB340**) and of 15% (**HB193**) is observed compared to the respective *n*-butyl substituted derivatives (**MD353**, **MD376**). For the larger propylene spacers the improvements are 33% (**HB330**) for the indandione and 55% (**HB194**) for the dicyanovinyl indandione acceptor. Only the dioxopyridone **HB331** showed a decrease in J_{SC} of 11% compared to **MD353**. Accordingly, in particular devices built with **HB194** reached a high PCE of 2.6%.

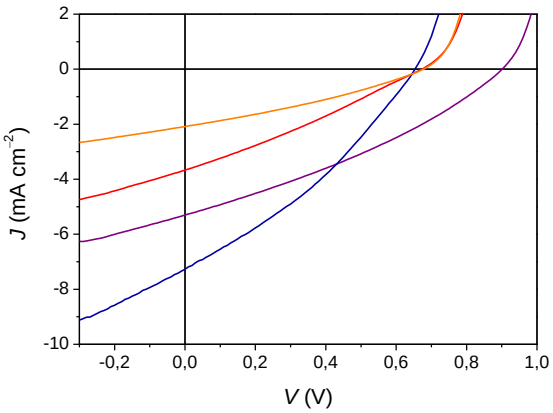

Figure 16. *J-V* response of the photovoltaic devices built with **MD248** (orange line, 75wt% $PC_{61}BM$), **MD353** (red line, 70wt% $PC_{61}BM$), **MD376** (magenta line, 75wt% $PC_{61}BM$) and **MD319** (blue line, 75wt% $PC_{61}BM$) measured under simulated AM 1.5 illumination at an irradiation intensity of 100 mW cm^{-2}.

The dye series bearing the dicycanovinyl indandione acceptor (**MD376**, **HB194** and **HB193**) clearly pinpoints the influence of the newly designed bridging units. The best solar cell devices built with **MD376** having the flexible alkyl substituent reach power conversion efficiencies of 1.5% at an optimized $PC_{61}BM$ content of 75wt%. The introduction of the

ethylene bridging unit in **HB193** entailed an improved PCE of 1.6% due to J_{SC} of 6.1 mA cm^{-2} at a $PC_{61}BM$ content of 65wt%. In the case of **HB194**, a further enhancement of PCE is observed. The maximum device performance is achieved at a $PC_{61}BM$ content of 55wt%, resulting in a significantly increased efficiency of 2.6%, which originates from an improved J_{SC} from 5.3 mA cm^{-2} for **MD376** to 8.2 mA cm^{-2} in the case of **HB194**. This improvement in J_{SC} of **HB194** and **HB193** may be attributed to the significantly enhanced absorbance in the visible region due to higher dye content in the solar cell. The quite high dye content in the best **HB194**:$PC_{61}BM$ photovoltaic devices compared to other small molecule based BHJ solar cells is indeed striking. Notably, the hole carrier mobility of **HB194** is the highest among this MC dye series and does not significantly decrease upon blending with $PC_{61}BM$ (Table 9). Both the substantial photocurrent and the high hole mobility are indicative for well-separated donor and acceptor phases consisting of densely packed MC dyes and $PC_{61}BM$. In contrast, for **MD376** a drop of mobility by more than one order of magnitude is observed for a $PC_{61}BM$ blend compared to that of the pristine dye, pointing at a deficient formation of percolation pathways (Table 9). In contrast to J_{SC}, the open circuit voltages for the three MC dyes **MD376**, **HB193** and **HB194** vary only slightly around the high level of 0.9 V, which can be explained in terms of their very similar HOMO and LUMO energies (Table 8).

2.2.5 X-ray diffraction of thin films

In order to gain insight into the morphology of the active layers in the solar cells drop-casted MC:$PC_{61}BM$ films of this leading dicyanovinyl indandione series, i.e **MD376**, **HB193** and **HB194** were studied by X-ray diffraction (XRD) and compared with the one of pristine dyes and $PC_{61}BM$, respectively (Figure 17). Additionally, differential scanning calorimetry (DSC) studies were performed with drop-casted MC:$PC_{61}BM$ films (Figure 19, Appendix). In the case of **HB194**:$PC_{61}BM$ (55wt%), we observed the presence of crystalline material by XRD and could assign each reflex to a corresponding one from the single components of the blend (Figure 17a). The DSC measurements confirmed the presence of crystalline material but showed a significantly lower melting point of 254 °C compared to that of pristine **HB194** of 291°C (Figure 19). Such a decrease of melting point is indicative for only small-sized crystalline domains and/or contamination of these domains by $PC_{61}BM$.

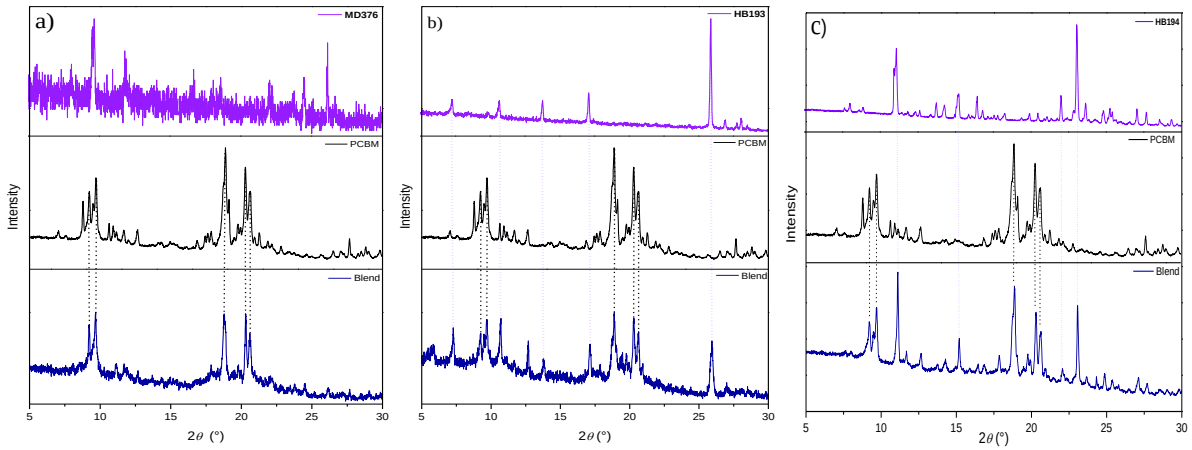

Figure 17. Powder X-ray diffractograms of a) **MD376** (top), $PC_{61}BM$ (middle) and a **MD376**:$PC_{61}BM$ (75wt%, bottom) blend. b) **HB193** (top), $PC_{61}BM$ (middle) and **HB193**:$PC_{61}BM$ (65wt%, bottom) blend. c) **HB194** (top), $PC_{61}BM$ (middle) and a **HB194**:$PC_{61}BM$ (55wt%, bottom) blend; all blends were obtained by drop-casting from chlorobenzene solution onto a glass substrate.

In the case of **HB193**, a lower degree of crystallinity was found by XRD analysis for blends with $PC_{61}BM$ (Figure 17b). In the case of **MD376**, the crystallinity is even more decreased, as no reflexes could be assigned to the single dye, but only these of $PC_{61}BM$ were found (Figure 17a). Furthermore, the melting enthalpy ΔH_m of 23.3 J g^{-1} of the blend determined by DSC (Figure 19d) is significantly lower than ΔH_m of blends of **HB194**:$PC_{61}BM$ (51.4 J g^{-1}). Accordingly, the ethylene and in particular the propylene bridging unit led to a distinctly higher grade of crystallinity of these dyes in BHJ blends. This might explain the higher charge carrier mobility and photocurrent of dye **HB194** (Table 9). As almost all chromophores with the rigid indolenine donors showed an increase in J_{SC} compared to the devices containing the corresponding dyes with *n*-butyl chain (Table 9), we expect this phenomenon to be generally linked to the presented modification of the donor part and the following higher tendency to crystallize.

2.4 Conclusion

In conclusion, an easy synthetic access to merocyanine dyes via three different routes is presented. By using these approaches a series of chromophores with five acceptor moieties with varying electron-accepting strengths was synthesized. The indolenine unit was applied as donor moiety, whereas its substitution pattern was diversified from *n*-butyl to an ethylene and propylene bridging unit, respectively. Due to the interaction of the Fischer base donor and the different acceptor parts, absorption maxima over the whole visible spectral range were generated. Analysis of the solid state packing by X-ray single crystal analysis showed

for six of the seven investigated samples a slipped antiparallel stacking motif with vanished dipolarity on the supramolecular level, allowing sufficient charge transport in the active layer of the solar cells. The rigidification of the donor by applying the ethylene and propylene spacer resulted in nearly all cases in a significant increase in J_{SC} of up to 55% (**HB194**) compared to the respective *n*-butyl derivatives. Solution-processed organic BHJ solar cells based on blends of **HB194** with $PC_{61}BM$ (55wt%) achieved a good power conversion efficiency of 2.6%.

2.5 Experimental section

2.5.1 Materials and methods

Solvents and reagents were obtained from commercial suppliers and purified and dried according to standard procedures.[89] Column chromatography was performed with commercial glass columns using silica gel (particle size 0.063-0.2 mm) as stationary phase. ^{1}H NMR spectra were recorded with a Bruker Advance 400 spectrometer at 25 °C using residual solvent peaks as internal standard. Coupling constants are given in Hz. High resolution ESI mass spectroscopy was carried out on a microTOF focus instrument (Bruker Daltronik GmbH) in positive mode with MeCN or $CHCl_3$ as solvent. UV-vis spectra were measured on a Perkin Elmer Lambda 950 UV-vis spectrophotometer using a conventional quartz cell (light path 1cm). Temperature was regulated by a PTP-1 Peltier element (Perkin Elmer).

CV was performed on a standard commercial electrochemical analyzer (EC epsilon; BAS Instrument, UK) in a three electrode single-compartment cell under argon. Dichloromethane (HPLC grade) was obtained from J. T. Baker and dried over calcium hydride and degassed prior to use. The supporting electrolyte tetrabutylammonium hexafluorophosphate (TBAHFP) was synthesized according to literature,[90] recrystallized from ethanol/water and dried in high vacuum. The measurements were carried out under exclusion of air and moisture at a concentration of 10^{-4} M with ferrocene as internal standard for the calibration of the potential. Working electrode: Pt disc; reference electrode: Ag/AgCl; auxiliary electrode: Pt wire.

X-ray powder diffraction (XRD) patterns were acquired on a STOE transmission diffractometer (STADI P) in a 2θ range of 5-30° by using $Cu_{K\alpha}$ radiation with a scanning rate of 1 deg min^{-1} in the case of **HB193** and **MD376** and a scanning rate of 0.075 deg min^{-1} in the case of **HB194**. A 8 mm aperture was used for all measurements. The samples for powder

XRD were prepared as follows: A thick film was prepared by drop-casting a chlorobenzene solution of the corresponding dye or MC:$PC_{61}BM$ mixture on a glass substrate. The film was then scratched off from the substrate and pestled to produce a homogeneous powder.
DSC measurements were performed with a TA Q1000 calorimeter using a heating/cooling rate of 10 °C min^{-1} in a nitrogen atmosphere. Two heating-cooling cycles were performed for each compound. The samples for DSC were prepared in the same way as for powder XRD.

2.5.2 Device fabrication

Charge carrier mobilities were determined in organic field effect transistors, where a spin-coated layer of the respective MC dye from chlorobenzene solution (20 mg mL^{-1}) was deposited on a pre-fabricated heavily doped p-type Si++/SiO_{-x} substrate with patterned source and drain gold contacts. The doped silicon substrate acts as the gate contact followed by a 230 nm thick SiO_{-x} insulating layer with a capacitance of 15 nF cm^{-2}. Channel length and width were 2.5, 10 or 20 μm and 1 cm, respectively. Devices were measured in a dry nitrogen atmosphere with a Keithley 4200-SCS semiconductor characterization system. Mobilities were calculated from the transconductance in the linear regime.
Solar cell fabrication: All devices were fabricated on commercial indium-tin oxide (ITO) coated glass. The ITO was etched with acid and subsequently cleaned using chloroform, acetone, mucasol detergent and de-ionized water in an ultrasonic bath. Next, the ITO substrates were exposed to ozone for 20 min and immediately spin-coated with poly(3,4-ethylene dioxythiophene):poly(styrene sulfonate) (PEDOT:PSS) (Baytron P AL 4083, HC Starck; ca. 40 nm). Afterwards, the samples were heat treated for 2 min at 110 °C to remove residual water and transferred into a N_2 glove box for further fabrication processing and measurement. $PC_{61}BM$ was obtained from Nano-C (Westwood, MA, USA), the merocyanine dyes were synthesized according to synthetic procedures described below. The active layers were spin-coated from heated (75 °C) chlorobenzene containing a mixture of MC and $PC_{61}BM$ with a concentration of 20 mg mL^{-1}. The substrates were moved to a high-vacuum chamber where the top electrode was evaporated through a mask (120 nm Al), leading to seven solar cells on each substrate with an active area of 0.08 cm^2. The *JV* characteristics of the solar cells were measured using a Keithley 2425 source measurement unit. The AM1.5 light was provided by a filtered Xe-lamp. The intensity of 100 mW cm^{-2} of the AM1.5 light was determined by using a calibrated inorganic solar cell from the Fraunhofer Institute for solar research in Freiburg (Germany) and a reference $PC_{61}BM$:P3HT cell measured by the

same institution. No spectral mismatch factor was included in the calculation of the efficiency. A Dektak surface profiler (Veeco) was used to determine the active layer thicknesses. The active layer thickness was 50-60 nm. UV-vis spectra were taken with a Varian Cary 50 spectrometer.

2.5.3 Electro-optical absorption measurements

Electro-optical absorption (EOA) measurements were carried out like described in the following. Dipole moments of the ground state μ_g and the dipole moment differences $\Delta\mu = \mu_e - \mu_g$ (μ_e: excited state dipole moment) of chromophores have been determined by means of EOA spectroscopy by which the difference of absorption of a solution with ($\varepsilon^E(\varphi, \tilde{\nu})$) and without ($\varepsilon(\tilde{\nu})$) an externally applied electric field **E** is measured with light parallelly (φ = 0°) and perpendicularly (φ = 90°) polarized to the direction of **E**.[91] For uniaxial phases, induced in a solution by both an alternating and a constant electric field of about 3×10^6 V m^{-1}, the dichroism $\varepsilon^E(\varphi, \tilde{\nu}) - \varepsilon(\tilde{\nu})$ depends on the orientational order of the molecules due to their ground state dipole moment μ_g, the shift of the absorption band proportional to the dipole moments difference $\Delta\mu$, and on the electric field dependence of the electric transition dipole moment $\mu_{eg}(E)$. UV-vis spectra, required for the evaluation of the integral absorption (μ_{eg}^2), were recorded with a Perkin-Elmer Lambda 900 or 950 spectrophotometer at 298 K. All measurements were carried out in dioxane.

2.5.4 Crystal structure determination

The crystal data of **HB194** were collected at Bruker APEX diffractometer with CCD area detector and graphite monochromated $Mo_{K\alpha}$ radiation. The structure was solved using direct methods, refined with SHELX software package (G. Sheldrick, University of Göttingen, Germany 1997) and expanded using Fourier techniques. All non-hydrogen atoms were refined anisotropically. Hydrogen atoms were assigned idealized positions and were included in structure factors calculations.

Crystal data for **HB194**: $C_{27}H_{21}N_3O$, M_r = 403.47, dark block-shaped crystal, 0.09×0.2×0.26, monoclinic space group P2(1)/n, a = 8.1678(6)Å, b = 21.9108(17)Å, c = 23.0033(18)Å, α = 90.00°, β = 94.1810(10)°, γ = 90.00°, V = 4105.8(5)Å^3, Z = 8, ρ_{calcd} = 1.305 g·cm^{-3}, μ = 0.081 mm^{-1}, $F(000)$ = 1696, T = 173(2) K, R_1 = 0.0863, wR^2 = 0.1309, 10265 independent reflections [2θ≤56.76°] and 567 parameters.

Crystallographic data of **HB194** have been deposited with the Cambridge Crystallographic Data Center as supplementary publication no. CCDC-740220. These data can be obtained free of charge from The Cambridge Crystallographic Data Center via www.ccdc.cam.ac.uk/data_request/cif

Crystal data for **MD353**: $C_{27}H_{33}N_3O_2$, M_r = 431.56 g mol^{-1}, red block-shaped crystal, 0.337×0.404×0.509 mm^3, triclinic space group P–1, a = 8.805(8) Å, b = 10.732(10) Å, c = 12.982(12) Å, α = 81.125(12)°, β = 74.333(12)°, γ = 89.545(12)°, V = 1166.3(18) Å^3, Z = 2, ρ_{calcd} = 1.229 g cm^{-3}, μ = 0.078 mm^{-1}, F(000) = 464, T = 174(2) K, R_1 = 0.0527, wR^2 = 0.1344, 5760 independent reflections [2θ≤56.56°] and 294 parameters.

Crystal data for **MD376**: $C_{28}H_{25}N_3O$, M_r = 419.51 g mol^{-1}, dark block-shaped crystal, 0.05×0.12×0.24 mm^3, a = 10.2335(11) Å, b = 21.690(2) Å, c = 10.0187(11) Å, α = 90°, β = 96.670(6)°, γ = 90°, V = 2208.7(4) Å^3, Z = 4, ρ_{calcd} = 1.262 g cm^{-3}, μ = 0.078 mm^{-1}, F(000) = 888, T = 100(2) K, R_1 = 0.0764, wR^2 = 0.1447, 9703 independent reflections [2θ≤70.18°] and 289 parameters.

Crystal data for **HB364**: $C_{26}H_{30}N_4S$, M_r = 430.60 g mol^{-1}, blue block-shaped crystal, 0.15×0.15×0.20 mm^3, monoclinic space group P2(1)/n, a = 13.0466(3) Å, b = 7.5537(2) Å, c = 23.8222(6) Å, α = 90°, β = 91.0020(10)°, γ = 90°, V = 2347.32(10) Å^3, Z = 4, ρ_{calcd} = 1.218 g cm^{-3}, μ = 1.367 mm^{-1}, F(000) = 920, T = 103(2) K, R_1 = 0.0350, wR^2 = 0.0940, 3503 independent reflections [2θ≤124.74°] and 285 parameters.

Crystal data for **MD319**: $C_{28}H_{26}N_4S$, M_r = 450.59 g mol^{-1}, green block-shaped crystal, 0.095×0.158×0.205 mm^3, triclinic space group P–1, a = 7.531(4) Å, b = 12.987(6) Å, c = 14.187(7) Å, α = 63.346(6)°, β = 78.552(6)°, γ = 78.555(6)°, V = 1205.9(10) Å^3, Z = 2, ρ_{calcd} = 1.241 g cm^{-3}, μ = 0.157 mm^{-1}, F(000) = 476, T = 173(2) K, R_1 = 0.0679, wR^2 = 0.1461, 5961 independent reflections [2θ≤62.37°] and 301 parameters.

Crystal data for **HB330**: $C_{24}H_{21}NO_2$, M_r = 355.42 g mol^{-1}, red block-shaped crystal, 0.24×0.27×0.31 mm^3, monoclinic space group P2(1)/c, a = 8.0432(14) Å, b = 14.495(3) Å, c = 15.715(3) Å, α = 90°, β = 101.195(2)°, γ = 90°, V = 1797.4(5) Å^3, Z = 4, ρ_{calcd} = 1.314 g cm^{-3}, μ = 0.083 mm^{-1}, F(000) = 752, T = 173(2) K, R_1 = 0.0515, wR^2 = 0.1305, 4363 independent reflections [2θ≤56.14°] and 246 parameters.

Crystal data for **HB331**:$C_{26}H_{29}N_3O_2$, M_r = 415.52 g mol^{-1}, red block-shaped crystal, 0.098×0.150×0.160 mm^3, monoclinic space group P2(1)/c, a = 11.870(2) Å, b = 15.311(3) Å, c = 12.268(2) Å, α = 90°, β = 98.366(2)°, γ = 90°, V = 2205.9(7) Å^3, Z = 4,

ρ_{calcd} = 1.251 g cm^{-3}, μ = 0.080 mm^{-1}, F(000) = 888, T = 173(2) K, R_1 = 0.0589, wR^2 = 0.1306, 5449 independent reflections [2θ≤56.50°] and 288 parameters.

2.5.5 Synthesis and characterization

The synthesis of **MD353** is given in reference 83.

2-[2-(1-Butyl-3,3-dimethyl-1,3-dihydro-indol-2-ylidene)-ethylidene]-indan-1,3-dione HB248

A 5 mL Ac_2O solution of (1-butyl-3,3-dimethyl-1,3-dihydro-indol-2-ylidene)-acetaldehyde (1.20 g, 4.93 mmol) and 1,3-indandione (720 mg, 4.93 mmol) was heated to 90 °C for 30 min, before the solvent was removed under vacuum. After column chromatography (1. CH_2Cl_2 with 0.1% MeOH, 2. CH_2Cl_2:EtOAc=9:1), the obtained solid was dissolved in CH_2Cl_2 and precipitated with *n*-hexane. Yield 765 mg (2.10 mmol, 42%). Mp. 207–209 °C. ^{1}H NMR (CD_2Cl_2, 400 MHz): δ 8.09 (d, ^3J = 14.1, 1H), 7.74 (m, 2H), 7.63 (m, 2H), 7.49 (d, ^3J = 14.1, 1H), 7.34 (m, 2H), 7.16 (m, 1H), 7.02 (m, 1H), 3.97 (t, ^3J = 7.5, 2H), 1.83 (m, 2H), 1.73 (s, 6H), 1.53 (m, 2H), 1.04 (t, ^3J = 7.4, 3H). UV-vis (CH_2Cl_2): λ_{max} (ε): 496 (114600 M^{-1} cm^{-1}). HRMS (ESI): calcd for $C_{25}H_{25}NO_2$ [M]$^+$: 371.1885, found: 371.1880. Elemental analysis (%) calcd for $C_{25}H_{25}NO_2$: C, 80.83; H, 6.78; N, 3.77. Found: C, 80.66; H, 6.85; N, 3.79. CV data: E_p^{ox} = 607 mV vs Fc, $E_{1/2}^{red}$ = –1935 mV vs Fc.

2-[2-(1,1-Dimethyl-5,6-dihydro-1*H*,4*H*-pyrrolo[3,2,1-*ij*]quinolin-2-ylidene)-ethylidene]-indan-1,3-dione HB330

A 1.5 mL Ac_2O solution of (1,1-dimethyl-5,6-dihydro-1*H*,4*H*-pyrrolo[3,2,1-*ij*]quinolin-2-ylidene)-acetaldehyde (340 mg, 1.50 mmol) and 1,3-indandione (219 mg, 1.50 mmol) was heated to 90 °C for 30 min, before the solvent was removed under vacuum. After column chromatography (CH_2Cl_2), the obtained solid was solved in CH_2Cl_2 and precipitated with *n*-hexane. Yield 440 mg (1.24 mmol, 83%). Mp. 245–248 °C. ^{1}H NMR ($CDCl_3$, 400 MHz): δ 8.08 (d, ^3J = 14.2, 1H), 7.77 (m, 2H), 7.60 (m, 2H), 7.37 (d, ^3J = 14.2, 1H), 7.15 (m, 1H), 7.06 (m, 2H), 3.93 (bs, 2H), 2.86 (t, ^3J = 6.1, 2H), 2.21 (m, 2H), 1.74 (s, 6H). UV-vis (CH_2Cl_2): λ_{max} (ε): 500 (111200 M^{-1} cm^{-1}). HRMS (ESI): calcd for $C_{24}H_{21}NO_2$ [M]$^+$: 355.1572, found: 355.1567. Elemental analysis (%) calcd for $C_{24}H_{21}NO_2$: C, 81.10; H, 5.96; N, 3.94. Found: C, 80.75; H, 5.96; N, 4.10. CV data: E_p^{ox} = 527 mV vs Fc, $E_{1/2}^{red}$ = –1927 mV vs Fc.

1-Butyl-5-[2-(1,1-dimethyl-5,6-dihydro-1*H*,4*H*-pyrrolo[3,2,1-*ij*]quinolin-2-ylidene)-ethylidene]-4-methyl-2,6-dioxo-1,2,5,6-tetrahydro-pyridine-3-carbonitrile HB331

A 1.5 mL Ac_2O solution of (1,1-dimethyl-5,6-dihydro-1*H*,4*H*-pyrrolo[3,2,1-*ij*]quinolin-2-ylidene)-acetaldehyde (341 mg, 1.50 mmol) and 1-butyl-6-hydroxy-4-methyl-2-oxo-1,2-dihydro-pyridine-3-carbonitrile[92] (309 mg, 1.50 mmol) was heated to 90 °C for 30 min, before the solvent was removed under vacuum. The residual solid was dissolved in CH_2Cl_2 and precipitated with *n*-hexane, before column chromatography (CH_2Cl_2) was performed. Subsequently, the product was obtained after recrystallization from CH_2Cl_2/*n*-hexane. Yield 304 mg (0.73 mmol, 49%). Mp. 247–249 °C. ^{1}H NMR ($CDCl_3$, 400 MHz): δ 8.00 (d, ^3J = 14.0, 1H), 7.87 (d, ^3J = 14.0, 1H), 7.21 (m, 1H), 7.16 (m, 2H), 4.03 (t, ^3J = 5.9, 2H), 3.99 (t, ^3J = 7.6, 2H), 2.90 (t, ^3J = 6.1, 2H), 2.51 (s, 3H), 2.23 (m, 2H), 1.72 (s, 6H), 1.63 (m, 2H), 1.39 (m, 2H), 0.94 (t, ^3J = 7.4, 3H). UV-vis (CH_2Cl_2): λ_{max} (ε): 529 (133500 M^{-1} cm^{-1}). HRMS (ESI): calcd for $C_{26}H_{30}N_3O_2$ $[M+H]^+$: 416.2333, found: 416.2335. Elemental analysis (%) calcd for $C_{26}H_{29}N_3O_2$: C, 75.15; H, 7.03; N, 10.11. Found: C, 74.54; H, 7.00; N, 10.03. CV data: $E_{1/2}^{ox}$ = 613 mV vs Fc, $E_{1/2}^{red}$ = –1720 mV vs Fc.

1-Butyl-5-[2-(1,1-dimethyl-4,5-dihydro-1*H*-pyrrolo[3,2,1-*hi*]indol-2-ylidene)-ethylidene]-4-methyl-2,6-dioxo-1,2,5,6-tetrahydro-pyridine-3-carbonitrile HB340

A 5.0 mL Ac_2O solution of 1,1-dimethyl-2-methylene-1,2,4,5-tetrahydro-pyrrolo[3,2,1-*hi*]indole (926 mg, 5.00 mmol), 1-butyl-6-hydroxy-4-methyl-2-oxo-1,2-dihydro-pyridine-3-carbonitrile[92] (1.03 g, 5.00 mmol) and DMF (550 mg, 7.50 mmol, 0.58 mL) was heated to 90 °C for 1 h, before the solvent was removed under vacuum. The residual solid was solved in CH_2Cl_2 and precipitated with *n*-hexane, before column chromatography (CH_2Cl_2 with 2% MeOH) was performed. Subsequently, the product was obtained after recrystallization from DCM/*n*-hexane. Yield 666 mg (1.66 mmol, 33%). Mp. 246–249 °C. ^{1}H NMR (DMSO–d_6, 400 MHz): δ 7.78 (d, ^3J = 14.5, 1H), 7.57 (d, ^3J = 14.5, 1H), 7.39 (d, ^3J = 7.3, 1H), 7.31 (d, ^3J = 6.9, 1H), 7.21 (t, ^3J = 7.3, 1H), 4.73 (m, 2H), 3.84 (t, ^3J = 7.4, 2H), 3.77 (t, ^3J = 6.8, 2H), 2.47 (s, 3H), 1.58 (s, 6H), 1.47 (m, 2H), 1.27 (m, 2H), 0.90 (t, ^3J = 7.4, 3H). UV-vis (CH_2Cl_2): λ_{max} (ε): 537 (117400 M^{-1} cm^{-1}). HRMS (ESI): calcd for $C_{25}H_{28}N_3O_2$ $[M+H]^+$: 402.2176, found: 402.2176. Elemental analysis (%) calcd for $C_{25}H_{27}N_3O_2$: C, 74.79; H, 6.78; N, 10.47. Found: C, 74.36; H, 6.73; N, 10.58. CV data: $E_{1/2}^{ox}$ = 558 mV vs Fc, E_p^{red} = –1710 mV vs Fc.

General procedure for MD376, HB193 and **HB194:**

One equivalent of indolenine, 1 equivalent of 2-(3-oxo-indan-1-ylidene)-malononitrile **56** and 1.5 equivalents of ethyl orthoformate in 1 mL ethanol/equivalent were heated to reflux for 1 h. After removal of the solvent, the product was isolated by column chromatography (DCM) and further purified by precipitation from dichloromethane and *n*-hexane.

2-{2-[2-(1-*n*-Butyl-3,3-dimethyl-1,3-dihydro-indol-2-ylidene)-ethylidene]-3-oxo-indan-1-ylidene}-malononitrile MD376

Yield 50%. Mp. 173 °C. ^{1}H NMR ($CDCl_3$, 400 MHz): δ 9.05 (d, ^3J = 13.9, 1H), 8.57 (m, 1H), 8.07 (d, ^3J = 13.8, 1H), 7.73 (m, 1H), 7.59 (m, 2H), 7.37 (m, 2H), 7.24 (m, 1H), 7.07 (m, 1H), 4.06 (t, ^3J = 7.5, 2H), 1.88 (m, 2H), 1.80 (s, 6H), 1.53 (m, 2H), 1.04 (t, ^3J = 7.4, 3H). UV-vis (CH_2Cl_2): λ_{max} (ε) = 477 (21000), 576 (66400 M^{-1} cm^{-1}). HRMS (ESI): calcd for $C_{28}H_{26}N_3O$ $[M+H]^+$: 420.2070, found: 420.2071. Elemental analysis (%) calcd for $C_{28}H_{25}N_3O$: C, 80.16; H, 6.01; N, 10.02. Found: C, 80.09; H, 6.03; N, 9.91. CV data: $E_{1/2}^{ox}$ = 648 mV vs Fc, $E_{1/2}^{red}$ = –1515 mV vs Fc.

2-{2-[2-(1,1-Dimethyl-4,5-dihydro-1*H*-pyrrolo[3,2,1-*hi*]indol-2-ylidene)-ethylidene]-3-oxo-indan-1-ylidene}-malononitrile HB193

Yield 19%. Mp. 277 °C. ^{1}H NMR (DMSO-d_6, 400 MHz): δ 8.55 (d, ^3J = 14.0, 1H), 8.34 (m, 1H), 7.58-7.73 (m, 4H), 7.39 (m, 1H), 7.31 (m, 1H), 7.22 (t, ^3J = 7.3, 1H), 4.64 (m, 2H), 3.77 (t, ^3J = 6.2, 2H), 1.65 (s, 6H). UV-vis (CH_2Cl_2): λ_{max} (ε) = 486 (20300), 586 (51100 M^{-1} cm^{-1}). HRMS (ESI): calcd for $C_{26}H_{20}N_3O$ $[M+H]^+$: 390.1600, found: 390.1599. Elemental analysis (%) calcd for $C_{26}H_{19}N_3O \times {}^2/_3\ H_2O$: C, 77.79; H, 5.11; N, 10.47. Found: C, 77.80; H, 4.85; N, 10.49. CV data: $E_{1/2}^{ox}$ = 563 mV vs Fc, $E_{1/2}^{red}$ = –1538 mV vs Fc.

2-{2-[2-(1,1-Dimethyl-5,6-dihydro-1*H*,4*H*-pyrrolo[3,2,1-*ij*]quinolin-2-ylidene)-ethylidene]-3-oxo-indan-1-ylidene}-malononitrile HB194

Yield 60%. Mp. 291 °C. ^{1}H NMR ($CDCl_3$, 400 MHz): δ 9.00 (d, ^3J = 14.0, 1H), 8.56 (m, 1H), 7.92 (d, ^3J = 13.8, 1H), 7.70 (m, 1H), 7.58 (m, 2H), 7.15 (m, 3H), 4.05 (bs, 2H), 2.90 (t, ^3J = 6.1, 2H), 2.25 (m, 2H), 1.79 (s, 6H). UV-vis (CH_2Cl_2): λ_{max} (ε) = 482 (21700), 578 (60300 M^{-1} cm^{-1}). HRMS (ESI): calcd for $C_{27}H_{21}N_3O$ $[M]^+$: 403.1685, found: 403.1679. Elemental analysis (%) calcd for $C_{27}H_{21}N_3O$: C, 80.37; H, 5.25; N, 10.41. Found: C, 80.10; H, 5.30; N, 10.37. CV data: $E_{1/2}^{ox}$ = 602 mV vs Fc, $E_{1/2}^{red}$ = –1550 mV vs Fc.

2-{4-Butyl-5-[2-(1-butyl-3,3-dimethyl-1,3-dihydro-indol-2-ylidene)-ethylidene]-5*H*-thiazol-2-ylidene}-malononitrile HB364

A 8.0 mL Ac_2O solution of (1-butyl-3,3-dimethyl-1,3-dihydro-indol-2-ylidene)-acetaldehyde (1.98 g, 8.0 mmol) and 2-(4-*n*-butyl-thiazol-2(5*H*)-ylidene)malononitrile (1.50 g, 7.30 mmol) was heated to 90 °C for 95 min, before *n*-hexane was added and the solution was decanted. The residue was stirred first with *iso*-propanol, filtrered off and recrystallized from CH_2Cl_2/*n*-hexane. Yield 2.24 g (5.2 mmol, 71%). Mp. 263–265 °C. ^{1}H NMR (CD_2Cl_2, 400 MHz): δ 7.97 (d, ^3J = 13.5, 1H), 7.40 (m, 2H), 7.26 (m, 1H), 7.09 (m, 1H), 5.72 (d, ^3J = 13.6, 1H), 2.89 (m, 2H), 1.79 (m, 2H), 1.69 (s, 6H), 1.48 (m, 2H), 1.00 (t, ^3J = 7.4, 3H). UV-vis (CH_2Cl_2): λ_{max} (ε) = 618 (137100 M^{-1} cm^{-1}). HRMS (ESI): calcd for $C_{26}H_{30}N_4S$ $[M]^+$: 430.2191, found: 430.2185. Elemental analysis (%) calcd for $C_{26}H_{30}N_4S$: C, 72.52; H, 7.02; N, 13.01; S, 7.45. Found: C, 72.56; H, 7.02; N, 13.02; S, 7.42. CV data: $E_{1/2}^{ox}$ = 470 mV vs Fc, E_p^{red} = –1474 mV vs Fc.

2-{5-[2-(1-Butyl-3,3-dimethyl-1,3-dihydro-indol-2-ylidene)-ethylidene]-4-phenyl-5*H*-thiazol-2-ylidene}-malononitrile MD319

A 1.5 mL Ac_2O solution of (1-butyl-3,3-dimethyl-1,3-dihydro-indol-2-ylidene)-acetaldehyde (365 mg, 1.50 mmol) and 2-(4-phenyl-5*H*-thiazol-2-ylidene)-malononitrile (338 mg, 1.50 mmol) was heated to 70 °C for 30 min. Washing of the precipitate with diethylether was followed by column chromatography (CH_2Cl_2 with 10% MeOH). Yield 470 mg (1.04 mmol, 70%). Mp. 317–319 °C. ^{1}H NMR ($CDCl_3$, 400 MHz): δ 7.96 (d, ^3J = 13.6, 1H), 7.74 (m, 2H), 7.53 (m, 4H), 7.37 (m, 1H), 7.30 (m, 1H), 7.23 (m, 1H), 7.05 (d, ^3J = 8.0, 1H), 3.94 (t, ^3J = 7.4, 2H), 1.81 (m, 2H), 1.54 (s, 6H), 1.48 (m, 2H), 1.03 (t, ^3J = 7.3, 3H). UV-vis (CH_2Cl_2): λ_{max} (ε) = 632 (111800 M^{-1} cm^{-1}). HRMS (ESI): calcd for $C_{28}H_{27}N_4S$ $[M+H]^+$: 451.1951, found: 451.1952. Elemental analysis (%) calcd for $C_{28}H_{26}N_4S \times \frac{1}{3}\ H_2O$: C, 73.17; H, 5.92; N, 12.19; S, 6.98. Found: C, 72.97; H, 5.71; N, 12.43; S, 7.20. CV data: $E_{1/2}^{ox}$ = 467 mV vs Fc, E_p^{red} = –1344 mV vs Fc.

2.6 Appendix

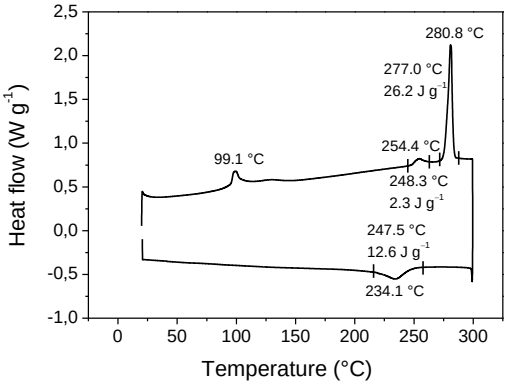

Figure 18. DSC measurement of $PC_{61}BM$ powder.

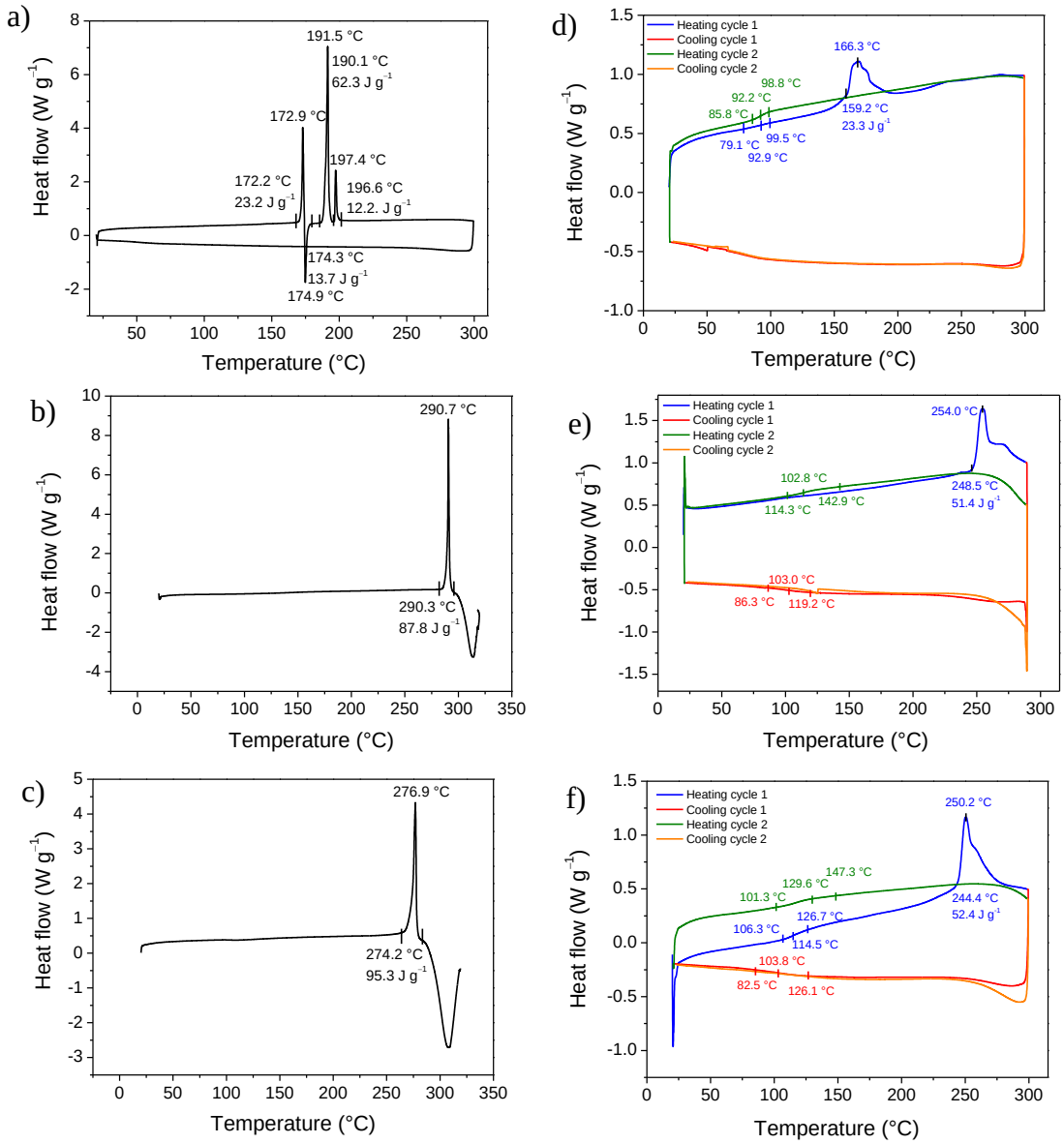

Figure 19. DSC measurements of powder of a) **MD376**. b) **HB194**. c) **HB193** and of drop-casted and dried samples of d) **MD376**:$PC_{61}BM$ (75wt%). e) **HB194**:$PC_{61}BM$ (55wt%). f) **HB193**:$PC_{61}BM$ (65wt%).

Chapter 3

Efficient solution-processed bulk heterojunction solar cells by antiparallel supramolecular arrangement of merocyanine dyes

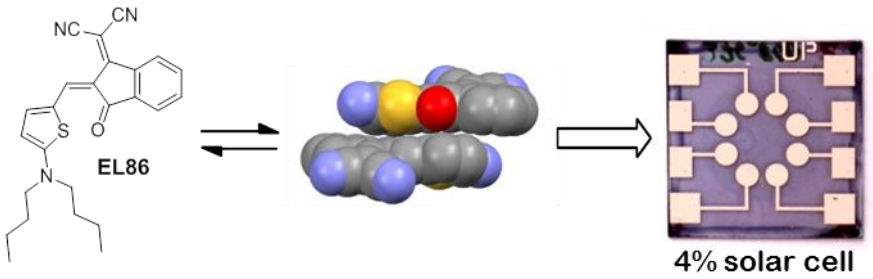

Abstract: In this chapter, a series of merocyanine dyes with aminothiophene donor and different acceptor units is reported. By modulation of the acceptor strength, absorption bands over the whole visible spectrum are accessible as well as adjustment of the frontier molecular orbital levels. The performance of the chromophores in blends with fullerene acceptors in solution-processed bulk heterojunction solar cells was studied and related to the molecular properties of the dyes. In particular, the effect of the large ground state dipole moments of these dyes was investigated by X-ray single crystal analysis. In all samples antiparallel dimers were formed, resulting in an annihilating of the dipole moments. Thus, we propose the prevalence of the centrosymmetric dimer in the active layers of the solar cells as well. This specific feature explains the good performance of merocyanine dyes in molecular organic photovoltaics. With blends of **EL86**/$PC_{71}BM$ we achieved a highly efficient solar cell with V_{OC} of 1.0 V, J_{SC} of 10.6 mA cm^{-2} and power conversion efficiency of 4.0%.*

* Solar devices were built by Dr. N. M. Kronenberg; the optimization of the device containing **EL86** was performed by M. Lenze (University of Köln). Single crystal analyses were measured by M. Gsänger, electro-optical absorption measurements by Dr. M. Stolte and cyclic voltammetry by A.-M. Krause; synthetic support was given by Dr. E. Tulyakova (**EL**), M. Kaiser (**MD**) and P. Seufert-Baumbach (University of Würzburg).

3.1 Introduction

In recent years, organic photovoltaic has inspired not only significant academic, but also industrial research as a potential low-cost alternative to current silicon solar cells. Organic solar cells belong to the so-called excitonic solar cells, which are characterized by the formation of strongly bound electron-hole pairs (excitons) upon excitation with light. The localized excitons prevail due to the low dielectric constants in organic semiconductors, being insufficient to affect the direct generation of free charge carriers like in their highly dielectric inorganic counterparts. Exciton dissociation occurs almost exclusively at the interface between two materials with different electron affinities: the electron acceptor and the electron donor. Therefore, only excitons created within the distance of the exciton diffusion length of ~10–20 nm[16] from the interface can dissociate and contribute to the electrical current of the external circuit. The design of the so-called bulk heterojunction (BHJ)[18] which uses a blend of donor and acceptor materials forming an interpenetrating, phase-separated network with nanoscale morphology, allows for concomitantly efficient exciton diffusion to the interface and effective light absorption imparted by an optimized layer thickness typically in the range of 100 nm.

The active layer comprising the electron donor and acceptor can be deposited by two techniques: vacuum-deposition and solution-processing. In the case of vacuum-deposition, the most promising results with power conversion efficiencies of ~5% were obtained with small-molecule donor materials like phthalocyanines.[63] A well-known and exhaustively explored electron donor in the field of solution-processing is the polymer poly(3-hexylthiophene) (P3HT) with record efficiencies around 5%.[22a,21c] Besides, irrespective of the preparation method, the almost ubiquitous use of electron accepting fullerenes like [6,6]-phenyl-C_{61}-butyric-acid methyl ester ($PC_{61}BM$) in solution-processed and C_{60} in vacuum-deposited devices represents a common feature in organic photovoltaics. The high electron affinity,[93] excellent ability to transport charge[94] and its commercial availability turn fullerenes into the best acceptor components currently available for these devices.

After innumerous publications about photovoltaic devices based on blends of P3HT/$PC_{61}BM$ it becomes clear that room for optimization is getting increasingly smaller. One challenge is the high-lying LUMO of P3HT, which is significantly higher than needed for an efficient electron transfer to the fullerene.[19a] One strategy for increasing the device performance by raising the open-circuit voltage (V_{OC}) is the modification of the fullerene, which was recently achieved by applying an indene-C_{60} adduct as acceptor material in a blend with P3HT.[95]

Furthermore, new donor materials exhibiting smaller band gaps[96] and low-lying frontier molecular orbital (FMO) levels were developed in order to enhance the overlap of the absorption spectrum with the solar emission and to maximize the V_{OC}. This concept is translated into a variety of small-band gap polymers like poly(2,7-carbazole), poly(2,1,3-benzothiadiazole) or copolymers containing thieno[3,4-*b*]thiophene and benzodithiophene monomeric units, showing PCEs (power conversion efficiency) of >7%.[76,97] In these polymers, the concept of using alternating electron-rich and electron-poor units connected by a π-conjugated moiety results in the desired bathochromic shift of t76he absorption edge. An interesting example represents the work of Huang *et.al*, where an electron-rich polymer backbone was connected via a π-bridge with acceptor units at the end of side-chains. These polymers show promising solar cell performance with PCE up to 4.7%.[98]

Alongside the research on polymeric materials, the number of publications concerning the application of small molecules in solution-processed solar cells is rising rapidly. Besides the impressive examples of Nguyen[53] with a diketopyrrolopyrrole dye and recently Forrest[58c] employing a squarylic acid achieving PCE >4%, several other dye classes were successfully applied in solution-processed organic photovoltaics.[33a,g,27,29,35,41,60,56,66-62,68,69-71]

In our research approach a similar strategy like with small-band gap polymers is applied by using merocyanine (MC) dyes, which are characterized by their typical donor-π-acceptor structure. These small molecules exhibit the advantages of easy syntheses and purification processes, are monodisperse and show high absorption coefficients. Additionally, MCs provide low-lying HOMO levels, conferring high V_{OC} values for the resulting solar devices. By careful modulation of both donor and acceptor moieties of the chromophores, absorption starting from the shorter wavelength regime up to the near-infrared region is feasible.[99] The intensity of the optical transition is dependent on the combination of the donor and acceptor component and their reciprocal effects with each other.[91b] Typically, sharp and intense absorption bands occur in the *cyanine limit*, where the two resonance structures of a push-pull system contribute equally to the ground and excited state. This is tantamount to equal dipole moments in the ground and the excited state and minimized reorganization upon excitation. Broader absorption bands with lower absorption coefficients are often observed for chromophores far from the *cyanine limit*.[7,100] Furthermore, merocyanine dyes are known for their tendency to form centrosymmetric aggregates, triggered by their large ground state dipole moments.[101]

Besides their good solubility, these molecules can also be evaporated thermally under high-vacuum conditions. By taking advantage of these unique properties, we have recently started to elucidate the potential of MC dyes as donor components in vacuum-deposited BHJ solar cells and observed an encouraging increase in PCE from 2.6% (solution-processing) to 4.9% (vacuum-deposition).[4,102]

In this chapter the synthesis and characterization of the electro-optical, electro-chemical and photovoltaic properties of a series of merocyanine dyes bearing the same donor unit, dibutyl-aminothiophene, but seven different acceptor moieties with varying electron-accepting strengths (Scheme 2) is presented. As dipolar chromophores are known to aggregate in concentrated solutions in centrosymmetric dimers,[101] the behavior of the reported dyes was now also investigated in the solid state by single crystal analysis. Solution-processed bulk heterojunction solar cells were built with all synthesized dyes and PCE values up to 4% were achieved in combination with $PC_{71}BM$.

3.2 Results

3.2.1 Synthesis

Scheme 2 outlines the synthetic route, which follows our earlier work on merocyanine dyes for photovoltaic materials.[4,102] The chromophores were obtained by a Knoevenagel condensation, where the aldehyde **63** was combined with the CH-acidic acceptor units in acetic anhydride at 90°C. The reactions took 30–90 min to achieve a nearly complete consumption of the starting materials and resulted in the corresponding products with yields of 51–77%. The detailed synthetic procedures and characterization data are described in the experimental section.

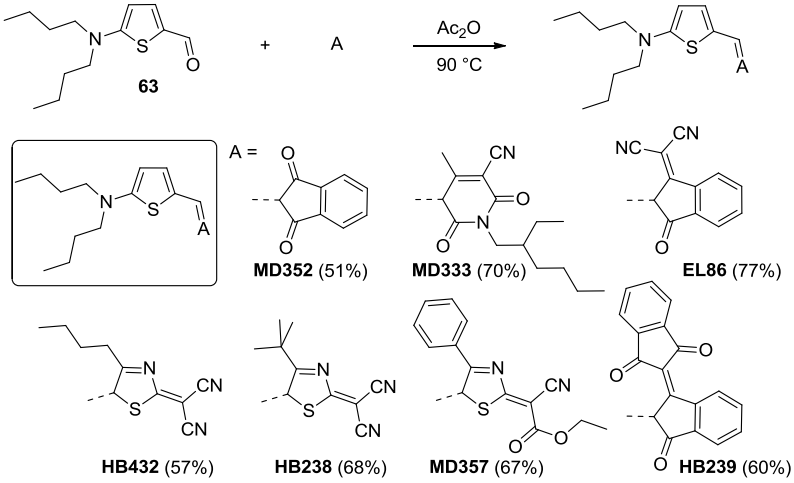

Scheme 2. Syntheses (yields in parentheses) and molecular structures of the investigated MC dyes.

3.2.2. Electro-optical and electro-chemical properties

The optical properties of the synthesized merocyanine dyes were investigated by UV-vis spectroscopy and electro-optical absorption measurements.[91] Furthermore, cyclic voltammetry was performed for each dye to obtain information on their HOMO and LUMO levels.[103] Figure 20a displays representative absorption spectra of the reported dye series in dichloromethane, whereas Figure 20b visualizes the position of the FMO energies of the chromophores with regard to the electron acceptor $PC_{61}BM$. The significant electro-optical and electro-chemical properties are summarized in Table 12.

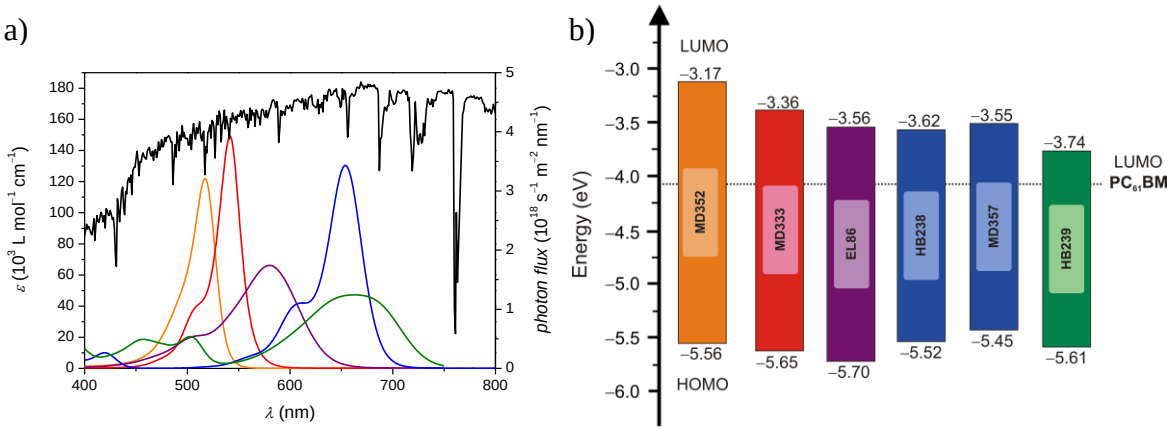

Figure 20. a) UV-vis spectra of **MD352** (orange line), **MD333** (red line), **EL86** (violet line), **MD357** (blue line) and **HB239** (green line) in CH_2Cl_2 ($c_0 \sim 10^{-5}$ mol L^{-1}) at 298 K and photon flux at 1.5 AM conditions (black line). The spectra of **HB238** and **HB432** are similar to **MD357**; thus they are not depicted here for clarity reasons. b) FMO levels of dyes **MD352**, **MD333**, **EL86**, **HB238**, **MD357** and **HB239** and their relative position to the LUMO of $PC_{61}BM$ (the solid area represents the band gap and FMO levels, respectively).

Increasing the acceptor strength from the weakest acceptor unit indandione (**MD352**) to the stronger electron-acceptors thiazole (**HB238**, **HB432**, **MD357**) and bis-indandione (**HB239**) entails a significant red-shift of the absorption maxima from 517 nm (**MD352**) to 654 nm (**MD357**) and 660 nm (**HB239**), respectively. Thus, by varying the acceptor unit, the absorption properties are tunable over the whole region of the visible spectrum. The extinction coefficients at λ_{max} vary from ~5×10^5 L mol^{-1} cm^{-1} for **HB239** to ~1.5×10^6 L mol^{-1} cm^{-1} for **MD333**. However, this does not necessarily reflect the absorption strength of a chromophore, as a dye with a sharp and intense absorption profile can absorb the same amount of photons as one with a broad, but less intense UV-vis band. In order to evaluate the absorption strength, we defined the physical parameter $\mu^2_{eg}\, M^{-1}$ (absorption density), which represents the transition dipole moment μ^2_{eg} divided by the molecular weight M of the compound and is therefore directly related to the tinctorial strength of the respective

chromophore. The absorption densities of the reported dye all range at 0.22 ± 0.02 D^2 mol g^{-1}, except for **HB239**, which displays a significantly reduced tinctorial strength. If we apply the same procedure to determine the absorption density of P3HT, we calculate a distinctly lower value of only 0.14 D^2 mol g^{-1}. Regarding the electro-optical properties we found that the dyes **MD333**, **HB432**, **HB238** and **MD357** show large ground state dipole moments of 12–13 D and small changes of the dipole moment upon optical excitation, whereas **MD352**, **EL86** and **HB239** exhibit distinctly lower μ_g and higher $\Delta\mu$ values. As expected, the dyes close to the *cyanine limit* show the largest transition dipole moments (Table 10).

Figure 20b illustrates one of the major benefits of merocyanine dyes with regard to organic solar cells: all dyes show favorable low-lying HOMO levels, although the examples **MD352** and **MD333** display rather large band gaps. Low-lying HOMO levels enable high open-circuit voltages.[104] Within the presented dye series, the HOMO energies vary by only 0.25 eV. On the other hand, the respective acceptor unit has a significantly stronger influence on the LUMO level, which is shifted by 0.57 eV from **MD352** to **HB239**. The dyes with the stronger acceptor units exhibit low-lying LUMO levels, however, still with an energy offset to the LUMO of PCBM close to the ideal value of 0.3–0.4 eV.[19] Hence, these dyes match ideally with PCBM owing to small energy loss upon electron transfer from the dye to the fullerene acceptor. Accordingly, by modulation of the acceptor unit, not only absorption properties are adjusted, but also the FMO levels of the respective chromophore.

Table 10. Electro-optical and electro-chemical properties of the investigated dyes

MC dye	λ_{max} (nm)[a]	ε (L mol^{-1} cm^{-1})[a]	μ^2_{ag} (D^2)[a]	μ^2_{ag} M^{-1} (D^2 mol g^{-1})[a]	μ_g (D)[b]	$\Delta\mu$ (D)[b]	E_{HOMO} (eV)[c]	E_{LUMO} (eV)[d]
MD352	517	121900	82	0.22	5.7	4.2	–5.56*	–3.17
MD333	542	149400	95	0.20	12.6	1.7	–5.65	–3.36
EL86	580	66200	97	0.23	8.6	4.1	–5.70	–3.56
HB432	645	130400	100	0.23	13.2	2.0	–5.52	–3.60
HB238	651	143200	102	0.24	13.1	2.5	–5.52	–3.62
MD357	654	130500	104	0.21	12.1	2.3	–5.45*	–3.55
HB239	663	47300	74	0.15	6.1	4.6	–5.61*	–3.74

[a] UV-vis measurements for dilute solution (c_0 ~10^{-5} M) in CH_2Cl_2. [b] 1,4-dioxane (c_0 ~ 10^{-6} M). [c] Calculated from CV measurements ($E_{1/2}^{ox}$/*E_p) in CH_2Cl_2 calibrated against the ferrocene/ferrocenium couple (Fc/Fc^+, –5.15 eV) as internal standard. [d] $E_{LUMO} = E_{HOMO} + (hc/\lambda_{max})$.

3.2.3 Crystal structures

For two characteristic dyes of our series, **EL86** and **HB239**, we have grown single crystals that could be resolved by single crystal X-ray analysis. As shown in Figure 21 and Figure 22

the chromophores are located in planes parallel to each other arranged in discrete stacks, whereas each molecule features one close and one distant neighbor, forming close and distant centrosymmetric dimeric units. The CC bond lengths of the methine bridges alter only marginally, indicating a fully conjugated system close to the *cyanine limit*.[7,100]

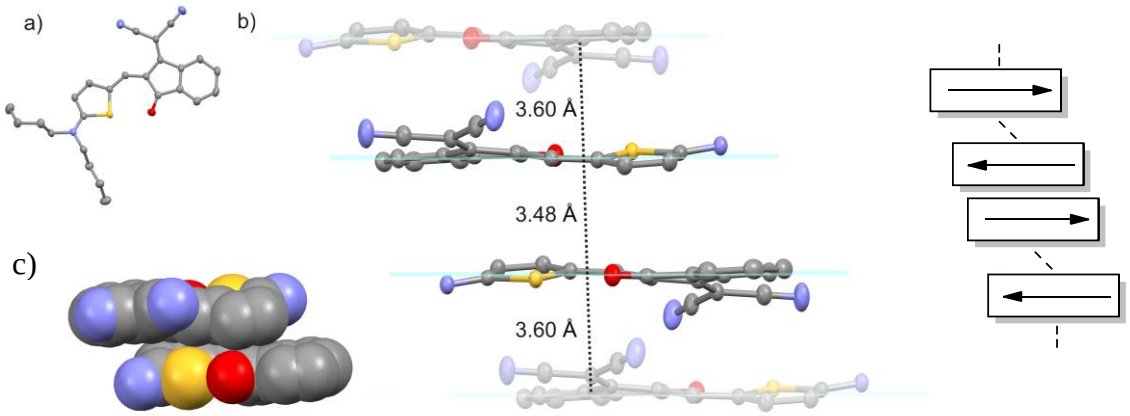

Figure 21. a) Molecular crystal structure of **EL86** in the solid state. b) π-Stack of **EL86** with antiparallel packing motif. c) Spacefill view of the close dimer of **EL86** (for clarity, the alkyl chains in b) and c) and all protons are omitted). d) Schematic representation of a **EL86** stack with one close and one more distant neighbor and antiparallel orientation of the dipole moments (arrows).

In the single crystal structure of **EL86**, the molecule itself is slightly distorted, with a torsion angle between the donor and acceptor unit of 13°. Within the stacks, almost equal distances of the close (3.48 Å) and the distant (3.60 Å) centrosymmetric dimer results in a one-dimensional stack of closely packed chromophores (Figure 21b). These show only a small longitudinal displacement to each other leading to a pronounced contact area between the π-surfaces of neighboring molecules. The displacement is more pronounced in the case of the distant dimer. By contrast, whilst a tightly bound antiparallel dimer unit is preserved in crystals of **HB239** (3.47 Å distance), here the distant dimer show a significantly increased interspace of 4.89 Å, being 41% longer than the one of the close dimer (Figure 22b). Adjoining molecules are shifted longitudinally to each other. Additionally, the chromophores of the distant dimer exhibit a transversal displacement, further reducing the $\pi\pi$–contact area between adjacent molecules. Both effects are probably caused by the strongly distorted molecular structure of **HB239**, as the angle between the two indandione units of the acceptor accounts to 32°. The twisted acceptor moiety acts like a spacer between the centrosymmetric distant dimers and prevents the formation of a closely packed π-stack as it is provided in the case of **EL86**.

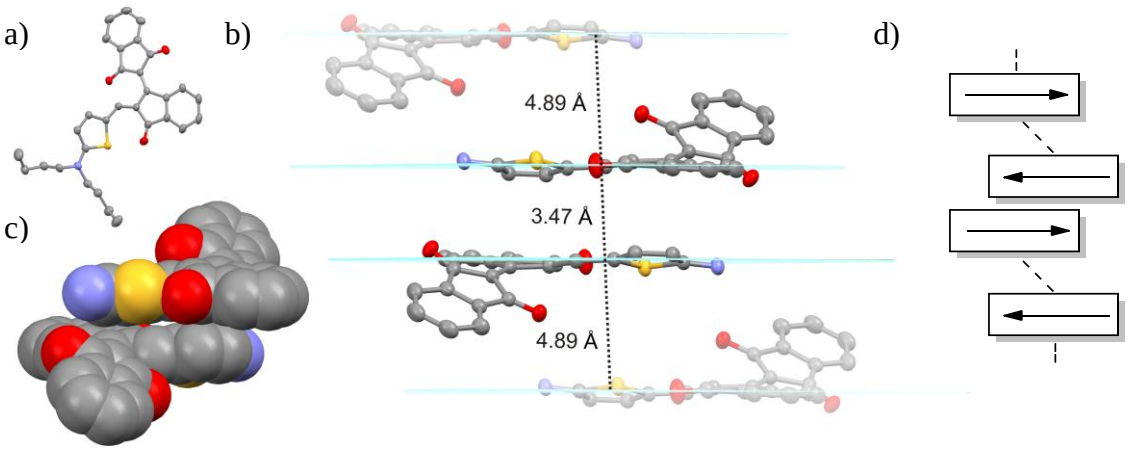

Figure 22. a) Molecular crystal structure of **HB239** in the solid state. b) π-Stack of **HB239** with antiparallel packing motif. b) Spacefill view of the close dimer of **HB239** (for clarity, the alkyl chains in b) and c) and all protons are omitted). d) Schematic representation of a **HB239** stack with one close and one more distant neighbor and antiparallel orientation of the dipole moments (arrows).

3.2.4 Bulk heterojunction solar cells.

The power conversion efficiency η of solar cells is defined as:

$$\eta = \frac{FF \cdot J_{SC} \cdot V_{OC}}{P_{in}} \qquad (1)$$

where FF is the fill factor, J_{SC} the short-circuit current density, V_{OC} the open-circuit voltage and P_{in} the power density of the incoming light. All described MC dyes were evaluated in combination with the fullerene acceptor $PC_{61}BM$ in solution-processed BHJ solar cells displaying the following simple device structure ITO/PEDOT:PSS(40 nm)/ dye/$PC_{61}BM$/Al(120 nm) at an illumination intensity of 100 mW cm^{-2}. Solar devices containing merocyanine dyes were spin-coated from solutions of chlorobenzene. The solar cells were optimized with respect to their active layer thickness and the dye/$PC_{61}BM$ ratio. Both V_{OC} and fill factor were usually barely influenced by different dye/$PC_{61}BM$ ratios. However, the short-circuit current density and consequently PCE typically displayed a maximum at 70–75wt% $PC_{61}BM$. Concerning the active layers, optimized conditions were created for film thicknesses of 50–60 nm. For detailed device fabrication procedures, see experimental section. The following section provides an overview of the determined solar cell characteristics, which are listed in Table 11.

The absorption spectra of all solar cells show a bathochromic shift of λ_{max} compared to the corresponding solution spectra in dichloromethane and a significant band broadening often observed in solid state absorption. This shift, ranging from 14 nm for **MD333** to 37 nm for

HB239 could be originated by dispersion forces. Except for **MD352** and **MD333**, all reported compounds show absorption maxima in the region of the solar flux with the highest intensity (600–800 nm, Figure 20a).

The open-circuit voltages determined for this series of dyes range around 0.7 V. **MD357** shows the lowest V_{OC} of 0.47 V, which is in good agreement with the highest HOMO level of this dye series (Figure 20b). Likewise, the dye with the lowest HOMO level, **EL86** reached the highest V_{OC} of 0.96 V. The short-circuit current density is strongly dependent on the light harvesting efficiency as well as the charge carrier properties of the active layer of a photovoltaic cell. Here, most investigated device showed moderate values for J_{SC} of ~4 mA cm^{-2}. Cells built with **MD352** exhibited a lower performance with J_{SC} of 2.9 mA cm^{-2}, whereas a significantly higher J_{SC} of 5.8 mA cm^{-2} was determined for devices with **EL86**. Notably, for this dye a higher dye loading of 40wt% resulted in the best solar cell performance. Fill factors of ~0.3 were measured for all solar devices with a maximum value of 0.41 for cells built with **EL86**. The power conversion efficiencies range between 0.5–1.1% with one clear outlier, **EL86**, showing 2.3%.

Table 11. Photovoltaic characteristics of the investigated solution-cast dye:$PC_{61}BM$ BHJ solar cells[a]

MC dye	λ_{max} (nm)[b]	μ_h^{dye} (cm^2 V^{-1} s^{-1})	μ_h^{blend} (cm^2 V^{-1} s^{-1})	V_{OC} (V)	J_{SC} (mA cm^{-2})	FF	η (%)
MD352	532	n. d.		0.63	2.9	0.27	0.5
MD333	556	n. d.		0.73	4.0	0.32	0.9
EL86	595	1×10^{-5}	1×10^{-6}	0.96	5.8	0.41	2.3
HB432	666	n. d.		0.67	3.5	0.36	0.9
HB238	682	4×10^{-4}	3×10^{-7}	0.72	4.5	0.35	1.1
MD357	689	n. d.		0.47	4.0	0.27	0.5
HB239	700	no field effect		0.68	4.0	0.36	1.0

[a] For each dye/PCBM combination results for the optimized ratio are presented, which are 70wt% PCBM for **MD352**, **MD333** and **MD357**, 60wt% PCBM for **EL86** and 75wt% PCBM for **HB432**, **HB238** and **HB239**. [b] UV-vis measurements of a thin film of the blend.

For the most promising dye of this series **EL86**, an optimization of the cell setup was performed.[105] Here, the PEDOT-PSS layer was treated with ozone directly before the spin-coating of the active layer to decrease the work function and as electrode a combination of Ca and Ag was used. Furthermore, $PC_{61}BM$ was substituted by $PC_{71}BM$ to enhance the absorption and small amounts of *n*-butanol were added as a cosolvent to the solvent chlorobenzene. The result of this optimization afforded a highly improved solar cell with PCE of 4.0% (Figure 23). Dye **DPP(TBFu)$_2$** (Figure 23, inset), which exhibits one of the best device performance among solution-processed small-molecule BHJ solar cells with an

equally simple device setup,[53] was included as donor component in our study for comparison. Figure 4 shows the *J*–*V* curve of both the optimized device containing **EL86** and a reference device based on **DPP(TBFu)$_2$**/$PC_{71}BM$. Although we use significantly lower dye contents the J_{SC} of 10.6 mA cm^{-2} of our chromophore **EL86** matches the obtained 9.6 mA cm^{-2} (Ref 53: 10.0 mA cm^{-2}) for **DPP(TBFu)$_2$**. Furthermore, the high V_{OC} of 1.0 V compared to 0.91 V (Ref 53: 0.92 V) for **DPP(TBFu)$_2$** results in a device efficiency of 4.0%, whilst **DPP(TBFu)$_2$** exhibits 4.1% (Ref 53: 4.4%). Notably, devices containing **DPP(TBFu)$_2$** need to be annealed at 110 °C for 10 min to reach high performance, whereas cells built with **EL86** afford 4.0% without post treatment.

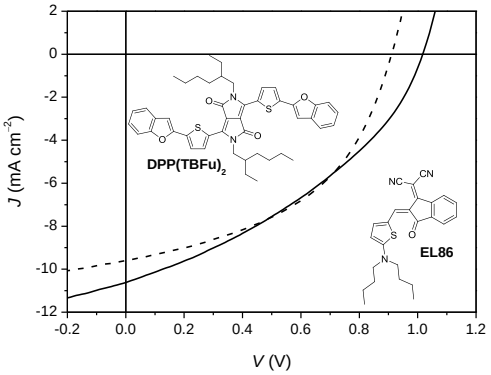

Figure 23. *J*–*V* response of the solar cells built with **EL86** (solid line, 60wt% $PC_{71}BM$) and **DPP(TBFu)$_2$** (dashed line, 40wt% $PC_{71}BM$) measured under simulated solar illumination (AM1.5, 100 mW cm^{-2}).

3.3 Discussion

Merocyanine dyes are known for large dipole moments due to charge transfer from the electron donor units to the acceptor units of the molecules (Table 10).[6] According to the Bässler model,[85] completely randomly arranged highly dipolar molecules are supposed to limit the transport of charge carriers in amorphous solid state materials due to a broadening of the density of states. This might restrict the application of these materials as organic semiconductors. However, the concept of merocyanine dyes as active component in organic solar cells is based on the following assumption: merocyanine dyes arrange in centrosymmetric dimers with low transversal or longitudinal displacement, resulting in the annihilation of the dipole moment on the supramolecular level leading to an entirely new situation within the Bässler model. Thus, whilst many merocyanine dyes with large dipole moments failed in nonlinear optics owing to the formation of such antiparallel dimers[106] they become beacons of hope for organic photovoltaics.

To verify this arrangement for the presented dyes we analyzed the solid state behavior by using the examples of **EL86** and **HB239**. Actually, both dyes form stacks of antiparallel arranged dimers in single crystals. The almost planar chromophore **EL86** shows small interplanar distances to both of its neighbors, resulting in a densely packed crystal with good contact area between the π-systems, as required for efficient charge transport. Actually, this dye showed the highest hole mobility in a blend with $PC_{61}BM$ of this dye series and a peak in performance at a relatively high dye loading of 40wt%, allowing for high J_{SC} values. Furthermore, in blends with $PC_{71}BM$ this dye led to a highly efficient photovoltaic device with a PCE up to 4%.

In contrast, **HB239** exhibits a strongly distorted chromophore in the single crystal forcing a long distance of 4.89 Å between every second molecule. Here, the long distance between two π-systems and the transversal shift of the distant dimers prevent strong electronic coupling. For these reason, we supposed charge transport properties inferior to the one determined for **EL86**. In fact, no field effect at all could be detected for OFETs containing the dye **HB239**. Furthermore, photovoltaic devices built with the latter did not exceed PCEs of 1% due to low fill factor and short-circuit current density, which could both be influenced by a low hole mobility. **HB239** with the distorted geometry also displayed the lowest absorption density of the presented dyes, which in turn has a negative influence on the light harvesting properties.

Additionally to the presented data in this chapter, the same structural arrangement of the chromophores, the antiparallel dimer, was observed in the single crystal of a derivative of **MD333** in earlier work on nonlinear optics.[101b] As the centrosymmetric dimer was evidenced in all investigated crystalline samples, we assume this to be the general packing motif of merocyanine dyes both in the solid state as well as short-range order in thin films. Thus, we suppose the prevailing dye arrangement in the active layer of merocyanine solar cells to be a centrosymmetric dimer exhibiting a negligible dipole moment. Due to this packing motif, the charge transport properties are not necessarily impaired by the large ground state dipole moment of the monomeric molecules. For this reason, hole mobilities for pure dye films such as 1×10^{-5} cm^2 V^{-1} s^{-1} for **EL86** and 4×10^{-4} cm^2 V^{-1} s^{-1} for **HB238** are possible for the presented dyes, which are comparable to the mobilities of highly efficient non-dipolar dyes applied in solution-processed BHJ solar cells.[27,53]

In the case of **HB238**, the hole mobility of dye/PCBM blends drops by three orders of magnitude compared to the device with dye only. From this observation we deduce a deficient phase separation in the blend containing **HB238** entailing an adverse morphology

for charge transport. If charges created in the active layer recombine before being extracted at the electrodes due to deficient percolation pathways, this would reduce the J_{SC} significantly. Actually, the short-circuit current density of 4 mA cm^{-2} of a **HB238** device is lower than expected for a cell showing an absorption maximum around 680 nm, coinciding with the maximal intensity of the photon flux (Figure 20a). Upon blending **EL86** with $PC_{61}BM$ the ability to transport charges is preserved to a large degree. Combined with the broad absorption band around 600 nm this contributes to the high J_{SC} values obtained with cells containing **EL86**. Furthermore, this dye displays the lowest HOMO level of this dye series, explaining the high V_{OC} of ~1 V, which is among the best in the field. With an optimized cell setup and $PC_{71}BM$ as electron acceptor, a considerable PCE of 4% was obtained. Although the device exhibits a relatively low fill factor, the high J_{SC} and V_{OC} values hold promise that merocyanine dye based solar devices may surpass the currently only two examples[53,58c] with higher performance in solution-processed BHJ devices.

3.4 Conclusion

We have synthesized and characterized a series of merocyanine dyes with an aminothiophene donor unit and seven different heterocyclic acceptor moieties. The variation of the acceptor groups had a strong impact on absorption properties and the LUMO levels whilst the influence on the HOMO levels was only small. Single crystals of **EL86** and **HB239** verified the presence of centrosymmetric dimeric packing units, confirming the assumed antiparallel arrangement of the dipolar molecules. As the centrosymmetric dimer was found as general packing motif in our and earlier[101b,106] studies, we suppose the presence of the same packing motif in the active layer of the merocyanine solar cells. The antiparallel arrangement of dipoles results in the annihilation of the dipolarity of the single molecules and an amalgamation of the charge distribution. This explains dye **EL86** being a highly efficient electron donor in solar devices in combination with $PC_{71}BM$. Here, the very high V_{OC} (1.0 V) and J_{SC} (10.6 mA cm^{-2}) result in a cell with a considerable PCE of 4%. Using **DPP(TBFu)$_2$** as one of the actual most efficient dyes for comparison in our experimental setup revealed similar performances for both dyes. Consequently, we could both explain the substantial achievements made for merocyanine dyes in the field of organic solar cells as well as improve them by tailoring the dye structure to match one of today's record holder.

3.5 Experimental section

3.5.1 Materials and methods

Solvents and reagents were obtained from commercial sources and purified and dried according to standard procedures.[107] 1,3-Indandione (97%), 1-chloro-3,3-dimethyl-2-butanone (93%), 2-bromo-1-phenylethanone (98%) and 5-bromothiophene-2-carboxaldehyde (95%) were purchased from commercial suppliers. Column chromatography was performed with commercial glass columns using silica gel (particle size 0.063 – 0.2 mm) as stationary phase. ^{1}H NMR were recorded with a 400 MHz spectrometer using residual solvent peaks as internal standard. UV-vis spectra were measured on a conventional Perkin-Elmer Lambda 950 spectrophotometer equipped with temperature controllers. CV was performed on a standard commercial electrochemical analyzer (EC epsilon; BAS Instrument, UK) in a three electrode single-compartment cell under argon. Dichloromethane (HPLC grade) was dried over calcium hydride and degassed prior to use. The supporting electrolyte tetrabutylammonium hexafluorophosphate (TBAHFP) was synthesized according to literature,[90] recrystallized from ethanol/water and dried under high vacuum. The measurements were carried out under exclusion of air and moisture at a concentration of 10^{-4} M with ferrocene as internal standard for the calibration of the potential. Working electrode: Pt disc; reference electrode: Ag/AgCl; auxiliary electrode: Pt wire.

Electro-optical absorption (EOA) measurements were carried out according to the following description: Dipole moments of the ground state μ_g and the dipole moment differences $\Delta\mu = \mu_e - \mu_g$ (μ_e: excited state dipole moment) of chromophores were determined by means of EOA spectroscopy by which the difference of absorption of a solution with ($\varepsilon^E(\varphi, \tilde{\nu})$) and without ($\varepsilon(\tilde{\nu})$) an externally applied electric field **E** is measured with light parallelly (φ = 0°) and perpendicularly (φ = 90°) polarized to the direction of **E**.[91] For uniaxial phases, induced in a solution by both an alternating and a constant electric field of about 3×10^6 V m^{-1}, the dichroism $\varepsilon^E(\varphi, \tilde{\nu}) - \varepsilon(\tilde{\nu})$ depends on the orientational order of the molecules due to their ground state dipole moment μ_g, the shift of the absorption band proportional to the dipole moments difference $\Delta\mu$, and on the electric field dependence of the electric transition dipole moment μ_{eg}(**E**). UV-vis spectra that were required for the evaluation of the integral absorption (μ_{eg}^2) were recorded with a Perkin-Elmer Lambda 950 spectrophotometer at 298 K. All measurements were carried out in dioxane.

Crystal structure determination: The crystal data of **EL86** and **HB239** were collected at Bruker APEX diffractometer with CCD area detector and graphite monochromated $Mo_{K\alpha}$ radiation. The structure was solved using direct methods, refined with SHELX software package (G. Sheldrick, University of Göttingen, Germany 1997)[108] and expanded using Fourier techniques. All non-hydrogen atoms were refined anisotropically. Hydrogen atoms were assigned idealized positions and were included in structure factor calculations.

Crystal data for **EL86**: $C_{25}H_{25}N_3OS$, M_r = 415.54, blue block-shaped crystal, 0.18×0.28×0.38, triclinic space group P–1, a = 8.3309(11) Å, b = 10.3185(14) Å, c = 13.5744(18) Å, α = 101.648(2)°, β = 100.169(2)°, γ = 103.967(2)°, V = 1077.5(2) Å^3, Z = 2, ρ_{calcd} = 1.281 g·cm^3, μ = 0.172 mm^{-1}, F(000) = 440, T = 173(2) K, R_1 = 0.0441, wR^2 = 0.1074, 5322 independent reflections [2θ ≤ 56.56°] and 273 parameters.

Crystal data for **HB239**: $C_{31}H_{29}NO_3S$, M_r = 495.61, purple block-shaped crystal, 0.23×0.24×0.26, triclinic space group P–1, a = 9.231(4) Å, b = 9.721(4) Å, c = 15.343(6) Å, α = 98.104(4)°, β = 100.837(4)°, γ = 104.768(4)°, V = 1281.4(9) Å^3, Z = 2, ρ_{calcd} = 1.285 g·cm^{-3}, μ = 0.160 mm^{-1}, F(000) = 524, T = 173(2) K, R_1 = 0.0578, wR^2 = 0.1435, 6295 independent reflections [2θ ≤ 56.56°] and 325 parameters.

Crystallographic data have been deposited with the Cambridge Crystallographic Data Center as supplementary publication no. CCDC-835848 (**EL86**) and CCDC-835849 (**HB239**). These data can be obtained free of charge from The Cambridge Crystallographic Data Center via www.ccdc.cam.ac.uk/data_request/cif

3.5.2 Device fabrication

All devices were fabricated on commercial indium-tin oxide (ITO) coated glass. The ITO was etched with acid and subsequently cleaned using chloroform, acetone, mucasol detergent and de-ionized water in ultrasonic bath. Next, the ITO substrates were exposed to ozone for 20 minutes and immediately coated with poly(3,4-ethylene dioxythiophene):poly(styrene sulfonate) (PEDOT:PSS) (Baytron P AL 4083, HC Starck; ca. 40 nm). Afterwards the samples were heat treated for 2 minutes at 110 °C to remove residual water and transferred into a N_2 glove box for the fabrication of devices and measurement. $PC_{61}BM$ and $PC_{71}BM$ applied here were obtained from Nano-C.

The active layers were spin-coated from chlorobenzene containing the mixture of merocyanine and PCBM. The substrates were transferred to a high-vacuum chamber where the top electrode was evaporated through a mask. Here, either a 120 nm thick Al layer or a

combination of a 4 nm Ca layer (Aldrich, 99%) and a 150 nm Ag layer (Alfa Aesar, 99.9%) was applied. On each substrate, seven solar cells with an active area of 0.08 cm^2 were located. The *JV* characteristics of the solar cells were measured using a Keithley 2425 source measurement unit. The AM1.5 light was provided by a filtered Xe lamp. The intensity of 100 mW cm^{-2} of the AM1.5 light was determined by using a calibrated inorganic solar cell from the Fraunhofer Institute for solar research in Freiburg, Germany and a reference $PC_{61}BM$:P3HT cell measured by the same institute. No spectral mismatch factor was included in the calculation of the efficiency.

A Dektak surface profiler (Veeco) was used to determine the active layer thicknesses.

Charge carrier mobilities were determined in organic field effect transistors, where a spin-coated layer of the respective MC dye from chlorobenzene solution (20 mg/mL) was deposited on a pre-fabricated heavily doped p-type Si^{++}/SiO_{-x} substrate with patterned source and drain gold contacts. The doped silicon substrate acts as the gate electrode followed by a 230 nm thick SiO_{-x} insulating layer with a capacitance of 15 nF cm^{-2}. Channel length and width were 2.5, 10 or 20 μm and 1 cm, respectively. Devices were measured in a dry nitrogen atmosphere with a Keithley 4200-SCS semiconductor characterization system. Mobilities were calculated from the transconductance in the linear regime.

3.5.3 Synthetic procedures

The syntheses and characterization data of **MD352**[4] and **MD333**[109] were reported previously and those of the new merocyanine dyes are given here.

5-(Dibutylamino)-thiophene-2-carbaldehyde (63)[110]

5-Bromothiophene-2-carboxaldehyde (4.78 g, 25.0 mmol), dibutylamine (9.70 g, 12.8 mL, 75.0 mmol) and *p*-toluenesulfonic acid (250 mg, 1.45 mmol) were heated to 100 °C for 24 h, before 37 mL dest. H_2O were added. After the mixture was stirred at room temperature for 30 min, it was extracted with CH_2Cl_2 (3 × 25 mL) and the solvent was removed under vacuum. Purification by column chromatography (CH_2Cl_2) yielded the product as brown oil. Yield 4.20 g (18.0 mmol, 70%). ^{1}H NMR ($CDCl_3$, 400 MHz): δ 9.45 (s, 1H), 7.43 (d, ^3J = 4.5 Hz, 1H), 5.89 (d, ^3J = 4.5 Hz, 1H), 3.32 (m, 4H), 1.64 (m, 4H), 1.35 (m, 4H), 0.95 (t, ^3J = 7.4 Hz, 6H). MS (MALDI-TOF, matrix: DCTB): calcd for $C_{13}H_{21}NOS$: 239.1, found 239.1.

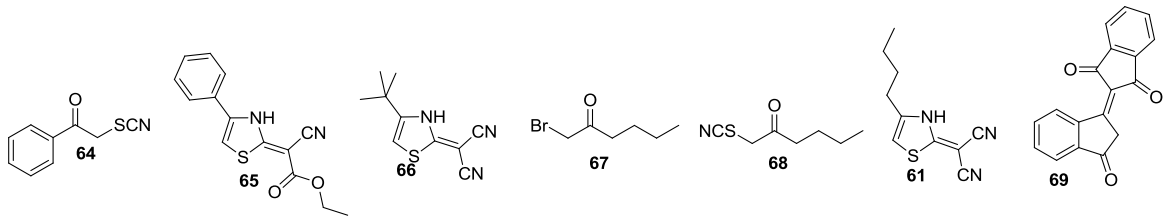

1-Phenyl-2-thiocyanato-ethanone 64

To a 300 mL ethanol solution of 2-bromo1-phenylethanone (15.0 g, 75.0 mmol) KSCN (7.35 g, 75.0 mmol) was added and the mixture heated to reflux for 3 h. Following a hot filtration, the mother liquor was cooled slowly to room temperature and the precipitate was filtered off. Washing with some cold ethanol and drying in vacuum yielded the product **3**. The reaction was carried out similar to reference 111. Yield 8.50 g (48.0 mmol, 64%). Mp = 74–75 °C. ^{1}H NMR ($CDCl_3$, 400 MHz): δ 7.94 (m, 2H), 7.67 (m, 1H), 7.54 (m, 2H), 4.74 (s, 2H). MS (EI): calcd for C_9H_7NOS: 177.0, found 177.0.

Cyano-(4-phenyl-5H-thiazol-2-ylidene)-acetic acid ethyl ester 65

A 17 mL DMF solution of 1-phenyl-2-thiocyanato-ethanone (10.0 g, 56.0 mmol) and cyano acetic acid ethyl ester (6.30 g, 56.0 mmol) was heated to 30 °C for 4 h prior to the addition of NEt_3 (16.6 g, 23 mL, 164 mmol) was added. After acidification with HOAc, the precipitate was filtered off, washed with water and dried under vacuum. The reaction was carried out similar to reference S112. Yield 14.2 g (52.0 mmol, 93%). Mp = 143–145 °C. ^{1}H NMR ($CDCl_3$, 400 MHz): δ 7.47 (m, 2H), 7.35 (m, 3H), 6.72 (s, 1H), 4.15 (q, ^3J = 7.1 Hz, 2H), 1.22 (t, ^3J = 7.1 Hz, 3H). MS (EI): calcd for $C_{14}H_{12}N_2O_2S$: 272.1, found 272.0.

2-(4-t*ert*-Butyl-5*H*-thiazol-2-ylidene)-malononitrile 66

To a 74 mL ethanol solution of 1-chloro-3,3-dimethyl-2-butanone (13.0 g, 97.0 mmol) NH_4SCN (7.30 g, 97.0 mmol) was added. The reaction mixture was heated to reflux for 4 h, before it was cooled down to room temperature. Then, malononitrile (6.38 g, 97.0 mmol) was added and the mixture was heated to 50 °C, before NEt_3 (9.85 g, 13.5 mL, 97.0 mmol) was added. Subsequently, the reaction was stirred at room temperature over night and was poured onto ice water. HOAc was added to acidify the mixture, before stirring for 1 h at room temperature. The precipitate was filtered off and washed with water. The reaction was carried out similar to reference S112. Yield 17.4 g (85.0 mmol, 87%). Mp = 265–268 °C. ^{1}H NMR ($CDCl_3$, 400 MHz): δ 6.15 (s, 1H), 1.20 (s, 9H). MS (EI): calcd for $C_{10}H_{11}N_3S$: 205.1, found 205.1.

1-Bromo-2-hexanone 67[113]

2-Hexanone (12.0 g, 0.12 mol, 14.5 mL) in 72 mL MeOH was cooled to -10 °C with a $CaCl_2 \times 6\,H_2O$ / ice frigorific mixture, before bromine (19.2 g, 0.12 mmol, 6.20 mL) was added slowly within 5 min. The mixture was first stirred at 0 °C for 45 min and then 45 min at 10 °C. The color of the solution changed from dark red to light yellow upon consumption of bromine. After 36 mL H_2O and 60 mL conc. H_2SO_4 (temperature control with ice bath!) were added, the reaction mixture was stirred over night at room temperature. The addition of 110 mL H_2O was followed by the extraction with diethylether (4 × 40 mL). The organic phases were combined and washed with 30 mL $NaHCO_3$ and twice with 30 mL H_2O. After removing the solvent under vacuum, the residue was distilled at 16 mbar at 75 °C. Yield 18.0 g (100 mmol, 90%). ^{1}H NMR ($CDCl_3$, 400 MHz): δ 3.93 (s, 2H), 2.62 (t, ^3J = 7.4 Hz, 2H), 1.59 (m, 2H), 1.32 (m, 2H), 0.90 (t, ^3J = 7.3 Hz, 3H).

1-Thiocyanato-2-hexanone 68

1-Bromo-2-hexanone (18.0 g, 100 mmol) and potassium thiocyanate (9.80 g, 0.10 mol) in 400 mL ethanol were heated under reflux for 3 h. After filtration of the hot solution, the solvent was removed under vacuum. The obtained orange oil was used directly in the next step. The reaction was carried out similar to reference S111. Yield 14.5 g (0.09 mmol, 92%). ^{1}H NMR ($CDCl_3$, 400 MHz): δ 4.02 (s, 2H), 2.56 (t, ^3J = 7.4 Hz, 2H), 1.61 (m, 2H), 1.34 (m, 2H), 0.91 (t, ^3J = 7.3 Hz, 3H).

2-(4-Butyl-5H-thiazol-2-ylidene)-malononitrile 61

1-Thiocyanato-2-hexanone (500 mg, 3.20 mmol) was mixed under argon atmosphere with 0.95 g of each dry triethylamine and DMF. Malononitrile (180 mg, 2.80 mmol) was added. After 3.5 h of stirring at room temperature, the mixture was poured onto 8 mL H_2O. The precipitate was filtrered off and dried under vacuum. The reaction was carried out similar to reference S112. Yield 570 mg (2.80 mmol, 87%). ^{1}H NMR ($CDCl_3$, 400 MHz): δ 11.08 (s, 1H), 6.20 (s, 1H), 2.54 (m, 2H), 1.62 (m, 2H), 1.39 (m, 2H), 0.96 (t, ^3J = 7.3 Hz, 3H). MS (MALDI-TOF, matrix: DCTB) calcd for $C_{10}H_{12}N_3S$: 206.1; found: 206.1.

[1,2']Biindenylidene-3,1'.3'-trione 69

A 24 mL dry ethanol solution of 1,3-indandione (2.04 g, 14.0 mmol) was stirred for 5 min, before NaOAc (1.53 g, 18.6 mmol) was added. After 1 h of stirring at room temperature, the reaction mixture was diluted with 50 mL of dest H_2O. The solution was then acidified with conc. HCl to a pH of ~1, the green precipitate was filtered off and dried under vacuum. The reaction was carried out similar to reference 82. Yield 2.54 g (9.26 mmol, 66%). Mp = 214–

215 °C. ^{1}H NMR ($CDCl_3$, 400 MHz): δ 9.68 (m, 1H), 8.03 (m, 1H), 7.97 (m, 2H), 7.86 (m, 1H), 7.82 (m, 2H), 7.75 (m, 1H), 4.17 (s, 2H). HRMS (ESI): calcd for $C_{18}H_{11}O_3$ $[M+H]^+$: 275.0703, found: 275.0704.

2-[2-(5-Dibutylamino-thiophen-2-yl-methylene)-3-oxo-indan-1-ylidene]-malononitrile EL86

A 1.0 mL Ac_2O solution of 5-dibutylamino-thiophene-2-carbaldehyde (239 mg, 1.00 mmol) and 2-(3-oxo-indan-1-ylidene)-malononitrile[82] (194 mg, 1.00 mmol) was heated to 90 °C for 1 h. After solvent removal, the product was isolated by column chromatography (CH_2Cl_2) and precipitation from CH_2Cl_2/*n*-hexane. Yield 320 mg (0.77 mmol, 77%). Mp = 201–202 °C. ^{1}H NMR (CD_2Cl_2, 400 MHz): δ 8.57 (s, 1H), 8.51 (m, 1H), 7.67 (m, 1H), 7.60 (m, 3H), 6.36 (d, ^3J = 5.1 Hz, 1H), 3.56 (m, 4H), 1.75 (m, 4H), 1.44 (m, 4H), 1.00 (t, ^3J = 7.3 Hz, 6H). UV-vis (CH_2Cl_2): λ_{max} (ε) = 580 (66200 M^{-1} cm^{-1}). HRMS (ESI): calcd for $C_{25}H_{25}N_3OS$ $[M]^+$: 415.1718, found: 415.1713. Elemental analysis (%) calcd for $C_{25}H_{25}N_3OS$: C, 72.26; H, 6.06; N, 10.11. Found: C, 72.40; H, 6.08; N, 10.12. CV data: $E_{1/2}^{ox}$ = 547 mV vs Fc, E_p^{red} = –1527 mV vs Fc.

2-[5-(5-Dibutylamino-thiophen-2-yl-methylene)-4-*n*-butyl-5*H*-thiazol-2-ylidene]-malononitrile HB432

A 1.1 mL Ac_2O solution of 5-dibutylamino-thiophene-2-carbaldehyde (256 mg, 1.07 mmol) and 2-(4-*n*-butyl-5*H*-thiazol-2-ylidene)-malononitrile (200 mg, 0.97 mmol) was heated to 90 °C for 30 min. The precipitate was filtered off and washed with *iso*-propanol and *n*-hexane, before it was recrystallized form *n*-hexane/CH_2Cl_2. Yield 236 mg (0.55 mmol, 57%). Mp = 162–165 °C. ^{1}H NMR (DMSO-d_6, 400 MHz): δ 8.69 (s, 0.1H), 8.35 (s, 1H), 8.26 (d, ^3J = 5.6 Hz, 0.1H), 7.98 (d, ^3J = 5.2 Hz, 1H), 7.34 (d, ^3J = 5.6 Hz, 0.1H), 6.95 (d, ^3J = 5.3 Hz, 1H), 3.77–3.85 (m, 0.4H), 3.68 (t, ^3J = 7.3 Hz, 4H), 3.03 (t, ^3J = 7.0 Hz, 0.2H), 2.85 (t, ^3J = 7.6 Hz, 2H), 1.66 (m, 6.6H), 1.36 (m, 6.6H), 0.92 (m, 9.9H). UV-vis (CH_2Cl_2): λ_{max} (ε) = 645 (130400 M^{-1} cm^{-1}). HRMS (ESI): calcd for $C_{23}H_{31}N_4S_2$ $[M]^+$: 426.1912, found: 426.1904. Elemental analysis (%) calcd for $C_{23}H_{30}N_4S_2$: C, 64.75; H, 7.09; N, 13.13; S, 15.03. Found: C, 64.39; H, 7.02; N, 13.09; S, 14.88. CV data: $E_{1/2}^{ox}$ = 371 mV vs Fc, E_p^{red} = –1348 mV vs Fc.

For **HB432** two isomers were determined by NMR spectroscopy. 2D NMR studies revealed that the main isomer with 90% is isomer A (Figure 24) and isomer B occurs with 10%.

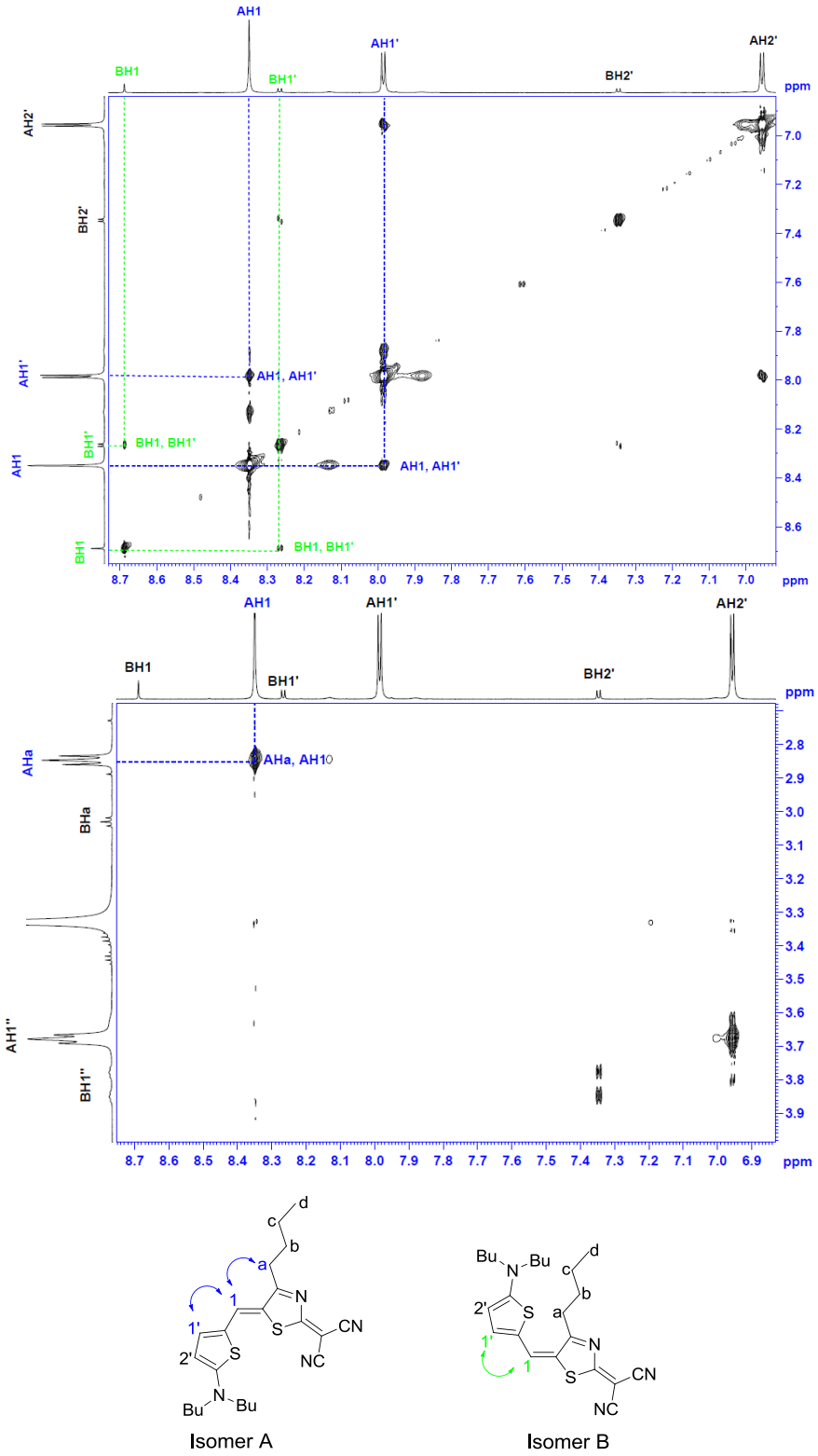

Figure 24. ROESY spectrum (600 MHz, DMSO-d_6, 298 K) of **HB432**. Both isomers A and B show NOE effects for protons H1 and H1'. Isomer A shows a *Z* configuration, which is confirmed by an additional NOE effect for H1 and Ha, whereas isomer B shows no NOE effect for H1 and Ha and displays therefore an *E* configuration.

2-[5-(5-Dibutylamino-thiophen-2-yl-methylene)-4-*tert*-butyl-5*H*-thiazol-2-ylidene]-malononitrile HB238

A 1.0 mL Ac_2O solution of 5-dibutylamino-thiophene-2-carbaldehyde (224 mg, 0.94 mmol) and 2-(4-*tert*-butyl-5*H*-thiazol-2-ylidene)-malononitrile (192 mg, 0.94 mmol) was heated to 90 °C for 30 min. The precipitate was filtered off and washed with *iso*-propanol and *n*-hexane. Yield 273 mg (0.64 mmol, 68%). Mp = 215–217 °C. ^{1}H NMR (CD_2Cl_2, 400 MHz): δ 8.06 (s, 1H), 7.50 (d, ^3J = 4.8 Hz, 1H), 6.30 (d, ^3J = 4.8 Hz, 1H), 3.51 (m, 4H), 1.72 (m, 4H), 1.52 (s, 9H), 1.41 (m, 4H), 0.99 (t, ^3J = 7.4 Hz, 6H). UV-vis (CH_2Cl_2): λ_{max} (ε) = 651 (143200 M^{-1} cm^{-1}). HRMS (ESI): calcd for $C_{23}H_{31}N_4S_2$ $[M+H]^+$: 427.1985, found: 427.1986. Elemental analysis (%) calcd for $C_{23}H_{30}N_4S_2$: C, 64.75; H, 7.09; N, 13.13; S, 15.03. Found: C, 64.84; H, 6.87; N, 13.11; S, 15.23. CV data: $E_{1/2}^{ox}$ = 369 mV vs Fc, E_p^{red} = –1392 mV vs Fc.

Cyano-[5-(5-dibutylamino-thiophen-2-yl-methylene)-4-phenyl-5*H*-thiazol-2-ylidene]-acetic acid ethyl ester MD357

A 6.0 mL Ac_2O solution of 5-dibutylamino-thiophene-2-carbaldehyde (1.44 g, 6.00 mmol) and cyano-(4-phenyl-5*H*-thiazol-2-ylidene)-acetic acid ethyl ester (1.63 g, 6.00 mmol) was heated to 70 °C for 1.5 h. The precipitate was filtered off and washed with *iso*-propanol and *n*-hexane. Yield 1.99 g (4.03 mmol, 67%). Mp = 151–152 °C. ^{1}H NMR ($CDCl_3$, 400 MHz): δ 7.75 (m, 2H), 7.67 (bs, 1H), 7.51 (m, 3H), 7.36 (bs, 1H), 6.19 (d, ^3J = 4.8 Hz, 1H), 4.34 (m, 2H), 3.46 (t, ^3J = 7.7 Hz, 4H), 1.70 (m, 4H), 1.41 (m, 7H), 0.99 (t, ^3J = 7.3 Hz, 6H). UV-vis (CH_2Cl_2): λ_{max} (ε) = 654 (130500 M^{-1} cm^{-1}). HRMS (ESI): calcd for $C_{27}H_{32}N_3O_2S_2$ $[M+H]^+$: 494.1930, found: 494.1929. Elemental analysis (%) calcd for $C_{27}H_{31}N_3O_2S_2$: C, 65.69; H, 6.33; N, 8.51; S, 12.99. Found: C, 65.15; H, 6.28; N, 8.35; S, 12.96. CV data: E_p^{ox} = 297 mV vs Fc, E_p^{red} = –1371 mV vs Fc.

2-(5-Dibutylamino-thiophen-2-yl-methylene)-[1,2']biindenylidene-3,1',3'-trione HB239

A 1.0 mL Ac_2O solution of 5-dibutylamino-thiophene-2-carbaldehyde (193 mg, 0.80 mmol) and [1,2']biindenylidene-3,1',3'-trione (221 mg, 0.80 mmol) was heated to 90 °C for 30 min. The precipitate was filtered off and washed with *iso*-propanol and *n*-hexane. The product was purified by column chromatography (CH_2Cl_2 with 0.5% MeOH). Yield 239 mg (0.48 mmol, 60%). Mp = 186–189 °C. ^{1}H NMR (CD_2Cl_2, 400 MHz): δ 8.37 (d, ^3J = 7.7 Hz, 1H), 8.02 (s, 1H), 7.79 (m, 2H), 7.66 (m, 2H), 7.59 (m, 2H), 7.48 (m, 2H), 6.31 (d, ^3J = 5.0 Hz, 1H), 3.49 (t, ^3J = 7.6 Hz, 4H), 1.75 (m, 4H), 1.43 (m, 4H), 0.92 (t, ^3J = 7.4 Hz, 6H). UV-vis (CH_2Cl_2): λ_{max} (ε) = 663 (47300 M^{-1} cm^{-1}). HRMS (ESI): calcd for $C_{31}H_{29}NO_3S$ $[M]^+$: 495.1868,

found: 495.1863. Elemental analysis (%) calcd for $C_{31}H_{29}NO_3S$: C, 75.12; H, 5.90; N, 2.83; S, 6.47. Found: C, 75.08; H, 5.94; N, 2.98; S, 6.59. CV data: E_p^{ox} = 458 mV vs Fc, $E_{1/2}^{red}$ = –1292 mV vs Fc.

3.6 Appendix

Cyclic voltammograms

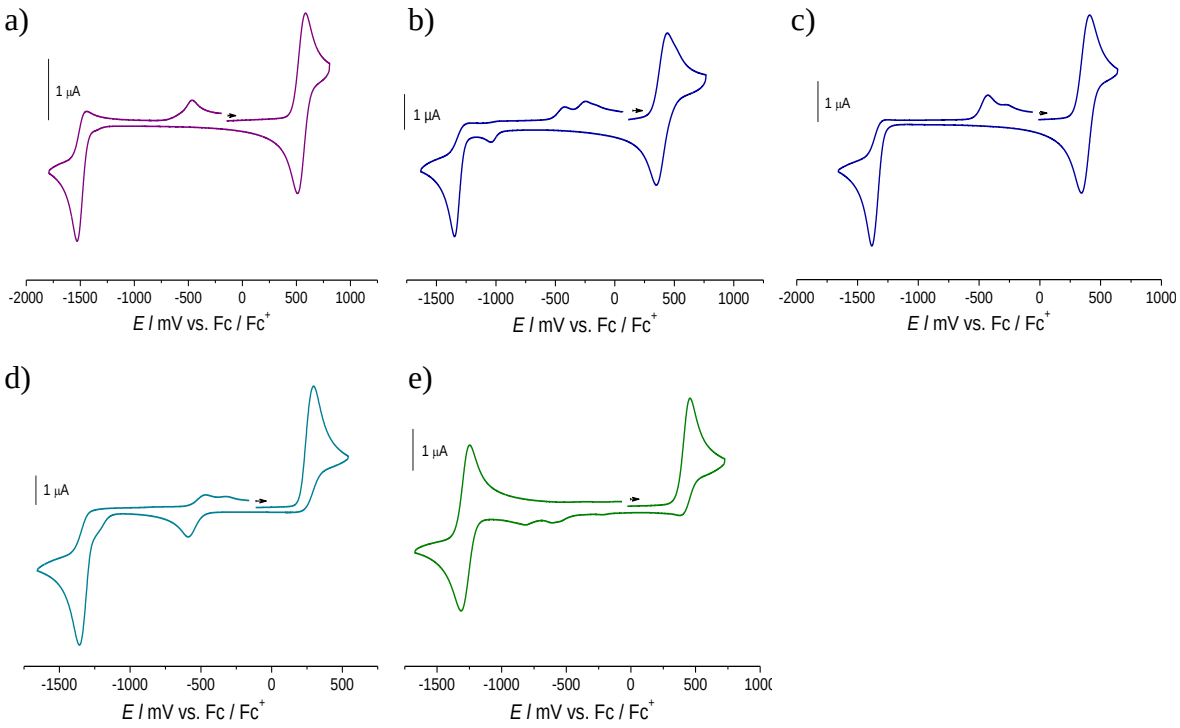

Figure 25. Cyclic voltammogram of a) **EL86**. b) **HB432**. c) **HB238**. d) **MD357**. e) **HB239** (10^{-4} M, CH_2Cl_2, calibrated against the Fc/Fc^+ couple, scan rate 100 mV s^{-1}; supporting electrolyte TBAHFP (0.1 M)).

Electro-optical absorption measurements

Table 12. Optical and electrical properties of merocyanine dyes **MD333**, **EL86**, **HB238**, **HB432**, **MD357** and **HB239** determined by analysis of their UV-vis and EOA spectra measured in 1,4-dioxane at 298 K.

	λ_{max} (nm)	ε_{max} (L mol^{-1} cm^{-1})	μ_{eg} (D)	μ_g [a] (D)	$\Delta\mu$ [a] (D)	c^2
MD333	536	99700	8.2	12.6 ± 0.3	1.7 ± 0.2	0.448 ± 0.007
EL86	576	76500	9.8	8.6 ± 0.1	4.1 ± 0.1	0.397 ± 0.003
HB238	650	85500	9.9	13.1 ± 0.7	2.5 ± 0.7	0.438 ± 0.018
HB432	644	85800	9.9	13.2 ± 0.7	2.0 ± 0.9	0.448 ± 0.021
MD357	653	86200	9.8	12.1 ± 0.6	2.3 ± 0.7	0.442 ± 0.018
HB239	660	52000	8.7	6.1 ± 0.1	4.6 ± 0.2	0.372 ± 0.005

[a] The solvent effect was corrected according to the Onsager's continuum model[114] to the vacuum state.

The linear combinations $L_p = 6\,[L(\lambda, 0°) - 3\,L(\lambda, 90°)]$ is proportional to the square of μ_g (Figure 26: $L_p \sim (\mu_g)^2$). Notably, the wave number independence of L_p ensures that only homogeneously polarized spectral regions were used for the evaluation of the molecular properties from the EOA spectra.

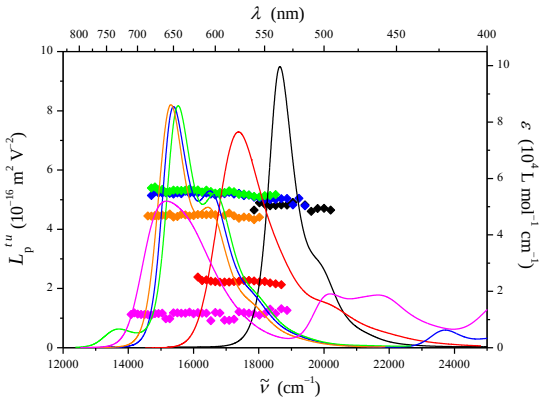

Figure 26. UV-vis spectra (solid line) and the linear combination L_p (symbol) of merocyanine dyes **MD333** (black), **EL86** (red), **HB238** (blue), **HB432** (green), **MD357** (orange) and **HB239** (magenta) measured in 1,4-dioxane at 298 K.

Chapter 4

Near-Infrared Absorbing Merocyanine Dyes for Bulk Heterojunction Solar Cells*

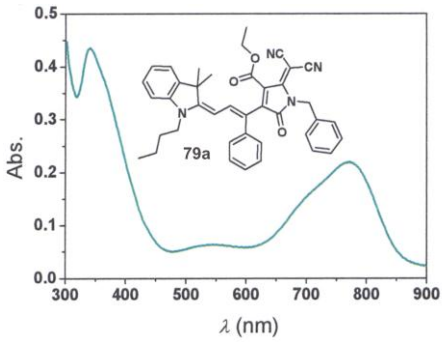

79a:$PC_{61}BM$ (25/75wt%)

Abstract: A series of near-infrared absorbing merocyanine dyes bearing the strong electron accepting 2-oxo-5-dicyanomethylene-pyrrolidine unit was synthesized and applied in combination with $PC_{61}BM$ and $PC_{71}BM$ in solution-processed photoactive layers of bulk heterojunction solar cells, exhibiting a remarkable performance range with power conversion efficiencies from 0.01 to 1.00%.

* This chapter was published by: Bürckstümmer, H.; Kronenberg, M. N.; Meerholz, K.; Würthner, F. *Org. Lett.* **2010**, *12*, 3666–3669. Reproduced with permission from American Chemical Society.
Solar cell devices were built by N. M. Kronenberg (University of Köln). Synthetic support was given by M. Kaiser and cyclic voltammetry by A.-M. Krause (University of Würzburg).

4.1 Introduction

Merocyanine dyes represent a traditional class of chromophores with a general structural feature consisting of an electron donating and an electron accepting moiety that are connected by a polymethine chain. Their unique dipolar and polarizability properties enable applications in nonlinear optics and as photorefractive materials.[7,100,115] The absorption wavelengths as well as band gaps of these chromophores are easily tunable by variation of the chain length and the donor and acceptor groups.[7,100,115] These features in combination with their high tinctorial strengths add up to materials well-suited for implementation in organic photovoltaics. Recently, we have shown the application of merocyanine dyes as donors in solution-processed and vapor-deposited bulk heterojunction (BHJ) organic solar cells in combination with a fullerene as an acceptor.[4,102] Moreover, merocyanine dyes have been used in dye-sensitized solar cells (also called Graetzel cells).[9]

In the field of solution-processed BHJ organic solar cells, great attention has been paid particularly to the combination of the polymeric donor poly(3-hexylthiophene) (P3HT) and the electron accepting fullerene derivative $PC_{61}BM$ with enormous research efforts on the optimization of structural features such as regioregularity of the P3HT polymer and the morphology of the active BHJ layer by post-treatment of the devices.[21] More recently, in order to improve the absorption properties and harvest more photons, low-bandgap polymers have been developed and very high power conversion efficiencies (PCEs) exceeding 7% have been achieved.[76,97,116] Another recent strategy towards BHJ solar cells is based on substitution of the polymeric donor by small molecules whose monodispersity enables facile synthesis and convenient optimization of the absorption and redox properties. In the last years, increasingly promising results were reported with various types of dyes such as oligothiophene,[25,41] squaraine,[56,57] cyanine,[117] BODIPY,[64] diketopyrrolopyrrole (DPP),[52-53] indigoid,[60] acene[35] and dibenzo[*b*,*def*]chrysene,[38] leading to PCEs up to 4.4%.[53]

The photon flux of sun light displays a maximum at ~690 nm (1.8 eV).[118] Thus, to achieve an ideal spectral overlap of the absorption of solar cells with the solar irradiation, materials with absorption reaching in the near-infrared (NIR) are required.[119] Moreover, photovoltaics with NIR absorption render transparent solar cells for sun shading and solar power window applications possible.[120] Here, we report the synthesis and characterization of the optical, electrochemical and photovoltaic properties of a series of new merocyanine (MC) dyes containing the strong electron acceptor moiety 2-oxo-5-dicyanomethylene-pyrrolidine **62** (Scheme 3), which imparts absorption of the MC dyes in the NIR.[121] Application of the

present merocyanine chromophores in solution-processed solar cells based on blends with $PC_{71}BM$ yielded devices with PCEs of up to 1%.

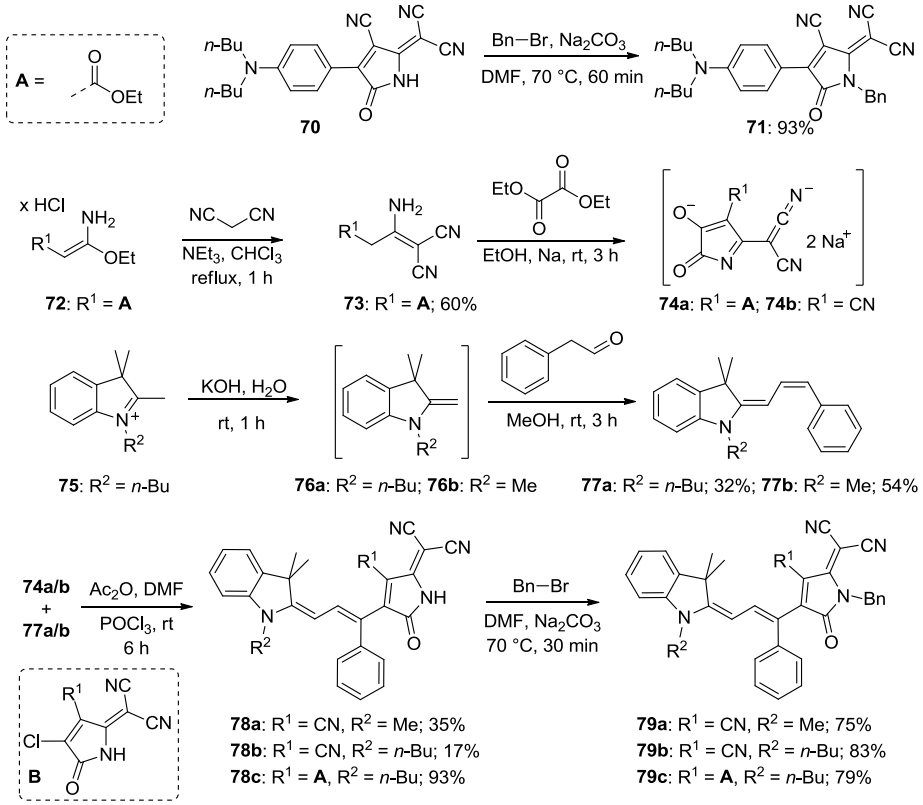

Scheme 3. Syntheses of the merocyanine dyes **59** and **67a**–**c**.

4.2 Results and discussion

The reference chromophore **71** consisting of an aniline donor and the heterocyclic acceptor that are directly connected was synthesized by the alkylation of **70**[122] with benzyl bromide in a high yield of 93% (Scheme 3). The synthesis of more extended merocyanine dyes **79a**–**c** involves three major sequences: the syntheses of the acceptor and the donor moieties and the condensation of these two moieties into the desired chromophores. The synthesis of the acceptor **74a** starts with the reaction of enolate **72** with malononitrile in the presence of triethylamine as a base to afford the intermediate **73** in 60% yield.[123] The subsequent condensation reaction of **73** with diethyl oxalate under basic conditions resulted in the acceptor **74a**,[124] which exhibits poor solubility and thus was used in the further reaction as obtained. The donor component **77a** was built up by deprotonation of indolenine **75** ("Fischer base")[125] followed by condensation with phenylacetaldehyde in methanol.[126] The two-step reaction afforded **77a** in a rather poor yield of 32%. A higher yield of 54% was obtained for the methyl derivative **77b** by condensation of the commercially available indolenine **76b** with phenylacetaldehyde.[126] The coupling of the donor and acceptor moieties comprises the in-situ

generation of component **B** by chlorination and protonation of the dianionic acceptor **74**, followed by addition of component **77** to **B** leading to elimination of one equivalent HCl to result in chromophores **78a**–**c**. A high yield of 93% was obtained in the case of **78c,** while the dyes **78a**,**b** resulting from acceptor **74b**[124] were obtained in significantly lower yields of 17–35%. The final step involving the alkylation of the secondary amine **78** with benzyl bromide afforded the dyes **79a**–**c** in 79–83% yield.

Figure 27 displays the UV-vis spectra and the cyclic voltammograms of reference **71** and merocyanine dye **79a** in CH_2Cl_2. Further data along with those of dyes **79b**,**c** are listed in Table 14. The HOMO levels were derived from the half-wave oxidation potentials determined by cyclic voltammetry (CV), whereas the LUMO energies are calculated by the equation: $E_{LUMO}=E_{HOMO}+(hc/\lambda_{max})$. All of these dyes possess one oxidation and two reduction waves, both processes being fully reversible (Figure 27).

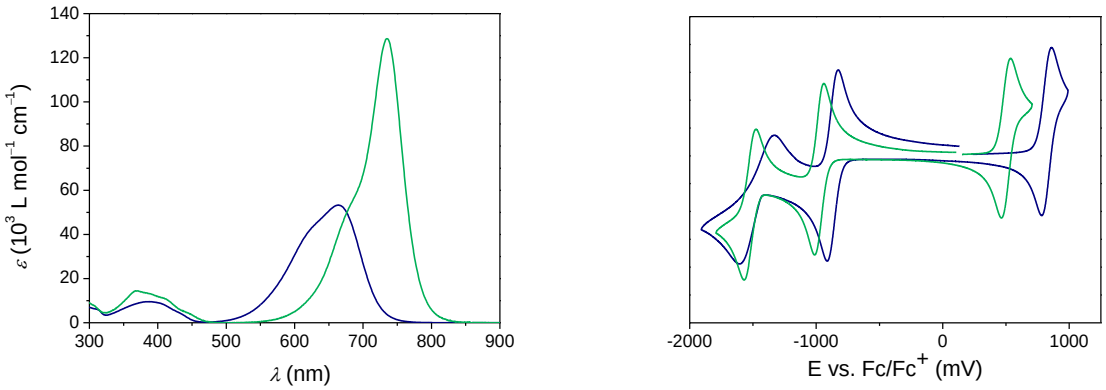

Figure 27. UV-vis absorption spectra (left, 2×10^{-5} M, CH_2Cl_2) and cyclic voltammograms (right, CH_2Cl_2, calibrated against Fc/Fc^+ couple) of **71** (blue line) and **79a** (green line).

Chromophore **71** exhibits an absorption maximum at 664 nm with a molar extinction coefficient of 53300 M^{-1} cm^{-1}. The rather low tinctorial strength and the broad absorption band indicate a more polyene-like character of this dye.[127] Notably, **71** shows very low-lying HOMO and LUMO levels at –5.98 eV and –4.11 eV, respectively. Dyes **79a** and **79b** with extended π-systems differ only by the alkyl substituent (Me vs. *n*-Bu) at the donor unit and show a bathochromic shift of the absorption maxima of 70 nm compared with that of **79** and sharp cyanine-like absorption bands with high extinction coefficients of 121800–128600 M^{-1} cm^{-1}. Their HOMO levels range at –5.65 eV, while their LUMOs are situated at energies around –3.96 eV. Replacement of the cyano substituent R^1 at the oxo-pyrrolidino acceptor unit by an ethyl ester group in compound **79c** results in a shift of both HOMO and LUMO levels by 0.18 eV to higher energies compared to those of **79a**,**b**, but without any alteration of the absorption features.

The presented dyes were characterized in solution-processed BHJ solar cell devices with the general structure: ITO/PEDOT:PSS (~40 nm)/dye : $PC_{61}BM$ (25/75% by weight; ~ 50 nm)/Al (120 nm). The details for device fabrication are given in section 4.4.1. The photovoltaic characteristics of the solar cells are presented in Table 13.

Table 13. Optical and Electrochemical Properties of **71** and **79a**–**c** and Photovoltaic Characteristics of BHJ Solar Cell Devices Containing a MC Dye:$PC_{61}BM$ Blend.

MC dye	**71**	**79a**	**79b**	**79c**	**79c**[e]
λ_{max} (nm)[a]	664	735	738	736	
ε (M^{-1} cm^{-1})[a]	53300	128600	121800	87400	
λ_{max} (nm)[b]	640	783	783	771	
E_{HOMO} (eV)[c]	–5.98	–5.65	–5.66	–5.48	
E_{LUMO} (eV)[d]	–4.11	–3.96	–3.98	–3.80	
wt% PCBM	70	70	75	75	75
V_{OC} (V)	0.55	0.71	0.74	0.64	0.66
J_{SC} (mA cm^{-2})	0.05	2.28	2.00	3.33	4.83
FF	0.31	0.28	0.29	0.31	0.31
PCE (%)	0.01	0.46	0.43	0.66	1.00

[a] UV-vis measurements in CH_2Cl_2. [b] UV-vis measurements of a thin film of the blend. [c] From CV measurements ($E_{1/2}^{ox}$) in CH_2Cl_2 calibrated against ferrocene/ferrocenium couple (Fc/Fc^+, –5.15 eV) as internal standard. [d] $E_{LUMO} = E_{HOMO} + (hc/\lambda_{max})$. [e] Solar cell with $PC_{71}BM$ as acceptor.

For the device of reference **71** a very low PCE of 0.01% was observed. This low efficiency arises from the small short-circuit photocurrent (J_{SC}) of 50 µA cm^{-2} which is very likely caused by a lack of driving force for charge-carrier separation owing to the low LUMO level of –4.11 eV. The latter energy level is not sufficiently high for electron injection into the LUMO level of the $PC_{61}BM$ acceptor (–4.08 eV, Figure 28).

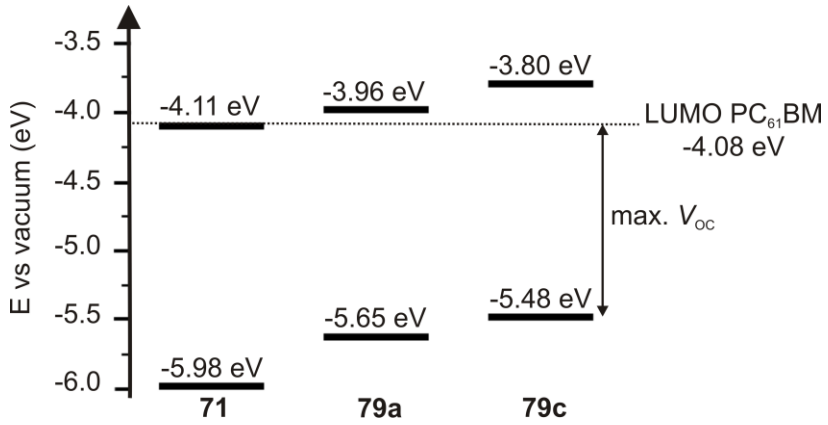

Figure 28. Illustration of the HOMO and LUMO energies of dyes **71**, **79a** and **79c** in comparison with the LUMO energy of $PC_{61}BM$.

The introduction of the indolenine donor group in merocyanine dyes lead to the extension of the π-system and entailed better matched HOMO levels for the dyes **79a**–**c**. Moreover, these dyes afforded solar cells with absorption in the NIR region, and thus enabling the production of devices that are transparent in the visible range (Figure 29).

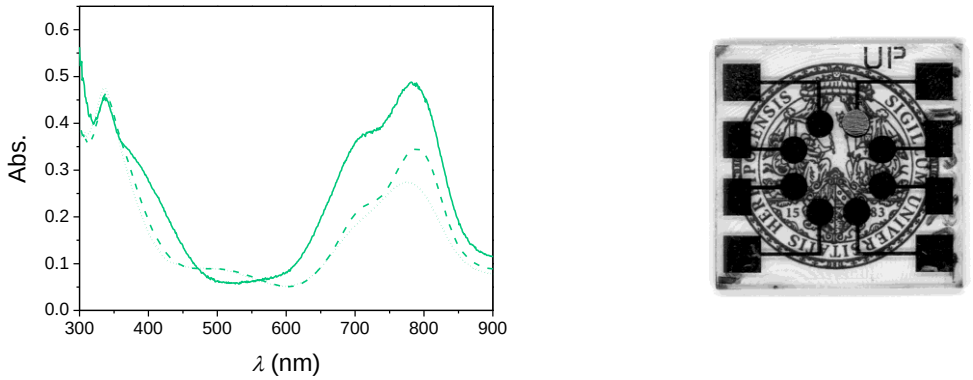

Figure 29. Left: UV-vis thin film absorption spectra of dye:$PC_{61}BM$ blends (25/75% by weight) of **79a** (solid line), **79b** (dashed line) and **79c** (dotted line). Right: Picture of a transparent device containing a blend of **79c**:$PC_{61}BM$ (25/75wt%) lying on the seal of the Universität Würzburg.

The devices built with **79a**–**c** exhibit appreciable open-circuit voltage (V_{OC}) values of 0.64–0.74 V, in particular, if we consider their low bandgap. The observed fill factors (FF) of 0.3 are typical for solution-processed MC-based solar cells.[99,102] Devices containing **79a** and **79b**, whose chromophores solely differ by the side chains, displayed similar J_{SC} of 2.28 and 2.00 mA cm^{-2}, respectively, and PCEs of 0.43–0.46%. Though their LUMO energies are still quite similar to the LUMO of $PC_{61}BM$, imparting a driving force of only ~0.1 eV for electron transfer according to the solution data (which may, however, shift in the solid state).[4] In the literature, an offset of 0.3–0.4 eV is proposed as tradeoff between sufficient driving force and minimized energy loss upon charge injection.[19] To increase the LUMO energy level, we have synthesized dye **79c** which bears a slightly weaker acceptor moiety owing to the replacement of one cyano group by an ester group. Actually, both frontier molecular orbitals of **79c** are shifted to higher energies by 0.18 eV compared to those of dyes **79a**,**b** (Table 1). While the higher-lying HOMO of dye **79c** leads to a lowering of V_{OC} of the respective solar cell (0.64 V) relative to the cells fabricated with **79a** (0.71 V), the increased LUMO confers a stronger driving force for electron transfer from the MC to the fullerene and, thus, enhances the J_{SC} values by 46%, resulting in an overall performance of 0.7% for **79c**.

The high symmetry of $PC_{61}BM$ renders forbidden low-energy optical transitions and results in only weak absorption in the visible spectral region. For this reason $PC_{71}BM$ has been applied in BHJ solar cells as its lower degree of symmetry affords an improved absorbance in

the visible range.[20b,128] Thus, we have built devices containing a spin-coated **79c**:$PC_{71}BM$ (25/75% by weight) blend. Upon changing the acceptor material, the fill factor and the V_{OC} were not altered but the photocurrent is increased by 45%, reaching a value of 4.83 mA cm^{-2} and a PCE of 1% (Table 13). The EQE characteristics emphasize that the enhanced absorption of $PC_{71}BM$ especially in the range of 400–600 nm, is the origin of this significant improvement (Figure 30).

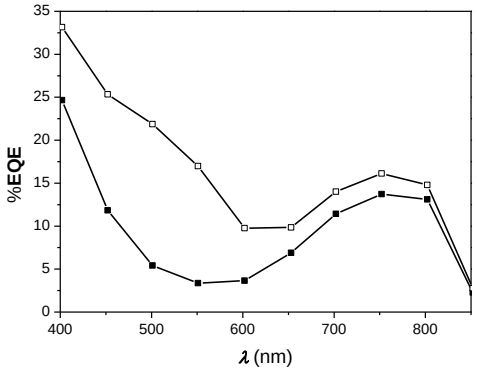

Figure 30. EQE characteristics of devices containing blends of **79c** with $PC_{61}BM$ (filled squares) and $PC_{71}BM$ (empty squares) (each 75wt% PCBM).

4.3 Conclusion

In summary, a series of novel functional merocyanine chromophores is presented that feature NIR absorption for bulk heterojunction solar cells. Upon optimizing the electronic properties, dye **79c** was obtained whose HOMO and LUMO levels are well-suited for application in organic solar cells with PCBM fullerenes as electron accepting materials. Solar cells fabricated with the newly synthesized merocyanine dyes afford appreciably high open-circuit voltages of up to 0.74 V despite the low bandgap and maximum power conversion efficiency of 1.0%. Due to their absorption in the NIR region, these merocyanine dyes are promising materials for solar power windows or sun shading technologies as well as for tandem cell devices.

4.4 Experimental section

4.4.1 Materials and methods

Solvents and reagents were obtained from commercial sources and purified and dried according to standard procedures.[107] Ethyl-3-ethoxy-3-imino-propionate hydrochloride, phenylacetaldehyde, malononitrile, diethyl oxalate, 1,3,3-trimethyl-2-methyleneindoline, $PC_{61}BM$ and $PC_{71}BM$ were purchased from commercial sources.

Column chromatography was performed with commercial glass columns using silica gel (particle size 0.063–0.2 mm) as stationary phase. ^{1}H NMR spectra were recorded with a 400 MHz spectrometer using the residual solvent peaks as internal standard. Coupling constants are given in Hz. UV-vis spectra were measured on a conventional spectrophotometer equipped with temperature controllers. Cyclic voltammetry (CV) was performed on a standard commercial electrochemical analyzer (EC epsilon; BAS Instrument, UK) in a three electrode single-compartment cell under argon. Dichloromethane (HPLC grade) was dried over calcium hydride and degassed prior to use. The supporting electrolyte tetrabutylammonium hexafluorophosphate (TBAHFP) was synthesized according to literature[90] and recrystallized from ethanol/water and dried in high vacuum. The measurements were carried out under exclusion of air and moisture at a concentration of 10^{-4} M with ferrocene as an internal standard for the calibration of the potential. Working electrode: Pt disc; reference electrode: Ag/AgCl; auxiliary electrode: Pt wire.

Device fabrication. All solar cell devices were fabricated on commercial indium tin oxide (ITO) coated glass. The ITO was etched with acid and subsequently cleaned using chloroform, acetone, mucasol detergent and deionized water in ultrasonic bath. Next, the ITO substrates were exposed to ozone for 20 min and immediately coated with poly(3,4-ethylene dioxythiophene):poly(styrene sulfonate) (PEDOT:PSS) (Baytron P AL 4083, HC Starck; ca. 40 nm) from aqueous solution. Afterwards the samples were heat treated for 2 min at 110 °C to remove residual water and stored in a N_2 glove box. The active layers were spin-coated from chlorobenzene containing the mixture of the merocyanine dye and PCBM using a concentration of 20 mg mL^{-1}.

The substrates were transferred to a high-vacuum chamber where the top electrode (120 nm Al) was evaporated through a mask, resulting in seven solar cells on each substrate with an active area of 0.08 cm^2 each (see Figure 29 right). The *JV* characteristics of the solar cells were measured using a Keithley 2425 source measurement unit. The AM1.5 light was provided by a filtered Xe-lamp. The intensity of 100 mW cm^{-2} of the AM1.5 light was determined using a calibrated inorganic solar cell from the Fraunhofer Institute for solar research in Freiburg (Germany) and a reference $PC_{61}BM$:P3HT cell measured by the same institution. No spectral mismatch factor was included in the calculation of the efficiency. A Dektak surface profiler (Veeco) was used to determine the active layer thickness, which was 50 ± 5 nm for the present layers. UV-vis spectra were taken with a Varian Cary 50 spectrometer. EQE measurements were performed by filtering the Xe lamp using Melles

Griot interference filters with an FWHM of 10 nm. The power of the filtered light was measured using an Optical Power Meter (Newport, Model 1830 C).

4.4.2 Synthetic procedures and characterization

2-[1-Benzyl-3-cyano-5-oxo-4-(4-dibutylamino-phenyl)-1,5-dihydro-pyrrol-2-ylidene]-malononitrile 71

A 50 mL DMF solution of 2-[3-cyano-4-(4-dibutylamino-phenyl)-5-oxo-1,5-dihydro-pyrrol-2-ylidene]-malononitrile **70**[122] (934 mg, 2.50 mmol) and Na_2CO_3 (132 mg, 1.25 mmol) was heated to 70 °C under argon atmosphere, before benzyl bromide (0.36 mL, 513 mg, 3.00 mmol) was added. After 1 h, the solvent was removed under vacuum and the product was purified by column chromatography (CH_2Cl_2) and subsequent precipitation from CH_2Cl_2/*n*-hexane. Yield 1.08 g (2.33 mmol, 93%). Mp. 174–176 °C. ^{1}H NMR (CD_2Cl_2, 400 MHz): δ 8.54 (m, 2H), 7.35 (m, 3H), 7.17 (m, 2H), 6.81 (m, 2H), 5.35 (s, 2H), 3.48 (m, 4H), 1.67 (m, 4H), 1.41 (m, 4H), 0.99 (t, ^3J = 7.4, 3H). ^{13}C NMR (CD_2Cl_2, 101 MHz): δ 168.2 (C), 156.3 (C), 154.1 (C), 142.3 (C), 135.4 (C), 134.3 (CH), 129.5 (CH), 128.6 (CH), 127.0 (CH), 116.5 (C), 114.7 (C), 113.9 (C), 113.6 (CH), 112.4 (C), 94.7 (C), 51.9 (CH_2), 45.0 (CH_2), 30.2 (CH_2), 20.8 (CH_2), 14.2 (CH_3). UV-vis (CH_2Cl_2): λ_{max} (ε) = 665 (53800 M^{-1} cm^{-1}). HRMS (ESI): calcd for $C_{29}H_{29}N_5O$ $[M]^+$: 463.2372, found: 463.2377. Elemental analysis (%) calcd for $C_{29}H_{29}N_5O$: C 75.14, H 6.31, N 15.11; found: C 75.37, H 6.46, N 15.21. CV data: $E_{1/2}^{ox}$ = 826 mV vs Fc, $E_{1/2}^{red}$ = –851 mV vs Fc, $E_{1/2}^{red}$ = –1417 mV vs Fc.

3-Amino-4,4-dicyano-but-3-enoic acid ethyl ester 73[123]

A 77 mL $CHCl_3$ solution of ethyl-3-ethoxy-3-imino-propionate hydrochloride **72** (15.0 g, 76.7 mmol), malononitrile (5.06 g, 76.7 mmol) and triethylamine (7.74 g, 76.7 mmol) was refluxed for 1 h. The cooled reaction mixture was extracted with water, before the solvent was removed under vacuum to give the product as light brown oil. Yield 8.31 g (46.4 mmol, 60%). ^{1}H NMR ($CDCl_3$, 400 MHz): δ 7.49 (bs, 1H), 6.56 (bs, 1H), 4.26 (q, ^3J = 7.1, 2H), 3.61 (s, 2H), 1.32 (t, ^3J = 7.1 Hz, 3H). MS (EI) calcd for $C_8H_9N_3O_2$: 179.1; found: 179.1.

1-Butyl-3,3-dimethyl-2-(3-phenyl-allylidene)-2,3-dihydro-1*H*-indole 77a

1-Butyl-2,3,3-trimethyl-3H-indolium iodide **75**[125] (12.5 g, 36.0 mmol) was stirred in a 50 mL KOH solution (1 M) for 1 h and the reaction mixture was extracted with CH_2Cl_2, the solvent removed under vacuum and the crude product dried under vacuum. After adding 10 mL MeOH, phenylacetaldehyde (1.60 g, 133 mmol) in 10 mL MeOH were added and the mixture was stirred at room temperature for 3 h. The solvent was removed under vacuum, followed

by column chromatography (CH_2Cl_2), which yielded the desired product. Due to a fast degradation, the product was immediately used in the next reaction. The first step was carried out according to the procedure reported in reference 129 and the second step according to reference 126. Yield 3.68 g (11.6 mmol, 32%). ^{1}H NMR ($CDCl_3$, 400 MHz): δ 7.29–7.40 (m, 5H), 7.15 (m, 3H), 6.80 (m, 1H), 6.59 (d, ^3J = 7.7, 1H), 6.30 (d, ^3J = 14.9, 1H), 5.47 (d, ^3J = 11.7, 1H), 3.60 (t, ^3J = 7.5, 2H), 1.67 (m, 8H), 1.45 (m, 2H), 1.01 (t, ^3J = 7.4, 3H). HRMS (ESI): calcd for $C_{23}H_{27}N$ $[M]^+$: 317.2143, found: 317.2138.

1,3,3-Trimethyl-2-(3-phenyl-allylidene)-2,3-dihydro-1*H*-indole 77b[126]

To 1,3,3-trimethyl-2-methylene-2,3-dihydro-1*H*-indole **76b** (2.60 g, 15.0 mmol) in 20 mL MeOH, phenylacetaldehyde (2.40 g, 20.0 mmol) in 10 mL MeOH were added and the mixture stirred at room temperature for 3 h. After removal of the solvent, the subsequent column chromatography (*n*-hexane:CH_2Cl_2=9:1) afforded the desired product. Due to a fast degradation, the product was immediately used in the next reaction. Yield 2.24 g (8.10 mmol, 54%). ^{1}H NMR ($CDCl_3$, 400 MHz): δ 7.27–7.37 (m, 5H), 7.13 (m, 3H), 6.81 (m, 1H), 6.58 (d, ^3J = 7.9, 1H), 6.30 (d, ^3J = 15.1, 1H), 5.43 (d, ^3J = 11.3, 1H), 3.13 (s, 3H), 1.64 (s, 6H). HRMS (ESI): calcd for $C_{20}H_{21}N$ $[M]^+$: 276.1674, found: 276.1670.

2{3-Cyano-5-oxo-4-[1-phenyl-3-(1,3,3-trimethyl-1,3-dihydro-indol-2-ylidene)-propenyl]-1,5-dihydro-pyrrol-2-ylidene}-malononitrile 78a

A 17 mL DMF solution of Ac_2O (0.37 mL, 3.40 mmol), 1,3,3-trimethyl-2-(3-phenyl-allylidene)-2,3-dihydro-1*H*-indole **77b** (1.40 g, 5.00 mmol) and compound **74b**[124] (767 mg, 3.40 mmol) was cooled to 0 °C and $POCl_3$ (1.50 g, 10.0 mmol) was added slowly in 30 min. The reaction was stirred at room temperature for 6 h and afterwards poured into ice water. The precipitate was filtered off, washed with water and dried under vacuum. The product was purified by column chromatography (CH_2Cl_2 with 5% MeOH) and precipitation from CH_2Cl_2/*n*-hexane. Yield 525 mg (1.20 mmol, 35%). Mp. 324–327 °C. ^{1}H NMR (CD_2Cl_2, 400 MHz): δ 9.62 (d, ^3J = 14.3, 1H), 7.90 (s, 1H), 7.50 (m, 3H), 7.45 (m, 2H), 7.31 (m, 3H), 7.12 (d, ^3J = 7.9, 1H), 5.83 (d, ^3J = 14.2, 1H), 3.34 (s, 3H), 1.75 (s, 6H). ^{13}C NMR (CD_2Cl_2, 101 MHz): δ 176.6 (C), 167.7 (C), 158.2 (C), 149.4 (CH), 142.4 (C), 142.2 (C), 141.0 (C), 135.4 (C), 131.2 (CH), 129.5 (C), 129.34 (CH), 129.27 (CH), 126.7 (CH), 123.0 (CH), 115.1 (C), 112.8 (C), 111.5 (CH), 104.9 (CH), 50.6 (C), 31.9 (CH_3), 28.2 (CH_3). HRMS (ESI): calcd for $C_{28}H_{21}N_5NaO$ $[M+Na]^+$: 466.1638, found: 466.1637.

2{3-Cyano-5-oxo-4-[1-phenyl-3-(1-butyl-3,3-dimethyl-1,3-dihydro-indol-2-ylidene)-propenyl]-1,5-dihydro-pyrrol-2-ylidene}-malononitrile 78b

A 7.5 mL DMF solution of Ac_2O (0.17 mL, 1.50 mmol), 1-butyl-3,3-dimethyl-2-(3-phenyl-allylidene)-2,3-dihydro-1*H*-indole **77a** (700 mg, 2.20 mmol) and compound **74b**[124] (345 mg, 1.50 mmol) was cooled to 0 °C and $POCl_3$ (660 mg, 4.40 mmol) was added slowly in 30 min. The reaction mixture was stirred at room temperature for 6 h and afterwards poured into ice water. The precipitate was filtered off, washed with water and dried under vacuum. The product was purified by column chromatography (CH_2Cl_2) and subsequent precipitation from CH_2Cl_2/*n*-hexane. Yield 123 mg (0.25 mmol, 17%). Mp. 289–292 °C. ^{1}H NMR ($CDCl_3$, 400 MHz): δ 9.58 (d, ^3J = 14.2, 1H), 7.81 (s, 1H), 7.48 (m, 3H), 7.39 (m, 3H), 7.29 (m, 2H), 7.05 (d, ^3J = 7.9, 1H), 5.78 (d, ^3J = 14.1, 1H), 3.68 (m, 2H), 1.75 (s, 6H), 1.57 (m, 2H), 1.21 (m, 2H), 0.82 (t, ^3J = 7.4, 3H). ^{13}C NMR (101 MHz, CD_2Cl_2): δ 175.8 (C), 168.4 (C), 158.8 (C), 149.2 (CH), 142.4 (C), 142.3 (C), 140.7 (C), 135.5 (C), 131.1 (CH), 129.4 (C), 129.2 (CH), 129.1 (CH), 126.6 (CH), 123.1 (CH), 115.3 (C), 113.2 (C), 111.6 (CH), 105.4 (CH), 50.5 (C), 44.9 (CH_2), 29.8 (CH_2), 28.2 (CH_3), 20.5 (CH_2), 13.8 (CH_3). HRMS (ESI)*:* calcd for $C_{31}H_{27}N_5O$ $[M]^+$: 485.2216, found: 485.2209.

4-[3-(1-Butyl-3,3-dimethyl-1,3-dihydro-indol-2-ylidene)-1-phenyl-propenyl]-2-dicyanomethylene-5-oxo-2,5-dihydro-1*H*-pyrrole-3-carboxylic acid ethyl ester 78c

Natrium (180 mg, 7.90 mmol) in small pieces was dissolved in 2.5 mL absolute EtOH. After cooling to 0 °C, 3-amino-4,4-dicyano-but-3-enoic acid ethyl ester **73** (510 mg, 2.80 mmol) and diethyl oxalate (0.53 mL, 575 mg, 4.00 mmol) were added. The mixture was kept for 3 h at room temperature and after that 130 g benzene was added. The precipitate was filtered off and dried under vacuum and directly used for the next step. A 17 mL DMF solution of Ac_2O (0.37 mL, 3.40 mmol), 1-butyl-3,3-dimethyl-2-(3-phenyl-allylidene)-2,3-dihydro-1*H*-indole **77a** (1.60 g, 5.00 mmol) and compound **74a** (765 mg, 2.80 mmol) was cooled to 0 °C and $POCl_3$ (1.50 g, 10.0 mmol) was added slowly in 30 min. The reaction was stirred at room temperature for 6 h and then it was poured into ice water. The precipitate was filtered off, washed with water and dried under vacuum. The product was purified by column chromatography (CH_2Cl_2 with 2% MeOH) and subsequent precipitation from CH_2Cl_2/*n*-hexane. Yield 1.40 g (2.60 mmol, 93%). Mp. 254–256 °C. ^{1}H NMR ($CDCl_3$, 400 MHz): δ 9.2 (d, ^3J = 13.6, 1H), 7.72 (s, 1H), 7.28–7.43 (m, 5H), 7.23 (m, 2H), 7.13 (m, 1H), 6.87 (d, ^3J = 7.9, 1H), 5.53 (d, ^3J = 13.8, 1H), 3.55 (m, 2H and q, ^3J = 7.2, 2H), 1.71 (s, 6H), 1.51 (m, 2H), 1.20 (m, 2H), 1.10 (t, ^3J = 7.2, 3H), 0.81 (t, ^3J = 7.4, 3H). ^{13}C NMR (CD_2Cl_2, 101 MHz):

δ 171.1 (C), 169.0 (C), 163.4 (C), 157.7 (C), 145.9 (CH), 143.2 (C), 141.5 (C), 137.6 (C), 136.6 (C), 131.1 (CH), 128.9 (CH), 128.8 (CH), 128.4 (CH), 126.4 (C), 124.4 (CH), 122.8 (CH), 114.9 (C), 114.6 (C), 113.2 (C), 109.9 (CH), 100.9 (CH), 62.0 (CH_2), 49.1 (C), 43.9 (CH_2), 29.4 (CH_2), 28.5 (CH_3), 20.6 (CH_2), 13.9 (CH_3), 13.8 (CH_3). HRMS (ESI)*:* calcd for $C_{33}H_{32}N_4O_3$ $[M]^+$: 532.2474, found: 532.2470.

2-{1-Benzyl-3-cyano-5-oxo-4-[1-phenyl-3-(1,3,3-trimethyl-1,3-dihydro-indol-2-ylidene)-propenyl]-1,5-dihydro-pyrrol-2-ylidene}-malononitrile 79a

A 7.0 mL DMF solution of 2-{4-[3-(1-methyl-3,3-dimethyl-1,3-dihydro-indol-2-ylidene-1-phenyl-propenyl]-3-cyano-5-oxo-1,5-dihydro-pyrrol-2-ylidene-malononitrile **78a** (150 mg, 0.34 mmol) and Na_2CO_3 (18 mg, 0.17 mmol) was heated to 70 °C under argon atmosphere and benzyl bromide (70 mg, 0.41 mmol, 50 μL) was added. After 30 min, the solvent was removed and the crude product was purified by column chromatography (CH_2Cl_2) and subsequent precipitation from CH_2Cl_2/*n*-hexane. Yield 135 mg (0.25 mmol, 75%). Mp. 266–268 °C. ^{1}H NMR ($CDCl_3$, 400 MHz): δ 9.58 (d, ^3J = 14.2, 1H), 7.49 (m, 3H), 7.38 (m, 4H), 7.30 (m, 4H), 7.21 (m, 2H), 7.03 (m, 1H), 5.76 (d, ^3J = 14.0, 1H), 5.38 (s, 2H), 3.02 (s, 3H), 1.75 (s, 6H). ^{13}C NMR (CD_2Cl_2, 101 MHz): δ 175.9 (C), 168.8 (C), 157.8 (C), 149.2 (CH), 143.0 (C), 142.0 (C), 139.5 (C), 136.2 (C), 135.6 (C), 131.2 (CH), 129.3 (CH), 129.3 (CH), 129.23 (CH), 129.20 (CH), 128.3 (CH), 126.8 (CH), 126.4 (CH), 122.9 (CH), 115.7 (C), 113.9 (C), 111.3 (CH), 104.5 (CH), 50.3 (C), 44.8 (CH_2), 31.7 (CH_3), 28.3 (CH_3). UV-vis (CH_2Cl_2): λ_{max} (ε) = 735 (124800 M^{-1} cm^{-1}). HRMS (ESI): calcd for $C_{35}H_{27}N_5NaO$ $[M+Na]^+$: 556.2108, found: 556.2119. Elemental analysis (%) calcd for $C_{35}H_{27}N_5O$: C 78.78, H 5.10, N 13.12; found: C 78.34, H 5.43, N 12.68. CV data: $E_{1/2}^{ox}$ = 500 mV vs Fc, $E_{1/2}^{red}$ = –975 mV vs Fc, $E_{1/2}^{red}$ = –1517 mV vs Fc.

2-{1-Benzyl-3-cyano-5-oxo-4-[1-phenyl-3-(1-butyl-3,3-dimethyl-1,3-dihydro-indol-2-ylidene)-propenyl]-1,5-dihydro-pyrrol-2-ylidene}-malononitrile 79b

A 2.5 mL DMF solution of 2-{4-[3-(1-butyl-3,3-dimethyl-1,3-dihydro-indol-2-ylidene-1-phenyl-propenyl]-3-cyano-5-oxo-1,5-dihydro-pyrrol-2-ylidene-malononotrile **78b** (60 mg, 0.12 mmol) and Na_2CO_3 (7.0 mg, 66 μmol) was heated to 70 °C under argon atmosphere and benzyl bromide (26 mg, 0.15 mmol) was added. After 30 min of stirring at 70 °C, the solvent was evaporated and the crude product was purified by column chromatography (CH_2Cl_2 with 10% MeOH) and subsequent precipitation from CH_2Cl_2/*n*-hexane. Yield 57 mg (99 μmol, 83%). Mp. 256–258 °C. ^{1}H NMR (CD_2Cl_2, 400 MHz): δ 9.63 (d, ^3J = 14.1, 1H), 7.50 (m, 3H), 7.27–7.43 (m, 8H), 7.21 (m, 2H), 7.08 (d, ^3J = 7.9, 1H), 5.82 (d, ^3J = 14.2, 1H), 5.36 (s,

2H), 3.69 (t, ^3J = 7.3, 2H), 1.74 (s, 6H), 1.55 (m, 2H), 1.22 (m, 2H), 0.82 (t, ^3J = 7.3, 3H). ^{13}C NMR (CD_2Cl_2, 101 MHz): δ 175.6 (C), 168.7 (C), 157.8 (C), 149.1 (CH), 142.27 (C), 142.26 (C), 138.8 (C), 136.2 (C), 135.6 (C), 131.2 (CH), 129.4 (CH), 129.3 (CH), 129.2 (CH), 129.1 (CH), 128.1 (CH), 126.8 (CH), 126.6 (CH), 123.0 (CH), 115.9 (C), 114.1 (C), 111.7 (CH), 105.5 (CH), 50.4 (C), 44.9 (CH_2), 44.7 (CH_2), 29.8 (CH_2), 28.2 (CH_3), 20.5 (CH_2), 13.8 (CH_3). UV-vis (CH_2Cl_2): λ_{max} (ε) = 739 (143000 M^{-1} cm^{-1}). HRMS (ESI): calcd for $C_{38}H_{34}N_5O$ $[M+H]^+$: 576.2758, found: 576.2758. Elemental analysis (%) calcd for $C_{38}H_{33}N_5O$: C 79.28, H 5.78, N 12.16; found: C 79.00, H 5.72, N 12.16. CV data: $E_{1/2}^{ox}$ = 511 mV vs Fc, $E_{1/2}^{red}$ = –999 mV vs Fc, $E_{1/2}^{red}$ = –1537 mV vs Fc.

1-Benzyl-4-[3-(1-butyl-3,3-dimethyl-1,3-dihydro-indol-2-ylidene)-1-phenyl-propenyl]-2-dicyanomethylene-5-oxo-2,5-dihydro-1*H*-pyrrole-3-carboxylic-acid ethyl ester 79c

A 20 mL DMF solution of 4-[3-(1-butyl-3,3-dimethyl-1,3-dihydro-indol-2-ylidene)-1-phenyl-propenyl]-2-dicyanomethylene-5-oxo-2,5-dihydro-1H-pyrrole-3-carboxylic acid ethyl ester **78c** (500 mg, 0.94 mmol) and Na_2CO_3 (50 mg, 0.47 mmol) was heated to 70 °C under argon atmosphere and benzyl bromide (193 mg, 1.13 mmol) was added. After 30 min, the solvent was removed and the crude product was purified by column chromatography (CH_2Cl_2) and subsequent precipitation from CH_2Cl_2/*n*-hexane. Yield 460 mg (0.74 mmol, 79%). Mp. 204–205 °C. ^{1}H NMR ($CDCl_3$, 400 MHz): δ 9.21 (d, ^3J = 13.5, 1H), 7.40 (m, 5H), 7.27 (m, 7H), 7.08 (t, ^3J = 7.3, 1H), 6.81 (d, ^3J = 8.1, 1H), 5.40 (d, ^3J = 13.1, 1H), 5.37 (s, 2H), 3.49 (m, 4H), 1.70 (s, 6H), 1.47 (m, 2H), 1.18 (m, 2H), 1.10 (t, ^3J = 7.2, 3H), 0.80 (t, ^3J = 7.4, 3H). ^{13}C NMR (101 MHz, CD_2Cl_2): δ 170.1 (C), 169.8 (C), 164.1 (C), 157.4 (C), 145.0 (CH), 136.5 (C), 136.4 (C), 134.9 (C), 131.4 (CH), 129.3 (CH), 128.8 (CH), 128.7 (CH), 128.4 (CH), 128.2 (CH), 126.9 (CH), 126.0 (C), 123.9 (CH), 122.7 (CH), 115.3 (C), 114.2 (C), 109.5 (CH), 100.3 (CH), 62.2 (CH_2), 56.9 (C), 53.5 (C), 48.7 (C), 44.6 (CH_2), 43.7 (CH_2), 29.3 (CH_2), 28.6 (CH_3), 20.7 (CH_2), 13.9 (CH_3), 13.7 (CH_3). UV-vis (CH_2Cl_2): λ_{max} (ε) = 736 (86400 M^{-1} cm^{-1}). HRMS (ESI)*:* calcd for $C_{40}H_{38}N_4O_3$ $[M]^+$: 622.2944, found: 622.2938. Elemental analysis (%) calcd for $C_{40}H_{38}N_4O_3$: C 77.15, H 6.15, N 9.00; found: C 76.93, H 6.14, N 8.99. CV data: $E_{1/2}^{ox}$ = 335 mV vs Fc, $E_{1/2}^{red}$ = –1123 mV vs Fc, $E_{1/2}^{red}$ = –1629 mV vs Fc.

Chapter 5

Structure-property relationships for merocyanine dyes and their application in BHJ organic solar cells

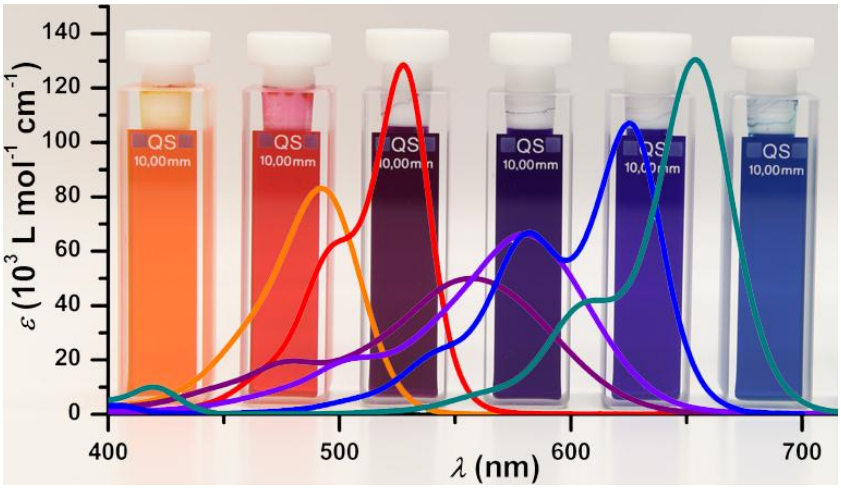

Abstract: The synthesis and complete characterization of a comprehensive series of merocyanine dyes is reported. As small soluble molecules, they offer the advantages of facile synthesis and purification, high tinctorial strength and monodispersity. By carefully modifying the electronic structure of the dyes, the absorption as well as the electrochemical properties are adjustable. Application of blends comprising MC dyes as electron donor material and fullerene derivatives as electron acceptor enables the fabrication of efficient solution-processed bulk heterojunction (BHJ) solar cells. Evaluation of the molecular properties of the chromophores in correlation with the respective solar cell characteristics resulted in a set of design rules for producing auspicious chromophores for organic solar cells. The most promising device with an open-circuit voltage (V_{OC}) of 0.99 V and a power conversion efficiency (PCE) of 3.3% is among the most efficient solution-processed BHJ solar cells containing only small soluble molecules.*

* Solar cell devices were built by N. M. Kronenberg and M. Lenze (University of Köln). Electro-optical absorption measurements were performed by Dr. M. Stolte and cyclic voltammetry by A.-M. Krause; synthetic support was given by Dr. E. Tulyakova (**EL**), M. Kaiser (**MD**) and P. Seufert-Baumbach (University of Würzburg).

5.1 Introduction

In chapter 5, a library of merocyanine dyes consisting of six dye series is presented and correlations are drawn between the structure and the molecular properties of the chromophores and the solar cell characteristics. After a short presentation of the synthesis in section 5.2.1, sections 5.2.2 and 5.2.3 provide an overview on the molecular properties of the dye series and their performance in photovoltaic cells. In the following section 5.3 a discussion of the prevailing correlations mainly on the basis of scatter plots is presented. Individual correlations are highlighted exemplarily. In section 5.2.2 and the following, the reported compounds are classified according to the following color code to allow a better overview:

- **Black** represents dyes, which result in non-efficient solar cells exhibiting PCEs of less than 0.5%.
- **Blue** marks chromophores, which yield solar devices with PCEs in the range of 0.5–1.3%.
- The color **red** highlights the best-performing dyes with PCEs of more than 1.3%.
- Chromophores marked in **grey** produced inhomogeneous films during solar cell processing mostly originated by low solubility and therefore ambiguous results. Consequently, their solar cell results are only listed in Table 17 and were not included in the discussion.

In each chart and table the chromophores are arranged corresponding to the absorption maxima in dichloromethane solution, starting with the absorption at the shortest wavelength. The important acceptor and donor units used to generate the reported merocyanine dyes are displayed below.

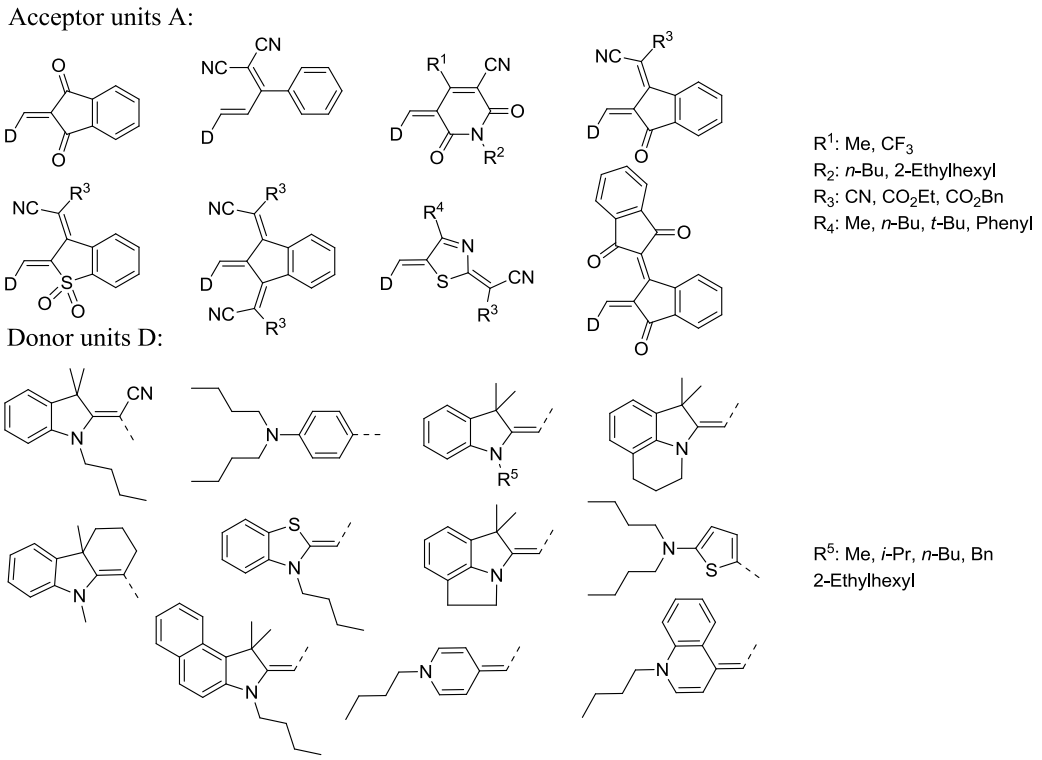

5.2 Results

5.2.1 Synthesis

Scheme 4 outlines three synthetic routes, which were applied to obtain the merocyanine dyes investigated in this work by using the examples of **EL85**, **MD347** and **HB193**. In most cases, the chromophores were obtained by a Knoevenagel condensation like in the case of **EL85**, where the CH-acidic acceptor compound **58** was combined with aldehyde **80** in acetic anhydride. After 60 min at 90°C a nearly complete consumption of the starting materials was achieved and the product isolated with good yield of 67%. Both the reaction time and yield are typical for most of the presented merocyanine dyes. For some donor compounds like quinoline or pyridine, the generation of the corresponding aldehyde was not feasible. Therefore, the pyridone **59** was first converted to the enamine in a mixture of DMF in Ac_2O, before 3-ethyl-2-methylquinolinium iodide **81** and one equivalent of base (e. g. NEt_3) were added.[83] The yield for this type of reaction depends strongly on the used donor compound. In the case of **MD347** a high yield of 90% could be obtained, whereas the coupling of the ethylpyridinium donor for example resulted in a low yield of 26% for **MD577** (for structure see Chart 7). For the coupling of indolenine **54a** with the indandione acceptor **58**, a third strategy was advantageous. Here, a three-component condensation reaction of the donor **54a** and acceptor compound **58** occurred in the presence of triethyl orthoformate yielding the dye

HB193 with a yield of 19%.[83,130] All synthesized dyes were characterized by ^{1}H-NMR, HRMS, UV-vis spectroscopy and mostly cyclic voltammetry (CV) and elemental analysis. Details concerning the synthesis and structural characterization are given in section 5.5.3.

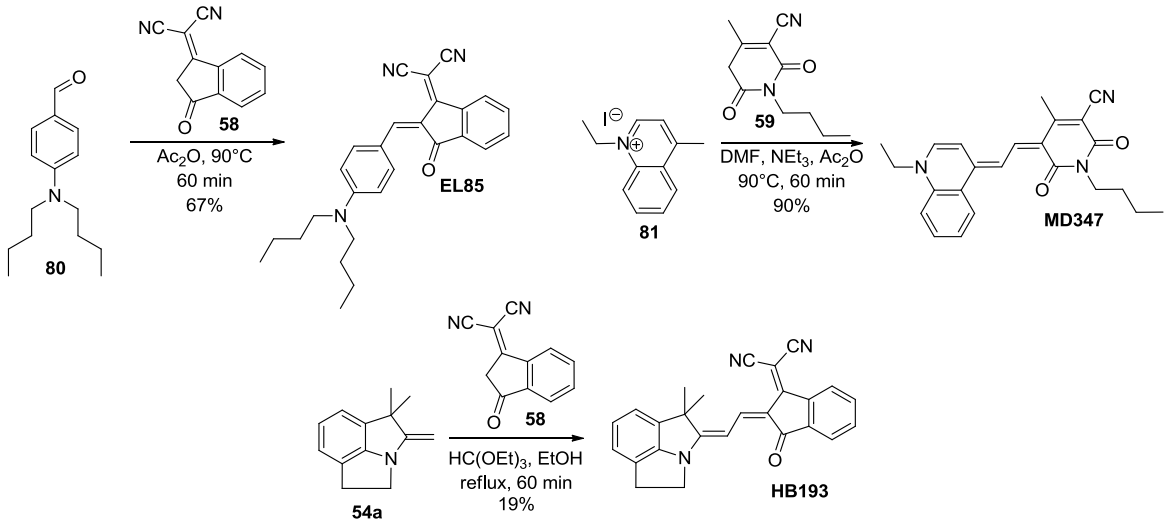

Scheme 4. Exemplary syntheses of three investigated MC dyes.

5.2.2 Optical and electrochemical properties

Figure 31 displays the UV-vis spectra of representative merocyanine dyes investigated in this work. The diagram illustrates that absorption over the whole visible range with absorption maxima (λ_{max}) from 490–660 nm was realized with the studied chromophores, displaying intense $\pi\pi^*$ transitions with charge-transfer character. In the past, an evaluation of this character by the resonance parameter c^2 was established, which allows the classification of donor-π-acceptor chromophores such as merocyanine dyes from polyene-type ($c^2 \approx 0$) via cyanine-type (*cyanine limit*, $c^2 \approx 0.5$) to betaine-type molecules ($c^2 \approx 1$).[7,100] In the case of $c^2 \approx 0$, the ground state of the respective chromophore is governed by the neutral resonance structure, whereas the ground state of the betaine-type is characterized by the zwitterionic resonance structure. In the *cyanine limit*, both ground and excited state are equally described by the neutral and the zwitterionic resonance structure, resulting in minimized reorganization upon excitation. In merocyanine dyes, the character of the push-pull system is reflected by the UV-vis spectra: polyene-like dyes exhibit broad absorption bands with lower absorption coefficients like aniline **EL79** (Chart 4), whereas cyanine-like dyes show sharp absorption bands with intense absorption like indolenine **MD319** (Chart 8). The majority of the presented dyes show narrow absorption bands pointing to the prevalence of cyanine-like chromophores (Figure 31). The figure $\mu^2_{ag}\ M^{-1}$, which we defined as absorption density, represents the transition dipole moment μ^2_{ag} divided by the molecular weight M of the

compound and is correlated with the tinctorial strength of the respective chromophore. For application in solar cells a chromophore ideally exhibits a small molecular mass, but high absorbance, creating a high optical density in thin films.

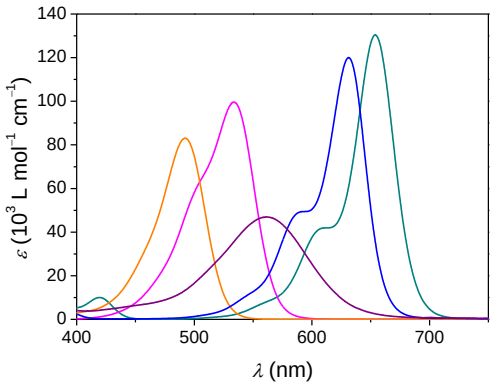

Figure 31. UV-vis spectra of **HB249** (orange), **HB312** (pink), **EL79** (magenta), **MD319** (blue) and **MD357** (blue-green) in CH_2Cl_2 (2×10^{-5} M, 25 °C).

The first investigated series, which is called in the following ***series In1*** is depicted in Chart 3. Table 14 and 15 compile all optical, electrochemical, electro-optical and solubility properties of the presented dyes. The HOMO levels based on irreversible oxidation potentials are calculated from the peak potentials (E_p) and marked with an asterisk (*) in Table 14 and 15, whereas the HOMO values based on reversible oxidation waves are calculated from the half-wave potentials ($E_{1/2}^{ox}$). The indandione acceptor is one of the weakest presented in this work and was combined with compounds of varying donor strength to give dyes with colors in dichloromethane from orange (**HB249**, λ_{max} = 492 nm) to blue (**EL44**, λ_{max} = 596 nm). For a survey of donor and acceptor strengths of various heterocycles, see references 7 and 100. The dyes show mostly sharp absorption bands, pointing to cyanine-type dyes. Their absorption densities $\mu^2_{ag}\, M^{-1}$ are located in a high range of 0.21 – 0.37 D^2 mol g^{-1}. Solely chromophore **HB249** bearing an aniline as donor unit represents a dye with a rather polyene-like π-system and exhibits a broad absorption band with relatively low absorption coefficient,[127] but nevertheless a $\mu^2_{ag}\, M^{-1}$ of 0.23 D^2 mol g^{-1}. This dye also displays the absorption maximum at the shortest wavelength of 492 nm, but a HOMO level at relatively low energy of –5.74 eV. In this series, the HOMO levels range from –5.76 eV to –5.35 eV, whereas the LUMOs are located at rather high energies of –3.05 eV to –3.33 eV. As expected, the HOMO levels of the dyes are significantly more affected by the variation of the donor component than the LUMO energies.

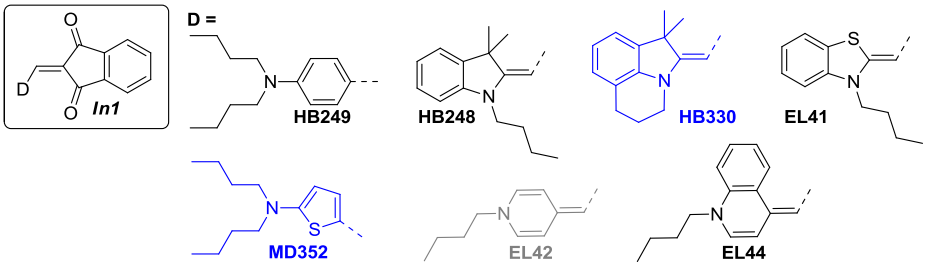

Chart 3. Chemical structures of ***series In1***

Chart 4 displays the chemical structures of the ***indandione series In2***. The acceptor strength of ***In2*** is increased compared to ***In1*** by the condensation of indandione with malononitrile, which afforded mostly systems close to the *cyanine limit* and violet color. In this series the substitution pattern of the indolenine (Fischer base) donor was extensively varied, which barely influenced the absorption or the electrochemical properties. The absorption bands of indolenine based chromophores are usually centered at 576 nm with absorption densities of 0.21–0.24 D^2 mol g^{-1}, the HOMO as well as the LUMO levels are situated at pretty low energies of –5.85 eV to –5.71 eV and –3.68 eV to –3.53 eV, respectively. The introduction of an additional cyano group in **HB276** led to a significant blue shift of the absorption maximum to 537 nm and shift of both FMO levels to lower energies.

Table 14. Optical, electro-optical, solubility and electrochemical properties of ***series In1–3*** and ***M***.

MC dye	λ_{max} (nm)[a]	ε (L mol^{-1} cm^{-1})	$\mu^2_{ag}\,M^{-1}$ (D^2 mol g^{-1})	c^2 [b]	μ_g [b] (D)	Solubility (g/L)	E_{HOMO} (eV)[c]	E_{LUMO} (eV)[d]
			Series In1					
HB249	492	83200	0.23	0.26	4.0	10.6	–5.74	–3.22
HB248	496	114600	0.25	/	/	10.8	–5.76*	–3.26
HB330	500	111200	0.27	/	/	8.6	–5.68*	–3.20
EL41	510	115400	0.21	/	/	/	–5.66*	–3.23
MD352	517	121900	0.22	0.39[131]	5.7[131]	27.2	–5.56*	–3.17
EL42	539	146900	0.32	/	/	/	–5.35*	–3.05
EL44	596	202800	0.37	/	/	2.3	–5.41*	–3.33
			Series In2					
HB276	537	38200	0.13	/	/	/	–6.21	–3.90
HB391	545	34800	0.14	/	/	/	–6.12	–3.84
EL79	562	47000	0.18	0.17	3.1	13.0	–5.85	–3.65
EL85	570	69500	0.25	0.24	5.9	/	–5.81	–3.64
HB345	572	72400	0.23	/	/	3.9	–5.82	–3.65
HB329	572	70600	0.21	/	/	2.7	–5.85	–3.68
HB280	574	25800	0.13	/	/	/	–5.69	–3.53
MD518	575	64000	0.24	/	/	/	–5.80	–3.64
MD376	576	66400	0.23	0.40	6.2	27.0	–5.80	–3.65
MD504	577	59000	0.18	/	/	/	–5.82	–3.66
HB374	577	65600	0.27	/	/	/	/	/
HB194	578	60300	0.24	0.40	6.7	3.0	–5.75	–3.60
HB366	578	64500	0.24	/	/	/	/	/
EL18	579	52400	0.20	/	/	1.8	–5.76*	–3.62
EL86	580	66200	0.23	0.40	8.6	2.5	–5.70	–3.56
HB193	586	51100	0.24	0.42	6.3	5.5	–5.71	–3.59
EL54	594	31900	0.11	/	/	8.4	–5.77	–3.68
			Series In3					
HB218	653	47400	0.13	/	/	2.2	–5.73*	–3.83
HB077	655	43600	0.14	0.36	4.2	6.2	–5.68*	–3.79
HB096	660	48000	0.13	/	/	/	–5.70*	–3.83
HB094	660	48300	0.14	0.36	4.4	/	–5.70*	–3.82
HB239	663	47300	0.15	0.37	6.1	17.3	–5.61*	–3.74
HB257	665	46500	0.14	/	/	4.6	–5.65*	–3.79
HB342	669	35400	0.11	/	/	/	–5.62*	–3.77
			Series M					
MD342	490	57100	0.27	0.49	6.7	6.0	–5.77	–3.24
MD344	506	90900	0.18	/	/	37.2	–5.70*	–3.25
HB312	533	99700	0.28	0.32	9.4	11.0	–5.57	–3.24
MD564	557	50000	0.19	/	/	/	–5.71*	–3.48
HB209	566	44900	0.13	0.32	4.7	/	–5.72	–3.53
HB095	571	49300	0.14	/	/	47.0	–5.68	–3.51
HB092	573	48900	0.15	/	/	/	–5.68	–3.51
MD426	580	60300	0.19	/	/	1.1	–5.89	–3.76
HB244	596	37900	0.12	0.32	4.7	/	–5.85*	–3.76
HB204	597	44800	0.14	/	/	/	–5.84*	–3.77
HB205	604	47000	0.13	/	/	/	–5.87*	–3.81
HB208	599	81700	0.19	/	/	/	–5.85	–3.78
HB091	603	58000	0.19	/	/	5.8	–5.97	–3.92
HB093	603	88000	0.19	/	/	/	–5.97	–3.91
MD519	641	33800	0.14	/	/	5.6	–5.78	–3.85

[a] UV-vis measurements for dilute solution (~10^{-5} M) in CH_2Cl_2. [b] Determined by electro-optic measurements. [c] Calculated from CV measurements ($E_{1/2}^{ox}$/*E_p) in CH_2Cl_2 calibrated against the ferrocene/ferrocenium couple (Fc/Fc^+, –5.15 eV) as internal standard. [d] $E_{LUMO} = E_{HOMO} + (hc/\lambda_{max})$.

Table 15. Optical, electro-optical, solubility and electrochemical properties of ***series Py***, ***Th***, **DPP(TBFu)$_2$** and P3HT.

MC dye	λ_{max} (nm)[a]	ε (L mol^{-1} cm^{-1})	$\mu^2_{ag}\,M^{-1}$ (D^2 mol g^{-1})	c^2 [b]	μ_g [b] (D)	Solubility (g/L)	E_{HOMO} (eV)[c]	E_{LUMO} (eV)[d]
			Series Py					
MD346	527	122000	0.25	/	/	5.7	–5.82	–3.47
MD353	528	129900	0.25	/	/	4.9	–5.82	–3.47
HB331	529	133500	0.26	/	/	/	–5.76	–3.42
MD343	535	78700	0.24	0.28[132]	10.8[132]	46.9	–5.77	–3.45
HB340	537	117400	0.26	0.46	11.8	3.5	–5.71	–3.40
MD324	538	84000	0.17	0.39[132]	10.1[132]	31.8	–5.91	–3.61
HB236	540	159700	0.23	0.45[133]	14.2[133]	/	–5.65	–3.36
HB136	541	120100	0.18	/	/	/	–6.00	–3.67
MD347	618	111500	0.27	0.56[132]	16.2[132]	0.6	–5.48*	–3.48
MD305	527	124800	0.22	/	/	166	–5.81	–3.46
MD301	528	129700	0.22	/	/	17.6	–5.82	–3.47
MD333	542	149400	0.20	0.45	12.6	4.2	–5.65	–3.36
MD577	549	114600	0.26	/	/	5.0	–5.43*	–3.17
MD330	617	120500	0.25	0.56	15.7	2.3	–5.47*	–3.46
			Series Th					
EL31	594	115000	0.25	/	/	/	–5.51	–3.42
EL84	620	62200	0.22	/	/	2.8	–5.71	–3.71
HB347	624	116100	0.30	/	/	1.3	–5.59	–3.60
HB231	624	128500	0.27	/	/	0.3	–5.58	–3.60
MD530	624	131000	0.28	/	/	/	–5.58	–3.59
MD304	625	107000	0.24	0.44	12.5	3.2	–5.61	–3.62
HB356	624	95500	0.20	/	/	/	–5.63	–3.65
HB247	626	124000	0.24	/	/	/	/	/
HB255	627	146100	0.28	/	/	1.1	–5.53	–3.55
EL32	631	120000	0.24	0.51	15.0	/	–5.54*	–3.57
EL53	640	65600	0.12	0.44	13.7	3.6	–5.56	–3.62
EL30	640	61000	0.19	/	/	/	–5.28*	–3.34
HB238	651	142200	0.24	0.44	13.1	6.3	–5.52	–3.61
MD499	654	117300	0.22	/	/	4.4	–5.43	–3.53
HB277	605	65800	0.22	/	/	/	–5.89	–3.84
MD319	632	112000	0.25	/	/	2.3	–5.62	–3.66
MD303	635	105700	0.23	/	/	0.6	–5.63	–3.68
HB256	635	123200	0.27	/	/	0.7	–5.56	–3.61
MD323	643	86000	0.25	0.28[91b]	12.3[91b]	7.1	–5.75	–3.82
MD356	659	131100	0.23	/	/	1.3	–5.56	–3.68
MD565	626	74000	0.21	/	/	13.4	–5.64*	–3.66
HB101	627	106000	0.22	/	/	6.1	–5.57*	–3.60
MD372	625	114700	0.25	/	/	/	–5.53*	–3.55
MD375	627	116700	0.23	/	/	5.2	–5.54*	–3.56
EL38	635	56800	0.12	/	/	/	–5.47*	–3.52
MD357	654	130500	0.21	0.44	12.1	4.5	–5.45*	–3.55
MD321	647	67000	0.14	/	/	/	–5.46	–3.54
HB364	616	133000	0.29	/	/	/	–5.62	–3.61
HB281	627	112000	0.27	/	/	/	–5.39	–3.41
HB075	626	116800	0.21	/	/	/	–5.56*	–3.58
DPP (TBFu)$_2$	628	62700	0.14	/	/	/	–5.56	–3.59
P3HT	449	/	0.14	/	/	/	–5.6*	–2.8

[a] UV-vis measurements for dilute solution (~10^{-5} M) in CH_2Cl_2. [b] Determined by electro-optic measurements. [c] Calculated from CV measurements ($E_{1/2}^{ox}$/*E_p) in CH_2Cl_2 calibrated against the ferrocene/ferrocenium couple (Fc/Fc^+, –5.15 eV) as internal standard. [d] $E_{LUMO} = E_{HOMO} + (hc/\lambda_{max})$.

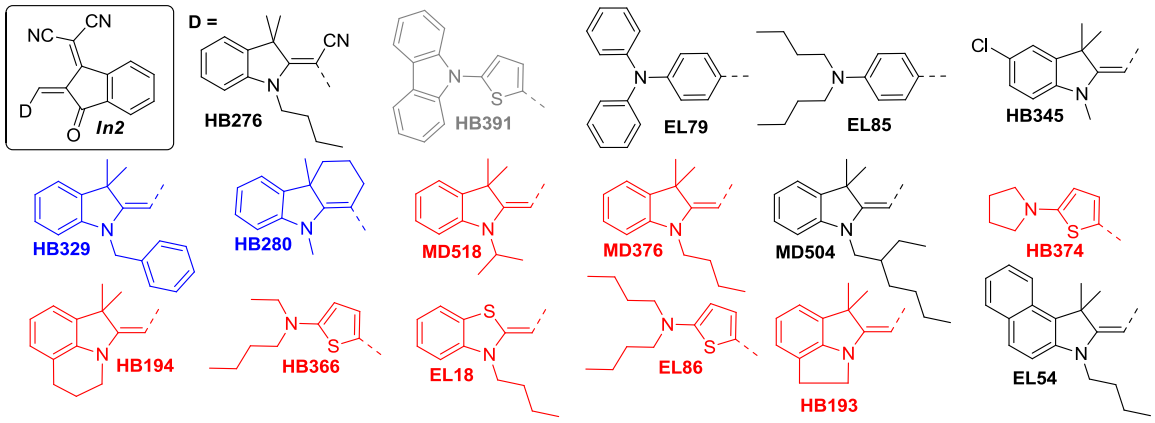

Chart 4. Chemical structures of ***series In2***.

A third series, using a bisindandione derivative as acceptor (***series In3***) is represented in Chart 5. The bisindandione acceptor, resulting from a condensation of two molecules of indandione, was combined with different indolenine derivatives and aminothiophene to give a series of green dyes. The interaction between the donor moieties and the acceptor results in a distinct bathochromic shift of λ_{max} to ~660 nm compared to ***series In2*** and lower absorption densities of ~0.13 D^2 mol g^{-1}. The HOMO energies of ***series In3*** lay between –5.61 eV and –5.73 eV, whereas the LUMO are further shifted to lower energies compared to ***series In2*** with a range from –3.74 eV to –3.83 eV. Here, aminothiophene **HB239** shows very similar characteristics compared to the indolenine based chromophores.

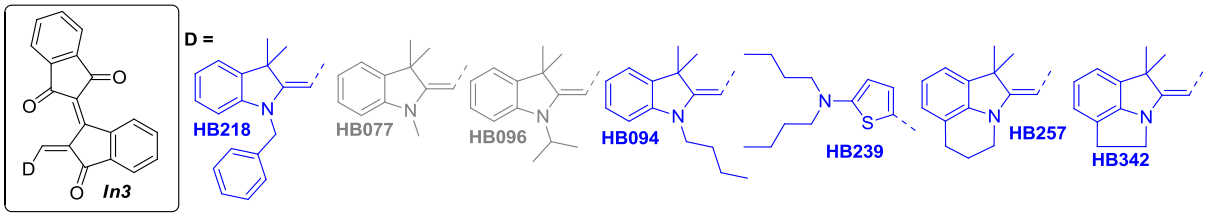

Chart 5. Chemical structures of the ***series In3***

Chart 6 shows the structures of dye ***series M*** (miscellaneous acceptors), where indolenine and aminothiophene derivatives serve as donor units. The acceptor moieties are mainly based on the structural concept of the indandione acceptor with various alterations. This series covers dyes with colors from orange (indolenine **MD342**, λ_{max} =490 nm) to blue (indolenine **MD519**, λ_{max} = 641 nm) with HOMO levels reaching from –5.97 eV (indolenine **HB091**) to –5.57 eV (indolenine **HB312**). Due to the very different acceptor units the LUMO range from high levels of –3.24 eV (**HB312**) to very low energies of –3.92 eV (**HB091**). The absorption densities in this series are usually below 0.2 D^2 mol g^{-1}, whereas indolenine **HB312** displays

a high value of 0.28 D^2 mol g^{-1}. This dye is structurally closely related to ***series In2***, but the weaker acceptor results in an absorption maximum at shorter wavelength of 533 nm and a shift of the FMO levels to higher energies was determined. Indolenine **MD564** describes a derivative of **MD376** (Chart 4), where one cyano group was replaced by an ester substituent, which entailed a shift of the absorption maximum by 9 nm to the blue and a reduced absorption density. Both FMO levels are shifted to higher energies by each ~0.1 eV. In indolenine **HB091**, the keto group of the indandione acceptor ***In2*** is substituted by a sulfonyl functional unit. This result in a stronger acceptor and a consequent bathochromic shift of the absorption maximum of 28 nm compared to indolenine **MD518** with very low-lying HOMO and LUMO levels.

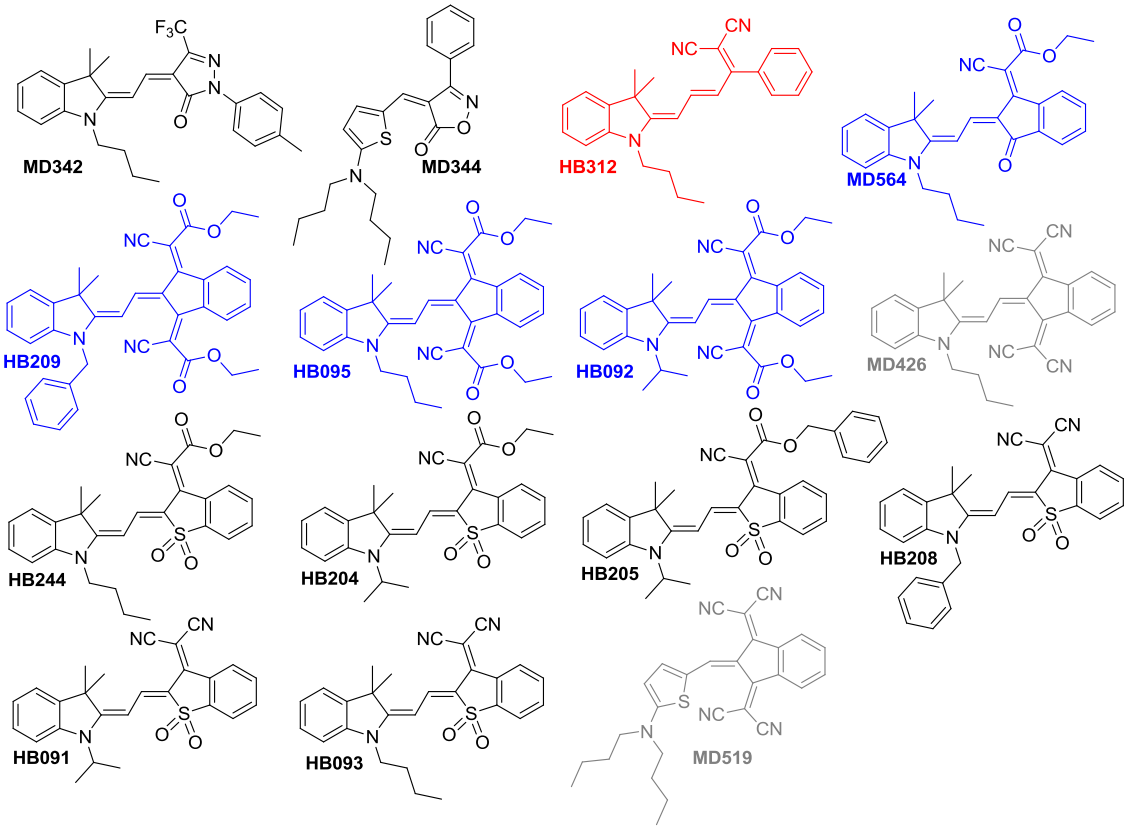

Chart 6. Chemical structures of ***series M***

The pyridone acceptor represents a widely investigated moiety in the earlier work of Würthner's group concerning materials for nonlinear optics.[7] From this work it is known that brilliant red dyes with a perfectly balanced electron distribution are accessible for pyridone acceptors in combination with indolenine and aminothiophene donors.[127] Two acceptor units with different alkyl chains were tested to identify the optimum between solubility and minimized amount of non-absorbing side-chains (Chart 7). The acceptor strength of ***series Py***

is located between indandione ***In1*** and ***In2***. Consequently, the absorption maxima of the compounds with donors like indolenine or aniline are observed in the range of 527–537 nm with good absorption densities of 0.20–0.26 D^2 mol g^{-1}. Their HOMO potentials were found around -5.7 eV, which is comparable to ***series In2***, but higher LUMO levels around –3.5 eV were determined. By using the thiazole donor of **MD324** or attaching a trifluoromethyl group to the acceptor in **HB136** the location of the FMO levels can be strongly influenced without changing the optical band gap. In both cases, λ_{max} is still located around 540 nm, but the FMO levels are shifted to lower energies by 0.2–0.3 eV.

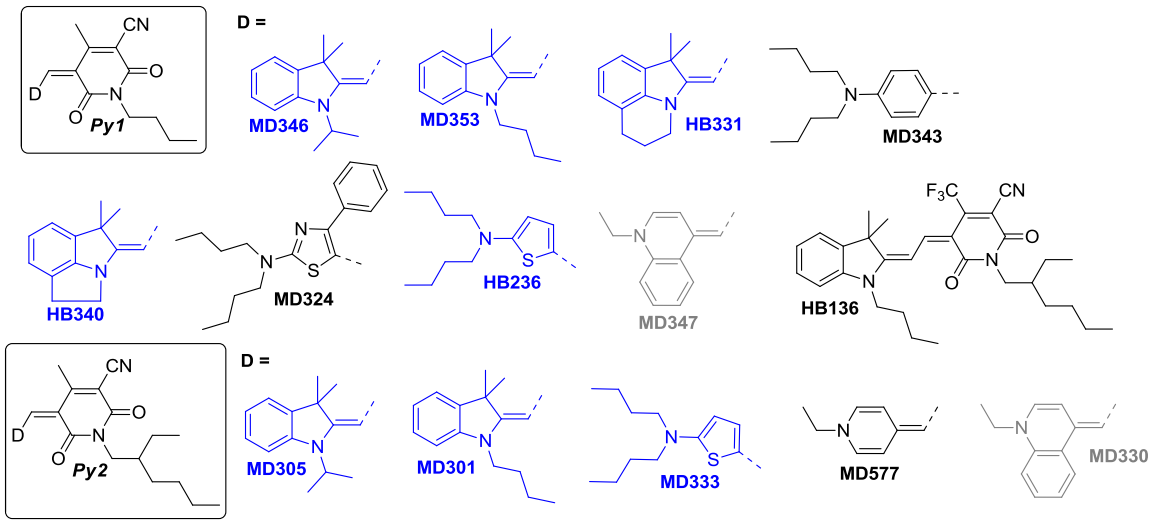

Chart 7. Chemical structures of ***series Py***

Chart 8 illustrates the structures of dye ***series Th*** bearing thiazole-like acceptors. The acceptor units are characterized by the heterocyclic thiazole unit substituted with *tert*-butyl, *n*-butyl, phenyl or methyl. The substituents were chosen to generate different packing behaviors in the solid state. Additionally, an effect on the solubility of the dyes was expected. To further strengthen the acceptor and enlarge the π-system, a malononitrile unit is attached in ***Th1*** and ***Th2***. Indeed all dyes except **EL31** exhibit absorption maxima > 600 nm with blue or green colors and sharp absorption band indicating cyanine-type chromophores. In the case of component ***Th3***, one cyano group is replaced by an ethyl ester to provide higher solubility in organic solvents. The chromophores with indolenine donor and acceptor Th1 display absorption maxima at ~625 nm with high tinctorial strentghs of 0.22–0.30 D^2 mol g^{-1}. The HOMO levels of the ***Th series*** range around –5.60 eV with corresponding LUMOs of –3.60 eV. Pyridine **EL30** and indolenine **EL53** show very similar absorption properties with maxima at 640 nm and reduced absorption densities of 0.19 and 0.12 D^2 mol g^{-1},

respectively. Though, both HOMO and LUMO levels of **EL30** are shifted to higher energies by 0.28 eV compared to **EL53**. Replacing the *tert*-butyl of compound ***Th1*** by the phenyl group in ***Th2*** yielded a slightly red-shifted λ_{max} for chromophores with the indolenine donor, while similar values were observed for the absorption densities and HOMO levels. The LUMO energies are located around –3.65 eV. The acceptor strength of ***Th3*** is slightly diminished compared to ***Th1*** and ***Th2*** due to the less electron-withdrawing ester group compared to a cyano group, which influences slightly the UV-vis and CV properties. Interestingly, the use of the bridged donor unit in **HB281** entailed a red-shift of λ_{max} compared to **HB364** of 11 nm and a shift of both FMO levels to higher energies by ~0.2 eV.

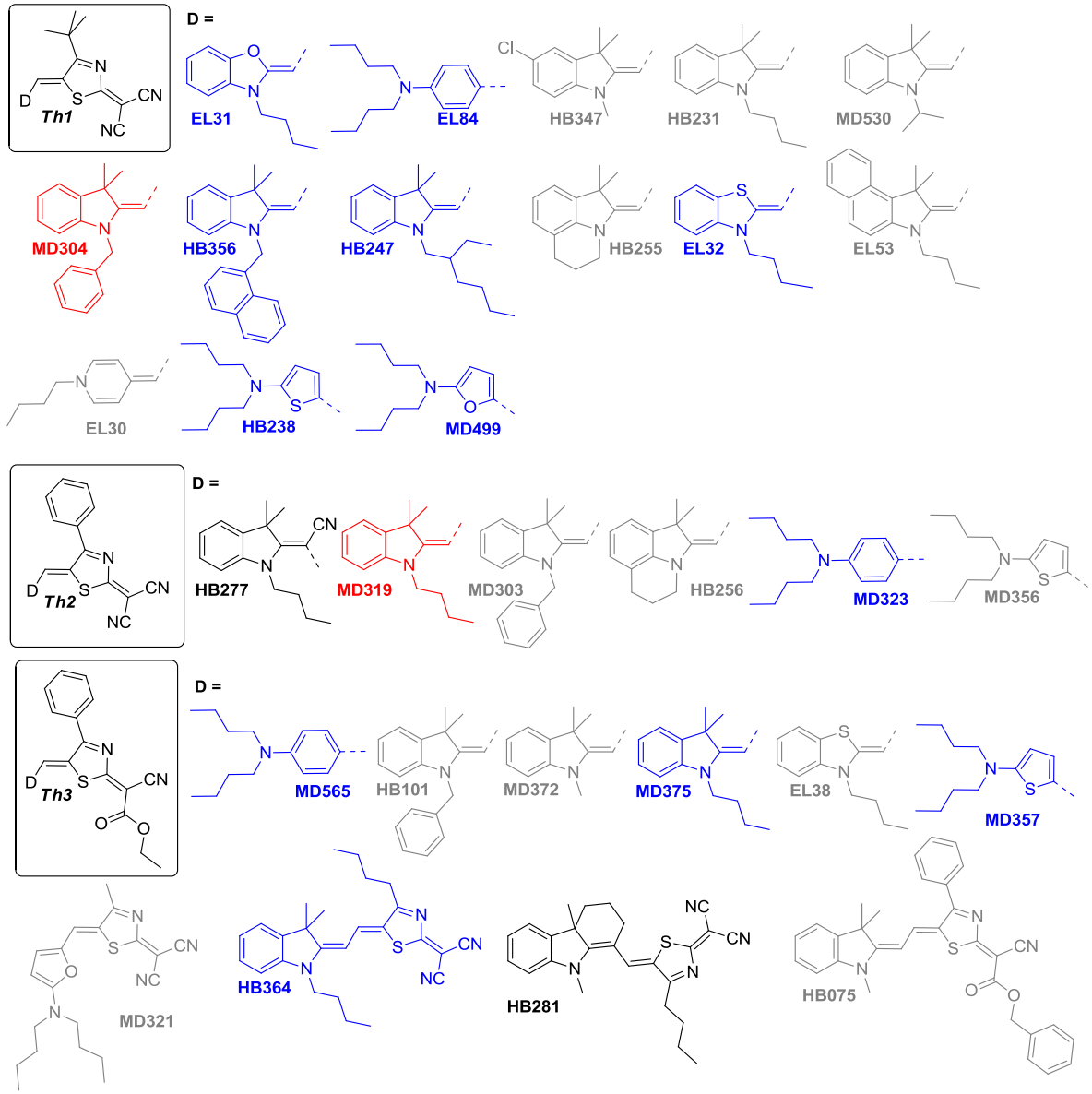

Chart 8. Chemical structures of ***series Th***

5.2.3 Photovoltaic properties

All MC dyes were evaluated in solution-processed BHJ solar cells, whose device structure is displayed in Figure 32a, in combination with the fullerene acceptor $PC_{61}BM$ (Figure 32b). **DPP(TBFu)$_2$** exhibiting one of the best device performances among solution-processed small-molecule BHJ solar cells,[53] was synthesized in our group and utilized in solar cells combined with PCBM according to literature for comparison. Unless stated otherwise, the solar devices were spin-coated from dye:$PC_{61}BM$ (25:75wt%) solutions of chlorobenzene.

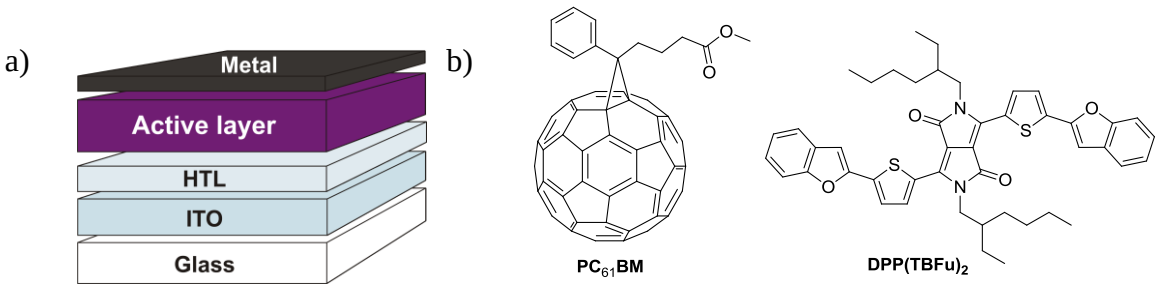

Figure 32. a) Schematic diagram of the device structure. b) Chemical structures of the fullerene acceptor $PC_{61}BM$ and the reference dye **DPP(TBFu)$_2$**.

Promising solar cells were optimized with respect to the dye:$PC_{61}BM$ ratio and active layer thickness. Both V_{OC} and fill factor (FF) were usually barely influenced by different dye:$PC_{61}BM$ ratios. However, J_{SC} and consequently PCE normally displayed a broad maximum at $PC_{61}BM$ weight percentages of 60–80 as shown in Figure 33 by using the example of **HB236**.

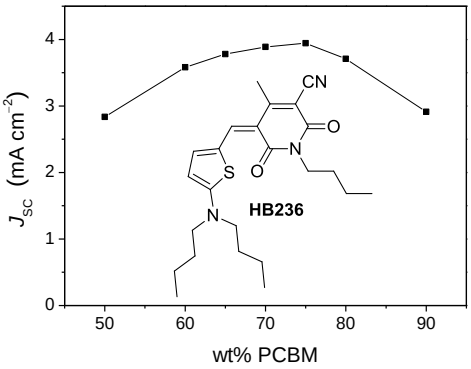

Figure 33. Dependence of J_{SC} on the $PC_{61}BM$ content in **HB236**:$PC_{61}BM$ solar cells.

Concerning the active layers, optimized conditions were created for film thicknesses of 50-60 nm. The PCE depends linearly on the fill factor (FF), the short-circuit current density (J_{SC}), the open-circuit voltage (V_{OC}) and reciprocally on the incident optical power (P_{in}) according to equation (1).

$$\eta = \frac{FF \cdot J_{SC} \cdot V_{OC}}{P_{in}} \quad (1)$$

Figure 34a exemplifies the dependence of the possible V_{OC} based on the LUMO level of $PC_{61}BM$ and the HOMO level of the corresponding donor compound by using the examples of P3HT and the indolenine dyes **HB312**, **HB194**, **MD304** and **HB091**. The solid area represents the band gap and the FMO levels of the material derived from the onsets of the redox waves (method 1). In the case of merocyanine dyes, this is usually equivalent to the band gap calculated by the absorption onset. However, the determination of onsets of redox waves or absorption bands is ambiguous. For this reason, we decided to calculate the HOMO level from the half wave potential $E_{1/2}^{ox}$, or, in case of irreversible oxidations, from the peak potential of the oxidation wave E_p. The LUMO energy was calculated by the following equation: $E_{LUMO} = E_{HOMO} + (hc/\lambda_{max})$ (method 2). The band gap and FMO levels derived by this calculation are clearly defined and symbolized by the dashed areas in Figure 34. For P3HT, the oxidation wave measured by CV is rather broad (Figure 34b), rendering the determination of the HOMO via the peak potential difficult. Furthermore, no LUMO energy could be derived by method 1, as no reduction was observed in the CV measurement. For discussion and in Table 14 and Table 15, values derived by method 2 are used.

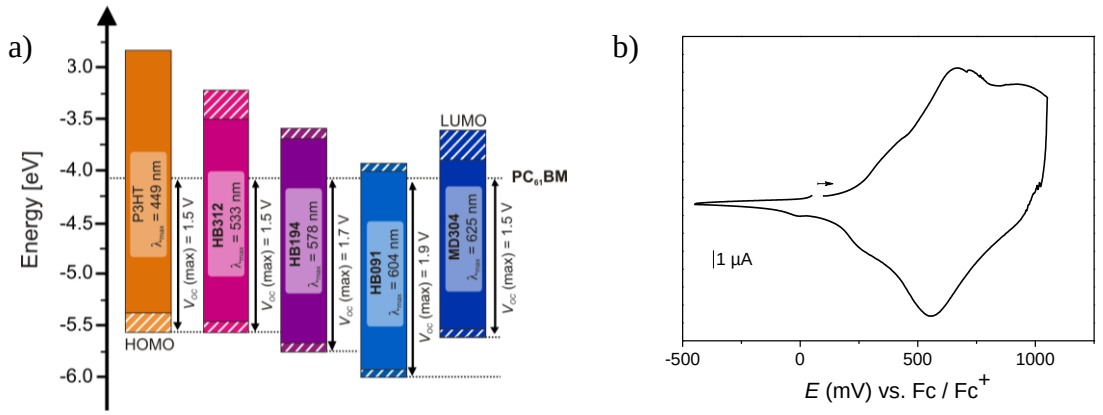

Figure 34. a) FMO levels of P3HT, **HB312**, **HB194**, **HB091** and **MD304** and their relative position to the LUMO of $PC_{61}BM$; solid area: band gap and FMO levels derived from the onsets of the redox waves; dashed area: $E_{HOMO} = -5.15\ eV - E_{1/2}^{ox}$; $E_{LUMO} = E_{HOMO} + (hc/\lambda_{max})$. b) Cyclic voltammogram (CH_2Cl_2, calibrated against the Fc/Fc^+ couple) of P3HT.

The HOMO level of P3HT accounts to about –5.6 eV and enables a possible V_{OC} of 1.5 V. However, the open-circuit voltages of BHJ solar cells comprising P3HT do usually not exceed ~0.6 V.[22a] In the literature, an offset between the LUMO of the electron acceptor and the LUMO of the donor material of 0.3–0.4 eV is described as necessary driving force for efficient charge separation.[19] The LUMO of P3HT around –2.8 eV is by far higher as necessary and results in a loss of more than 1 eV upon electron transfer. **HB312** (Chart 6) exhibits a comparable HOMO potential of –5.57 eV like P3HT, but a significantly lower

LUMO level of –3.24 eV. Nevertheless, a substantial part of the absorbed energy is lost upon transferring electrons to $PC_{61}BM$. An almost ideal set of FMO levels is given for the case of **HB194**: the low-lying HOMO allows for a possible V_{OC} of 1.7 V, whereas the offset LUMO (Donor) – LUMO (Acceptor) accounts for ~0.4 eV. The blue dye **MD304** exhibits a similar LUMO energy like **HB194**. However, due to the smaller band gap compared to **HB194**, the HOMO is shifted to –5.61 eV, which reduces the possible V_{OC} to 1.5 V. **HB091** provides a very low HOMO energy of –5.97 eV, which should enable a large V_{OC} up to 1.9 V. However, the LUMO is also located at low energy of –3.92 eV, possibly providing not enough driving force for an efficient charge transfer to the electron acceptor. These examples represent the scope of the investigated dyes and emphasizes, that even MC dyes with band gaps of ≥ 2.0 eV like **HB194** and **MD304** provide favorably low-lying FMO levels.

Table 16 and 17 display the photovoltaic properties of the built photovoltaic devices. For all dyes a significant broadening of the absorption spectrum accompanied with a bathochromic shift of the absorption maxima in the blend compared to λ_{max} determined in dichloromethane solution was observed. For ***series In1*** this shift accounts for 10–20 nm. Solar cells containing dyes of this series showed low fill factors of 0.23–0.32 and PCEs of only 0.1–0.6%. The low fill factors are typical for photovoltaic devices containing MC dyes and could be caused by unbalanced charge transport of holes and electrons due to low charge carrier mobility of the donor materials. However, this aspect was not explored further. The J_{SC} values range between 1.2 mA cm^{-2} (quinoline **EL44**) and 2.9 mA cm^{-2} (aminothiophene **MD352**). For V_{OC}, a maximum of 0.68 V was obtained for the two indolenine dyes **HB248** and **HB330**, whereas **EL41** showed the lowest value of 0.37 V of this series. The bridging unit in **HB330** seems to have a beneficial influence, as device with this chromophore showed an increase in J_{SC} of 30% compared to the one of **HB248**, which displays the same basic chromophore. In this series, solar cells containing dyes with aniline, pyridine or quinoline donor displayed almost no photovoltaic effect.

Series In2 was the morst successful one with eight dyes showing PCEs > 1.3% (Chart 4). For this series, the red shift of the λ_{max} in the blends is larger than in ***series In1*** and amounts to ~30 nm. One exception represents benzothiazole **EL18**, where a hypsochromic shift of the first λ_{max} of 5 nm was measured. Actually, the absorption spectrum of the blended **EL18** displays two absorption maxima, the one at 608 nm showing a red shift of 28 nm (Figure 35a) being in accordance with the other compounds of this series.

Table 16. Photovoltaic characteristics of the investigated solution-cast dye:$PC_{61}BM$ BHJ solar cell.

MC dye	λ_{max} (nm)[i]	V_{OC} (V)	J_{SC} (mA cm^{-2})	FF	η (%)	MC dye	λ_{max} (nm)[a]	V_{OC} (V)	J_{SC} (mA cm^{-2})	FF	η (%)
Series In1						**HB244**[c]	624	0.72	1.9	0.27	0.4
HB249	507	0.61	1.6	0.25	0.2	**HB204**	622	0.69	1.9	0.27	0.4
HB248	508	0.68	2.1	0.31	0.4	**HB205**	629	0.65	1.4	0.25	0.2
HB330	513	0.68	2.8	0.32	0.6	**HB208**	629	0.71	0.2	0.27	<0.1
EL41	526	0.37	1.3	0.23	0.1	**HB091**	635	0.79	0.8	0.28	0.2
MD352[a]	532	0.63	2.9	0.27	0.5	**HB093**	633	0.75	0.6	0.27	0.1
EL44[b]	617	0.38	1.2	0.24	0.1	***Series Py***					
Series In2						**MD346**[a]	545	0.65	3.9	0.29	0.7
HB276	559	0.60	0.1	0.30	<0.1	**MD353**[a]	545	0.67	3.7	0.28	0.7
EL79	588	0.70	0.5	0.26	0.1	**HB331**	549	0.76	3.3	0.33	0.8
EL85	595	0.70	2.2	0.28	0.4	**MD343**[a]	548	0.49	2.2	0.20	0.2
HB345[c]	603	0.97	1.7	0.27	0.4	**HB340**	557	0.79	4.0	0.36	1.1
HB329	603	0.90	1.8	0.29	0.5	**MD324**	557	0.62	0.9	0.28	0.2
HB280	636	0.71	2.2	0.30	0.5	**HB236**	557	0.68	3.9	0.31	0.8
MD518	606	0.84	5.7	0.30	1.5	**HB136**[j]	561	0.47	0.3	0.27	<0.1
MD376	605	0.90	5.3	0.32	1.5	**MD305**[a]	546	0.67	3.4	0.27	0.6
MD504	605	0.67	2.4	0.26	0.4	**MD301**[a]	544	0.77	4.0	0.29	0.9
HB374[c]	590	0.90	5.1	0.37	1.7	**MD333**[a]	556	0.73	4.0	0.32	0.9
HB194[d]	612	0.94	8.2	0.34	2.6	**MD577**[k]	544	0.70	1.1	0.26	0.2
HB366[c,e]	591	0.93	6.0	0.42	2.3	***Series Th***					
EL18[c]	574	0.92	6.0	0.32	1.8	**EL31**[c]	612	0.72	3.3	0.32	0.7
EL86[f]	595	0.96	5.8	0.41	2.3	**EL84**	650	0.70	3.3	0.31	0.7
HB193[g]	621	0.78	6.3	0.29	1.4	**MD304**[c]	649	0.72	7.8	0.32	1.8
EL54	626	0.37	0.3	0.21	<0.1	**HB356**[c]	649	0.64	4.6	0.28	0.8
Series In3						**HB247**	646	0.64	4.8	0.37	1.2
HB218	677	0.75	4.4	0.31	1.1	**EL32**[c]	606	0.66	4.4	0.41	1.2
HB094	683	0.71	4.2	0.33	1.0	**HB238**	682	0.72	4.5	0.35	1.1
HB239	700	0.68	4.0	0.36	1.0	**MD499**	680	0.63	3.8	0.29	0.7
HB257[c]	689	0.71	4.6	0.30	1.0	**HB277**[c]	636	0.75	1.5	0.29	0.3
HB342[c]	693	0.60	3.2	0.27	0.5	**MD319**[c]	659	0.65	7.3	0.33	1.6
Series M						**MD323**[c]	679	0.75	3.0	0.30	0.7
MD342[a]	485	0.60	1.2	0.25	0.2	**MD565**	658	0.60	4.7	0.27	0.8
MD344[h]	515	0.57	2.8	0.28	0.4	**MD375**[a]	660	0.52	4.7	0.29	0.7
HB312	552	0.85	4.3	0.38	1.4	**MD357**[a]	689	0.47	4.0	0.27	0.5
MD564	578	0.79	4.5	0.33	1.2	**HB364**[c]	650	0.60	4.5	0.33	0.9
HB209	587	0.76	3.5	0.28	0.7	**HB281**[c]	639	0.70	1.7	0.35	0.4
HB095	594	0.73	3.2	0.28	0.7	**DPP(TBFu)$_2$**[c,l]	595	0.91	6.7	0.59	3.6
HB092	595	0.71	3.7	0.28	0.7						

[a] 70wt% $PC_{61}BM$. [b] ODCB. [c] Chloroform. [d] 55wt% $PC_{61}BM$. [e] 50wt% $PC_{61}BM$. [f] 60wt% $PC_{61}BM$. [g] 65wt% $PC_{61}BM$. [h] 80wt% $PC_{61}BM$. [i] UV-vis measurements of a thin film of the blend. [j] 88 mW cm^{-2}. [k] Chlorobenzene with 20% Pyridine. [l] 40wt% $PC_{61}BM$ and annealed at 110°C for 10 min.

Table 17. Photovoltaic characteristics of the MC:$PC_{61}BM$ BHJ solar cells with inhomogeneous layers.

MC	λ_{max} (nm)[e]	$PC_{61}BM$ wt%	V_{OC} (V)	J_{SC} (mA cm^{-2})	FF	η (%)
Series In1						
EL42[a]	n.d.	75	0.54	0.9	0.53	0.3
Series In3						
HB077[b]	n.d.	75	0.59	3.8	0.31	0.7
HB096[b]	n.d.	75	0.73	3.7	0.33	0.9
Series M						
MD426[a]	609	75	0.90	0.4	0.28	0.1
MD519[b]	658	75	0.73	0.6	0.27	0.1
Series Py						
MD347[a]	n.d	75	0.45	1.5	0.35	0.2
MD330[c]	/	80	0.67	3.2	0.38	0.8
Series Th						
HB347[a]	n.d.	75	0.61	1.6	0.43	0.4
HB231[d]	-	-	-	-	-	-
HB255[a]	598	75	0.65	3.9	0.35	0.9
EL53[b]	662	75	0.53	0.9	0.23	0.1
EL30[d]	-	-	-	-	-	-
MD303[d]	-	-	-	-	-	-
HB256[a]	606	75	0.69	4.3	0.40	1.2
MD356[a]	691	50	0.71	2.8	0.37	0.7
HB101[b]	655	75	0.67	3.3	0.31	0.7
MD372[d]	-	-	-	-	-	-
EL38[a]	606	75	0.54	2.5	0.32	0.4
MD321[d]	-	-	-	-	-	-
HB075[d]	-	-	-	-	-	-

[a] Chloroform; [b] Chlorobenzene with 20% Pyridine.; [c] Chlorobenzene with each 6% Pyridine and Chloroform; [d] Solubility insufficient for device fabrication; [e] UV-vis measurements of a thin film of the blend;

For many of the devices containing dyes of ***series In2*** high V_{OC} up to 0.96 V were observed consistent with the low HOMO levels. The fill factor range around ~0.3, whereas the J_{SC} display a large distribution from 0.1–8.2 mA cm^{-2}. Efficient photovoltaic devices with PCE >1% exhibit photocurrents of 5–6 mA cm^{-2}. Here, the highest values for PCE of >2% in this work were achieved for the indolenine **HB194** and aminothiophenes **HB366** and **EL86**. Solar cells built with e. g. aniline **EL85** or indolenine **EL54** exhibited considerably lower voltages and also low J_{SC} and PCE. The *JV* characteristics of these solar cells displayed s-shaped curves, suggesting adverse processes like strong recombination due to high series resistance or charge accumulation caused by low carrier mobilities (Figure 35b). Here, also the lowest fill factors of 0.28 (**EL85**) and 0.21 (**EL54**) of this dye series were observed.

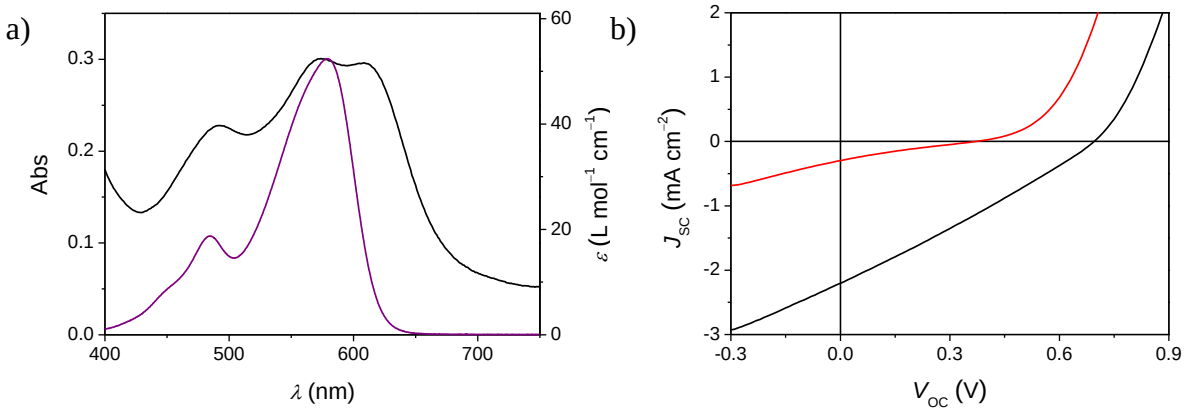

Figure 35. a) Absorption spectra of a device built with a blend of **EL18** (75wt% $PC_{61}BM$, black line) and a CH_2Cl_2 solution of **EL18** (~10^{-5} M, magenta line). b) *JV* response of devices built with blends of **EL85** (75wt% $PC_{61}BM$, red line) and **EL54** (75wt% $PC_{61}BM$, black line).

Notably, devices with **HB276**, exhibiting the lowest HOMO level of this series, showed almost no efficiency at all due to very low J_{SC} values. This could be explained by its very low LUMO nergy of −3.90 eV providing possibly a low driving force for electron transfer to $PC_{61}BM$. Benzothiazole **EL18** could not be processed from chlorobenzene due to insufficient solubility. However, solution-processing from chloroform yielded an efficient solar device with both high values for open-circuit voltage (0.92 V) and short-circuit current density (6.0 mA cm^{-2}), yielding an overall PCE of 1.8%.

Furthermore, acceptor ***In2*** was combined with several derivatives of the indolenine donor. By comparing *iso*-propyl compound **MD518** with *n*-butyl derivative **MD376**, the observed differences of the solar cell characteristics are negligible. In contrast, applying the more bulky benzyl in **HB329** or 2-ethylhexyl group in **MD504** significantly reduced J_{SC}. The introduction of the rigidifying bridging unit in **HB194** and **HB193** showed a beneficial influence on the short-circuit current densities. By reaching a notable value of 8.2 mA cm^{-2} in the case of **HB194**, a highly efficient solar device exhibiting a power conversion efficiency of 2.6% could be achieved. The V_{OC} was comparable like the reference device containing a **DPP(TBFu)$_2$**:$PC_{61}BM$ blend (0.91 V). However, the low fill factor of 0.34 for devices with **HB194** (compared to 0.59 for **DPP(TBFu)$_2$** cells) resulted in a lower performance compared to the reference cell. The highest values for voltage (0.96 V) and fill factor (0.41) of this series were achieved by using aminothiophene **EL86**. Combined with a good J_{SC} of 5.8 mA cm^{-2} a high efficiency of 2.3% was reached here. Figure 36 displays the *JV* response of the devices built with **EL86**, **HB194** and **DPP(TBFu)$_2$**. Notably, the slope of **HB194** at the intersection with *J*-axis is much steeper than for the two other devices. The series resistances can be determined from the slope of the graph at the intersection with the *V*-axis. For

DPP(TBFu)$_2$, a resistivity of 17 Ω cm^{-2} was measured, whereas **EL86** and **HB194** exhibit significantly higher values of 49 Ω cm^{-2} and 61 Ω cm^{-2}, respectively. These measurements are in accordance with the reduced fill factors of the devices comprising the MC dyes compared to the reference dye **DPP(TBFu)$_2$** and appear as the major deficiency of MC dye based BHJ photovoltaics. Notably, for the two best dyes of this series, **HB194** and aminothiophene **EL86**, closely packed $\pi\pi$-stacks were observed in the single crystal (see Ref 102a and Chapter 3), which appear to be a favorable packing for charge transport.

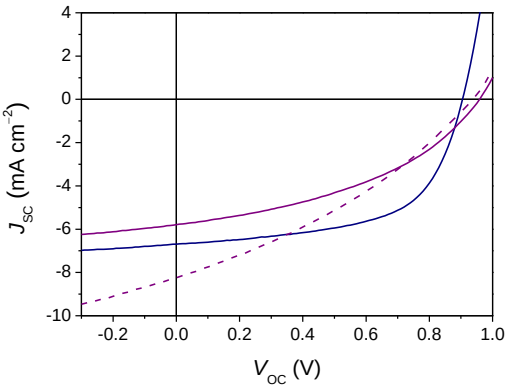

Figure 36. *JV* response of the devices built with blends of **EL86** (60wt% $PC_{61}BM$, solid magenta line), **HB194** (55wt% $PC_{61}BM$, dashed magenta line) and **DPP(TBFu)$_2$** (40wt% $PC_{61}BM$, solid blue line).

Dye ***series In3*** show absorption maxima in the blend with a bathochromic shift of ~24 nm compared to the solution spectra. Thus, λ_{max} is located around 700 nm, where the photon flux exhibits a maximum. The voltages of this series vary around 0.7 V, which is ~0.2 V lower than in ***series In2***. Except for the surprisingly poor performance of indolenine **HB342** (0.5%)**,** all dyes of ***series In3*** showed similar device performance of ~1%, whereas their J_{SC} values range between 4.0–4.6 mA cm^{-2}. Unlike in ***series In2***, the steric demand of the side-chains attached to the donor unit appear to have a negligible influence on the quality of the solar device. Presumably the more bulky acceptor unit in ***series In3*** allows for a more bulky donor part in centrosymmetric π-stacks.

Series M is the least homogeneous one owing to different acceptor units and abroad spread of coloristic properties from orange to blue. Nevertheless, devices with chromophores of dye ***series M*** display relatively similar V_{OC} values of ~0.7 V and typical FF of ~0.3. However, the PCE range from 0.1–1.4%. This is originated by the significant differences in J_{SC}, showing a minimum value of 0.2 mA cm^{-2} (**HB208**) and a maximum value of 4.5 mA cm^{-2} (**MD564**). Indolenine **HB312** was the best performing dye of this series. Despite its quite high HOMO energy of –5.57 eV, which is comparable with the dye ***series Th*** and also P3HT, a high open-

circuit voltage of 0.85 V was observed. In combination with the current density of 4.3 mA cm^{-2} and the high fill factor of 0.38, a good PCE of 1.4% was achieved with this magenta colored dye that absorbs rather in the high-energy regime of the solar spectrum. Indolenine **MD564**, which is a derivative of **MD376**, showed high V_{OC} of 0.8 V. The reached photocurrent of the respective devices of 4.5 mA cm^{-2} is appreciable, but still less than 5.3 mA cm^{-2} for **MD376**. Nevertheless, an efficient device displaying a PCE of 1.2% could be fabricated. The three indolenine dyes **HB209**, **HB095** and **HB092** describe a series with the same chromophore, but varying side-chains. In this example, no significant deviations of the solar cell features of the corresponding devices were observed and PCE of ~0.7% were obtained. Indolenine **HB091** and **HB093**, carrying a sulfonyl group at the acceptor, exhibit very low-lying HOMO and LUMO levels. Here, very low J_{SC} of 0.8 mA cm^{-2} and 0.6 mA cm^{-2} and PCEs of 0.2% and 0.1%, respectively, were obtained. The FMO levels were shifted to higher energies in **HB244** and **HB204**. Compared to **HB091** J_{SC} was increased significantly (1.9 mA cm^{-2}) in devices comprising **HB244**, which resulted also in an enhanced PCE of 0.4%.

For ***series Py***, two differently substituted pyridine acceptors ***Py1*** and ***Py2*** were used to vary the solubility of the dyes. Again, a bathochromic shift of the absorption bands of 20–30 nm occurs in the thin films compared to the solutions of these magenta dyes, yielding λ_{max} of 544–561 nm. The dyes of this series show comparable HOMO energies to those of ***series In2***, but the obtained V_{OC} did not exceeded 0.7–0.8 V. Here, the current densities varied significantly from 0.3–4.0 mA cm^{-2} with resulting PCE of 0.1–1.1%. By comparing the four compounds with indolenine donors, **MD346**, **MD353**, **MD305** and **MD301**, similar J_{SC} values of 3.4-4.0 mA cm^{-2} and open-circuit voltages of ~0.66 V were found. Solely **MD301** displayed a higher V_{OC} of 0.77 V, resulting in a more efficient solar cell with a PCE of 0.9%, while the other three compounds yielded PCEs of ~0.7%. The *JV* responses of all four devices showed steep slopes at the intersection with the *J*-axis suggestive for severe problems with the charge extraction (Figure 37a). The application of the bridging units in **HB331** and **HB340** resulted in slightly enhanced V_{OC} though higher HOMO levels. Besides similar current densities, the fill factors increased up to 0.36, which was also reflected by the *JV* graphs (Figure 37b). In contrast to ***series In2***, here, the ethylene bridging unit (**HB340**) resulted in the best solar cell with a PCE of 1.1%. In accordance with the findings of the previous series, aniline **MD343** exhibited poor solar cell characteristics with low V_{OC} of 0.49 V and fill factor of only 0.2. Both aminothiophene derivatives **HB236** and **MD333**

achieved J_{SC} of ~4 mA cm^{-2}, which is the maximal value obtained within this series. The overall efficiency was comparable to the indolenine compounds.

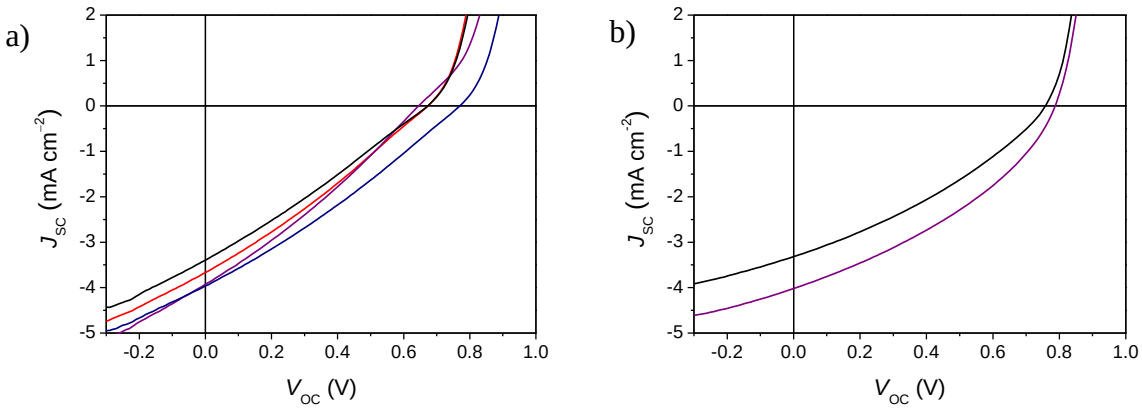

Figure 37. a) *JV* response of the devices built with blends of **MD353** (70wt% $PC_{61}BM$, red line), **MD346** (70wt% $PC_{61}BM$, violet line), **MD301** (70wt% $PC_{61}BM$, blue line) and **MD305** (70wt% $PC_{61}BM$, black line). b) *JV* response of the devices built with blends of **HB331** (75wt% $PC_{61}BM$, black line) and **HB340** (75wt% $PC_{61}BM$, violet line).

Generally, dyes of ***series Th*** showed a decreased solubility compared to other series in this work (Table 14 and 15), which might originate from their high dipole moments. Therefore, half of the synthesized dyes could not be processed or yielded devices with inhomogeneous layers and thus unreliable results. These are compiled in Table 17. For most of the dyes, chloroform was chosen as solvent for spin-coating. The red-shift of λ_{max} of 25–35 nm resulted in absorption bands centered at 612–689 nm in the thin films. The V_{OC} in this series ranged between 0.6–0.7 V, whereas J_{SC} showed mostly high values of 4–5 mA cm^{-2}. Combined with relatively good fill factors with an average of 0.34 for this series, PCE ranging from 0.4–1.8% were reached. Indolenine **MD304** (***series Th1***) represents the most promising dye of the thiazol series, as devices containing this dye achieved satisfying V_{OC} values of 0.72 V, fill factors of 0.32 and very high current densities of 7.8 mA cm^{-2}, resulting in an overall solar cell efficiency of 1.8%. In ***series Th1***, both benzothiazole and benzooxazole donors were applied in **EL32** and **EL31**. Devices containing **EL32** produce comparable high fill factors of 0.41 and appreciable photocurrent densities of 4.4 mA cm^{-2}, realizing a solar cell with PCE of 1.2%. Benzooxazole **EL31** showed reduced current densities and consequently a lower PCE of 0.7%.

Dyes with 4-phenyl group at thiazole acceptor ***Th2*** showed differing solubility and film forming behaviors compared to ***series Th1***. Indolenine **MD319** (***Th2***) bearing a butyl substituent formed homogeneous layers in chloroform, which was not possible with **HB231** (***Th1***). By contrast, the benzyl compound **MD303** (***Th2***) could not be processed from any

solvent, whereas **MD304** was the best candidate of ***series Th1***. The absorption spectrum of the device containing **MD319** displayed a typical red shift of 27 nm compared to solution data and its solar cell yielded a high photocurrent of 7.3 mA cm^{-2}. With a voltage of 0.65 V, a promising PCE of 1.6% was obtained. Compared to the indolenine derivatives, the aniline **MD323** showed inferior solar cell characteristics. By applying acceptor ***Th3***, which provided an enhanced solubility, an opposed trend was observed in the case of the aniline donor. Compared to aniline **MD323** (0.75 V), **MD565** showed a lower V_{OC} of 0.60 V, which correlates to the higher HOMO energy. However, the strong photocurrent of 4.7 mA cm^{-2} of cells with **MD565** outweighed this disadvantage and resulted in a higher PCE of 0.8%.

5.2.4 Device optimization

Besides the standard characterization of the presented dyes in solution-processed BHJ solar cells, device optimizations following known procedures were performed for slected dyes. For the best dye, indolenine **HB194**, neither the replacement of $PC_{61}BM$ by $PC_{71}BM$ nor the variation of the metal electrode led to better cell performance. For this reason, cells with aminothiophene **EL86** were optimized. First, the standard acceptor $PC_{61}BM$ was replaced with $PC_{71}BM$, enabling enhanced absorption at longer wavelengths due to its lower symmetry.[20b,128,134] The results of the optimization procedures are presented in Table 18, while the *JV* response is shown in Figure 38. For comparison, the *JV* response of a **DPP(TBFu)$_2$**:$PC_{71}BM$ device manufactured according to reference 53 was measured on the same experimental setup (Figure 38a). The cell characteristics of these devices are included in Table 18 fr comparison.

Table 18. Photovoltaic characteristics of cells with **EL86** (60wt% PCBM) and **DPP(TBFu)$_2$** (40wt% $PC_{71}BM$).

MC dye	HTL	cathode	PC_xBM	R_s (Ω cm^{-2})	V_{OC} (V)	J_{SC} (mA cm^{-2})	FF	η (%)
EL86	PEDOT	Al[b]	61	49.0	0.96	5.8	0.41	2.3
	PEDOT	Al[b]	71	50.9	0.96	7.2	0.39	2.7
	MoO_3	Al[b]	71	24.0	0.98	7.1	0.46	3.2
	MoO_3	Ca/Ag[c]	71	24.7	0.99	7.6	0.44	3.3
DPP(TBFu)$_2$[c]	PEDOT	Al[b]	71	21.0	0.91	9.6	0.47	4.1

[a] annealing at 110°C for 10 min. [b] 150 nm. [c] 6 nm/120 nm.

The fill factor was barley altered by application of $PC_{71}BM$, indicating similar miscibility of $PC_{61}BM$ and $PC_{71}BM$ with **EL86**. Furthermore, comparable V_{OC} were observed owing to

similar LUMO levels. By contrast, the photocurrent could be significantly enhanced due to enhanced light absorption (Figure 38b). The second optimization step concerns the interfaces of the solar device, which can strongly influence the efficiency of the cells.[135] Therefore, the usually employed PEDOT:PSS was substituted by a ~20 nm thick MoO_3 layer applied by evaporation. Thus, the detrimental series resistance could be significantly reduced from 51 Ω cm^{-2} to 24 Ω cm^{-2} accompanied by an improved fill factor of 0.46. Now, both series resistance and fill factor are comparable to the reference device. The photocurrent was slightly reduced, which was already observed in other experiments with comparable MoO_3 layer thicknesses.[136] Finally, the interface between metal and blend was optimized by modifying the cathode material. The application of a Ca/Ag cathode preserved the high voltage of 0.99 V and J_{SC} increased to 7.6 mA cm^{-2}, yielding an excellent efficiency of 3.3%. This could be explained by the increased built-in electrostatic potential upon application of an electrode with a higher work function, which improves charge separation and transport.

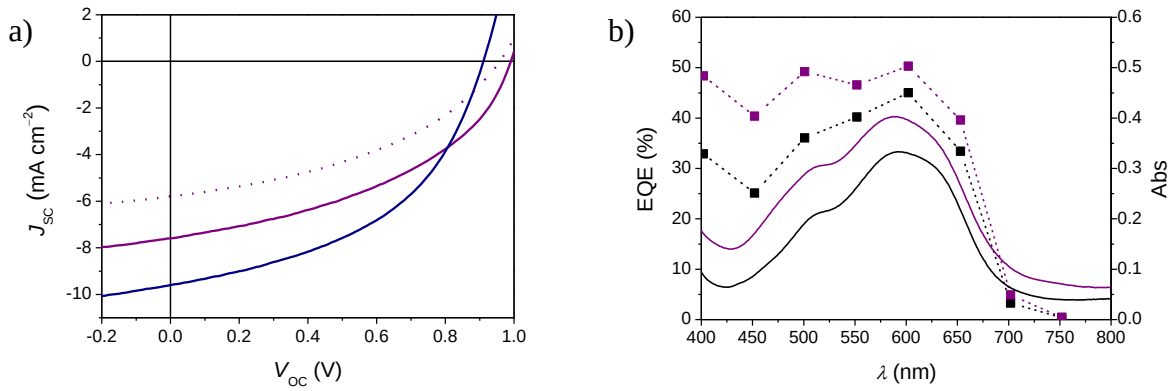

Figure 38. a) *JV* response of devices containing **EL86** (60wt% PCBM); dotted magenta line: $PC_{61}BM$, PEDOT, Al; solid magenta line: $PC_{71}BM$, MoO_3, Ca/Ag and **DPP(TBFu)$_2$** (40wt% $PC_{71}BM$, solid blue line). b) EQE (dashed line) and Absorption spectra (solid line) of the devices built with blends of **EL86** (60wt% $PC_{61}BM$ [black line] or $PC_{71}BM$ [violet line]); HTL: PEDOT; Cathode: Al.

5.3 Discussion

In order to evaluate the obtained data and elucidate possible relationships between the structure of the dyes and the performance in the respective solar cells, key features such as solubility, FMO levels, absorption properties and the molecular structure of the presented dyes were analyzed.

5.3.1 Solubility

The ability of the chromophores to form homogenous films in the solar devices was investigated. Here, the solubility of the dye in the applied solvent is essential. Therefore,

solubility experiments were carried out for a majority of the compounds (Table 14 and 15). From these experiments we learned that a solubility of less than ~2 mg mL^{-1}, under the reported conditions, usually resulted in inhomogeneous films and reduced PCEs (Figure 39 and Table 17). Furthermore, the results of the 7 cells on the same substrate differed strongly from each other. Therefore, measurements based on solar cells with inhomogeneous films were not included in the discussion. Please note that the solubility is significantly higher under the condition of the actual solar cell processing, which proceeds by stirring the dye solution for 3 days at elevated temperatures (up to 70 °C). For **HB194** an enhancement from 3 mg mL^{-1} to 15 mg mL^{-1} was observed at the higher temperatures of 70°C of solar cell processing.

For some components showing low solubility in chlorobenzene, 20% pyridine was added, enhancing the solubility of the respective dyes to 5–6 mg mL^{-1}. Interestingly, most of these solar devices showed mediocre cell performances and most of their active layers turned out to be inhomogeneous. As this coincidence between relatively high solubility and deficient film forming properties occurred only for this solvent mixture, we assume that the tendency to form non-uniform films on the given substrate is an intrinsic property of this solvent mixture. Upon considering the discussed film quality in combination with the solubility of the chromophores, 22 dyes (24%) are excluded from the discussion. Their molecular structures are shown in grey color in charts 3-8 and their cell results are collected in Table 17.

Interestingly, the dyes showing the highest solubilities of 30-166 mg mL^{-1} also result in relatively low performances with low values for J_{SC} and PCE of usually < 0.5%. Besides, even small changes in the structure can influence the solubility drastically, e.g. the substitution of the *n*-butyl chain in **MD301** by *iso*-propyl in **MD305** led to a tenfold increase of the solubility factor.

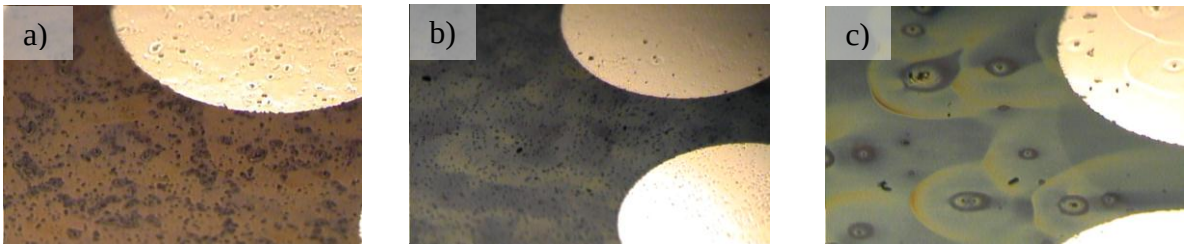

Figure 39. Images obtained under optical microscope of solar cells built with a) **HB255** (75wt% $PC_{61}BM$, chloroform); b) **HB101** (75wt% $PC_{61}BM$, chlorobenzene with 20% pyridine) and c) **MD356** (75wt% $PC_{61}BM$, chloroform). The light area represents the electrode material, the dark area the active layer between the single cells on one substrate.

5.3.2 HOMO and LUMO levels

The HOMO and LUMO energy levels were assessed in terms of the properties of the resulting solar cells. Concerning the position of the LUMO level, two opposing aspects need to be considered. First, the LUMO levels of the dye and the $PC_{61}BM$ need to be well-aligned to enable a rapid and unidirectional electron transfer from the donor to the electron accepting material. In the literature an ideal offset of 0.3–0.4 eV is proposed to achieve sufficient thermodynamic driving force.[19] At the same time, this energy offset represents a loss in chemical potential of the respective electrons. Thus, this energy is lost for the solar cell performance by means of a decreased open-circuit voltage and accordingly needs to be minimized.

In Figure 40 a scatter plot between J_{SC} of the respective photovoltaic device and the LUMO energy of the MC dye is depicted. The dyes with the lowest LUMO levels (–3.9 eV) of this work, indolenine **HB091** and **HB093** (***series M***), exhibit very low J_{SC} of 0.8 and 0.6 mA cm^{-2}, respectively, which could be attributed to a low efficiency for charge separation. Replacing one of the cyano groups at the acceptor by ester functional units resulted in a shift of the HOMO to higher energies by ~0.1 eV. Actually, here higher J_{SC} values of 1.9 and 1.5 mA cm^{-2} (**HB244** and **HB205**) were obtained. In our work about NIR absorbing MC dye similar results were obtained. By chemical engineering of a given chromophore, the LUMO level could be changed from –4.11 eV to –3.80 eV, which came along with a raise in J_{SC} from 0.1 mA cm^{-2} to 3.3 mA cm^{-2}.[99] Dyes with LUMO levels of –3.8 eV can achieve photocurrents up to 4.6 mA cm^{-2}. However, these are dyes from ***series In3***, where higher values were expected due to the absorption band centered in the thin film at ~700 nm, where the solar flux peaks. Hence, the driving force for charge separation seems to be still low. The highest photocurrents of >5 mA cm^{-2} were achieved with cells containing dyes of ***series In2*** or ***Th*** exhibiting LUMO levels of –3.6±0.1 eV. Here, the energy offset is obviously high enough to entail efficient exciton splitting.

Interestingly, dyes with high-lying LUMO levels of >–3.4 eV also display low to moderate J_{SC} values. A possible explanation for this phenomenon is the absorption of these dyes, which is located in the high-energy regime of the solar spectrum. Thus, they can only harvest a fraction of the incoming light. Taking into account the presented results a LUMO energy of –3.6±0.1 eV was established as trade-off between the required driving force for charge injection and a minimal energy loss.

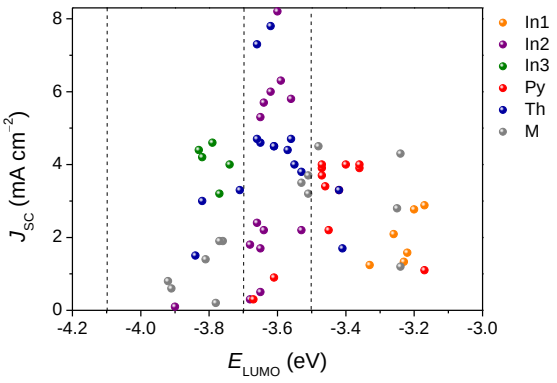

Figure 40. Dependence of J_{SC} of the MC:$PC_{61}BM$ solar cells on the LUMO level of the MC dye. The line at –4.1 eV represents the LUMO of $PC_{61}BM$, the lines at –3.7 eV and –3.5 eV embrace the determined optimal LUMO energy.

As shown in Figure 34, the relative position of the HOMO of the donor material to the LUMO of the electron acceptor determines the possible V_{OC} of the solar device. In several publications a linear relation of V_{OC} to the energy difference between the LUMO (acceptor) and the HOMO (donor) was observed.[137] Figure 41a displays a scatter plot of the HOMO levels as determined by CV of the presented MC dyes relative to the open-circuit voltages of the respective solar cells. It seems that irrespective of the particular HOMO level a relatively high V_{OC} in the range of 0.6–0.8 V can be reached with most of the dyes presented here. Higher V_{OC} were only achieved by dyes exhibiting HOMO levels below –5.7 eV. Remarkably, all of these dyes belong to the dye ***series In2***. The only exception is indolenine **HB312** (***series M***), which exhibits a high V_{OC} of 0.85 V despite a HOMO level of –5.57 eV. The high performance of this chromophore could be originated by the close structural relation of **HB312** to the dyes of ***series In2***. In general, devices containing dyes of ***series In2*** (HOMO ~ –5.8 eV) show significantly higher V_{OC} of ~0.9 V than e.g. cell with ***series In3*** (~0.7 V, HOMO ~ –5.65 V). Here, a direct correlation between the HOMO levels of the donor materials and the V_{OC} of the corresponding device was found. Dyes of ***series Th*** display a smaller band gap than chromophores of ***series In2*** and higher HOMOs of ~ –5.6 eV. The observed open-circuit voltages of 0.6–0.7 V reflect the difference in HOMO energies of ~0.2 eV. However, this rule does not apply in general to the investigated MC dyes, resulting in a strong deviation of the scatter plot from a linear relationship. This was also observed and investigated by Kelvin probe measurements in earlier work by Kronenberg *et. al.*[4] ***Series Py*** for example includes dyes, which show HOMO energies differing by ~0.4 eV, but the same open-circuit voltage of ~0.7 V. This observation could be explained by a strong deviation

between FMO levels in solution and in the solid state, band bending, Fermi level pinning,[138] or the influence of the morphology on the V_{OC}.[139]

Figure 41b depicts a scatter plot between J_{SC} and the HOMO energy of the respective chromophore. As expected, no correlation between the two quantities is observed. However, the strong decay of J_{SC} at HOMO levels below –5.82 eV is noteworthy. Considering the discrepancies of FMOs determined in solution and the solid state, these HOMO levels could be close to the HOMO of $PC_{61}BM$ (–6.1 eV) in the thin films.[41] Seemingly, a completely unidirectional electron transfer from the MC dye to the fullerene is no longer ensured, which could result in a reduction of J_{SC}.

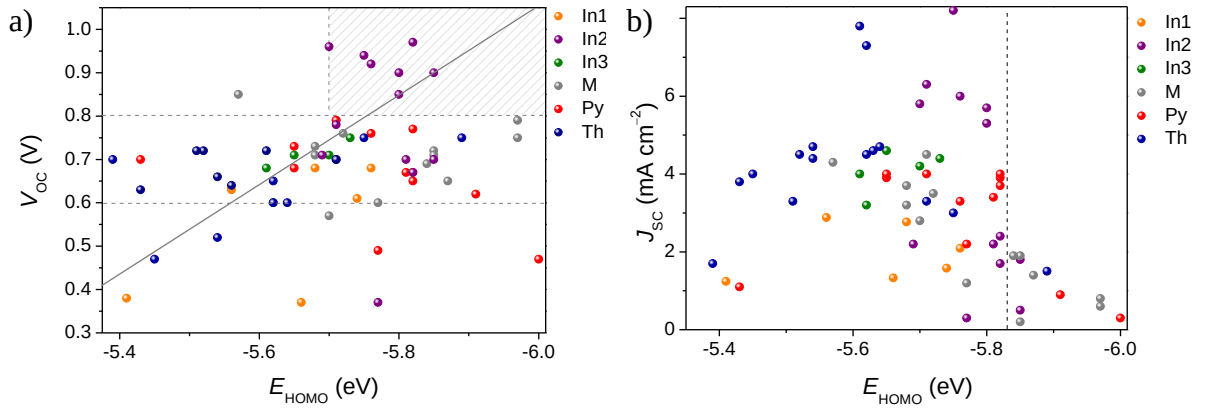

Figure 41. a) Dependence of V_{OC} of the investigated MC:$PC_{61}BM$ solar cells on the HOMO level of the MC dye; the solid line with a slope of 1 illustrates the theoretical relation between V_{OC} and HOMO; the horizontal lines represents the range of V_{OC} between 0.6 and 0.8 V; the horizontal line symbolizes the optimal HOMO level of –5.7 eV. b) Dependence of J_{SC} of the investigated MC:$PC_{61}BM$ solar cells on the HOMO level of the MC dye.

5.3.3 Absorption properties

If we now consider the identified values for the ideal LUMO level of –3.6±0.1 eV and the ideal HOMO level of –5.7±0.1 eV a maximal band gap of 2.1±0.2 eV can be deduced, which is equivalent to a range of λ_{max} = 540–650 nm in dichloromethane. Please note, that here the band gap is not equivalent to the onset of the absorption, but to the maximum of the absorption band in solution. However, although at the expense of V_{OC}, decreasing the band gap of a dye may result in the harvesting of more photons and enhanced J_{SC} owing to a better match of the absorption with the solar irradiation, displaying a maximum between 600-800 nm (Figure 42a). This assumption is partially confirmed by our results.

The scatter plot between the absorption maxima of the compounds in solution and J_{SC} of the respective devices in Figure 42b shows that devices comprising dyes of ***series In1*** display low J_{SC} of less than 3 mA cm^{-2}. The low value for short-circuit current density is

accompanied by a low PCE ≤0.6%. This can be explained with the spectral properties of this dye series, which exhibits the most hypsochromic absorption bands centered at ≤530 nm resulting in a suboptimal overlap with the solar spectrum. Thus, only a small fraction of the solar irradiation can be harvested and converted to electrons. A comparable picture is given with ***series Py***: the dyes display absorption maxima of 530–540 nm, which is just outside the determined optimal absorption range and results in the limitation of J_{SC} to a maximum of 4 mA cm^{-2} and PCE of ≤1%.

Figure 42b highlights, that only one dye (indolenine **HB312**) with an absorption maximum less than 540 nm exceeds J_{SC} of 4 mA cm^{-2}. The absorption band with optimal λ_{max} of ~576 nm enables dyes of ***series In2*** to harvest a significant amount of photons. Obviously, these are efficiently converted to electrons, as most of the devices built with dyes of ***In2*** show J_{SC} values exceeding 5 mA cm^{-2}. Cells with **HB194** reached the maximal value of 8.2 mA cm^{-2} in this work. Dye ***series Th*** shows absorption bands centered at ~630 nm, hence, within the determined optimal range. Here, the good overlap of the absorption with the irradiation entails high J_{SC} values >5 mA cm^{-2} for most of the devices, whereas cells containing **MD304** and **MD319** achieved considerable photocurrents of >7 mA cm^{-2}. In dye ***series In3***, the absorption is further shifted to longer wavelengths with λ_{max} in solution of ~660 nm, which should result in high values for J_{SC}. However, devices containing the green dyes could not exceed J_{SC} of 4.6 mA cm^{-2}. Besides the low driving force for electron transfer due to the low-lying LUMO level discussed in the previous section, their low tinctorial strengths could also reduce the harvesting of photons. The dyes of ***series In3*** show low absorption densities of 0.11–0.15 D^2 mol g^{-1}, whereas the majority of dyes presented here show values of >0.2 D^2 mol g^{-1}. The reduced oscillator strength could be originated by the distorted structure of the bisindandione acceptor, which was discussed in Chapter 3.

The significant number of dyes exhibiting absorption in the range of 540–650 nm, but nevertheless low performance emphasizes that optimal absorption properties are necessary, but not sufficient to result in high J_{SC} and consequently efficient solar cells. Additional to the number of absorbed photons, the morphology of the active layer, exciton diffusions lengths and charge transport properties of the materials are strongly influencing the short-circuit current density. Furthermore, a lower band gap like in the ***series Th*** or ***In3*** results in V_{OC} of usually less than 0.7 eV, restricting the overall PCE (Table 16). Within this work, the optimal trade-off between low HOMO level and consequently high V_{OC} and low band gap enabling high J_{SC} is given in ***series In2***. The correlation between spectral properties and solar cell

performance is visualized in Figure 42a, where in each case the UV-vis spectra of the best performing dyes of each wavelength regime are depicted and the obtained PCE values are stated.

Notably, most of the dyes with resonance parameter c^2 values of 0.4–0.5 resulted in efficient solar cells with PCEs of more than 1% (Table 14–16). Seemingly, systems close to the *cyanine limit* are more suitable for photovoltaic applications than polyene-like chromophores, which could be originated by their small reorganization energy.[125] Sytems with resonance parameters c^2 <0.3 like **HB249**, **EL79** or **MD343** showed poor solar cell performances with PCEs of 0.1–0.2%.

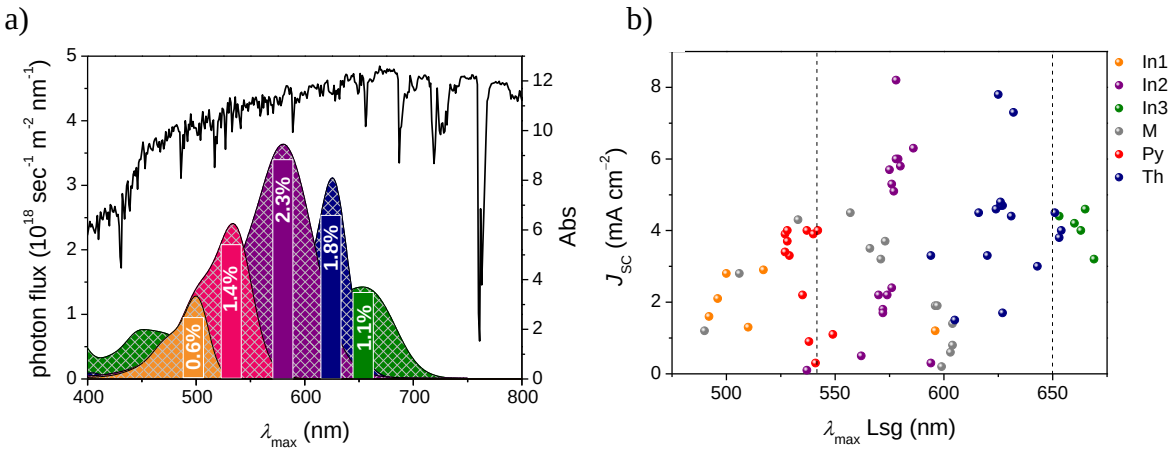

Figure 42. a) UV-vis absorption spectra of **HB330** (orange), **HB312** (red), **EL086** (violet), **MD304** (blue) and **HB218** (green) in CH_2Cl_2 (~10^{-5} M) with the PCE of the respective solar cell and the photon flux at AM1.5 conditions. The area of the absorption band correlates to the respective PCE. b) Dependence of J_{SC} on λ_{max} of the dye in solution; the determined optimal wavelength regime is marked by two dashed lines.

5.3.4 Molecular structure

Surprisingly simple conclusions were obtained after our extensive structural variation. Thus, within this work, the used acceptor units affect the absorption and electrochemical properties of the respective chromophore more strongly than the donor components. Chromophores with the acceptor ***In1*** shows absorption at rather short wavelengths and relatively high-lying LUMO levels. Consequently, the resulting solar cells show low short-circuit current densities and PCEs of ≤0.6%. The same holds true for the acceptor ***series Py***, although the bathochromic shift of the absorption entails higher J_{SC} and PCE of ~1%. The application of stronger acceptors such as in ***series In2*** resulted in favorable low-lying HOMO and LUMO levels and absorption at longer wavelengths. Within this series, the highest values of this work for V_{OC} (0.96 V), J_{SC} (8.2 mA cm^{-2}) and PCE (2.6%) could be achieved for cell with

HB194. Further modifications of the indandione motif in acceptor ***In3*** or the indolenines **HB091** and **HB209** did only result in decreased device performance, which could be caused by the non-planarity of the chromophores. In the case of ***series In3*** a strongly distorted molecular structure was verified for **HB239** by single crystal analysis (see Chapter 3). In all likelihood, the acceptor of **HB209**, **HB095** and **HB092** bearing two cyano acetic acid ester substituents on both sides of the indandione moiety is also not planar, due to the steric hindrance between the H-atoms of the phenyl group and the ethyl ester functionality. Furthermore, NMR studies detected Z/E-isomers of these dyes along the C-C double bond at the acceptor part. It is suggested, that both aspects contribute to a significantly more disordered packing of this chromophore with longer distances between the π-systems compared to **HB194** (Chapter 2). The acceptor ***series Th*** exhibit absorption at favorably long wavelength resulting in beneficial light harvesting abilities. However, this went at the expense of V_{OC} due to higher HOMO levels and could, in addition, not be linearly translated to higher J_{SC} values.

Within each series with varying donor units, compounds with an indolenine donor emerged as the most promising candidates. Besides low-lying FMO levels, the unique feature of this donor unit is given by the two methyl groups in position 3 of the indole, which creates a significant steric demand and imposes packing constraints. As a consequence these dyes usually exhibit good solubility without the necessity of extended alkyl chains. The application of bulky substituents like benzyl of 2-ethylhexyl did usually decrease the device performance due to significantly reduced photocurrents. Obviously, a more favorable packing is achieved for charge transport for substituents with less steric demand. In the case of distorted acceptors like ***In3***, this influence of the side-chains is outbalanced by the one caused by the different side-chains, which do consequently not alter the packing motif or device performance to a noticeable extent. However, none of these dyes is among the top performing ones. Furthermore, the rigidification of the chromophore with ethylene and propylene bridges at the donor moiety often resulted in enhanced J_{SC} and consequently PCE values. In chapter 2, this was rationalized by enhanced hole mobilites of the donor compounds in the blends with $PC_{61}BM$.

The second donor moiety resulting in dyes with excellent performances is the aminothiophene unit. Here again, sufficient solubilities and beneficially low-lying HOMO and LUMO levels were provided. The aniline component is in general among the low-performing donor units, which is possibly originated by the rather polyene-like π-system of

these chromophores. The donor moieties quinoline, pyridine and benzothiazole exhibit promising electronic properties. However, they usually result in low solubilities hampering the solution-processing of the solar cells.

5.4 Conclusion

In summary, the molecular and photovoltaic properties of a comprehensive series of merocyanine dyes with varying donor and acceptor components are presented. The analysis of their structural and electronic features and correlation with the characteristics of the respective solar cell resulted in efficient new chromophores for bulk heterojunction solar cells. According to the presented study, merocyanine dyes close to the *cyanine limit* with absorption maxima at 540–650 nm are most ideally suited for exploitation of solar light in single junction devices. Based on the electrochemical data, an optimal range for the FMO levels was identified with LUMO energy of –3.6±0.1 eV and HOMO energy of –5.7±0.1 eV allowing for efficient charge transfer from the electron donor to the electron acceptor with a minimal energy loss. By doing so, we could stress the advantages of merocyanine dyes like their predominant low-lying HOMO levels almost irrespective of the band gap or the high versatility of this dye class allowing absorption over the whole visible spectrum. However, this systematic study also disclosed the limitations of merocyanine dyes presented in this work: the highest open-circuit voltages were achieved with dyes exhibiting absorption maxima at wavelengths of ~580 nm, restricting the harvesting of photons. On the other hand, the chromophores with smaller band gaps were limited by V_{OC} of ~0.7 V. Additionally, the fill factors of merocyanine cells are usually low. Nevertheless, the application of MC dyes in blends with PCBM in solution-processed BHJ solar cells and the following optimization concerning the electron acceptor material and the hole transporting layer resulted in high-performing solar devices with PCE up to 3.3% and remarkably high V_{OC} of ~1 V. These results show not only the overall benefit of the class of MC dyes for the solar cell research, but contributes to the picture that, in the meantime, small molecules start to compete with their polymeric counterparts also in the area of solution-processed BHJ solar cells.

5.5 Experimental section

5.5.1 Materials and methods

Solvents and reagents were obtained from commercial sources and purified and dried according to standard procedures.[107]

1,3-Indandione (97%), 2-methylbenzothiazol (99%), 4-(diphenylamino)benzaldehyde (98%), 4-methyl-quinolin (99%), 1-bromo-3,3-dimethyl-2-butanone (93%), 2-bromo-1-phenylethanone (98%) were received from Acros Organics, 4-(dibutylamino)benzaldehyde (98%), 1-butyl-4-methylpyridinium iodide (99%), 5-bromthiophene-2-carboxaldehyde (95%) from Sigma Aldrich, 3-oxo-2,3-dihydrobenzo[*b*]thiophene-1,1-dioxide (97%) from Wako Chemicals and 5-dibutylamino-furan-2-carbaldehyde, dibutyl-(4-phenyl-thiazole-2-yl)-amine, 2-(1-phenyl-ethylidene)-malononitrile, 2,3,3-trimethylindolenine and 5-chloro-1,3,3-trimethyl-2-methylene-2,3-dihydro-1*H*-indole were kindly provided by the BASF SE.

Column chromatography was performed with commercial glass columns using silica gel (particle size 0.063 – 0.2 mm) as stationary phase. ^{1}H NMR spectra were recorded with a 400 MHz spectrometer using TMS or residual solvent peaks as internal standard. Coupling constants are given in Hz. UV-vis spectra were measured on a conventional spectrophotometer equipped with temperature controllers. CV was performed on a standard commercial electrochemical analyzer (EC epsilon; BAS Instrument, UK) in a three electrode single-compartment cell under argon. Dichloromethane (HPLC grade) was obtained from J. T. Baker and dried over calcium hydride and degassed prior to use. The supporting electrolyte tetrabutylammonium hexafluorophosphate (TBAHFP) was synthesized according to literature,[90] recrystallized from ethanol/water and dried in high vacuum. The measurements were carried out under exclusion of air and moisture at a concentration of 10^{-4} M with ferrocene as internal standard for the calibration of the potential. Working electrode: Pt disc; reference electrode: Ag/AgCl; auxiliary electrode: Pt wire. The solubility measurements were carried out according to the following procedure: an oversaturated solution of the dye in the solvent of the respective solar cells experiment was generated without stirring or heating. Consequently, the solution was filtered and 0.5 mL of the solution was filled in a weighed glass jar. The solvent was evaporated, the glass jar dried at 60 °C at 5×10^{-3} mbar and the amount of solved dye determined by differential weighing. Electro-optical absorption (EOA) measurements were carried out like described in the following. Dipole moments of the ground state μ_g and the dipole moment differences $\Delta\mu = \mu_e - \mu_g$ (μ_e: excited state dipole moment) of chromophores have been determined by means of EOA spectroscopy by which the difference of absorption of a solution with ($\varepsilon^E(\varphi, \tilde{\nu})$) and without ($\varepsilon(\tilde{\nu})$) an externally applied electric field **E** is measured with light parallelly ($\varphi = 0°$) and perpendicularly ($\varphi = 90°$) polarized to the direction of **E**.[91] For uniaxial phases, induced in a solution by both an alternating and a constant electric field of about 3×10^6 V m^{-1}, the dichroism

$\varepsilon^{E}(\varphi, \tilde{\nu}) - \varepsilon(\tilde{\nu})$ depends on the orientational order of the molecules due to their ground state dipole moment μ_g, the shift of the absorption band proportional to the dipole moments difference $\Delta\mu$, and on the electric field dependence of the electric transition dipole moment $\mu_{eg}(E)$. UV-vis spectra, required for the evaluation of the integral absorption (μ_{eg}^2), were recorded with a Perkin-Elmer Lambda 900 or 950 spectrophotometer at 298 K. All measurements were carried out in dioxane.

5.5.2 Device fabrication

All devices were fabricated on commercial indium tin oxide (ITO) coated glass. The ITO was etched with acid and subsequently cleaned using chloroform, acetone, mucasol detergent and de-ionized water in ultrasonic bath. Next, the ITO substrates were exposed to ozone for 20 minutes and immediately coated with poly(3,4-ethylene-dioxythiophene):poly(styrene sulfonate) (PEDOT:PSS) (Baytron P AL 4083, HC Starck; ca. 40 nm). Afterwards the samples were heat treated for 2 minutes at 110 °C to remove residual water and transferred into a N_2 glove box for the remainder of the fabrication and measurement. Alternatively, instead of PEDOT:PSS a hole transport layer of MoO_3 (Alfa Aesar, 99.95%; ca. 20 nm) was evaporated on the ITO substrate. $PC_{61}BM$ and $PC_{71}BM$ were obtained from Nano-C, the merocyanine dyes were synthesized according to synthetic procedures described below.

The active layers were spin-coated from the solvent (Chlorobenzene, Chlorobenzene with 20% Pyridine, *o*-Dichlorobenzene or Chloroform) containing the mixture of the MC and PCBM. The choice of solvent depended on the solubility of the dye and the film quality.

The substrates were moved to a high-vacuum chamber where the top electrode was evaporated through a mask. Here, either a 120 nm thick Al-layer or combination of a 6 nm Ba-layer (Aldrich, 99%) and 120 nm Ag-layer (Alfa Aesar, 99.9%) was applied. On each substrate, seven solar cells with an active area of 0.08 cm^2 are located. The *JV* characteristics of the solar cells were measured using a Keithley 2425 source measurement unit. The AM 1.5 light was provided by a filtered Xe-lamp. The intensity of 100 mW cm^{-2} of the AM 1.5 light was determined using a calibrated inorganic solar cell from the Fraunhofer Institute for solar research in Freiburg and a reference $PC_{61}BM$:P3HT cell measured by the same institution. No spectral mismatch factor was included in the calculation of the efficiency.

A Dektak surface profiler (Veeco) was used to determine the active layer thicknesses. UV-vis spectra were taken with a Varian Cary 50 spectrometer.

5.5.3 Synthetic procedures

The syntheses and characterization of **MD352**,[4] **MD376**,[4] **HB194**,[99a] **HB193**,[99a] **MD333**,[109] **MD301**,[83] **MD304**,[4] **MD353**,[83] **MD305**,[83] **HB236**,[109] **MD347**,[83] **MD344**[4] and **MD342**[140] were reported previously. The synthetic procedures and characterization data of the new merocyanine dyes are given blow.

5.5.3.1 Syntheses of precursors

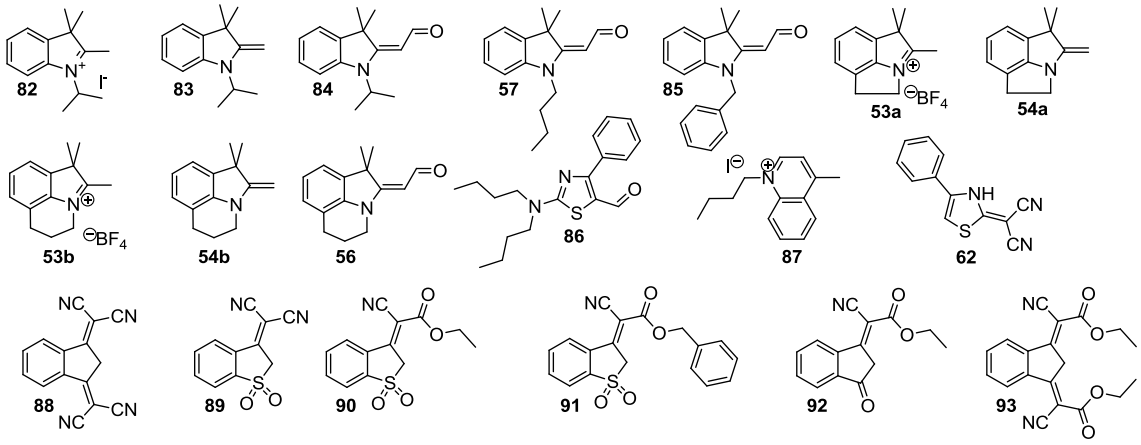

1-Isopropyl-2,3,3-trimethyl-3*H*-indolium iodide 82

2,3,3-Trimethylindolenine (9.37 g, 58.8 mmol) and 2-iodpropane (10.0 g, 58.8 mmol) were mixed and heated to 120 °C for 24 h. The solidified mixture was reduced to small pieces and washed with some cold diethylether. The reaction was carried out following to reference 141. Yield 16.9 g (51.1 mmol, 87%). Mp. 218–221°C. ^{1}H NMR ($CDCl_3$, 400 MHz): δ 7.88 (m, 1H), 7.52 (m, 3H), 5.44 (m, 1H), 3.24 (s, 3H), 1.85 (d, ^3J = 7.1 Hz, 6H), 1.60 (s, 6H). MS (EI): calcd for $C_{14}H_{20}N^+$: 202.2, found 202.1.

1-Isopropyl-3,3-dimethyl-2-methylene-2,3-dihydro-1*H*-indole 83

1-Isopropyl-2,3,3-trimethyl-3*H*-indolium iodide **(**16.9 g, 51.1 mmol) was stirred in 170 mL 1M KOH solution for 1 h at room temperature. After extraction with diethyl ether, the organic phase was dried over Na_2SO_4 and the solvent was evaporated afterwards. The reaction was carried out following reference 142. Yield 10.1 g (50.3 mmol, 98%).^{1}H NMR ($CDCl_3$, 400 MHz): δ 7.06 (m, 2H), 6.70 (m, 2H), 4.14 (m, 1H), 3.94 (s, 1H), 3.84 (s, 1H), 1.42 (d, ^3J = 7.1, 6H), 1.31 (s, 6H). MS (MALDI-TOF, matrix: DCTB): calcd for $C_{14}H_{19}N$: 201.15, found 201.15.

(1-Isopropyl-3,3-dimethyl-1,3-dihydro-indol-2-ylidene)-acetaldehyde 84

Dry DMF (11 mL) was cooled with an ice bath under argon atmosphere, before $POCl_3$ (10 g, 6.0 mL, 65 mmol) was added. Next 1-isopropyl-3,3-dimethyl-2-methylene-2,3-dihydro-1*H*-

indole (10.1 g, 50.3 mmol) in dry DMF (13 mL) was added dropwise and the reaction mixture was stirred at 40 °C for 1.5 h. The solution was poured on 100 mL ice water and the pH was adjusted to 10 with diluted NaOH solution. The mixture was first boiled up for 5 min and extracted with DCM, before the solvent was evaporated. The reaction was carried out following reference 143. Yield 11.4 g (49.5 mmol, 99%). Mp. 125–127 °C. ^{1}H NMR ($CDCl_3$, 400 MHz): δ 10.0 (d, ^{3}J = 8.8, 1H), 7.22 (m, 2H), 7.04 (m, 2H), 5,53 (d, ^{3}J = 8.8, 1H), 4.41 (m, 1H), 1.65 (s, 6H), 1.53 (d, ^{3}J = 7.1, 6H). MS (EI): calcd for $C_{15}H_{19}NO$: 229.1, found 229.1.

(1-Butyl-3,3-dimethyl-1,3-dihydro-indol-2-ylidene)-acetaldehyde 57

2,3,3-Trimethyl-indolenine (20.0 g, 126 mmol) and 1-iodbutan (23.2 g, 14.2 mL, 31.4 mmol) were heated to 120 °C for 24 h. The resulting vitreous solid was solved in DCM and stirred with a 1 M KOH solution (360 mL) for 1 h at room temperature. The mixture was extracted with DCM and the solvent removed under vacuum. Subsequently dry DMF (23 mL) was cooled with an ice bath under argon atmosphere, before $POCl_3$ (21 g, 12.7 mL, 140 mmol) was added. Next, the red oil from part one (25 g) in dry DMF (29 mL) was added dropwise and the reaction mixture was stirred at 40 °C for 1.5 h. The solution was poured on 10 mL ice water and the pH was adjusted to 10 using a diluted NaOH solution. The mixture was first boiled up for 5 min and extracted with ethyl acetate. The solvent was evaporated and the raw product purified by column chromatography (DCM with 1% MeOH). The reaction was carried out following references 141–143. Yield 14.7 g (61 mmol, 48% based on 2,3,3-trimethylindolenine). ^{1}H NMR ($CDCl_3$, 400 MHz): δ 9.93 (d, ^{3}J = 8.9, 1H), 7.22 (m, 2H), 7.02 (m, 1H), 6.80 (m, 1H), 5.34 (d, ^{3}J = 9.0, 1H), 3.64 (m, 2H), 1.63 (m. 8H), 1.36 (m, 2H), 0.89 (t, ^{3}J = 8.9, 3H). MS (MALDI-TOF, matrix: DCTB): calcd for $C_{16}H_{21}NO$: 243.16, found 243.16.

(1-Benzyl-3,3-dimethyl-1,3-dihydro-indol-2-ylidene)-acetaldehyde 85

2,3,3-Trimethyl-indolenine (5.00 g, 31.4 mmol) and benzylbromide (5.37 g, 3.7 mL, 31.4 mmol) were heated to 120 °C for 3 h. The resulting vitreous solid was chopped up and stirred with a 1 M KOH solution (90 mL) for 1 h at room temperature. The mixture was extracted with DCM and the solvent removed under vacuum. Subsequently dry DMF (6.6 mL) was cooled with an ice bath under argon atmosphere, before $POCl_3$ (6.0 g, 3.6 mL, 38.8 mmol) was added. Next, the red oil from part one (7.47 g) in dry DMF (7.9 mL) was added dropwise and the reaction mixture was stirred at 40 °C for 1.5 h. The solution was poured on 10 mL ice water and the pH was adjusted to 10 using a diluted NaOH solution.

The mixture was first boiled up for 5 min and extracted with ethyl acetate. The solvent was evaporated and the raw product purified by column chromatography (DCM with 1% MeOH). The reaction was carried out following references 141–143. Yield 5.47 g (19.7 mmol, 58% based on 2,3,3-trimethylindolenine). ^{1}H NMR ($CDCl_3$, 400 MHz): δ 10.02 (d, ^{3}J = 8.9, 1H), 7.29 (m, 5H), 7.22 (m, 1H), 7.17 (m, 1H), 7.07 (m, 1H), 6.81 (m, 1H), 5.43 (d, ^{3}J = 8.7, 1H), 4.90 (s. 2H), 1.72 (s. 6H). MS (MALDI-TOF, matrix: DCTB): calcd for $C_{19}H_{19}NO$: 277.15, found 277.15.

4,5,5-Trimethyl-2,5-dihydro-1*H*-pyrrolo[3,2,1-*hi*]indolylium tetrafluoro borate 53a

To a solution of HOAc (142 mL) and 2,3-dihydro-1*H*-indole (17.0 g, 143 mmol), sodium nitrite (10.9 g, 161 mmol) was added dropwise within 10 min. After stirring at room temperature for 30 min, 3-methyl-2-butanone (12.3 g, 143 mmol) was added at once and zinc powder (24.9 g, 380 mmol) in small portions. The reaction mixture was heated to reflux for 30 min. The chilled solution was poured in ice cold ammonia (660 mL) and extracted with diethyl ether. The organic layers were dropped into a solution of HBF_4 (12.5 g, 143 mmol) in ethanol (50 mL). The precipitate was filtered off and washed with diethyl ether. The reaction was carried out following reference 81. Yield 11.0 g (40 mmol, 28%). Mp. 217–220 °C. ^{1}H NMR (DMSO–d_6, 400 MHz): δ 7.51 (m, 3H), 4.70 (m, 2H), 3.81 (m, 2H), 2.62 (m, 3H), 1.56 (s, 6H). MS (EI): calcd for $C_{13}H_{16}N$: 186.1, found 186.0.

1,1,2-Trimethyl-1,2,4,5-tetrahydro-4*H*-pyrrolo[3,2,1-*hi*]indole 54a

A 13 mL ethanol solution of 4,5,5-trimethyl-2,5-dihydro-1*H*-pyrrolo[3,2,1-*hi*]indolylium tetrafluoro borate (1.00 g, 3.66 mmol) and KOH (411 mg, 7.32 mmol) was stirred at room temperature for 3 h, before the solvent was removed under vacuum and H_2O dest. was added. The mixture was extracted with diethyl ether, the organic phases dried over Na_2SO_4 and the solvent removed in vacuum. The reaction was carried out following reference 142. Yield 520 mg (2.81 mmol, 77%). ^{1}H NMR ($CDCl_3$, 400 MHz): δ 7.10 (m, 1H), 7.06 (m, 1H), 6.73 (m, 1H), 3.50 (m, 2H), 2.98 (m, 2H), 1.97 (s, 3H), 1.45 (s, 6H). HRMS (ESI): calcd for $C_{13}H_{16}N$ $[M+H]^+$: 186.1277, found 186.1277.

1,1,2-Trimethyl-1,4,5,6-tetrahydro-pyrrolo[3,2,1-*ij*]quinolinylium tetrafluoro borate 53b

To a solution of HOAc (300 mL) and 1,2,3,4-tetrahydro-quinoline (40.0 g, 300 mmol), sodium nitrite (23 g, 0.34 mmol) was added dropwise within 10 min. After stirring at room temperature for 30 min, 3-methyl-2-butanone (25.8 g, 300 mmol) was added at once and zinc powder (52.4 g, 0.8 mmol) in small portions. The reaction mixture was heated to reflux for 30 min. The chilled solution was poured in ice cold ammonia (1.4 L) and extracted with

diethyl ether. The organic layers were dropped into a solution of HBF_4 (26.4 g, 0.3 mmol) in ethanol (500 mL). The precipitate was filtered off and washed wit diethyl ether. The reaction was carried out following reference 81. Yield 15.2 g (53 mmol, 18%). Mp. 240–242 °C. ^{1}H NMR (DMSO–d_6, 400 MHz): δ 7.60 (m, 1H), 7.49 (t, ^{3}J = 8.9, 1H), 7.39 (m, 1H), 4.34 (m, 2H), 2.93 (m, 2H), 2.69 (s, 3H), 2.21 (m, 2H), 1.52 (s, 6H). MS (EI): calcd for $C_{14}H_{18}N$: 200.1, found 200.1.

1,1,2-Trimethyl-1,2,5,6-tetrahydro-4*H*-pyrrolo[3,2,1-*ji*]quinoline 54b

A 12 mL ethanol solution of 1,1,2-trimethyl-1,4,5,6-tetrahydro-pyrrolo[3,2,1-*ij*]quinolinylium tetrafluoro borate (1.00 g, 3.48 mmol) and KOH (390 mg, 6.96 mmol) was stirred at room temperature for 3 h, before the solvent was removed under vacuum and H_2O dest. was added. The mixture was extracted with diethyl ether, the organic phases dried over Na_2SO_4 and the solvent removed in vacuum. The reaction was carried out following reference 142. Yield 450 mg (2.26 mmol, 65%). ^{1}H NMR ($CDCl_3$, 400 MHz): δ 6.93 (m, 1H), 6.87 (m, 1H), 6.65 (m, 1H), 3.80 (m, 1H), 3.77 (m, 1H), 3.40 (m, 2H), 2.72 (m, 2H), 2.08 (m, 2H), 1.35 (s, 6H). HRMS (ESI): calcd for $C_{14}H_{18}N$ $[M+H]^+$: 200.1434, found 200.1434.

(1,1-Dimethyl-5,6-dihydro-1*H*,4*H*-pyrrolo[3,2,1-*ij*]quinoline-2-ylidene)-acetaldehyde 56

Dry DMF (3.0 mL) was cooled with an ice bath under argon atmosphere, before $POCl_3$ (1.85 g, 1.1 mL, 11.8 mmol) was added. Next, 1,1,2-trimethyl-1,2,5,6-tetrahydro-4*H*-pyrrolo[3,2,1-*ji*]quinoline (2.1 g, 10.5 mmol) in dry DMF (1.2 mL) was added dropwise and the reaction mixture was stirred at 35°C for 45 min. The solution was poured on 10 mL ice water and the pH was adjusted to 10 with diluted NaOH solution. The mixture was first boiled up for 5 min and cooled down to room temperature. The precipitate was filtered off and washed with water. The reaction was carried out following reference 143. Yield 1.90 mg (8.36 mmol, 80%). ^{1}H NMR ($CDCl_3$, 400 MHz): δ 9.95 (d, ^3J = 9.1, 1H), 7.06 (m, 1H), 7.01 (m, 1H), 6.94 (m, 1H), 5.32 (d, ^3J = 9.0, 1H), 3.59 (bs, 2H), 2.80 (m, 1H), 2.14 (m, 2H), 1.66 (s, 6H). HRMS (ESI): calcd for $C_{15}H_{18}NO$ $[M+H]^+$: 228.1383, found 228.1383.

2-Dibutylamino-4-phenyl-thiazole-5-carbaldehyde 86

To a solution of dry DMF (1.0 mL) and dibutyl-(4-phenyl-thiazole-2-yl)-amine (200 mg, 0.69 mmol) under argon atmosphere, $POCl_3$ (138 mg, 0.08 mL, 0.90 mmol) in 0.6 mL dry DMF was added. The reaction mixture was stirred at 40 °C for 4 h, before Na_2CO_3 solution was added to get a basic solution. After extraction with DCM, the solvent was removed under vacuum and the product purified by column chromatography (DCM with 2% MeOH). The reaction was carried out following reference 143. Yield 190 mg (0.6 mmol, 87%). ^{1}H NMR

(CD_2Cl_2, 400 MHz): δ 9.67 (s, 1H), 7.70 (m, 2H), 7.46 (m, 3H), 3.54 (bs, 4H), 1.70 (m, 4H), 1.40 (m, 4H), 0.98 (t, ^3J = 7.4, 6H). MS (MALDI-TOF, matrix: DIT): calcd for $C_{18}H_{25}N_2OS$ $[M+H]^+$: 317.17, found 317.17.

1-Butyl-4-methyl-quinolinium iodide 87

A 10 mL MeCN solution of 4-methyl-quinolin (5.0 g, 4.6 mL, 34.9 mmol) and 1-iodobutan (7.2 g, 4.5 mL, 34.9 mmol) was heated to reflux for 24 h. After removal of the solvent, the residual solid was washed with acetone and dried under vacuum. The reaction was carried out following reference 144. Yield 8.00 g (24.5 mmol, 70%). Mp. 129–130 °C. ^{1}H NMR (DMSO–d_6, 400 MHz): δ 9.42 (d, ^3J = 6.0, 1H), 8.60 (d, ^3J = 8.0, 1H), 8.54 (d, ^3J = 8.0, 1H), 8.26 (m, 1 H), 8.07 (d, ^3J = 6.0, 1H), 8.03 (m, 1H), 5.01 (m, 2H), 3.01 (s, 3H), 1.93 (m, 2H), 1.43 (m, 2H), 0.93 (t, ^3J = 7.3, 3H). MS (EI): calcd for $C_{14}H_{18}N$: 200.1, found 200.1.

2-(4-Phenyl-5*H*-thiazol-2-ylidene)-malononitrile 62

A 21 mL ethanol solution of 1-phenyl-2-thiocyanato-ethanone (3.00 g, 17 mmol) and malononitrile (1.12g, 17 mmol) was heated to 30 °C, before NEt_3 (1.5 g, 2.1 mL, 15 mmol) was added. The reaction was stirred at room temperature for 12 h, before 20 mL H_2O dest. were added and the mixture was acidified with HOAc. The precipitate was filtered off and washed with water. The reaction was carried out following reference 145.Yield 3.57 g (16 mmol, 93%). Mp. 244–246 °C. ^{1}H NMR (DMSO–d_6, 400 MHz): δ 7.72 (m, 2H), 7.46 (m, 3H), 7.32 (s, 1H). MS (MALDI-TOF, matrix: HCCA): calcd for $C_{12}H_8SN_3$ $[M+H]^+$: 226.04, found 226.04.

2-(3-Dicyanomethylene-indan-1-ylidene)-malononitrile 88

A 30 mL ethanol solution of 1,3-indandione (2.40 g, 16.0 mmol), malononitrile (2.70 g, 41.0 mmol) and ammonium acetate (1.25 g, 16.0 mmol) was heated to reflux for 30 min. After cooling down to room temperature, 25 mL H_2O dest. were added and the mixture was acidified by HCl. The precipitate was filtered off and recrystallized from acetic acid. The reaction was carried out following reference 146. Yield 3.14 g (13 mmol, 81%). Mp. 255–257 °C. ^{1}H NMR (DMSO–d_6, 400 MHz): δ 7.90 (m, 2H), 7.42 (m, 2H), 5.70 (s, 2H). MS (EI): calcd for $C_{15}H_6N_4$: 242.1, found 242.0.

2-(1,1-Dioxo-1,2-dihydro-1λ^6-benzo[b]thiophen-3-ylidene)-malononitrile 89

To a 4 mL dry ethanol solution of 3-oxo-2,3-dihydrobenzo[*b*]thiophene-1,1-dioxide (250 mg, 1.37 mmol) and malononitrile (100 mg, 1.51 mmol) under argon atmosphere and 5 drops of a mixture of piperidine:acetic acid=1:5 were added. The reaction was heated to 60 °C for 6 h. Then, additional malononitrile (50 mg, 0.76 mmol) in 0.5 mL dry ethanol was added. The

mixture was heated to 60 °C for 16 h. The precipitate was filtered off and washed with some cold ethanol. The reaction was carried out following reference 147. Yield 276 mg (1.20 mmol, 87%). Mp. 203–205 °C. ^{1}H NMR ($CDCl_3$, 400 MHz): δ 8.03 (m, 2H), 7.96 (m, 1H), 7.83 (m, 1H), 4.10 (s, 2H). MS (MALDI-TOF, matrix: DIT): calcd for $C_{11}H_6N_2O_2S$: 230.02, found 230.03.

Cyano-(1,1-dioxo-1,2-dihydro-1λ^6-benzo[*b*]thiophen-3-ylidene)-acetic acid ethyl ester 90

To a 1.6 mL dry ethanol solution of 3-oxo-2,3-dihydrobenzo[*b*]thiophene-1,1-dioxide (100 mg, 0.55 mmol) and cyano-acetic-acid ethyl ester (124 mg, 0.12 mL, 1.1 mmol) under argon atmosphere, three drops of a mixture of piperidine:acetic acid=1:5 were added. Afterwards the reaction was heated to 60 °C for 4 h. Then, additional cyano-acetic-acid ethyl ester (62 mg, 0.06 mL, 0.55 mmol) was added. The mixture was heated again to 60 °C for 17 h. The precipitate was filtered off and washed with some cold ethanol. The reaction was carried out following reference 147. Yield 85 mg (0.31 mmol, 56%). Mp. 204–206 °C. ^{1}H NMR ($CDCl_3$, 400 MHz): δ 8.89 (m, 1H), 7.95 (m, 1H), 7.84 (m, 2H), 4.83 (s, 2H), 4.40 (q, ^3J = 7.1, 2H), 1.42 (t, ^3J = 7.1, 3H). MS (MALDI-TOF, matrix: DHB): calcd for $C_{13}H_{11}NO_4S$ $[M+Na]^+$: 300.03, found 299.99.

Cyano-(1,1-dioxo-1,2-dihydro-1λ^6-benzo[*b*]thiophen-3-ylidene)-acetic acid benzyl ester 91

To a 1.6 mL dry ethanol solution of 3-oxo-2,3-dihydrobenzo[*b*]thiophene-1,1-dioxide (100 mg, 0.55 mmol) and cyano-acetic-acid benzyl ester (192 mg, 0.17 mL, 1.10 mmol) under argon atmosphere, three drops of a mixture of piperidine: acetic acid=1:5 were added. Afterwards the reaction was heated to 60 °C for 4 h. Then, additional cyano-acetic-acid benzyl ester (96 mg, 0.09 mL, 0.55 mmol) was added. The mixture was heated to 60 °C for 17 h. The precipitate was filtered off and washed with some cold ethanol. The reaction was carried out following reference 147. Yield 124 mg (0.37 mmol, 66%). Mp. 228–229 °C. ^{1}H NMR ($CDCl_3$, 400 MHz): δ 8.89 (m, 1H), 7.95 (m, 1H), 7.85 (m, 2H), 7.35-7.47 (m, 5H), 5.37 (s, 2H), 4.83 (s, 2H). MS (MALDI-TOF, matrix: DIT): calcd for $C_{18}H_{13}NO_4S$: 339.06, found 339.18.

Cyano-(3-oxo-indan-1-ylidene)-acetic acid ethyl ester 92

To a 33 mL ethanol solution with 1,3-indandione (4.38 g, 30.0 mol) cyano-acetic acid ethyl ester (6.79 g, 60.0 mol) was added. Before the mixture was heated to 55 °C for 1 h, NaOAc (2.50 g, 30.0 mol) was added in 5 portions. After adding 90 mL H_2O dest., the reaction was cooled down to room temperature and acidified to pH 2 with diluted HCl. The light green

precipitate was filtered off and dried under vacuum. The reaction was carried out following reference 146. Yield 4.40 g (18.2 mmol, 61%). ^{1}H NMR ($CDCl_3$, 400 MHz): δ 9.3 (m, 3H), 8.45 (m, 1H), 4.06 (q, ^3J = 7.0, 2H), 3.69 (s, 2H), 1.06 (t, ^3J = 7.0, 3H). MS (MALDI-TOF, matrix: DIT): calcd for $C_{14}H_{12}NO_3$ $[M+H]^+$: 242.08, found 242.06.

Cyano-[3-(cyano-ethoxycarbonyl-methylene)-indan-1-ylidene]-acetic ethyl ester 93

To a 15 mL dry ethanol solution with 1,3-indandione (1.00 g, 6.84 mmol) cyano acetic acid ethyl ester (4.64 g, 41.0 mmol) was added. Before the mixture was heated under reflux for 28 h, NaOAc (5.59 g, 41.0 mmol) was added in 5 portions. After adding 100 mL H2O dest., the reaction was cooled down to room temperature and acidified to pH 2 with diluted HCl. The mixture was extracted by DCM, the solvent removed under vacuum and the residue purified by column chromatography (DCM with 2% MeOH). The reaction was carried out following reference 146. Yield 1.24 g (3.70 mmol, 54%). Mp. 211–214 °C. ^{1}H NMR ($CDCl_3$, 400 MHz): δ 8.88 (m, 2H), 7.79 (m, 2H), 4.80 (s, 2H), 4.40 (q, ^3J = 7.1, 4H), 1.42 (t, ^3J = 7.1, 3H). HRMS (ESI): calcd for $C_{19}H_{20}N_3O_4$ $[M+NH_4]^+$: 354.1448, found: 354.1448.

5.5.3.2 Syntheses of ***series In1***

2-(4-Dibutylamino-benzylidene)-indan-1,3-dione HB249

A 7.0 mL Ac_2O solution of 4-dibutylamino-benzaldehyde (1.58 mg, 6.84 mmol) and 1,3-indandione (1.00 mg, 6.84 mmol) was heated to 90 °C for 30 min, before the solvent was removed under vacuum. After the column chromatography (DCM), the obtained solid was solved in DCM and precipitated with *n*-hexane. Yield 1.74 g (4.81 mmol, 70%). Mp. 127–129 °C. ^{1}H NMR (CD_2Cl_2, 400 MHz): δ 8.50 (d, ^3J = 8.8, 2H), 7.87 (m, 2H), 7.73 (m, 3H), 6.74 (m, 2H), 3.42 (t, ^3J = 7.9, 4H), 1.65 (m, 4H), 1.40 (m, 4H), 0.99 (t, ^3J = 7.4, 6H). UV-vis (DCM): λ_{max} (ε): 492 (83200 M^{-1} cm^{-1}). HRMS (ESI): calcd. for $C_{24}H_{28}NO_2$ $[M+H]^+$: 362.2115, found: 362.2115. Elemental analysis (%) calcd for $C_{24}H_{27}NO_2$: C, 79.74; H, 7.53; N, 3.87. Found: C, 79.76; H, 7.55; N, 3.91. CV data: $E_{1/2}^{ox}$ = 590 mV vs Fc, $E_{1/2}^{red}$ = −1761 mV vs Fc.

2-{2-[2-(3-Butyl-3*H*-benzothiazol-2-ylidene)-ethylidene]-3-oxo-indan-1-ylidene}-malononitril EL41

To a stirred solution of 1-butyl-2-methyl-1,3-benzothiazolium iodide[148] (668 mg, 2.00 mmol) in 7.0 mL ethanol 2-phenylaminomethylene-indan-1,3-dione[149] (498 mg, 2.00 mmol) was added. The mixture was refluxed under argon for 5 min, before piperidine (195 mg, 0.23 mL, 2.30 mmol) was added and the resulting solution refluxed overnight. After cooling to room

temperature the precipitate was filtered off and washed with *iso*-propanol. Yield 440 mg (1.22 mmol, 61%). Mp. 221–222 °C. ^{1}H NMR (DMSO–d_6, 400 MHz): δ 7.99 (dd, ^3J = 8.0, ^4J = 0.9, 1H), 7.76 (d, ^3J = 8.0, 1H), 7.53−7.44 (m, 4H), 7.60 (d, ^3J = 13.7, 1H), 7.55 (td, ^3J = 7.8, ^4J = 0.9, 1H), 7.47 (d, ^3J = 13.7, 1H), 7.41 (td, ^3J = 7.8, ^4J = 0.9, 1H), 4.32 (t, ^3J = 7.2, 2H), 1.79 (m, 2H), 1.46 (m, 2H), 1.00 (t, ^3J = 7.2, 3H). UV-vis (DCM): λ_{max} (ε) = 510 (115400 M^{-1} cm^{-1}). HRMS (ESI): calcd for $C_{22}H_{19}NO_2S$ $[M]^+$: 361.1136, found: 361.1131. Elemental analysis (%) calcd for $C_{22}H_{19}NO_2S$: C, 73.10; H, 5.30; N, 3.88; S, 8.87. Found: C, 72.95; H, 5.41; N, 3.92; S, 8.83. CV data: E_p^{ox} = 510 mV vs Fc, $E_{1/2}^{red}$ = –1882 mV vs Fc.

2-[2-(1-Butyl-1*H*-pyridin-4-ylidene)-ethylidene]-indan-1,3-dione EL42

To a stirred solution of 1-butyl-4-methylpyridinium iodide (554 mg, 2.00 mmol) in 7.0 mL ethanol was added 2-phenylaminomethylene-indan-1,3-dione[149] (498 mg, 2.00 mmol). The mixture was refluxed under argon for 5 min, before piperidine (0.23 mL, 2.30 mmol) was added and the resulting solution refluxed overnight. After cooling to room temperature the precipitate was filtered off and washed with *iso*-propanol. Yield 400 mg (1.31 mmol, 65%). Mp. 130–132 °C. ^{1}H NMR (DMSO–d_6, 400 MHz): δ 8.17 (d, ^3J = 6.7, 2H), 7.66 (d, ^3J = 14.9, 1H), 7.53−7.43 (m, 4H), 7.41 (d, ^3J = 5.3, 2H), 7.19 (d, ^3J = 14.9, 1H), 4.64 (t, ^3J = 7.4, 2H), 1.77 (m, 2H), 1.42 (m, 2H), 0.93 (t, ^3J = 7.4, 3H). UV-vis (DCM): λ_{max} (ε): 539 (147000 M^{-1} cm^{-1}). HRMS (ESI): calcd. for $C_{20}H_{19}NO_2$ $[M]^+$: 305.1416, found: 305.1410. Elemental analysis (%) calcd for $C_{20}H_{19}NO_2$: C, 78.66; H, 6.27; N, 4.59. Found: C, 78.70; H, 6.32; N, 4.63. CV data: E_p^{ox} = 200 mV vs Fc, $E_{1/2}^{red}$ = –1936 mV vs Fc.

2-[2-(1-Butyl-1*H*-quinolin-4-yliden)-ethylidene]-indan-1,3-dione EL44

To a stirred solution of 1-butyl-4-methylquinolinium iodide (654 mg, 2.00 mmol) in 7.0 mL ethanol was added 2-phenylaminomethylene-indan-1,3-dione (498 mg, 2.00 mmol). The mixture was refluxed under nitrogen for 5 min, before piperidine (0.23 mL, 2.30 mmol) was added and the resulting solution refluxed overnight. After cooling to room temperature the precipitate was filtered off and washed with *iso*-propanol. Yield 600 mg (1.69 mmol, 84%). Mp. 237–240 °C. ^{1}H NMR (DMSO–d_6, 400 MHz): δ 8.32 (dd, ^3J = 8.9, ^4J = 1.1, 1H), 8.27 (d, ^3J = 7.3, 1H), 8.14 (d, ^3J = 14.4, 1H), 8.03 (dd, ^3J = 8.9, ^4J = 1.1, 1H), 8.00 (d, ^3J = 14.4, 1H), 7.93 (m, 1H), 4.64 (m, 1H), 7.61−7.55 (m, 4H), 4.52 (m, 2H), 1.79 (m, 2H), 1.38 (m, 2H), 0.93 (t, ^3J = 7.5, 3H). UV-vis (DCM): λ_{max} (ε): 596 (202800 M^{-1} cm^{-1}). HRMS (ESI): calcd. for $C_{24}H_{21}NO_2$ $[M]^+$: 355.1572, found: 355.1567. Elemental analysis (%) calcd for $C_{24}H_{21}NO_2$: C, 81.10; H, 5.96; N, 3.94. Found: C 81.10; H, 5.89; N, 3.99. CV data: E_p^{ox} = 260 mV vs Fc, $E_{1/2}^{red}$ = –1666 mV vs Fc.

5.5.3.3 Syntheses of ***series In2***

2-{2-[2-(1-Butyl-3,3-dimethyl-1,3-dihydro-indol-2-ylidene)-2-cyano-ethylidene]-3-oxo-indan-1-ylidene}-malononitrile HB276

A 2.0 mL Ac_2O solution of 2-(1-butyl-3,3-dimethylindolin-2-ylidene)-3-oxopropanenitrile (300 mg, 1.11 mmol) and 2-(3-oxo-indan-1-ylidene)-malononitrile[82] (217 mg, 1.11 mmol) was heated to 90 °C for 45 min, before the solvent was removed. The residue was purified twice by column chromatography (DCM). Yield 332 mg (0.75 mmol, 67%). Mp. 211–213 °C. ^{1}H NMR (CD_2Cl_2, 400 MHz): δ 8.60 (d, ^3J = 7.3, 1H), 8.49 (d, ^3J = 7.8, 1H), 8.39 (s, 1H), 8.12 (s, 1H), 7.85 (d, ^3J = 7.0, 1H), 7.75 (m, 2H), 7.67 (m, 3H), 7.44 (m, 4H), 7.34 (m, 2H), 7.19 (m, 2H), 4.19 (m, 2H), 4.07 (m, 2H), 2.13 (m, 1H), 2.04 (m, 1H), 1.91 (m, 2H), 1.86 (s, 3H), 1.81 (s, 6H), 1.73 (s, 3H), 1.58 (m, 2H), 1,43 (m, 2H), 1.08 (t, ^3J = 7.3, 3H), 0.99 (t, ^3J = 7.3, 3H). UV-Vis (DCM): λ_{max} (ε): 537 (38200 M^{-1} cm^{-1}). HRMS (ESI): calcd for $C_{29}H_{25}N_4O$ $[M+H]^+$: 445.2023, found: 445.2023. CV data: E_p^{ox} = 1052 mV vs Fc, $E_{1/2}^{red}$ = –1307 mV vs Fc, E_p^{red} = –2000 mV vs Fc.

2-[2-(5-Carbazol-9-yl-thiophen-2-ylmethylene)-3-oxo-indan-1-ylidene]-malononitrile HB391

A 1.0 mL Ac_2O solution of 5-(9*H*-carbazol-9-yl)thiophene-2-carbaldehyde (300 mg, 1.08 mmol) and 2-(3-oxo-indan-1-ylidene)-malononitrile[82] (190 mg, 0.98 mmol) was heated to 90 °C for 90 min. The reaction mixture was suspended in *n*-hexane before the precipitate was filtered off and washed with *iso*-propanol. The residue was purified by column chromatography (DCM:*n*-hexane=2:1) and recrystallization from DCM/*n*-hexane. Yield 170 mg (0.37 mmol, 38%). Mp. 323–325 °C. ^{1}H NMR (CD_2Cl_2, 400 MHz): δ 8.94 (s, 1H), 8.71 (m, 1H), 8.15 (m, 2H), 8.03 (m, 1H), 7.94 (m, 1H), 7.88 (m, 2H), 7.80 (m, 2H), 7.54 (m, 2H), 7.50 (d, ^3J = 4.3, 1H), 7.40 (m, 2H). UV-vis (DCM): λ_{max} (ε): 545 (34800 M^{-1} cm^{-1}). HRMS (ESI): calc. for $C_{29}H_{16}N_3OS$ $[M+H]^+$: 454.1009, found: 454.1008. Elemental analysis (%) calcd for $C_{29}H_{15}N_3OS \times 0.4\ H_2O$: C, 74.82; H, 3.54; N, 9.03; S, 6.89. Found: C, 74.92; H, 3.38; N, 9.07; S, 6.65. CV data: $E_{1/2}^{ox}$ = 966 mV vs Fc, E_p^{red} = –1151 mV vs Fc.

2-[2-(4-Diphenylamino-benzylidene)-3-oxo-indan-1-ylidene]-malononitrile EL79

A 5.0 mL Ac_2O solution of 4-diphenylamino-benzaldehyde (1.37 g, 5.0 mmol) and 2-(3-oxo-indan-1-ylidene)-malononitrile[82] (970 mg, 5.0 mmol) was heated to 90 °C for 1 h. After solvent removal, the product was isolated by column chromatography (DCM) and precipitation from DCM/*n*-hexane. Yield 1.63 g (3.63 mmol, 72%). Mp. 225–227 °C. ^{1}H NMR (DMSO–d_6, 400 MHz): δ 8.49 (d, ^3J = 7.6, 1H), 8.35 (s, 1H), 8.21 (d, ^3J = 7.8, 2H),

7.96 (m, 1H), 7.87 (m, 2H), 7.48 (t, ^3J = 7.6, 4H), 7.31 (d, ^3J = 7.6, 6H), 6.85 (d, ^3J = 9.0, 2H). UV-vis (DCM): λ_{max} (ε) = 562 (47000 $M^{-1}cm^{-1}$). HRMS (ESI): calcd for $C_{31}H_{20}N_3O$ $[M+H]^+$: 450.1601, found: 450.1589. Elemental analysis (%) calcd for $C_{31}H_{19}N_3O$: C, 82.83; H, 4.26; N, 9.35. Found: C, 82.80; H, 4.23; N, 9.28. CV data: $E_{1/2}^{ox}$ = 704 mV vs Fc, E_p^{red} = –1260 mV vs Fc.

2-[2-(4-Dibutylamino-benzylidene)-3-oxo-indan-1-ylidene]-malononitrile EL85

A 1.0 mL Ac_2O solution of 4-dibutylamino-benzaldehyde (233 mg, 1.00 mmol) and 2-(3-oxo-indan-1-ylidene)-malononitrile[82] (194 mg, 1.00 mmol) was heated to 90 °C for 1 h. After solvent removal, the product was isolated by column chromatography (DCM) and precipitation from DCM/*n*-hexane. Yield 275 mg (0.67 mmol, 67%). Mp. 152–153 °C. ^{1}H NMR (DMSO–d_6, 400 MHz): δ 8.45 (d, ^3J = 7.8, 1H), 8.30 (s, 1H), 8.25 (d, ^3J = 9.2, 2H), 7.88 (m, ^3J = 4.5, ^4J = 1.0, 1H), 7.81 (dd, ^3J = 4.5, ^4J = 1.0, 1H), 6.91 (d, ^3J = 9.2, 2H), 3.50 (m, 4H), 1.58 (m, 4H), 1.38 (m, 4H), 0.95 (t, ^3J = 7.8, 6H). UV-vis (DCM): λ_{max} (ε) = 570 (69500 M^{-1} cm^{-1}). HRMS (ESI): calcd for $C_{27}H_{27}N_3O$ $[M]^+$: 409.2154, found: 409.2149. Elemental analysis (%) calcd for $C_{27}H_{27}N_3O$: C, 79.19; H, 6.65; N, 10.26. Found: C, 79.23; H, 6.70; N, 10.32. CV data: $E_{1/2}^{ox}$ = 661 mV vs Fc, E_p^{red} = –1378 mV vs Fc.

2-{2-[-(5-Chloro-1,3,3-trimethyl-1,3-dihydro-indol-2-ylidene)-ethylidene]-3-oxo-indan-1-ylidene}-malononitrile HB345

A 7.0 mL EtOH solution of 5-chloro-1,3,3-trimethyl-2-methylene-2,3-dihydro-1*H*-indole (416 mg, 2.00 mmol), 2-(3-oxo-indan-1-ylidene)-malononitrile[82] (388 mg, 2.00 mmol) and ethyl orthoformate (445 mg, 3.00 mmol) were heated to reflux for 1 h, before the solvent was removed under vacuum. After column chromatography (DCM), the obtained solid was solved in DCM and precipitated with *n*-hexane. Yield 441 mg (1.07 mmol, 54%). Mp. 327–330 °C. ^{1}H NMR ($CDCl_3$, 400 MHz): δ 9.03 (d, ^3J = 13.6, 1H), 8.59 (m, 1H), 7.94 (d, ^3J = 13.6, 1H), 7.74 (m, 1H), 7.61 (m, 2H), 7.32 (m, 2H), 6.97 (d, ^3J = 8.3, 1H), 3.58 (s, 3H), 1.80 (s, 6H). UV-vis (DCM): λ_{max} (ε) = 572 (724000 M^{-1} cm^{-1}). HRMS (ESI): calcd for $C_{25}H_{19}ClN_3O$ $[M+H]^+$: 412.1211, found: 412.1206. Elemental analysis (%) calcd for $C_{25}H_{18}ClN_3O$: C, 72.90; H, 4.40; N, 10.20. Found: C, 72.47; H, 4.34; N, 10.36. CV data: $E_{1/2}^{ox}$ = 669 mV vs Fc, $E_{1/2}^{red}$ = –1478 mV vs Fc.

2-{2-[2-(1-Benzyl-3,3-dimethyl-1,3-dihydro-indol-2-ylidene)-ethylidene]-3-oxo-indan-1-ylidene}-malononitrile HB329

A 2.0 mL ethanol solution of 1-benzyl-3,3-dimethyl-2-methylene-2,3-dihydro-1*H*-indole (499 mg, 2.00 mmol), 2-(3-oxo-indan-1-ylidene)-malononitrile[82] (388 mg, 2.00 mmol) and

ethyl orthoformate (445 mg, 3.00 mmol) were heated to reflux for 1 h. After solvent removal, the product was purified by column chromatography (DCM) and precipitation from DCM/*n*-hexane. Yield 232 mg (0.51 mmol, 26%). Mp. 263–267 °C. ^{1}H NMR ($CDCl_3$, 400 MHz): δ 9.07 (d, ^3J = 13.6, 1H), 8.57 (m, 1H), 8.12 (d, ^3J = 13.6, 1H), 7.71 (m, 1H), 7.59 (m, 2H), 7.35 (m, 7H), 7.23 (m, 1H), 7.07 (m, 1H), 5.24 (s, 2H), 1.85 (s, 6H). UV-vis (DCM): λ_{max} (ε) = 572 (70600 M^{-1} cm^{-1}). HRMS (ESI): calcd for $C_{31}H_{23}N_3O$ $[M]^+$: 453.1841, found: 453.1836. Elemental analysis (%) calcd for $C_{31}H_{23}N_3O$: C, 82.10; H, 5.11; N, 9.27. Found: C, 81.89; H, 5.13; N, 9.24. CV data: $E_{1/2}^{ox}$ = 700 mV vs Fc, $E_{1/2}^{red}$ = –1479 mV vs Fc.

2-[2-(4a,9-Dimethyl-3,4,4a,9-tetrahydro-2*H*-carbazol-1-ylmethylene)-3-oxo-indan-1-ylidene]-malononitrile HB280

A 1.3 mL Ac_2O solution of 4a,9-dimethyl-3,4,4a,9-tetrahydro-2*H*-carbazole-1-carbaldehyde (300 mg, 1.32 mmol) and 2-(3-oxo-indan-1-ylidene)-malononitrile[82] (256 mg, 1.32 mmol) was heated to 90 °C for 30 min. The precipitate was filtered and washed with *n*-hexane and *iso*-propanol, before purification by column chromatography (DCM with 1% MeOH). Yield 352 mg (0.87 mmol, 66%). Mp. 238–240 °C. ^{1}H NMR (CD_2Cl_2, 400 MHz): δ 8.31 (m, 1H), 7.74 (s, 1H), 7.51 (m, 2H), 7.43 (m, 2H), 7.34 (m, 3H), 3.28 (s, 3H), 2.96 (m, 1H), 2.77 (m, 1H), 2.48 (m, 1H), 2.20 (m, 1H), 1.87 (m, 1H), 1.75 (m, 1H), 1.67 (s, 3H). UV-vis (DCM): λ_{max} (ε): 574 (25800 M^{-1} cm^{-1}). HRMS (ESI): calcd for $C_{27}H_{21}N_3O$ $[M]^+$: 403.1685, found: 403.1679. Anal. Calcd. for $C_{27}H_{21}N_3O \times {}^1/_3\ H_2O$: C, 79.20; H, 5.33; N, 10.26; Found: C, 72.21; H, 5.24; N, 10.23. CV data: E_p^{ox} = 539 mV vs Fc, $E_{1/2}^{red}$ = –1450 mV vs Fc, E_p^{red} = –2112 mV vs Fc.

2-{2-[2-(1-Isopropyl-3,3-dimethyl-1,3-dihydro-indol-2-ylidene)-ethylidene]-3-oxo-indan-1-ylidene}-malononitrile MD518

A 5.0 mL ethanol solution of 1-*iso*-propyl-3,3-dimethyl-2-methylene-2,3-dihydro-1*H*-indole (742 mg, 3.68 mmol), 2-(3-oxo-indan-1-ylidene)-malononitrile[82] (715 mg, 3.68 mmol) and ethyl orthoformate (818 mg, 5.53 mmol) was heated to reflux for 30 min. After cooling down to room temperature the solvent was evaporated and the raw product purified by column chromatography (DCM) and precipitation from DCM/*n*-hexane. Yield 282 mg (0.70 mmol, 19%). Mp. 215–217 °C. ^{1}H NMR ($CDCl_3$, 400 MHz): δ 9.06 (d, ^3J = 13.8, 1H), 8.58 (m, 1H), 8.25 (d, ^3J = 13.8, 1H), 7.72 (m, 1H), 7.58 (m, 2H), 7.36 (m, 2H), 7.23 (m, 2H), 4.84 (m, 1H), 1.80 (s, 6H), 1.73 (d, ^3J = 6.9, 6H). UV-vis (DCM): λ_{max} (ε) = 575 (64500 M^{-1} cm^{-1}). HRMS (ESI): calcd for $C_{27}H_{24}N_3O$ $[M+H]^+$: 406.1914, found: 406.1921. Elemental analysis (%)

calcd for $C_{27}H_{23}N_3O$: C, 79.97; H, 5.72; N, 10.36. Found: C, 79.28; H, 5.66; N, 10.30. CV data: $E_{1/2}^{ox}$ = 647 mV vs Fc, $E_{1/2}^{red}$ = –1532 mV vs Fc.

2-(2-{2-[1-(2-Ethylhexyl)-3,3-dimethyl-1,3-dihydro-indol-2-ylidene]-ethylidene}-3-oxo-indan-1-ylidene)-malononitrile MD504

A 5.0 mL ethanol solution of 1-(2-ethylhexyl)-3,3-dimethyl-2-methylene-2,3-dihydro-1*H*-indole (1.00 g, 3.68 mmol), 2-(3-oxo-indan-1-ylidene)-malononitrile[82] (715 mg, 3.68 mmol) and ethyl orthoformate (818 mg, 5.53 mmol) was heated to reflux for 30 min. After cooling down to room temperature the solvent was evaporated and the crude product was purified by column chromatography (DCM) and precipitation from DCM/*n*-hexane. Yield 286 mg (0.60 mmol, 16%). Mp. 150–154 °C. ^{1}H NMR ($CDCl_3$, 400 MHz): δ 9.06 (d, ^3J = 13.8, 1H), 8.57 (m, 1H), 8.08 (d, ^3J = 13.8, 1H), 7.73 (m, 1H), 7.58 (m, 2H), 7.36 (m, 2H), 7.22 (m, 1H), 7.05 (m, 1H), 3.95 (d, ^3J = 7.6, 2H), 2.10 (m, 1H), 1.81 (s, 6H), 1.24–1.50 (m, 8H), 1,01 (t, ^3J = 7.4, 3H), 0.87 (t, ^3J = 7.9, 3H). UV-vis (DCM): λ_{max} (ε) = 576 (59000 M^{-1} cm^{-1}). HRMS (ESI): calcd for $C_{32}H_{33}N_3O$ $[M]^+$: 475.2624, found: 475.2618. Elemental analysis (%) calcd for $C_{32}H_{33}N_3O$: C, 80.81; H, 6.99; N, 8.83. Found: C, 80.29; H, 7.26; N, 8.17. CV data: $E_{1/2}^{ox}$ = 667 mV vs Fc, $E_{1/2}^{red}$ = –1527 mV vs Fc.

2-{2-[5-(Butyl-ethyl-amino)-thiophen-2-ylmethylene]-3-oxo-indan-1-ylidene}-malononitrile HB366

A 5.0 mL Ac_2O solution of 5-(butyl(ethyl)amino)thiophene-2-carbaldehyde (0.90 g, 4.6 mmol) and 2-(3-oxo-indan-1-ylidene)-malononitrile[82] (0.81 g, 4.2 mmol) was heated to 90 °C for 1 h, before *n*-hexane was added and the solution was decanted. The residue was stirred with *iso*-propanol, filtered off and recrystallized from DCM/*n*-hexane. Yield 1.16 g (3.0 mmol, 72%). Mp. 231–232 °C. ^{1}H NMR (CD_2Cl_2, 400 MHz): δ 8.58 (s, 1H), 8.51 (m, 1H), 7.67 (m, 1H), 7.59 (m, 3H), 6.37 (d, ^3J = 5.0, 1H), 3.63 (q, ^3J = 7.2, 2H), 3.50 (m, 2H), 1.75 (m, 2H), 1.43 (m, 2H), 1.36 (t, ^3J = 7.2, 2H), 1.00 (t, ^3J = 7.3, 3H). UV-vis (DCM): λ_{max} (ε): 578 (64500 M^{-1} cm^{-1}). HRMS (ESI): calcd for $C_{23}H_{21}N_3OS$ $[M]^+$: 387.1405, found: 387.1400. Elemental analysis (%) for $C_{23}H_{21}N_3OS$ × ½ H_2O: C, 69.67; H, 5.59; N, 10.60; S, 8.09. Found: C, 68.82; H, 5.29; N, 10.69; S, 8.07.

2-[3-Oxo-2-(5-pyrrolidin-1-yl-thiophen-2-ylmethylene)-indan-1-ylidene]-maloninitrile HB374

A 2.0 mL Ac_2O solution of 5-(pyrrolodin-1-yl)thiophene-2-carbaldehyde (400 mg, 2.21 mmol) and 2-(3-oxo-indan-1-ylidene)-malononitrile[82] (390 mg, 2.01 mmol) was heated to 90 °C for 80 min. The reaction mixture was suspended in *n*-hexane, before the precipitate

was filtered off and washed with *iso*-propanol. The residue was purified by column chromatography (DCM:EtOAc=30:1) and recrystallization from DCM/*n*-hexane. Yield 360 mg (1.01 mmol, 50%). Mp. 295–296 °C. ^{1}H NMR (CD_2Cl_2, 400 MHz): δ 8.59 (s, 1H), 8.51 (m, 1H), 7.68 (m, 1H), 7.60 (m, 3H), 6.31 (d, ^3J = 5.0, 1H), 3.62 (m, 4H), 2.17 (m, 4H). UV-vis (DCM): λ_{max} (ε): 577 (65600 M^{-1} cm^{-1}). HRMS (ESI): calcd for $C_{21}H_{15}N_3OS$ $[M]^+$: 357.0936, found: 357.0930. Elemental analysis (%) for $C_{21}H_{15}N_3OS$: C, 70.57; H, 4.23; N, 11.76; S, 8.97. Found: C, 70.20; H, 4.27; N, 11.50; S, 8.61.

2-{2-[2-(3-Butyl-3*H*-benzothiazol-2-ylidene)-ethylidene]-3-oxo-indan-1-ylidene}-malononitrile EL18

A 1.0 mL Ac_2O solution of 3-butyl-2-methyl-1,3-benzothiazolium bromide[148] (285 mg, 1.00 mmol) and *N*,*N*′-diphenyl-formamidine (196 mg, 1.00 mmol) was heated to 140 °C for 1 h, before KOAc (98.0 mg, 1.00 mmol) and 2-(3-oxo-indan-1-ylidene)-malononitrile[82] (194 mg, 1.00 mmol) was added. The mixture was heated to 140 °C for 3 h before solvent removal. The residual solid was purified by column chromatography (DCM). Yield 41 mg (0.10 mmol, 10%). Mp. 303–305 °C. ^{1}H NMR (DMSO–d_6, 400 MHz): δ 8.58 (d, ^3J = 14.0, 1H), 8.32 (d, ^3J = 8.0, 1H), 8.18 (d, ^3J = 8.0, 1H), 8.04 (d, ^3J = 14.0, 1H), 7.97 (d, ^3J = 8.2, 1H), 7.69–7.62 (m, 4H), 7.52 (t, ^3J = 8.2, 1H), 4.48 (t, ^3J = 7.2, 2H), 1.83 (m, 2H), 1.50 (m, 2H), 1.00 (t, ^3J = 7.2, 3H). UV-vis (DCM): λ_{max} (ε) = 579 (52400 M^{-1} cm^{-1}). HRMS (ESI): calcd for $C_{25}H_{19}N_3OS$ $[M]^+$: 409.1249, found: 409.1243. Elemental analysis (%) calcd for $C_{25}H_{19}N_3OS$: C, 73.32; H, 4.68; N, 10.26; S, 7.83. Found: C, 73.45; H, 4.60; N, 10.32; S, 7.90. CV data: E_p^{ox} = 610 mV vs Fc, E_p^{red} = –1582 mV vs Fc.

2-{2-[2-(3-Butyl-1,1-dimethyl-1,3-dihydro-benzo[*e*]indol-2-ylidene)-ethylidene]-3-oxo-indan-1-ylidene}-malononitrile EL54

A 0.5 mL Ac_2O solution of (3-butyl-1,1-dimethyl-1,3-dihydro-benzo[*e*]indol-2-ylidene)-acetaldehyde (293 mg, 1.00 mmol) and 2-(3-oxo-indan-1-ylidene)-malononitrile[82] (194 mg, 1.00 mmol) was heated to 90 °C for 1 h. After solvent removal, the product was isolated by column chromatography (DCM) and precipitation from DCM/*n*-hexane. Yield 375 mg (0.80 mmol, 80%). Mp. 108–110 °C. ^{1}H NMR (DMSO–d_6, 400 MHz): δ 8.99 (d, ^3J = 14.0, 1H), 8.38 (d, ^3J = 8.0, 1H), 8.29 (d, ^3J = 8.5, 1H), 8.10 (t, ^3J = 9.5, 1H), 8.08 (t, ^3J = 9.5, 1H), 8.06 (d, ^3J = 14.0, 1H), 7.85 (d, ^3J = 8.5, 1H), 7.72 (m, 3H), 7.57 (t, ^3J = 8.0, 1H), 4.30 (t, ^3J = 7.8, 2H), 2.00 (s, 6H), 1.50 (m, 2H), 1.00 (t, ^3J = 7.4, 3H). UV-vis (DCM): λ_{max} (ε) = 594 (31900 M^{-1} cm^{-1}). HRMS (ESI): calcd for $C_{32}H_{27}N_3O$ $[M]^+$: 469.2154, found: 469.2225.

Elemental analysis (%) calcd for $C_{32}H_{27}N_3O$: C, 81.85; H, 5.80; N, 8.95. Found: C, 81.90; H, 5.82; N, 8.89. CV data: $E_{1/2}^{ox}$ = 621 mV vs Fc, $E_{1/2}^{red}$ = –1530 mV vs Fc.

5.5.3.4 Syntheses of ***series In3***

2-[2-(1-Benzyl-3,3-dimethyl-1,3-dihydro-indol-2-ylidene)-ethylidene]-[1,2']biindenylidene-3,1',3'-trione HB218

A 1.5 mL Ac_2O solution of (1-benzyl-3,3-dimethyl-1,3-dihydro-indol-2-ylidene)-acetaldehyde (1.00 g, 3.60 mmol) and [1,2']biindenylidene-3,1'.3'-trione (1.00 g, 3.60 mmol) was heated to 90 °C for 45 min. The precipitate was filtered off and washed with *n*-hexane and *iso*-propanol, before purification by column chromatography (DCM). Yield 788 mg (1.45 mmol, 41%). Mp. 289–292 °C. ^{1}H NMR (CD_2Cl_2, 400 MHz): δ 8.58 (d, ^3J = 14.2, 1H), 8.50 (m, 1H), 8.06 (m, 1H), 7.89 (m, 2H), 7.69 (m, 2H), 7.64 (m, 1H), 7.48 (m, 2H), 7.38 (m, 1H), 7.31 (m, 6H), 7.23 (m, 1H), 7.09 (d, ^3J = 7.7, 1H), 5.30 (s, 2H), 1.77 (s, 6H). UV-vis (DCM): λ_{max} (ε) = 653 (47400 M^{-1} cm^{-1}). HRMS (ESI): calcd for $C_{37}H_{28}NO_3$ $[M+H]^+$: 534.2064, found: 534.2063. Elemental analysis (%) calcd for $C_{37}H_{27}NO_3 \times ¼\ H_2O$: C, 82.58; H, 5.15; N, 2.60. Found: C, 82.80; H, 5.15; N, 2.63. CV data: E_p^{ox} = 579 mV vs Fc., $E_{1/2}^{red}$ = –1292 mV vs Fc.

2-[2-(1,3,3-Trimethyl-1,3-dihydro-indol-2-ylidene)-ethylidene]-[1,2]biindenylidene-3,1',3'-trione HB077

A 5.0 mL Ac_2O solution of (1,3,3-trimethyl-1,3-dihydro-indol-2-ylidene)-acetaldehyde (1.00 g, 5.00 mmol) and [1,2']biindenylidene-3,1',3'-trione (1.37 g, 5.00 mmol) was heated to 90 °C for 30 min. The precipitated dye was filtered off, washed with *iso*-propanol and *n*-hexane and recrystallized from acetic anhydride. Yield 1.14 g, (2.49 mmol, 50%). Mp. 268–271 °C. ^{1}H NMR (DMSO–d_6, 400 MHz): δ 8.50 (d, ^3J = 14.7, 1H), 8.30 (m, 1H), 7.86 (m, 1H), 7.76 (m, 4H), 7.66 (d, ^3J = 7.5, 1H), 7.53−7.59 (m, 4H), 7.47 (m, 1H), 7.35 (m, 1H), 3.03 (s, 3H), 1.66 (s, 6H). UV-vis (DCM): λ_{max} (ε) = 450 (26100), 655 (44500 M^{-1} cm^{-1}). HRMS (ESI): calcd for $C_{31}H_{23}NO$ $[M]^+$: 457.1677, found: 457.1677. Elemental analysis (%) calcd for $C_{31}H_{23}NO$: C, 81.38; H, 5.07; N, 3.06. Found: C, 81.26; H, 5.00; N, 3.06. CV data: E_p^{ox} = 534 mV vs Fc, $E_{1/2}^{red}$ = –1307 mV vs Fc, E_p^{red} = – 1948 mV vs Fc.

2-[2-(1-Isopropyl-3,3-dimtehyl-1,3-dihydro-indol-2-ylidene)-ethylidene]-[1,2'] biindenylidene-3,1',3'-trione HB096

A 1.0 mL Ac_2O solution of (1-*iso*-propyl-3,3-dimethyl-1,3-dihydro-indol-2-ylidene)-acetaldehyde (200 mg, 0.88 mmol) and [1,2']biindenylidene-3,1'.3'-trione (241 mg,

0.88 mmol) was heated to 90 °C for 30 min. The solvent evaporation was followed by column chromatography (DCM with 0.3% MeOH). Yield 220 mg (0.45 mmol, 51%). Mp. 288–290 °C. ^{1}H NMR (CD_2Cl_2, 400 MHz): δ 8.58 (d, ^3J = 14.3, 1H), 8.45 (m, 1H), 8.21 (m, 1H), 7.83 (m, 2H), 7.68 (m, 2H), 7.60 (m, 1H), 7.49 (m, 2H), 7.37 (m, 3H), 7.26 (m, 1H), 4.93 (m, 1H), 1.76 (d, ^3J = 7.1, 6H), 1.70 (s, 6H). UV-vis (DCM): λ_{max} (ε) = 660 (45000 M^{-1} cm^{-1}). HRMS (ESI): calcd for $C_{33}H_{27}NO_3$ $[M]^+$: 485.1991, found: 485.1986. Elemental analysis (%) calcd for $C_{33}H_{27}NO_3 \times ½ H_2O$: C, 80.14; H, 5.71; N, 2.83. Found: C, 80.15; H, 5.62; N, 2.81. CV data: E_p^{ox} = 554 mV vs Fc, $E_{1/2}^{red}$ = –1335 mV vs Fc, E_p^{red} = – 1961 mV vs Fc.

2-[2-(1-Butyl-3,3-dimethyl-1,3-dihydro-indol-2-ylidene)-ethylidene]-[1,2']biindenylidene-3,1',3'-trione HB094

A 0.6 mL Ac_2O solution of (1-butyl-3,3-dimethyl-1,3-dihydro-indol-2-ylidene)-acetaldehyde (100 mg, 0.41 mmol) and [1,2']biindenylidene-3,1',3'-trione (112 mg, 0.41 mmol) was heated to 90 °C for 30 min. The solvent evaporation was followed by column chromatography (DCM with 0.1% MeOH). Yield 104 mg (0.21 mmol, 51%). Mp. 220–222 °C. ^{1}H NMR (CD_2Cl_2, 400 MHz): δ 8.50 (d, ^3J = 14.4, 1H), 8.37 (d, ^3J = 7.2, 1H), 7.95 (m, 1H), 7.75 (m, 2H), 7.60 (m, 2H), 7.53 (m, 1H), 7.41 (m, 2H), 7.32 (m, 2H), 7.18 (m, 1H), 7.09 (d, ^3J = 8.6, 1H), 4.04 (m, 2H), 2.04 (s, 2H), 1.83 (m, 2H), 1.63 (s, 6H), 1.45 (m, 2H), 0.97 (t, ^3J = 7.3, 3H). UV-vis (DCM): λ_{max} (ε) = 660 (51100 M^{-1} cm^{-1}). HRMS (ESI): calcd for $C_{34}H_{30}NO_3$ $[M+H]^+$: 500.2220, found: 500.2214. Elemental analysis (%) calcd for $C_{34}H_{29}NO_3 \times ⅓ H_2O$: C, 80.77; H, 5.91; N, 2.75. Found: C, 80.58; H, 5.87; N, 2.80. CV data: E_p^{ox} = 548 mV vs Fc, $E_{1/2}^{red}$ = –1332 mV vs Fc, E_p^{red} = – 1973 mV vs Fc.

2-[2-(1,1-Dimethyl-5,6-dihydro-1*H*,4*H*-pyrrolo[3,2,1-*ij*]quinolin-2-ylidene)-ethylidene]-[1,2']biindenylidene-3,1',3'-trione HB257

A 1.0 mL Ac_2O solution of (1,1-dimethyl-5,6-dihydro-1*H*,4*H*-pyrrolo[3,2,1-*ij*]quinolin-2-ylidene)-acetaldehyde (200 mg, 0.88 mmol) and [1,2']biindenylidene-3,1'.3'-trione (240 mg, 0.88 mmol) was heated to 90 °C for 1 h. The precipitate was filtered off and washed with *iso*-propanol and *n*-hexane. Yield 339 mg (0.70 mmol, 80%). Mp. 254–257 °C. ^{1}H NMR (CD_2Cl_2, 400 MHz): δ 8.51 (d, ^3J = 14.6, 1H), 8.42 (m, 1H), 7.85 (m, 3H), 7.67 (m, 2H), 7.59 (m, 2H), 7.43 (m, 2H), 7.22 (m, 1H), 7.17 (m, 1H), 4.12 (m, 2H), 2.91 (m, 2H), 2.26 (m, 2H), 1.70 (s, 6H). UV-vis (DCM): λ_{max} (ε): 665 (46500 M^{-1} cm^{-1}). HRMS (ESI): calcd. for $C_{33}H_{26}NO_3$ $[M+H]^+$: 484.1907, found 484.1908. Elemental analysis (%) calcd for

$C_{33}H_{25}NO_3$: C, 81.97; H, 5.21; N, 2.90. Found: C, 81.62; H, 5.19; N, 2.92. CV data: E_p^{ox} = 503 mV vs Fc, $E_{1/2}^{red}$ = –1348 mV vs Fc.

2-[2-(1,1-Dimethyl-5,6-dihydro-1*H*,4*H*-pyrrolo[3,2,1-*ij*]quinolin-2-ylidene)-ethylidene]-[1,2']biindenylidene-3,1',3'-trione HB342

A 7.0 mL EtOH solution of 1,1-dimethyl-2-methylene-1,2,4,5-tetrahydro-pyrrolo[3,2,1-*hi*]indole (370 mg, 2.00 mmol), [1,2']biindenylidene-3,1'.3'-trione (548 mg, 2.00 mmol) and ethyl orthoformate (430 mg, 2.90 mmol) was heated to reflux for 1 h, before the solvent was removed under vacuum. After the column chromatography (DCM), the obtained solid was dissolved in DCM and precipitated with *n*-hexane. Yield 97 mg (0.21 mmol, 10%). Mp. 269–272 °C. ^{1}H NMR ($CDCl_3$, 400 MHz): δ 8.43 (m, 1H), 8.13 (bs, 1H), 7.84 (m, 2H), 7.65 (m, 4H), 7.48 (m, 2H), 7.17 (m, 3H), 4.46 (t, ^3J = 6.9, 2H). 3.80 (t, ^3J = 6.9, 2H), 1.65 (s, 6H). UV-vis (DCM): λ_{max} (ε): 669 (35400 M^{-1} cm^{-1}). HRMS (ESI): calcd for $C_{32}H_{24}NO_3$ $[M+H]^+$: 470.1751, found: 470.1751. CV data: E_p^{ox} = 473 mV vs Fc, $E_{1/2}^{red}$ = –1315 mV vs Fc.

5.5.3.5 Syntheses of ***series M***

2-[4-(1-Butyl-3,3-dimethyl-1,3-dihydro-indol-2-ylidene)-1-phenyl-but-2-enylidene]-malononitrile HB312

A 7.0 mL Ac_2O solution of (3,3-dimethyl-1-butyl-1,3-dihydro-indol-2-ylidene)-acetaldehyde (1.50 g, 6.16 mmol) and 2-(1-phenyl-ethylidene)-malononitrile (1.04 g, 6.16 mmol) was heated to 70 °C for 30 min. The solvent removal was followed by column chromatography (DCM) and precipitation from DCM/*n*-hexane. Yield 1.63 g (4.14 mmol, 67%). Mp. 200–202 °C. ^{1}H NMR ($CDCl_3$, 400 MHz): δ 7.51 (m, 3H), 7.33 (m, 2H), 7.24 (m, 1H), 7.14 (m, 2H), 7.01 (m, 1H), 6.81 (d, ^3J = 7.9, 1H), 6.71 (d, ^3J = 13.6, 1H), 5.70 (d, ^3J = 13.0, 1H), 3.72 (t, ^3J = 7.5, 2H), 1.69 (m, 2H), 1.45 (m, 2H), 1.23 (s, 6H), 1.01 (t, ^3J = 7.4, 3H). UV-vis (DCM): λ_{max} (ε) = 533 (99700 M^{-1} cm^{-1}). HRMS (ESI): calcd for $C_{27}H_{27}N_3$ $[M]^+$: 393.2205, found: 393.2200. Elemental analysis (%) calcd for $C_{27}H_{27}N_3$: C, 82.41; H, 6.92; N, 10.68. Found: C, 82.24; H, 6.88; N, 10.63. CV data: $E_{1/2}^{ox}$ = 418 mV vs Fc, $E_{1/2}^{red}$ = –1761 mV vs Fc.

{2-[2-(1-Butyl-3,3-dimethyl-1,3-dihydro-indol-2-ylidene)-ethylidene]-3-oxo-indan-1-ylidene}-cyano acetic acid ethyl ester MD564

A 5.0 mL ethanol solution of 1-butyl-3,3-dimethyl-2-methylene-2,3-dihydro-1*H*-indole (1.08 g, 5.00 mmol), cyano-(3-oxo-indan-1-ylidene)-acetic acid ethyl ester (1.21 g, 5.00 mmol) and ethyl orthoformate (1.11 mg, 7.50 mmol) was heated to reflux for 1 h.

Subsequently, the solvent was evaporated and the crude product purified by column chromatography (DCM). Yield 213 mg (0.46 mmol, 9%). Mp. 158–163 °C. ^{1}H NMR ($CDCl_3$, 400 MHz): δ 9.05 (d, ^3J = 13.6, 0.4H), 8.78 (d, ^3J = 7.6, 0.5H), 8.67 (d, ^3J = 13.9, 0.5H), 8.16 (m, 0.5H), 8.02 (2 × d, 2 × ^3J = 13.6, 1H), 7.72 (m, 1H), 7.53 (m, 2H), 7.35 (m, 2H), 7.18 (m, 1H), 7.02 (m, 1H), 4.41 (2 × q, 2 × ^3J = 7.1, 2H), 4.02 (t, ^3J = 7.3, 2H), 1.86 (m, 2H), 1.80 (s, 2.7H), 1.70 (s, 3.3H), 1.53 (m, 2H), 1.43 (t, ^3J = 7.1, 3H), 1.02 (2 × t, 2 × ^3J = 7.3, 3H). UV-vis (DCM): λ_{max} (ε) = 557 (50000 M^{-1} cm^{-1}). HRMS (ESI): calcd for $C_{30}H_{31}N_2O_3$ $[M+H]^+$: 467.2329, found: 467.2323. Elemental analysis (%) calcd for $C_{30}H_{30}N_2O_3$: C, 77.23; H, 6.48; N, 6.00. Found: C, 77.08; H, 6.70; N, 5.83. CV data: E_p^{ox} = 556 mV vs Fc, $E_{1/2}^{red}$ = –1511 mV vs Fc.

2-{2-[2-(1-Benzyl-3,3-dimethyl-1,3-dihydro-indol-2-ylidene)ethylidene]-3-(cyano-ethoxycarbonyl-methylene)-indan-1-ylidene]-cyano-acetic acid ethyl ester HB209

A 1.5 mL Ac_2O solution of (1-benzyl-3,3-dimethyl-1,3-dihydro-indol-2-ylidene)-acetaldehyde (100 mg, 0.36 mmol) and cyano-[3-(cyano-ethoxycarbonyl-methylene)-indan-1-ylidene]-acetic ethyl ester (121 mg, 0.36 mmol) was heated to 90 °C for 30 min. The solvent evaporation was followed by column chromatography (DCM) and precipitation from DCM/*n*-hexane. Yield 130 mg (0.22 mmol, 61%). Mp. 191–193 °C. ^{1}H NMR (CD_2Cl_2, 400 MHz): δ 8.63 (m, 1.4H), 8.56 (m, 0.3H), 8.45 (m, 0.3H), 8.29 (m, 0.3H), 8.09 (d, ^3J = 13.8, 0.7H), 7.55 (m, 1.4H), 7.47 (m, 0.6H), 7.22-7.39 (m, 7H), 7.16 (m, 1H), 7.01 (d, ^3J = 7.9, 1H), 5.57 (m, 1H), 5.02 (bs, 2H), 4.38 (q, ^3J = 7.1, 0.7H), 4.22 (q, ^3J = 7.1, 2.7H), 4.12 (q, ^3J = 7.1, 0.6H), 1.73 (s, 2H), 1.64 (s, 4H), 1.41 (t, ^3J = 7.1, 1.1H), 1.34 (t, ^3J = 7.1, 4H), 1.27 (t, ^3J = 7.1, 0.9H). UV-vis (DCM): λ_{max} (ε) = 566 (44900 M^{-1} cm^{-1}). HRMS (ESI): calcd for $C_{38}H_{33}N_3O_4$ $[M]^+$: 595.2471, found: 595.2462. CV data: $E_{1/2}^{ox}$ = 572 mV vs Fc, $E_{1/2}^{red}$ = –1373 mV vs Fc.

[2-[2-(1-Butyl-3,3-dimethyl-1,3-dihydro-indol-2-ylidene)-ethylidene]3-(cyano-ethoxycarbonyl-methylene)-indan-1-ylidene]-cyano-acetic acid ethyl ester HB095

A 0.8 mL Ac_2O solution of (1-butyl-3,3-dimethyl-1,3-dihydro-indol-2-ylidene)-acetaldehyde (100 mg, 0.41 mmol) and cyano-[3-(cyano-ethoxycarbonyl-methylene)-indan-1-ylidene]-acetic ethyl ester (138 mg, 0.41 mmol) was heated to 90 °C for 30 min. Solvent evaporation was followed by column chromatography (DCM) and precipitation from DCM/*n*-hexane. Yield 80 mg (0.14 mmol, 35%). Mp. 198–201 °C. ^{1}H NMR (CD_2Cl_2, 400 MHz): δ 8.68 (m, 1.4H), 8.63 (m, 0.3H), 8.48 (m, 0.3H), 8.28 (d, ^3J = 13.8, 0.3H), 8.07 (d, ^3J = 14.2, 0.7H), 7.57 (m, 1.4H), 7.50 (m, 0.6H), 7.33 (m, 2H), 7.16 (m, 1H), 7.01 (m, 1H), 5.61 (d, ^3J = 13.7,

0.3H), 5.53 (d, ^3J = 14.1, 0.7H), 4.31 (q, ^3J = 7.1, 0.7H), 4.20 (q, ^3J = 7.1, 2.8H), 4.14 (q, ^3J = 7.1, 0.5H), 3.81 (m, 2H), 1.70 (m, 4H), 1.60 (s, 4H), 1.46 (m, 2H), 1.33 (t, ^3J = 7.1, 1H), 1.28 (t, ^3J = 7.1, 4.3H), 1.22 (t, ^3J = 7.1, 0.7H), 0.94 (t, ^3J = 7.3, 3H). UV-vis (DCM): λ_{max} (ε) = 571 (49300 M^{-1} cm^{-1}). HRMS (ESI): calcd for $C_{35}H_{35}N_3O_4$ $[M]^+$: 561.2628, found: 561.2618. Elemental analysis (%) calcd for $C_{35}H_{35}N_3O_4$: C: 74.84, H: 6.28, N: 7.48. Found: C: 74.64, H: 6.40, N: 7.47. CV data: $E_{1/2}^{ox}$ = 529 mV vs Fc, $E_{1/2}^{red}$ = –1388 mV vs Fc.

[2-[2-(1-Isopropyl-3,3-dimethyl-1,3-dihydro-indol-2-ylidene)-ethylidene]3-(cyano ethoxycarbonyl-methylene)-indan-1-ylidene]-cyano-acetic acid ethyl ester HB092

A 0.4 mL Ac_2O solution of (1-*iso*-propyl-3,3-dimethyl-1,3-dihydro-indol-2-ylidene)-acetaldehyde (58 mg, 0.25 mmol) and cyano-[3-(cyano-ethoxycarbonyl-methylene)-indan-1-ylidene]-acetic ethyl ester (85 mg, 0.25 mmol) was heated to 90 °C for 40 min. The solvent evaporation was followed by column chromatography (DCM) and precipitation from DCM/*n*-hexane. Yield 70 mg (0.13 mmol, 51%). Mp. 231–233 °C. ^{1}H NMR (CD_2Cl_2, 400 MHz): δ 8.70 (m, 1.4H), 8.65 (m, 0.3H), 8.50 (m, 0.3H), 8.43 (d, ^3J = 13.8, 0.3H), 8.20 (d, ^3J = 13.9, 0.7H), 7.54 (m, 1.4H), 7.47 (m, 0.6H), 7.30 (m, 2H), 7.19 (m, 1H), 7.13 (m, 1H), 5.77 (d, ^3J = 13.8, 0.3H), 5.72 (d, ^3J = 14.0, 0.7H), 4.51 (m, 1H), 4.40 (q, ^3J = 7.1, 0.7H), 4.28 (q, ^3J = 7.1, 2.7H), 4.18 (q, ^3J = 7.1, 0.6H), 1.70 (s, 2H), 1.60 (m, 10H), 1.42 (t, ^3J = 7.1, 1H), 1.37 (t, ^3J = 7.1, 4.1H), 1.29 (t, ^3J = 7.1, 0.9H). UV-vis (DCM): λ_{max} (ε) = 573 (48900 M^{-1} cm^{-1}). HRMS (ESI): calcd for $C_{34}H_{33}N_3O_4$ $[M]^+$: 547.2471, found: 547.2463. CV data: $E_{1/2}^{ox}$ = 526 mV vs Fc, $E_{1/2}^{red}$ = –1389 mV vs Fc, E_p^{red} = –2454 mV vs Fc.

2-{2-[2-(1-Butyl-3,3-dimethyl-1,3-dihydro-indol-2-ylidene)-ethylidene]-3-dicyanomethylene-indan-1-yliene}-malononitrile MD426

A 8.0 mL Ac_2O solution of (1-butyl-3,3-dimethyl-1,3-dihydro-indol-2-ylidene)-actaldehyde (1.95 g, 8.0 mmol) and 2-(3-dicyanomethylene-indan-1-ylidene)-malononitrile (1.94 mg, 8.0 mmol) was heated to 90 °C for 2 h. Following the solvent removal, the product was isolated after column chromatography (DCM) and precipitation from DCM/*n*-hexane. Yield 1.90 g (4.06 mmol, 51%). Mp. 274–277 °C. ^{1}H NMR ($CDCl_3$, 400 MHz): δ 8.48 (d, ^3J = 14.5, 1H), 8.47 (m, 2H), 7.52 (m, 2H), 7.33 (m, 2H), 7.24 (m, 1H), 7.07 (m, 1H), 5.89 (d, ^3J = 14.5, 1H), 4.03 (t, ^3J = 7.7, 2H), 1.81 (m, 2H), 1.74 (s, 6H), 1.45 (m, 2H), 0.98 (t, ^3J = 7.3, 3H). UV-vis (DCM): λ_{max} (ε) = 580 (60200). HRMS (ESI): calcd for $C_{31}H_{26}N_5$ $[M+H]^+$: 468.2183, found: 468.2183. Elemental analysis (%) calcd for $C_{31}H_{25}N_5 \times ½\ H_2O$: C. 78.13, H: 5.50, N: 14.70. Found: C: 78.22, H: 5.35, N: 14.57. CV data: $E_{1/2}^{ox}$ = 744 mV vs Fc, $E_{1/2}^{red}$ = –1282 mV vs Fc, $E_{1/2}^{red}$ = –1518 mV vs Fc.

{2-[2-(1-Butyl-3,3-dimethyl-1,3-dihydro-indol-2-ylidene)-ethylidene]-1,1-dioxo-1,2-dihydro-1λ^6-benzo[*b*]thiophene-3-ylidene}-cyano-acetic acid ethyl ester HB244

A 1.0 mL Ac_2O solution of 1-*n*-butyl-3,3-dimethyl-1,3-dihydro-indol-2-ylidene)-acetaldehyde (147 mg, 0.60 mmol) and cyano-(1,1-dioxo-1,2-dihydro-1λ^6-benzo[*b*]thiophen-3-ylidene)-acetic acid ethyl ester (167 mg, 0.60 mmol) was heated to 90 °C for 1 h. The precipitate was filtered off and washed with *n*-hexane and *iso-p*ropanol. The raw product purified by column chromatography (DCM). Yield 79 mg (0.16 mmol, 26%). Mp. 195–196 °C. ^{1}H NMR (DMSO–d_6, 400 MHz): δ 8.82 (bs, 1H), 8.33 (bs, 1H), 8.00 (m, 1H), 7.83 (m, 2H), 7.66 (m, 1H), 7.55 (m, 1H), 7.45 (m, 1H), 7.32 (m, 1H), 6.64 (d, ^3J = 14.9, 1H), 4.35 (q, ^3J = 7.1, 2H), 4.13 (m, 2H), 1.78 (m, 2H), 1.67 (s, 6H), 1.43 (m, 2H), 1.37 (t, ^3J = 7.1, 3H), 1.02 (t, ^3J = 7.4, 3H). UV-vis (DCM): λ_{max} (ε) = 596 (37900 M^{-1} cm^{-1}). HRMS (ESI): calcd for $C_{29}H_{31}N_2O_4S$ $[M+H]^+$: 503.1999, found: 503.1999. CV data: E_p^{ox} = 695 mV vs Fc, $E_{1/2}^{red}$ = –1236 mV vs Fc, $E_{1/2}^{red}$ = –1842 mV vs Fc.

Cyano-{2-[2-(1-isopropyl-3,3-dimethyl-1,3-dihydro-indol-ylidene)-ethylidene]-1,1-dioxo-1,2-dihydro-1λ^6-benzo[*b*]thiophen-3-ylidene)-acetic acid ethyl ester HB204

A 0.5 mL Ac_2O solution of 1-*iso*-propyl-3,3-dimethyl-1,3-dihydro-indol-2-ylidene)-acetaldehyde (41 mg, 0.18 mmol) and cyano-(1,1-dioxo-1,2-dihydro-1λ^6-benzo[*b*]thiophen-3-ylidene)-acetic acid ethyl ester (50 mg, 0.18 mmol) was heated to 90 °C for 45 min. The solvent evaporation was followed by column chromatography (DCM) and precipitation from *n*-hexane. Yield 51 mg (0.10 mmol, 58%). Mp. 233–235 °C. ^{1}H NMR (CD_2Cl_2, 400 MHz): δ 8.98 (d, ^3J = 7.8, 1H), 8.42 (d, ^3J = 14.7, 0.6H), 8.09 (m, 0.3H), 7.84 (m, 1H), 7.70 (m, 2H), 7.38 (m, 2H), 7.25 (m, 2H), 6.80 (d, ^3J = 14.5, 1H), 4.78 (m, 1H), 4.36 (q, ^3J = 7.1, 2H), 1.77 (s, 2.2H), 1.70 (d, ^3J = 7.1, 6H), 1.67 (s, 3.8H), 1.41 (t, ^3J = 6.9, 3H). UV-vis (DCM): λ_{max} (ε) = 597 (44800 M^{-1} cm^{-1}). HRMS (ESI): calcd for $C_{28}H_{29}N_2O_4S$ $[M+H]^+$: 489.1843, found: 489.1842. CV data: E_p^{ox} = 692 mV vs Fc, $E_{1/2}^{red}$ = –1257 mV vs Fc, $E_{1/2}^{red}$ = –1872 mV vs Fc.

Cyano-{2-[2-(1-isopropyl-3,3-dimethyl-1,3-dihydro-indol-ylidene)-ethylidene]-1,1-dioxo-1,2-dihydro-1λ^6-benzo[*b*]thiophen-3-ylidene)-acetic acid benzyl ester HB205

A 0.5 mL Ac_2O solution of cyano-(1,1-dioxo-1,2-dihydro-1λ^6-benzo[*b*]thiophen-3-ylidene)-acetic acid benzyl ester (50 mg, 0.15 mmol) and (1-*iso*-propyl-3,3-dimethyl-1,3-dihydro-indol-2-ylidene)-acetaldehyde (34 mg, 0.15 mmol) was heated to 90 °C for 30 min. After solvent removal the crude product was purified by column chromatography (DCM) and precipitation from DCM/*n*-hexane. Yield 50 mg (91 μmol, 61%). Mp. 182–185 °C. ^{1}H NMR

(CD_2Cl_2, 400 MHz): δ 9.01 (m, 1H), 8.41 (bs, 0.6H), 8.01 (bs, 0.3H), 7.84 (m, 1H), 7.71 (m, 2H), 7.50 (m, 2H), 7.40 (m, 5H), 7.26 (m, 2H), 6.82 (m, 1H), 5.35 (s, 2H), 4.79 (m, 1H), 1.77 (s, 2H), 1.71 (d, ^3J = 7.0 6H), 1.58 (s, 4H). UV-vis (DCM): λ_{max} (ε) = 604 (47000). HRMS (ESI): calcd for $C_{33}H_{31}N_2O_4S$ $[M+H]^+$: 511.1999, found: 511.2005. Elemental analysis (%) calcd for $C_{33}H_{30}N_2O_4S \times 1\ H_2O$: C, 69.70; H, 5.67; N, 4.93; S, 5.64. Found: C, 69.96; H, 5.50; N, 4.53; S, 5.46. CV data: E_p^{ox} = 717 mV vs Fc, $E_{1/2}^{red}$ = –1226 mV vs Fc, $E_{1/2}^{red}$ = –1840 mV vs Fc.

2-{2-[2-(1-Benzyl-3,3-dimethyl-1,3-dihydro-indol-2-ylidene)-ethylidene]-1,1-dioxo-1,2-dihydro-1λ^6-benzo[*b*]thiophen-3-ylidene}-malononitrile HB208

A 1.5 mL Ac_2O solution of 1-benzyl-3,3-dimethyl-1,3-dihydro-indol-2-ylidene)-acetaldehyde (120 mg, 0.43 mmol) and 2-(1,1-dioxo-1,2-dihydro-1λ^6-benzo[*b*]thiophen-3-ylidene)-malononitrile (100 mg, 0.43 mmol) was heated to 90 °C for 40 min. The solvent evaporation was followed by column chromatography (DCM). Yield 132 mg (0.27 mmol, 63%). Mp. 210–214 °C. ^{1}H NMR ($CDCl_3$, 400 MHz): δ 9.14 (d, ^3J = 14.3, 1H), 8.86 (m, 1H), 7.86 (m, 1H), 7.76 (m, 2H), 7.34 – 7.46 (m, 7H), 7.30 (m, 1H), 7.20 (m, 1H), 6.77 (d, ^3J = 14.4, 1H), 5.24 (s, 2H), 1.84 (s, 6H). UV-vis (DCM): λ_{max} (ε) = 599 (81700 M^{-1} cm^{-1}). HRMS (ESI): calcd for $C_{30}H_{23}N_3NaO_2S$ $[M+Na]^+$: 512.1403, found: 512.1403. Elemental analysis (%) calcd for $C_{30}H_{23}N_3O_2S \times ⅓\ H_2O$: C, 72.71; H, 4.81; N, 8.48; S, 6.47. Found: C, 72.86; H, 4.82; N, 8.45; S, 6.48. CV data: $E_{1/2}^{ox}$ = 702 mV vs Fc, $E_{1/2}^{red}$ = –1257 mV vs Fc, $E_{1/2}^{red}$ = –1872 mV vs Fc.

2-{2-[2-(1-Isopropyl-3,3-dimethyl-1,3-dihydro-indol-2-ylidene)-ethylidene]-1,1-dioxo-1,2-dihydro-1λ^6-benzo[*b*]thiophen-3-ylidene}-malononitrile HB091

A 0.9 mL Ac_2O solution of 1-*iso*-propyl-3,3-dimethyl-1,3-dihydro-indol-2-ylidene)-acetaldehyde (100 mg, 0.43 mmol) and 2-(1,1-dioxo-1,2-dihydro-1λ^6-benzo[*b*]thiophen-3-ylidene)-malononitrile (100 mg, 0.43 mmol) was heated to 90 °C for 40 min. The precipitate was filtered off and washed with *n*-hexane and *iso*-propanol. Yield 126 mg (0.29 mmol, 66%). Mp. 304–305 °C. ^{1}H NMR ($CDCl_3$, 400 MHz): δ 9.15 (d, ^3J = 14.5, 1H), 8.90 (m, 1H), 7.89 (m, 1H), 7.74 (m, 2H), 7.37 (m, 2H), 7.29 (m, 2H), 6.87 (d, ^3J = 14.5, 1H), 4.79 (m, 1H), 1.80 (s, 6H), 1.74 (d, ^3J = 7.1, 6H). UV-vis (DCM): λ_{max} (ε) = 604 (85200 M^{-1} cm^{-1}). HRMS (ESI): calcd for $C_{26}H_{24}N_3O_2S$ $[M+H]^+$: 422.1584, found: 442.1580. Elemental analysis (%) calcd for $C_{26}H_{23}N_3O_2S$: C, 70.72; H, 5.25; N, 9.52; S, 7.26. Found: C, 70.75; H, 5.32; N, 9.58; S, 7.33. CV data: $E_{1/2}^{ox}$ = 824 mV vs Fc, $E_{1/2}^{red}$ = –1271 mV vs Fc, $E_{1/2}^{red}$ = –1864 mV vs Fc.

2-{2-[2-(1-Butyl-3,3-dimethyl-1,3-dihydro-indol-2-ylidene)-ethylidene]-1,1-dioxo-1,2-dihydro-1λ^6-benzo[*b*]thiophen-3-ylidene}-malononitrile HB093

A 1.0 mL Ac_2O solution of 1-butyl-3,3-dimethyl-1,3-dihydro-indol-2-ylidene)-acetaldehyde (106 mg, 0.43 mmol) and 2-(1,1-dioxo-1,2-dihydro-1λ^6-benzo[*b*]thiophen-3-ylidene)-malononitrile (100 mg, 0.43 mmol) was heated to 90 °C for 40 min. The solvent evaporation was followed by column chromatography (DCM with 10% *n*-pentane). Yield 121 mg (0.27 mmol, 62%). Mp 262–264 °C. ^{1}H NMR ($CDCl_3$, 400 MHz): δ 9.17 (d, ^3J = 14.5, 1H), 8.89 (m, 1H), 7.91 (m, 1H), 7.74 (m, 2H), 7.39 (m, 2H), 7.28 (m, 1H), 7.12 (d, ^3J = 7.8, 1H), 6.73 (d, ^3J = 14.5, 1H), 4.06 (t, ^3J = 7.4, 2H), 1.88 (m, 2H), 1.81 (s, 6H), 1.51 (m, 2H), 1.04 (t, ^3J = 7.3, 3H). UV-vis (DCM): λ_{max} (ε) = 603 (88300 M^{-1} cm^{-1}). HRMS (ESI): calcd for $C_{27}H_{26}N_3O_2S$ $[M+H]^+$: 456.1740, found: 456.1748. CV data: $E_{1/2}^{ox}$ = 819 mV vs Fc, $E_{1/2}^{red}$ = –1276 mV vs Fc, $E_{1/2}^{red}$ = –1869 mV vs Fc.

2-[2-(5-Dibutylamino-thiophen-2-ylmethylene)-3-dicyanomethylene-indan-1-ylidene]-malononitrile MD519

A 1.2 mL Ac_2O solution of 5-dibutylamino-thiophene-2-carbaldehyde (383 mg, 1.60 mmol) and 2-(3-dicyanomethylene-indan-1-ylidene)-malononitrile (388 g, 1.60 mmol) was heated to 90 °C for 2 h. The precipitate was filtered off and washed with *iso*-propanol and *n*-hexane. Yield 648 mg (1.40 mmol, 87%). Mp. 246–249 °C. ^{1}H NMR ($CDCl_3$, 400 MHz): δ 8.62 (s, 1H), 8.44 (m, 2H), 7.76 (d, ^3J = 5.3, 1H), 7.52 (m, 2H), 6.42 (d, ^3J = 5.3, 1H), 3.60 (m, 4H), 1.77 (m, 4H), 1.44 (m, 4H), 1.02 (t, ^3J = 7.4, 6H). UV-vis (DCM): λ_{max} (ε) = 641 (34000 M^{-1} cm^{-1}). HRMS (ESI): calcd for $C_{28}H_{26}N_5S$ $[M+H]^+$: 464.1903, found: 464.1909. Elemental analysis (%) calcd for $C_{28}H_{25}N_5S$: C, 72.54; H, 5.44; N, 15.11; S, 6.92. Found: C, 72.37; H, 5.22; N, 14.74; S, 6.95. CV data: $E_{1/2}^{ox}$ = 633 mV vs Fc, $E_{1/2}^{red}$ = –1248 mV vs Fc, $E_{1/2}^{red}$ = –1498 mV vs Fc, $E_{1/2}^{red}$ = –1711 mV vs Fc.

5.5.3.6 Syntheses of ***series Py***

1-Butyl-5-[2-(1-isopropyl-3,3-dimethyl-1,3-dihydro-indol-2-ylidene)-ethylidene]-4-methyl-2,6-dioxo-1,2,5,6-tetrahydro-pyridine-3-carbonitrile MD346

A 0.4 mL Ac_2O solution of (1-*iso*-propyl-3,3-dimethyl-1,3-dihydro-indol-2-ylidene)-acetaldehyde (100 mg, 0.44 mmol) and 1-butyl-6-hydroxy-4-methyl-2-oxo-1,2-dihydro-pyridine-3-carbonitrile[92] (90 mg, 0.44 mmol) was heated to 140 °C for 30 min, before the solvent was removed under vacuum. The residual solid was purified by column chromatography (DCM with 10% MeOH) and precipitation from DCM/*n*-hexane. Yield

120 mg (0.29 mmol, 66%). Mp. 224–226 °C. ^{1}H NMR ($CDCl_3$, 400 MHz): δ 8.10 (m, 2H), 7.38 (m, 2H), 7.31 (m, 1H), 7.25 (m, 1H), 4.87 (m, 1H), 3.99 (m, 2H), 2.52 (s, 3H), 1.71 (s, 6H), 1.69 (d, ^3J = 7.1, 6H), 1.62 (m, 2H), 1.39 (m, 2H), 0.94 (t, ^3J = 7.4, 6H). UV-vis (DCM): λ_{max} (ε) = 527 (122000 M^{-1} cm^{-1}). HRMS (ESI): calcd for $C_{26}H_{31}N_3O_2$ $[M]^+$: 417.2416, found: 417.2411. Elemental analysis (%) calcd for $C_{26}H_{31}N_3O_2$: C, 74.79; H, 7.48; N, 10.06. Found: C, 74.67; H, 7.45; N, 10.01. CV data: $E_{1/2}^{ox}$ = 672 mV vs Fc, $E_{1/2}^{red}$ = –1707 mV vs Fc.

1-Butyl-5-(4-dibutylamino-benzylidene)-4-methyl-2,6-dioxo-1,2,5,6-tetrahydro-pyridine-3-carbonitrile MD343

A 1.5 mL Ac_2O solution of 4-(dibutylamino)-benzaldehyde (233 mg, 1.00 mmol) and 1-butyl-6-hydroxy-4-methyl-2-oxo-1,2-dihydro-pyridine-3-carbonitrile[92] (206 mg, 1.00 mmol) was heated to 90 °C for 1 h. The precipitate was filtered off and washed with *iso*-propanol and *n*-hexane. Yield 308 mg (0.73 mmol, 73%). Mp. 163–165 °C. ^{1}H NMR ($CDCl_3$, 400 MHz): δ 8.17 (d, ^3J = 9.1, 2H), 7.54 (s, 1H), 6.65 (d, ^3J = 9.3, 2H), 3.98 (t, ^3J = 7.5, 2H), 3.42 (t, ^3J = 7.9, 4H), 2.57 (s, 3H), 1.64 (m, 6H), 1.37 (m, 6H), 0.99 (t, ^3J = 7.4, 6H), 0.94 (t, ^3J = 7.3, 3H). UV-vis (DCM): λ_{max} (ε) = 535 (78700 M^{-1} cm^{-1}). HRMS (ESI): calcd for $C_{26}H_{36}N_3O_2$ $[M+H]^+$: 422.2802, found: 422.2802. Elemental analysis (%) calcd for $C_{26}H_{35}N_3O_2$: C, 74.07; H, 8.37; N, 9.97. Found: C, 74.05; H, 8.22; N, 9.94. CV data: $E_{1/2}^{ox}$ = 617 mV vs Fc, E_p^{red} = –1485 mV vs Fc.

1-Butyl-5-(2-dibutylamino-4-phenyl-thiazol-5-ylmethylene)-4-methyl-2,6-dioxo-1,2,5,6-tetrahydro-pyridine-3-carbonitrile MD324

A 1.5 mL Ac_2O solution of 2-(dibutylamino)-4-phenyl-thiazole-5-carbaldehyde (190 mg, 0.60 mmol) and 1-butyl-6-hydroxy-4-methyl-2-oxo-1,2-dihydro-pyridine-3-carbonitrile[92] (124 mg, 0.60 mmol) was heated to 140 °C for 30 min. The precipitate was purified by column chromatography (DCM with 7% MeOH). Yield 183 mg (0.36 mmol, 60%). Mp. 186–188 °C. ^{1}H NMR ($CDCl_3$, 400 MHz): δ 7.79 (s, 1H), 7.62 (m, 2H), 7.55 (m, 2H), 3.99 (m, 2H), 3.81 (bs, 2H), 3.54 (bs, 2H), 2.21 (s, 3H), 1.74 (bs, 4H), 1.62 (m, 2H), 1.33–1.49 (m, 6H), 0.99 (bs, 6H), 0.95 (t, ^3J = 7.3, 3H). UV-vis (DCM): λ_{max} (ε) = 538 (84000 M^{-1} cm^{-1}). HRMS (ESI): calcd for $C_{29}H_{36}N_4O_2S$ $[M]^+$: 504.2559, found: 504.2553. Elemental analysis (%) calcd for $C_{29}H_{36}N_4O_2S$: C, 69.02; H, 7.19; N, 11.10; S, 6.35. Found: C, 68.76; H, 7.10; N, 11.05; S, 6.61. CV data: $E_{1/2}^{ox}$ = 761 mV vs Fc, $E_{1/2}^{red}$ = –1447 mV vs Fc.

5-(2-(1-Butyl-3,3-dimethylindolin-2-ylidene)ethylidene)-1-(2-ethylhexyl)-2,6-dioxo-4-(trifluoromethyl)-1,2,5,6-tetrahydropyridine-3-carbonitrile HB136

A 5.0 mL Ac_2O solution of (1-butyl-3,3-dimethyl-1,3-dihydro-indol-2-ylidene)-acetaldehyde (1.22 g, 5.00 mmol) and 1-(2-ethylhexyl)-2,6-dioxo-4-(trifluoromethyl)-1,2,5,6-tetrahydropyridine-3-carbonitrile (1.58 mg, 5.00 mmol) was heated to 130 °C for 1 h, before the solvent was removed under vacuum. The residual solid was purified by column chromatography (DCM with 10% MeOH) and precipitation from DCM/*n*-hexane. Yield 360 mg (0.66 mmol, 13%). Mp. 148–152 °C. ^{1}H NMR ($CDCl_3$, 400 MHz): δ 8.24 (m, 2H), 7.43 (m, 2H), 7.36 (m, 1H), 7.18 (d, ^3J = 7.7, 1H), 4.12 (m, 2H), 3.96 (m, 2H), 1.87 (m, 3H), 1.70 (s, 6H), 1.50 (m, 2H), 1.31 (m, 10H), 1.03 (t, ^3J = 7.3, 3H), 0.90 (m, 6H). UV-vis (DCM): λ_{max} (ε) = 541 (120100 M^{-1} cm^{-1}). HRMS (ESI): calcd for $C_{31}H_{38}F_3N_3O_2$ $[M-H]^-$: 541.2849 found: 541.2848. Elemental analysis (%) calcd for $C_{31}H_{38}F_3N_3O_2$: C, 68.74; H, 7.07; N, 7.75. Found: C, 68.58; H, 7.47; N, 8.41. CV data: $E_{1/2}^{ox}$ = 849 mV vs Fc, $E_{1/2}^{red}$ = –1482 mV vs Fc.

1-(2-Ethylhexyl)-5-[2-(1-ethyl-1*H*-pyridin-4-ylidene)-ethylidene]-4-methyl-2,6-dioxo-1,2,5,6-tetrahydro-pyridine-3-carbonitrile MD577

A 3.0 mL Ac_2O solution of 1-(2-ethylhexyl)-6-hydroxy-4-methyl-2-oxo-1,2-dihydro-pyridine-3-carbonitrile[92] (787 mg, 3.00 mmol) and *N*,*N*'-diphenylformamidine (588 mg, 3.00 mmol) was stirred at room temperature for 1 h, before it was heated to 90 °C for 15 min. After adding KOAc (294 mg, 3.00 mmol) and 1-ethyl-4-methyl-pyridinium bromide (606 mg, 3.00 mmol) the solution was heated to 90 °C for 2 h. Following the solvent removal, the product was purified by column chromatography (DCM with 5% MeOH). Yield 306 mg (0.78 mmol, 26%). Mp. 201–202 °C. ^{1}H NMR ($CDCl_3$, 400 MHz): δ 7.71 (d, ^3J = 14.8, 1H), 7.66 (d, ^3J = 7.1, 2H), 7.50 (d, ^3J = 14.9, 1H), 7.23 (d, ^3J = 7.1, 2H), 4.27 (q, ^3J = 13.9, 2H), 3.90 (m, 4H), 2.28 (s, 3H), 1.88 (m, 1H), 1.62 (d, ^3J = 7.4, 3H), 1.29 (m, 6H), 0.88 (m, 6H). UV-vis (DCM): λ_{max} (ε) = 549 (114600 M^{-1} cm^{-1}). HRMS (ESI): calcd for $C_{24}H_{32}N_3O_2$ $[M+H]^+$: 394.2489, found: 394.2490. Elemental analysis (%) calcd for $C_{24}H_{31}N_3O_2$: C, 73.25; H, 7.94; N, 10.68. Found: C, 73.09; H, 7.98; N, 10.71. CV data: E_p^{ox} = 280 mV vs Fc, E_p^{red} = –1831 mV vs Fc.

1-(2-Ethylhexyl)-5-[2-(1-ethyl-1*H*-quinolin-4-ylidene)-ethylidene]-4-methyl-2,6-dioxo-1,2,5,6-tetrahydro-pyridine-3-carbonitrile MD330

A 5.0 mL Ac_2O solution of 1-(2-ethylhexyl)-6-hydroxy-4-methyl-2-oxo-1,2-dihydro-pyridine-3-carbonitrile[92] (1.31 g, 5.00 mmol) and DMF (548 mg, 7.50 mmol, 0.58 mL) was

heated to 90 °C for 15 min, before 1-ethyl-4-methylchinolinium iodide (1.49 g, 5.00 mmol) and KOAc (490 mg, 5.00 mmol) were added. After heating to 100 °C for 15 min, the product was precipitated by adding an acetone/*n*-hexane mixture and filtered off. The following column chromatography (DCM:MeOH=8:1) and precipitation from DCM/*n*-hexane yielded the pure product. Yield 943 mg (2.13 mmol, 43%). Mp. 243–245 °C. ^{1}H NMR ($CDCl_3$, 400 MHz): δ 8.66 (d, ^3J = 13.9, 1H), 8.56 (m, 1H), 7.97 (d, ^3J = 14.0, 1H), 7.85 (m, 1H), 7.73 (m, 1H), 7.69 (m, 1H), 7.6 (m, 1H), 7.35 (d, ^3J = 7.2, 1H), 4.46 (m, 2H), 3.89 (m, 2H), 2.46 (s, 3H), 1.90 (m, 1H), 1.64 (t, ^3J = 7.3, 3H), 1.32 (m, 8H), 0.88 (m, 6H). UV-vis (DCM): λ_{max} (ε) = 617 (120500 M^{-1} cm^{-1}). HRMS (ESI): calcd for $C_{28}H_{34}N_3O_2$ $[M+H]^+$: 444.2646, found: 444.2637. Elemental analysis (%) calcd for $C_{28}H_{33}N_3O_2$: C, 75.81; H, 7.50; N, 9.47. Found: C, 75.77; H, 7.49; N, 9.48. CV data: E_p^{ox} = 324 mV vs Fc, E_p^{red} = –1556 mV vs Fc.

5.5.3.7 Syntheses of ***series Th***

2-{4-*tert*-Butyl-5-[2-(3-butyl-3H-benzooxazol-2-ylidene)-ethylidene]-5*H*-thiazol-2-ylidene}-malononitrile EL31

A 1.5 mL Ac_2O solution of 3-butyl-2-methyl-1,3-benzooxazolium iodide[148] (317 mg, 1.00 mmol) and *N*,*N*′-diphenyl-formamidine (196 mg, 1.00 mmol) was heated to 140 °C for 1 h, before KOAc (98 mg, 1.00 mmol) and 2-(4-*tert*-butyl-5*H*-thiazol-2-ylidene)-malononitrile (204 mg, 1.00 mmol) were added. The mixture was heated to 100 °C for 4 h before the solvent removal. The residual solid was purified by column chromatography (DCM with 5% MeOH) and recrystallized from *iso*-propanol. Yield 25 mg (0.06 mmol, 7%). Mp. 328–330 °C. ^{1}H NMR (400 MHz, $CHCl_3$): δ 8.31 (d, ^3J = 12.8, 2H), 7.50 (d, ^3J = 7.9, ^4J = 0.8, 1H), 7.40 (m, ^3J = 7.9, ^4J = 0.8, 2H), 7.23 (d, ^3J = 7.9, ^4J = 0.8, 1H), 5.16 (d, ^3J = 12.8, 2H), 4.02 (t, ^3J = 7.5, 2H), 1.86 (m, ^3J = 7.5, 2H), 1.56 (s, 9H), 1.49 (m, ^3J = 7.5, 2H), 1.03 (t, ^3J = 7.5, 3H). UV-vis (DCM): λ_{max} (ε) = 594 (115000 M^{-1} cm^{-1}). HRMS (ESI): calcd for $C_{23}H_{25}N_4OS$ $[M+H]^+$: 405.1744, found: 405.1747. Elemental analysis (%) calcd for $C_{23}H_{24}N_4OS$: C, 68.29; H, 5.98; N, 13.85; S, 7.93. Found: C, 68.33; H, 6.01; N, 13.80; S, 7.98. CV data: $E_{1/2}^{ox}$ = 360 mV vs Fc, E_p^{red} = –1530 mV vs Fc.

2-[4-*tert*-Butyl-5-(4-dibutylamino-benzylidene)-5*H*-thiazol-2-ylidene]-malononitrile EL84

A 1.0 mL Ac_2O solution of 5-dibutylamino-benzaldehyde (233 mg, 1.00 mmol) and 2-(4-*tert*-butyl-5*H*-thiazol-2-ylidene)-malononitrile (205 mg, 1.00 mmol) was heated to 90 °C for 3 h. The solvent evaporation was followed by column chromatography (DCM) and precipitation

from DCM/*n*-hexane. Yield 220 mg (0.52 mmol, 52%). Mp. 217–218 °C. ^{1}H NMR (DMSO–d_6, 400 MHz): δ 8.26 (s, 1H), 7.82 (d, ^3J = 9.2, 2H), 6.96 (d, ^3J = 9.2, 2H), 3.46 (t, ^3J = 7.3, 4H), 1.58 (m, 4H), 1.54 (s, 9H), 1.35 (m, 4H), 0.93 (t, ^3J = 7.3, 6H). UV-vis (DCM): λ_{max} (ε) = 620 (66200 M^{-1} cm^{-1}). HRMS (ESI): calcd for $C_{25}H_{32}N_4S$ $[M]^+$: 420.2348, found: 420.2342. Elemental analysis (%) calcd for $C_{25}H_{32}N_4S$: C, 71.39; H, 7.67; N, 13.32; S, 7.62. Found: C, 71.25; H, 7.63; N, 13.35; S, 7.77. CV data: $E_{1/2}^{ox}$ = 562 mV vs Fc, E_p^{red} = -1335 mV vs Fc.

2-{4-*tert*-Butyl-5-[2-(5-chloro-1,3,3-trimethyl-1,3-dihydro-indol-2-ylidene)-ethylidene]-5*H*-thiazol-2-ylidene}-malononitrile HB347

A 2.0 mL Ac_2O solution of (5-chloro-1,3,3-trimethyl-1,3-dihydro-indol-2-ylidene)-acetaldehye (472 mg, 2.00 mmol) and 2-(4-*tert*-butyl-5*H*-thiazol-2-ylidene)-malononitrile (411 mg, 2.00 mmol) was heated to 90 °C for 1 h. The precipitate was filtered off and washed with *iso*-propanol and *n*-hexane. Yield 692 mg (1.64 mmol, 82%). Mp. 394–396 °C. ^{1}H NMR ($CDCl_3$, 400 MHz): δ 8.16 (d, ^3J = 13.0, 1H), 7.33 (m, 1H), 7.27 (1H), 6.91 (d, ^3J = 8.3, 1H), 5.44 (d, ^3J = 13.0, 1H), 3.44 (s, 3H), 1.67 (s. 6H), 1.54 (s, 9H). UV-vis (DCM): λ_{max} (ε): 624 (116100 M^{-1} cm^{-1}). HRMS (ESI): calcd for $C_{23}H_{24}ClN_4S$ $[M+H]^+$: 423.1405, found: 423.1395. Elemental analysis (%) calcd for $C_{23}H_{23}ClN_4S$: C, 65.31; H, 5.48; N, 13.25; S, 7.58. Found: C, 64.98; H, 5.51; N, 13.23; S, 7.96. CV data: $E_{1/2}^{ox}$ = 440 mV vs Fc, $E_{1/2}^{red}$ = –1369 mV vs Fc.

2-{4-*tert*-Butyl-5-[2-(1-butyl-3,3-dimethyl-1,3-dihydro-indol-2-ylidene)-ethylidene]-5H-thiazol-2-ylidene}-malononitrile HB231

A 4.9 mL Ac_2O solution of (1-butyl-3,3-dimethyl-1,3-dihydro-indol-2-ylidene)-acetaldehyde (1.20 g, 4.90 mmol) and 2-(4-*tert*-butyl-5*H*-thiazol-2-ylidene)-malononitrile (1.01 g, 4.90 mmol) was heated to 90 °C for 1 h. The precipitate was filtered off and washed with *n*-hexane and *iso*-propanol. Yield 965 mg (2.24 mmol, 46%). Mp. 350–352 °C. ^{1}H NMR (CD_2Cl_2, 400 MHz): δ 8.32 (d, ^3J = 13.4, 1H), 7.38 (m, 2H), 7.23 (m, 1H), 7.07 (m, 1H), 5.64 (d, ^3J = 13.4, 1H), 3.94 (m, 2H), 1.80 (m, 2H), 1.68 (s, 6H), 1.55 (s, 9H), 1.47 (m, 2H), 1.01 (t, ^3J = 7.4, 3H). UV-vis (DCM): λ_{max} (ε) = 624 (110100 M^{-1} cm^{-1}). HRMS (ESI): calcd for $C_{26}H_{31}N_4S$ $[M+H]^+$: 431.2264, found: 431.2258. Elemental analysis (%) calcd for $C_{26}H_{30}N_4S$ × ⅓ H_2O: C, 71.52; H, 7.08; N, 12.83; S, 7.34. Found: C, 71.61; H, 6.88; N, 12.77; S, 7.49. CV data: $E_{1/2}^{ox}$ = 434 mV vs Fc, $E_{1/2}^{red}$ = –1421 mV vs Fc.

2-(4-(*tert*-Butyl)-5-(2-(1-isopropyl-3,3-dimethylindolin-2-ylidene)ethylidene)thiazol-2(5*H*)-ylidene)malononitrile MD530

A 10.0 mL Ac_2O solution of (1-*iso*-propyl-3,3-dimethyl-1,3-dihydro-indol-2-ylidene)-acetaldehyde (2.50 g, 10.9 mmol) and 2-(4-*tert*-butyl-5*H*-thiazol-2-ylidene)-malononitrile (0.90 g, 4.40 mmol) was heated to 90 °C for 2 h. Subsequent to solvent removal, the crude product was purified by column chromatography (DCM). Yield 100 mg (0.24 mmol, 5%). Mp. 353–355 °C. ^{1}H NMR ($CDCl_3$, 400 MHz): δ 8.24 (d, ^3J = 13.1, 1H), 7.33 (m, 2H), 7.18 (m, 2H), 5.68 (d, ^3J = 13.1, 1H), 4.63 (m, 1H), 1.66 (d, ^3J = 7.4, 6H), 1.64 (s, 6H), 1.53 (s, 9H). UV-vis (DCM): λ_{max} (ε) = 624 (131000 M^{-1} cm^{-1}). HRMS (ESI): calcd for $C_{25}H_{29}N_4S$ $[M+H]^+$: 416.2035, found: 416.2029. Elemental analysis (%) calcd for $C_{25}H_{28}N_4S \times ½\ H_2O$: C, 70.55; H, 6.87; N, 13.16; S, 7.53. Found: C, 70.70; H, 6.33; N, 13.22; S, 7.51. CV data: $E_{1/2}^{ox}$ = 429 mV vs Fc, $E_{1/2}^{red}$ = –1433 mV vs Fc.

2-{4-*tert*-Butyl-5-[2-(3,3-dimethyl-1-naphthalen-1-ylmethyl-1,3-dihydro-indol-2-ylidene)-ethylidene]-5*H*-thiazol-2-ylidene}-malononitrile HB356

A 8.5 mL Ac_2O solution of 2-(3,3-dimethyl-1-(naphthalen-1-ylmethyl)indolin-2-ylidene)acetaldehyde (2.50 g, 8.4 mmol) and 2-(4-*tert*-butyl-5*H*-thiazol-2-ylidene)-malononitrile (1.72 mg, 8.4 mmol) was heated to 90 °C for 30 min, before the precipitate was filtered off and washed with *n*-hexane and *iso*-propanol. After column chromatography (DCM), the obtained solid was solved in DCM and precipitated with *n*-hexane. Purification with recycling GPC ($CHCl_3$) resulted in the pure product. Yield 450 mg (0.87 mmol, 10%). Mp. 301–302 °C. ^{1}H NMR ($CDCl_3$, 400 MHz): δ 8.02 (m, 2H), 7.87 (d, ^3J = 8.0, 1H), 7.69 (m, 2H), 7.39 (m, 2H), 7.25 (m, 3H), 6.98 (m, 1H), 6.88 (d, ^3J = 7.5, 1H), 5.60 (s, 2H), 5.42 (d, ^3J = 13.0, 1H), 1.74 (s, 6H), 1.54 (s, 9H). UV-vis (DCM): λ_{max} (ε): 625 (95500 M^{-1} cm^{-1}). HRMS (ESI): calcd for $C_{33}H_{30}N_4S$ $[M]^+$: 514.2191, found: 514.2185.

2-{4-*tert*-Butyl-5-{2-(1-(2-ethylhexyl)-3,3-dimethyl-1,3-dihydro-indol-2-ylidene)-ethylidene]-5*H*-thiazol-2-ylidene}-malononitrile HB247

A 4.0 mL Ac_2O solution of 1-(2-ethylhexyl)-3,3-dimethyl-2-methylene-2,3-dihydro-1*H*-indole (1.02 g, 3.4 mmol) and 2-(4-*tert*-butyl-5*H*-thiazol-2-ylidene)-malononitrile (700 mg, 3.4 mmol) was heated to 90 °C for 40 min, before the precipitate was filtered off and washed with *n*-hexane and *iso*-propanol. After column chromatography (1. DCM, 2. DCM with 0.1% EtOAc), the obtained solid was dissolved in DCM and precipitated with *n*-hexane. Yield 906 mg (1.9 mmol, 55%). Mp. 235–237 °C. ^{1}H NMR (CD_2Cl_2, 400 MHz): δ 8.31 (d, ^3J = 13.4, 1H), 7.36 (m, 2H), 7.23 (m, 1H), 7.06 (m, 1H), 5.66 (d, ^3J = 13.4, 1H), 3.83 (d, ^3J = 7.5,

2H), 2.08 (m, 1H), 1.69 (s, 6H), 1.55 (s, 9H), 1.24–1.44 (m, 8H), 0.98 (t, ^3J = 7.5, 3H), 0.89 (t, ^3J = 7.2, 3H). UV-vis (DCM): λ_{max} (ε): 626 (124000 M^{-1} cm^{-1}). HRMS (ESI): calcd for $C_{30}H_{38}N_4S$ $[M]^+$: 486.2817, found: 486.2812.

2-{4-*tert*-Butyl-5-[2-(1,1-dimethyl-5,6-dihydro-1*H*,4*H*-pyrrolo[3,2,1-*ij*]quinolin-2-ylidene)-ethylidene]-5*H*-thiazol-2-ylidene}-malononitrile HB255

A 1.0 mL Ac_2O solution of (1,1-dimethyl-5,6-dihydro-1*H*,4*H*-pyrrolo[3,2,1-*ij*]quinolin-2-ylidene)-acetaldehyde (200 mg, 0.88 mmol) and 2-(4-*tert*-butyl-5*H*-thiazol-2-ylidene)-malononitrile (181 mg, 0.88 mmol) was heated to 90 °C for 1 h. The precipitate was filtered off and washed with *iso*-propanol and *n*-hexane, before it was purified by column chromatography (DCM with 0.2% MeOH). Yield 235 mg (0.57 mmol, 64%). Mp. 343–345 °C. ^{1}H NMR (CD_2Cl_2, 400 MHz): δ 8.29 (d, ^3J = 13.5, 1H), 7.20 (m, 1H), 7.14 (m, 2H), 5.60 (d, ^3J = 13.6, 1H), 3.90 (m, 2H), 2.88 (m, 2H), 2.22 (m, 2H), 1.68 (s, 6H), 1.54 (s, 9H). UV-vis (DCM): λ_{max} (ε): 627 (146100 M^{-1} cm^{-1}). HRMS (ESI): calcd. for $C_{25}H_{26}N_4S$ $[M]^+$: 414.1878, found 414.1873. Elemental analysis (%) calcd for $C_{25}H_{26}N_4S$: C, 72.43; H, 6.32; N, 13.51; S, 7.73. Found: C, 72.14; H, 6.27; N, 13.33; S, 7.61. CV data: $E_{1/2}^{ox}$ = 376 mV vs Fc, $E_{1/2}^{red}$ = –1456 mV vs Fc.

2-{4-*tert*-Butyl-5-[2-(3-butyl-3H-benzothiazol-2-ylidene)-ethylidene]-5H-thiazol-2-ylidene}-malononitrile EL32

A 1.0 mL Ac_2O solution of 3-butyl-2-methyl-1,3-benzothiazolium iodide (333 mg, 1.00 mmol) and *N*,*N*′-diphenyl-formamidine (196 mg, 1.00 mmol) was heated to 140 °C for 1 h, before KOAc (98 mg, 1.00 mmol) and 2-(4-*tert*-butyl-5*H*-thiazol-2-ylidene)-malononitrile (204 mg, 1.00 mmol) was added. The mixture was heated to 120 °C for 1 h before the solvent removal. The residual solid was purified by column chromatography (DCM with 5% MeOH). Yield 34 mg (0.08 mmol, 8%). Mp. 329–330 °C. ^{1}H NMR ($CDCl_3$, 400 MHz): δ 7.99 (d, ^3J = 12.7, 1H), 7.63 (dd, ^3J = 7.6, ^4J = 0.9, 1H), 7.51 (dt, ^3J = 7.6, ^4J = 0.9, 1H), 7.32 (dt, ^3J = 7.6, ^4J = 0.9, 1H), 7.30 (d, ^3J = 7.7, 1H), 5.70 (d, ^3J = 12.7, 1H), 4.16 (t, ^3J = 7.5, 2H), 1.85 (q, 2H), 1.52 (m, 9H), 1.33 (m, 2H), 1.07 (t, ^3J = 7.5, 3H). UV-vis (DCM): λ_{max} (ε) = 631 (120000 M^{-1} cm^{-1}). HRMS (ESI): calcd. for $C_{23}H_{25}N_4S_2$ $[M+H]^+$: 421.1515, found: 421.1501. Elemental analysis (%) calcd for $C_{23}H_{24}N_4S_2$: C, 65.68; H, 5.75; N, 13.32; S, 15.25. Found: C, 65.50; H, 5.81; N, 13.37; S, 15.32. CV data: E_p^{ox} = 386 mV vs Fc, E_p^{red} = –1455 mV vs Fc.

2-{4-*tert*-Butyl-5-[2-(3-butyl-1,1-dimethyl-1,3-dihydro-beno[*e*]indol-2-ylidene)-ethylidene]-5*H*-thiazol-2-ylidene}-malononitrile EL53

A 1.0 mL Ac_2O solution of (3-butyl-1,1-dimethyl-1,3-dihydro-benzo[*e*]indol-2-ylidene)-acetaldehyde (495 mg, 1.69 mmol) and 2-(4-*tert*-butyl-5*H*-thiazol-2-ylidene)-malononitrile (346 mg, 1.69 mmol) was heated to 90 °C for 1 h. The precipitate was filtered off and washed with *iso*-propanol and *n*-hexane. Yield 540 mg (1.12 mmol, 66%). Mp. 243–245 °C. ^{1}H NMR (DMSO–d_6, 400 MHz): δ 8.50 (d, ^3J = 14.2, 1H), 8.33 (d, ^3J = 8.6, 1H), 8.12 (d, ^3J = 9.2, 1H), 8.10 (d, ^3J = 7.9, 1H), 7.85 (d, ^3J = 9.2, 1H), 7.67 (t, ^3J = 8.5, 1H), 7.57 (t, ^3J = 8.2, 1H), 6.63 (s, 1H), 6.12 (d, ^3J = 14.2, 1H), 4.42 (t, ^3J = 7.4, 2H), 1.80 (m, 2H), 1.52 (m, 6H), 1.42 (m, 2H), 1.27 (s, 9H), 0.95 (t, ^3J = 7.4, 3H). UV-vis (DCM): λ_{max} (ε) = 640 (65600 M^{-1} cm^{-1}). HRMS (ESI): calcd for $C_{30}H_{33}N_4S$ $[M+H]^+$: 481.2420, found: 481.2416. Elemental analysis (%) calcd for $C_{30}H_{32}N_4S$: C, 74.96; H, 6.71; N, 11.66; S, 6.67. Found: C, 74.88; H, 6.75; N, 11.52; S, 6.85. CV data: $E_{1/2}^{ox}$ = 406 mV vs Fc, $E_{1/2}^{red}$ = –1411 mV vs Fc.

2-{4-*tert*-Butyl-5-[2-(1-butyl-1*H*-pyridin-4-ylidene)-ethylidene]-5*H*-thiazol-2-ylidene}-malononitrile El30

A 1.5 mL Ac_2O solution of 1-butyl-4-methyl-pyridinium iodide (480 mg, 1.73 mmol) and N,N′-diphenyl-formamidine (340 mg, 1.73 mmol) was heated to 150 °C for 1 h, before KOAc (137 mg, 1.40 mmol) and 2-(4-*tert*-butyl-5*H*-thiazol-2-ylidene)-malononitrile (353 mg, 1.73 mmol) in 1.0 mL Ac_2O were added. The mixture was heated to 120 °C for 1 h before the solvent removal. The residual solid was purified by column chromatography (DCM with 5% MeOH). Yield 35 mg (0.10 mmol, 6%). Mp. 170–172 °C. ^{1}H NMR (DMSO–d_6, 400 MHz): δ 8.60 (d, ^{3}J = 6.9, 2H), 8.09 (d, ^{3}J = 15.0, 1H), 7.97 (d, ^{3}J = 6.9, 2H), 6.35 (d, ^{3}J = 15.0, 1H), 4.36 (t, ^{3}J = 7.5, 2H), 1.85 (m, 2H), 1.42 (s, 9H), 1.29 (m, 2H), 0.93 (t, ^{3}J = 7.5, 3H). UV-vis (DCM): λ_{max} (ε) = 640 (61000 M^{-1} cm^{-1}). HRMS (ESI): calcd for $C_{21}H_{25}N_4S$ $[M+H]^+$: 365.1794, found: 365.1787. Elemental analysis (%) calcd for $C_{21}H_{24}N_4S$: C, 69.20; H, 6.64; N, 15.37; S, 8.80. Found: C, 69.06; H, 6.70; N, 15.43; S, 8.91. CV data: E_p^{ox} = 130 mV vs Fc, $E_{1/2}^{red}$ = –1581 mV vs Fc.

2-[4-*tert*-Butyl-5-(5-dibutylamino-furan-2-ylmethylene)-5*H*-thiazol-2-ylidene]-malononitrile MD499

A 5.0 mL Ac_2O solution of 5-dibutylamino-furan-2-carbaldehyde (1.12 g, 5.02 mmol) and 2-(4-*tert*-butyl-5*H*-thiazol-2-ylidene)-malononitrile (1.03 g, 5.02 mmol) was heated to 90 °C for 30 min. After the solvent removal the product was isolated by column chromatography (DCM) and precipitation from DCM/*n*-hexane. Yield 1.45 g (3.53 mmol, 70%). Mp. 197–

199 °C. ^{1}H NMR (DMSO–d_6, 400 MHz): δ 8.00 (d, ^3J = 4.9, 1H), 7.74 (s, 1H), 6.76 (d, ^3J = 4.9, 1H), 3.66 (m, 4H), 1.67 (m, 4H), 1.43 (s, 9H), 1.39 (m, 4H), 0.92 (t, ^3J = 7.2, 6H). UV-vis (DCM): λ_{max} (ε) = 653 (117300 M^{-1} cm^{-1}). MS (MALDI-TOF, matrix: DCTB): calcd for $C_{23}H_{30}N_4OS$: 410.214, found 410.212. Elemental analysis (%) calcd for $C_{23}H_{30}N_4OS$: C, 67.28; H, 7.36; N, 13.65; S, 7.81. Found: C, 67.21; H, 6.99; N, 13.57; S, 8.04. CV data: $E_{1/2}^{ox}$ = 276 mV vs Fc, E_p^{red} = –1439 mV vs Fc.

2-{5-[2-(1-Butyl-3,3-dimethyl-1,3-dihydro-indol-2-ylidene)-2-cyano-ethylidene]-4-phenyl-5H-thiazol-2-ylidene}-malononitrile HB277

A 2.0 mL Ac_2O solution of 2-(1-butyl-3,3-dimethylindolin-2-ylidene)-3-oxopropanenitrile (300 mg, 1.11 mmol) and 2-(4-phenyl-5*H*-thiazol-2-ylidene)-malononitrile (252 mg, 1.11 mmol) was heated to 90 °C for 30 min, before the solvent was removed. The residue was purified twice by column chromatography (1. DCM with 1% MeOH; 2. DCM). Yield 403 mg (0.85 mmol, 76%). Mp. 285–286 °C. ^{1}H NMR (CD_2Cl_2, 400 MHz): δ 7.23 (s, 1H), 7.67 (m, 3H), 7.61 (m, 2H), 7.40 (m, 1H), 7.30 (m, 2H), 7.11 (m, 1H), 4.24 (m, 2H), 1.79 (m, 2H), 1.48 (s, 6H), 1.34 (m, 1H), 0.93 (t, ^3J = 7.4, 3H). UV-Vis (DCM): λ_{max} (ε): 605 (65800 M^{-1} cm^{-1}). HRMS (ESI): calcd for $C_{29}H_{25}N_5S$ $[M]^+$: 475.1831, found: 475.1825. Elemental analysis (%) calcd for $C_{29}H_{25}N_5S$: C, 73.23; H, 5.30; N, 14.73; S, 6.74. Found: C, 72.97; H, 5.38; N, 14.37; S, 6.47. CV data: E_p^{ox} = 742 mV vs Fc, E_p^{red} = –1193 mV vs Fc.

2-{5-[2-(1-Benzyl-3,3-dimethyl-1,3-dihydro-2-ylidene)-ethylidene]-4-phenyl-5*H*-thiazol-2-ylidene}-malononitrile MD303

A 1.0 mL Ac_2O solution of (1-benzyl-3,3-dimethyl-1,3-dihydro-indol-2-ylidene)-acetaldehyde (100 mg, 0.36 mmol) and 2-(4-phenyl-5*H*-thiazol-2-ylidene)-malononitrile (81 mg, 0.36 mmol) was heated to 90 °C for 1 h. The precipitate was filtered off and washed with *n*-hexane and *iso*-propanol. Yield 150 mg (0.31 mmol, 86%). Mp. 318–321 °C. ^{1}H NMR (CD_2Cl_2, 400 MHz): δ 7.97 (d, ^3J = 13.6, 1H), 7.70 (m, 2H), 7.57 (m, 3H), 7.38 (m, 5H), 7.24 (m, 3H), 7.07 (d, ^3J = 7.9, 1H), 5.84 (d, ^3J = 13.7, 1H), 5.17 (s, 2H), 1.60 (s, 6H). UV-vis (DCM): λ_{max} (ε) = 635 (105700 M^{-1} cm^{-1}). HRMS (ESI): calcd for $C_{31}H_{25}N_4S$ $[M+H]^+$: 485.1794, found: 485.1795. Elemental analysis (%) calcd for $C_{31}H_{24}N_4S$: C, 76.83; H, 4.99; N, 11.56; S, 6.62. Found: C, 76.64; H, 4.95; N, 11.51; S, 6.87. CV data: $E_{1/2}^{ox}$ = 485 mV vs Fc, E_p^{red} = –1295 mV vs Fc.

2-{5-[2-(1,1-Dimethyl-5,6-dihydro-1*H*,4*H*-pyrrolo[3,2,1-*ij*]quinolin-2-ylidene)-ethylidene]-4-phenyl-5*H*-thiazol-2-ylidene}-malononitrile HB256

A 1.0 mL Ac_2O solution of (1,1-dimethyl-5,6-dihydro-1*H*,4*H*-pyrrolo[3,2,1-*ij*]quinolin-2-ylidene)-acetaldehyde (200 mg, 0.88 mmol) and 2-(4-phenyl-5*H*-thiazol-2-ylidene)-malononitrile (200 mg, 0.88 mmol) was heated to 90 °C for 1 h. The precipitate was filtered off and washed with *n*-hexane and *iso*-propanol. After purification by column chromatography (DCM with 0.3% MeOH), the dye was precipitated from DCM/*n*-hexane. Yield 267 mg (0.61 mmol, 70%). Mp. 311–314 °C. ^{1}H NMR (CD_2Cl_2, 400 MHz): δ 7.99 (d, ^3J = 13.7, 1H), 7.73 (m, 2H), 7.59 (m, 3H), 7.17 (m, 3H), 5.83 (d, ^3J = 13.1, 1H), 3.96 (m, 2H), 2.89 (m, 2H), 2.23 (m, 2H), 1.55 (s, 6H). UV-vis (DCM): λ_{max} (ε): 635 (123200 M^{-1} cm^{-1}). HRMS (ESI): calcd. for $C_{27}H_{22}N_4S$ $[M]^+$: 434.1565, found 434.1559. CV data: $E_{1/2}^{ox}$ = 415 mV vs Fc, E_p^{red} = –1379 mV vs Fc.

2-[5-(4-Dibutylamino-benzylidene)-4-phenyl-5*H*-thiazol-2-ylidene]-malononitrile MD323

A 2.0 mL Ac_2O solution of 4-dibutylamino-benzaldehyde (467 mg, 2.00 mmol) and 2-(4-phenyl-5*H*-thiazol-2-ylidene)-malononitrile (450 mg, 2.00 mmol) was heated to 90 °C for 1 h. The solvent evaporation was followed by column chromatography (DCM) and precipitation from DCM/*n*-hexane. Yield 710 mg (1.61 mmol, 81%). Mp. 218–220 °C. ^{1}H NMR ($CDCl_3$, 400 MHz): δ 7.77 (m, 2H), 7.61 (m, 1H), 7.55 (m, 5H), 6.73 (d, ^3J = 9.2, 2H), 3.42 (t, ^3J = 7.7, 4H), 1.63 (m, 4H), 1.41 (m, 4H), 1.00 (t, ^3J = 7.3, 6H). UV-vis (DCM): λ_{max} (ε) = 643 (86000 M^{-1} cm^{-1}). HRMS (ESI): calcd for $C_{27}H_{29}N_4S$ $[M+H]^+$: 441.2107, found: 441.2103. Elemental analysis (%) calcd for $C_{27}H_{28}N_4S$: C, 73.60; H, 6.41; N, 12.72; S, 7.28. Found: C, 73.30; H, 6.38; N, 12.70; S, 7.26. CV data: $E_{1/2}^{ox}$ = 596 mV vs Fc, E_p^{red} = –1192 mV vs Fc.

2-[5-(5-Dibutylamino-thiophen-2-ylmethylene)-4-phenyl-5*H*-thiazol-2-ylidene]-malononitrile MD356

A 6.0 mL Ac_2O solution of 5-dibutylamino-thiophene-2-carbaldehyde (1.44 g, 6.00 mmol) and 2-(4-phenyl-5*H*-thiazol-2-ylidene)-malononitrile (1.35 g, 6.00 mmol) was heated to 90 °C for 30 min. The precipitate was filtered off and washed with *iso*-propanol and *n*-hexane. Yield 1.66 g (3.72 mmol, 62%). Mp. 280–283 °C. ^{1}H NMR (DMSO–d_6, 400 MHz): δ 8.10 (d, ^3J = 5.4, 1H), 8.01 (s, 1H), 7.68 (m, 2H), 7.58 (m, 3H), 7.06 (d, ^3J = 5.3, 1H), 3.73 (t, ^3J = 7.3, 4H), 1.90 (m, 4H), 1.37 (m, 4H), 0.94 (t, ^3J = 7.2, 6H). UV-vis (DCM): λ_{max} (ε) = 659 (131100 M^{-1} cm^{-1}). HRMS (ESI): calcd for $C_{25}H_{27}N_4S_2$ $[M+H]^+$: 447.1672, found:

447.1664. Elemental analysis (%) calcd for $C_{25}H_{26}N_4S_2$: C, 67.23; H, 5.87; N, 12.54; S, 14.36. Found: C, 67.10; H, 5.84; N, 12.57; S, 14.53. CV data: $E_{1/2}^{ox}$ = 408 mV vs Fc, $E_{1/2}^{red}$ = –1269 mV vs Fc.

Cyano-[5-(4-dibutylamino-benylidene)-4-phenyl-5H-thiazol-2-ylidene]-acetic acid ethyl ester MD565

A 1.5 mL Ac_2O solution of 4-dibutylamino-benzaldehyde (350 mg, 1.50 mmol) and cyano-(4-phenyl-5*H*-thiazol-2-ylidene)-acetic acid ethyl ester (409 mg, 1.50 mmol) was heated to 90 °C for 2.5 h. The solvent removal was followed by precipitation from DCM/*n*-hexane. Yield 130 mg (0.27 mmol, 18%). Mp. 187–189 °C. ^{1}H NMR ($CDCl_3$, 400 MHz): δ 7.79 (m, 2H), 7.64 (m, 2H), 7.55 (m, 4H), 6.70 (m, 2H), 4.38 (q, ^3J = 7.1, 2H), 3.39 (m, 4H), 1.63 (m, 4H), 1.40 (m, 7H), 0.99 (t, ^3J = 7.4, 6H). UV-vis (DCM): λ_{max} (ε) = 626 (74000 M^{-1} cm^{-1}). HRMS (ESI): calcd for $C_{29}H_{34}N_3O_2S$ $[M+H]^+$: 488.2366, found: 488.2366. Elemental analysis (%) calcd for $C_{29}H_{33}N_3O_2S$: C, 71.43; H, 6.82; N, 8.62; S, 6.58. Found: C, 71.12; H, 6.74; N, 8.47; S, 6.84. CV data: E_p^{ox} = 494 mV vs Fc, E_p^{red} = –1305 mV vs Fc.

{5-[2-(1-Benzyl-3,3-dimethyl-1,3-dihydro-indol-2-ylidene)-ethylidene]-4-phenyl-5*H*-thiazol-2-ylidene}-cyano-acetic acid ethyl ester HB101

A 3.0 mL Ac_2O solution of (1-benzyl-3,3-dimethyl-1,3-dihydro-indol-2-ylidene)-actaldehyde (1.11 g, 4.00 mmol) and cyano-(4-phenyl-5*H*-thiazol-2-ylidene)-acetic acid ethyl ester (1.09 g, 4.00 mmol) was heated to 70 °C for 45 min. The solvent evaporation was followed by column chromatography (DCM) and precipitation from DCM/*n*-hexane. Yield 176 mg (0.33 mmol, 8%). Mp. 270–273 °C. ^{1}H NMR ($CDCl_3$, 400 MHz): δ 7.93 (d, ^3J = 13.8, 1H), 7.74 (m, 2H), 7.52 (m, 3H), 7.27–7.39 (m, 5H), 7.17 (m, 3H), 6.92 (m, 1H), 5.91 (d, ^3J = 13.7, 1H), 5.11 (s, 2H), 4.32 (q, ^3J = 7.2, 2H), 1.61 (s, 6H), 1.37 (t, ^3J = 7.2, 3H). UV-vis (DCM): λ_{max} (ε) = 627 (106400 M^{-1} cm^{-1}). HRMS (ESI): calcd for $C_{33}H_{30}N_3O_2S$ $[M+H]^+$: 532.2053, found: 532.2053. Elemental analysis (%) calcd for $C_{33}H_{29}N_3O_2S$: C, 74.55; H, 5.50; N, 7.90; S, 6.03. Found: C, 74.35; H, 5.47; N, 7.89; S, 6.40. CV data: E_p^{ox} = 425 mV vs Fc, $E_{1/2}^{red}$ = –1363 mV vs Fc.

{5-[2-(1,3,3-trimethyl-1,3-dihydro-indol-2-ylidene)-ethylidene]-4-phenyl-5*H*-thiazol-2-ylidene}-cyano-acetic acid ethyl ester MD372

A 5.0 mL Ac_2O solution of (1,3,3-trimethyl-1,3-dihydro-indol-2-ylidene)-actaldehyde (1.01 g, 5.00 mmol) and cyano-(4-phenyl-5*H*-thiazol-2-ylidene)-acetic acid ethyl ester (1.36 g, 5.00 mmol) was heated to 70 °C for 30 min. The precipitate was filtered off and washed with *iso*-propanol and *n*-hexane. Yield 1.53 g (3.30 mmol, 67%). Mp. 288–290 °C.

^{1}H NMR ($CDCl_3$, 400 MHz): δ 7.95 (d, ^3J = 13.5, 1H), 7.77 (m, 2H), 7.53 (m, 3H), 7.35 (m, 1H), 7.27 (m, 1H), 7.17 (m, 1H), 7.00 (d, ^3J = 8.0, 1H), 5.86 (d, ^3J = 13.5, 1H), 4.34 (m, 2H), 3.48 (m, 3H), 1.55 (s, 6H), 1.37 (t, ^3J = 4.1, 3H). UV-vis (DCM): λ_{max} (ε) = 583 (58500), 625 (114700 M^{-1} cm^{-1}). HRMS (ESI): calcd for $C_{27}H_{26}N_3O_2S$ $[M+H]^+$: 456.1740, found: 456.1740. Anal. calcd for $C_{27}H_{25}N_3O_2S \times ⅓ H_2O$: C, 70.26; H, 5.60; N, 9.10; S, 6.95. Found: C, 70.26; H, 5.44; N, 9.18; S, 6.94.

{5-[2-(1-Butyl-3,3-dimethyl-1,3-dihydro-indol-2-ylidene)-ethylidene]-4-phenyl-5*H*-thiazol-2-ylidene}-cyano-acetic acid ethyl ester MD375

A 3.0 mL Ac_2O solution of (1-butyl-3,3-dimethyl-1,3-dihydro-indol-2-ylidene)-actaldehyde (730 g, 3.00 mmol) and cyano-(4-phenyl-5*H*-thiazol-2-ylidene)-acetic acid ethyl ester (820 g, 3.00 mmol) was heated to 70 °C for 30 min. The precipitate was filtered off and washed with *iso*-propanol and *n*-hexane. Yield 850 mg (1.71 mmol, 57%). Mp. 269–272 °C. ^{1}H NMR ($CDCl_3$, 400 MHz): δ 7.96 (d, ^3J = 13.2, 1H), 7.77 (m, 2H), 7.53 (m, 3H), 7.34 (m, 1H), 7.27 (m, 1H), 7.17 (m, 1H), 6.99 (d, ^3J = 8.0, 1H), 5.90 (d, ^3J = 13.4, 1H), 4.35 (m, 2H), 3.90 (t, ^3J = 7.4, 2H), 1.77 (m, 2H), 1.53 (s, 6H), 1.46 (m, 2H), 1.38 (t, ^3J = 7.1, 3H), 1.00 (t, ^3J = 7.1, 3H). UV-vis (DCM): λ_{max} (ε) = 627 (116700 M^{-1} cm^{-1}). HRMS (ESI): calcd for $C_{30}H_{32}N_3O_2S$ $[M+H]^+$: 498.2210, found: 498.2216. Elemental analysis (%) calcd for $C_{30}H_{31}N_3O_2S$: C, 72.40; H, 6.28; N, 8.44; S, 6.44. Found: C, 72.27; H, 6.21; N, 8.62; S, 6.30. CV data: E_p^{ox} = 388 mV vs Fc, E_p^{red} = –1439 mV vs Fc.

{5-[2-(3-Butyl-3*H*-benzothiazol-2-yliden)-ethyliden]-4-phenyl-5*H*-thiazol-2-yliden}-cyano-acetic acid ethyl ester EL38

A 1.0 mL Ac_2O solution of 3-butyl-2-methyl-1,3-benzothiazolium iodide (334 mg, 1.00 mmol) and *N*,*N*′-diphenyl-formamidine (196 mg, 1.00 mmol) was heated to 140 °C for 30 min, before KOAc (98 mg, 1.00 mmol) and cyano-(4-phenyl-5*H*-thiazol-2-ylidene)-acetic acid ethyl ester (270 mg, 1.00 mmol) was added. The mixture was heated to 110 °C for 3 h before the solvent removal. The residual solid was purified by column chromatography (DCM with 5% MeOH). Yield 100 mg (0.21 mmol, 21%). Mp. 320–322 °C. ^{1}H NMR (DMSO–d_6, 400 MHz): δ 8.58 (dd, ^3J = 8.2, ^4J = 1.0, 1H), 7.96 (d, ^3J = 8.5, 1H), 8.76 (d, ^3J = 14.0, 1H), 7.75−7.60 (m, 5H), 7.29 (t, ^3J = 7.4, 1H), 7.02 (m, ^3J = 7.4, 1H), 6.78 (d, ^3J = 14.0, 1H), 4.64 (t, ^3J = 7.6, 2H), 4.18 (t, ^3J = 7.1, 2H), 1.77 (m, 2H), 1.42 (m, 2H), 1.25 (t, ^3J = 7.1, 2H), 0.92 (t, ^3J = 7.6, 3H). UV-vis (DCM): λ_{max} (ε) = 635 (128600). HRMS (ESI): calcd for $C_{27}H_{26}N_3O_2S_2$ $[M+H]^+$: 488.1461, found: 488.1454. Elemental analysis (%) calcd for

$C_{27}H_{25}N_3O_2S_2$: C: 66.50, H: 5.17, N: 8.62, S: 13.15. Found: C: 66.61, H: 5.19, N: 8.59, S: 13.17. CV data: E_p^{ox} = 319 mV vs Fc, E_p^{red} = –1454 mV vs Fc.

2-[5-(5-Dibutylamino-furan-2-ylmethylene)-4-methyl-5*H*-thiazol-2-ylidene]-malononitrile MD321

A 1.5 mL Ac_2O solution of 5-dibutylamino-furan-2-carbaldehyde (223 mg, 1.00 mmol) and 2-(4-methyl-5*H*-thiazol-2-ylidene)-malononitrile (162 mg, 1.00 mmol) was heated to 70 °C for 75 min. The precipitate was filtered off and washed with *iso*-propanol and *n*-hexane. Yield 255 mg (0.70 mmol, 70%). Mp. 179–181 °C. ^{1}H NMR ($CDCl_3$, 400 MHz): δ 7.32 (d, ^3J = 4.5, 1H), 6.99 (s, 1H), 5.80 (d, ^3J = 4.4, 1H), 3.54 (t, ^3J = 7.9, 4H), 2.52 (s, 3H), 1.73 (m, 4H), 1.46 (m, 4H), 1.01 (t, ^3J = 7.4, 1H). UV-vis (DCM): λ_{max} (ε) = 604 (25100), 647 (67000 M^{-1} cm^{-1}). HRMS (ESI): calcd for $C_{20}H_{25}N_4OS$ $[M+H]^+$: 369.1744, found: 369.1740. Elemental analysis (%) calcd for $C_{20}H_{24}N_4OS$: C, 65.19; H, 6.56; N, 15.20; S, 8.70. Found: C, 65.41; H, 6.58; N, 15.22; S, 8.75. CV data: $E_{1/2}^{ox}$ = 307 mV vs Fc, E_p^{red} = –1417 mV vs Fc.

2-[4-Butyl-5-(4a,9-dimethyl-3,4,4a,9-tetrahydro-2*H*-carbazol-1-ylmethylene)-5*H*-thiazol-2-ylidene]-malononitrile HB281

A 1.3 mL Ac_2O solution of 4a,9-dimethyl-3,4,4a,9-tetrahydro-2*H*-carbazole-1-carbaldehyde (300 mg, 1.32 mmol) and 2-(4-*n*-butylthiazol-2(5*H*)-ylidene)malononitrile (271 mg, 1.32 mmol) was heated to 90 °C for 15 min, before the solvent was removed. The precipitate was filtered and washed with *n*-hexane and *iso*-propanol, before purification by column chromatography (DCM with 1.5% MeOH). Yield 468 mg (1.13 mmol, 86%). Mp. 245–247 °C. ^{1}H NMR (CD_2Cl_2, 400 MHz): δ 7.83 (s, 1H), 7.44 (m, 3H), 7.31 (m, 1H), 7.21 (m, 1H), 3.83 (s, 3H), 3.02 (m, 1H), 2.87 (m, 3H), 2.37 (m, 1H), 2.20 (m, 1H), 1.93 (m, 1H), 1.72–1.86 (m, 3H), 1.47 (m, 2H), 1.41 (s, 3H), 0.98 (t, ^3J = 7.3, 3H). UV-vis (DCM): λ_{max} (ε): 627 (112000 M^{-1} cm^{-1}). HRMS (ESI): calcd for $C_{25}H_{26}N_4S$ $[M]^+$: 414.1878, found: 414.1873. Elemental analysis (%) calcd for $C_{25}H_{26}N_4S \times ½\ H_2O$: C, 70.89; H, 6.42; N, 13.23; S, 7.57. Found: C, 70.76; H, 6.19; N, 13.03; S, 7.30. CV data: $E_{1/2}^{ox}$ = 240 mV vs Fc, E_p^{red} = –1493 mV vs Fc.

Benzyl-2-cyano-2-(4-phenyl-5-(2-(1,3,3-trimethylindolin-2-ylidene)ethylidene)thiazol-2(5*H*)-ylidene)acetate HB075

A 3.5 mL Ac_2O solution of benzyl-2-cyano-2-(4-phenylthiazol-2-(5*H*)-ylidene)acetate (829 mg, 2.48 mmol) and (1,3,3-trimethyl-1,3-dihydro-indol-2-ylidene)-actaldehyde (500 mg, 2.48 mmol) was heated to 70 °C for 30 min. The precipitate was filtered off and

washed with *iso*-propanol and *n*-hexane. The residual solid was purified by column chromatography (DCM with 2% MeOH). Yield 1.10 mg (2.12 mmol, 86%). Mp 289–290 °C. ^{1}H NMR (CD_2Cl_2, 400 MHz): δ 8.02 (d, ^{3}J = 13.7, 1H), 7.75 (m, 2H), 7.58 (m, 3H), 7.46 (m, 2H), 7.39 (m, 3H), 7.33 (m, 2H), 7.22 (m, 1H), 7.08 (d, ^{3}J = 7.8, 1H), 5.98 (d, ^{3}J = 13.8, 1H), 5.31 (s, 2H), 3.53 (s, 3H), 1.54 (s, 6H). UV-vis (DCM): λ_{max} (ε) = 626 (116800). HRMS (ESI): calcd for $C_{32}H_{28}N_3O_2S$ $[M+H]^+$: 517.1824, found: 517.1819. Elemental analysis (%) calcd for $C_{32}H_{27}N_3O_2S \times 1\ H_2O$: C. 71.75, H: 5:46, N: 7:84, S: 5.99. Found: C: 71.89, H: 5.24, N: 7.87, S: 6.12. CV data: E_p^{ox} = 411 mV vs Fc, E_p^{red} = –1408 mV vs Fc.

Chapter 6 Summary

The technology of organic photovoltaics offers the possibility of low-cost devices due to easy fabrication procedures and low material consumption and at the same time high flexibility concerning the applied substrates or design features such as the color palette. Owing to these benefits, this research field is highly active, being reflected by the continuously rising number of publications.

Chapter 1 gives an extensive overview of a part of these reports, namely the field of solution-processed BHJ organic solar cells using small molecules as electron-donating materials. In the early years of this research area (2006-2008), well known hole transporting materials such as triphenylamine based chromophores, oligothiophenes and polyaromatic hydrocarbons were applied. However, many of these dyes lacked absorption at longer wavelengths and were therefore limited in their light harvesting qualities. Later, chromophores based on low band gap systems consisting of electron-donating and electron-accepting units showing internal charge transfer overcame this handicap. Today, donor-substituted diketopyrrolopyrroles (D-A-D chromophores), squaraines (D-A-D chromophores) and acceptor substituted oligothiophenes (A-D-A chromophores) are among the most promising dyes for small molecule based organic solar cells with PCEs of 4-5%.

This work is based on the findings of the groups of Würthner and Meerholz, which tested merocyanine dyes for the first time in organic BHJ solar cells.[4] According to the Bässler theory[85], the high dipolarity of these dyes should hamper the charge transport, but the obtained first results with PCE of 1.7% proved the potenital of this class of dyes for this application. Merocyanine dyes offer the advantages of facile synthesis and purification, high tinctorial strength and monodispersity. Additionally, the electronic structure of the dyes, namely the absorption as well as the electrochemical properties, can be adjusted by using the right combination of donor and acceptor units. For these reasons, this class of dye is highly interesting for the application in organic solar cells.

It was the aim of the thesis to build more knowledge about the potential and limitations of merocyanines in BHJ photovoltaic devices. By screening a variety of donor and acceptor groups a comprehensive data set both for the molecular materials as well as for the respective solar devices was generated and analyzed. As one focus, the arrangement of the chromophores in the solid state was investigated to gain insight about the packing in the solar cells and its relevance for the performance of the latter. To do so, X-ray single crystal

analyses were performed for selected molecules. By means of correlations between molecular properties and the characteristics of the corresponding solar cells, several design rules to generate efficient chromophores for organic photovoltaics were developed.

The different donor and acceptor moieties applied in this work are depicted in the following.

Acceptor units A:

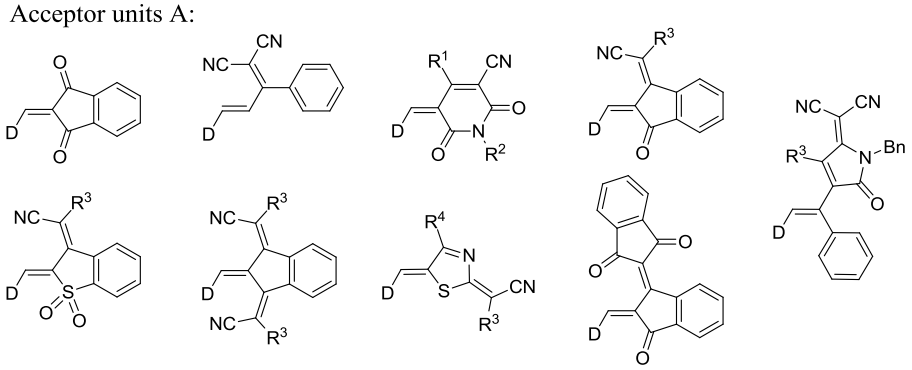

R^1: Me, CF_3; R_2: *n*-Bu, 2-Ethylhexyl; R_3: CN, CO_2Et, CO_2Bn; R_4: Me, *n*-Bu, *t*-Bu, Phenyl

Donor untis D:

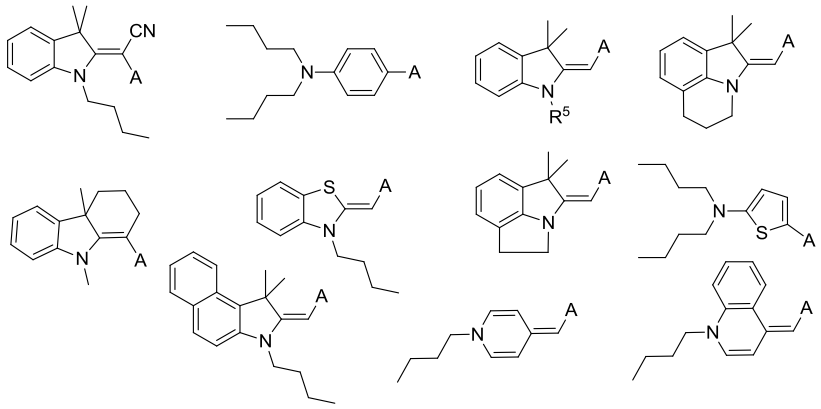

R^5: Me, *i*-Pr, *n*-Bu, Bn, 2-Ethylhexyl

Both groups are arranged according to the strength of the acceptor and donor, respectively, starting each with the weakest unit. The synthesis of these dyes and their electronic characterization by means of UV-vis spectroscopy and cyclic voltammetry are described in *Chapters 2-5*. The substitution pattern (R^1–R^5) of both donor and acceptor units were varied to investigate the influence of bulky substituents on the packing behaviour and to find the optimum between solubility and the least amount of non-absorbing alkyl chains. It was found, that long solubilizing alkyl chains like 2-ethylhexyl are only beneficial if the chromophore shows a poor solubility, like in the case of dyes with a pyridine or quinoline donor. Moreover, bulky substituents displayed a negative influence on the performance of corresponding solar cells in case of planar chromophores like for example **MD376** and its derivatives. In the case of strongly distorted chromophores like **HB094** and derivatives, no significant influence was detected.

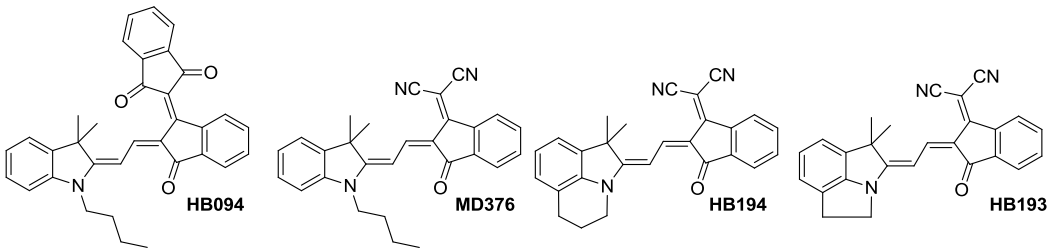

In *Chapter 2*, chromophores with an indolenine donor ("Fischer base") unit are reported. Besides an variation of the acceptor unit, the flexible butyl chain at the donor unit was substituted by an ethylene and propylene bridging units. In all described examples, these modifications resulted in better solar cell characteristics, especially with improved short-circuit current density. Solar cells containing **HB194** achieved a PCE of 2.6%. By using the example of one chromophore series, **MD376**, **HB194** and **HB193**, the phenomenon was studied in detail by means of charge transport analysis in organic field effect transistors, powder diffraction experiments and differential scanning calorimetry. The dyes with bridging units, in particular **HB194** showed higher charge carrier mobility and stronger tendency to crystallize in blends with $PC_{61}BM$. Single crystal analysis displayed in six of seven investigated examples an antiparallel arrangement of the chromophores, which results in an annihilation of the dipole moment on the supramolecular level.

Chapter 3 describes the synthesis and characterization of a dye series with aminothiophene donor and different acceptor units. The absorption properties and the LUMO energies of the chromophores were strongly affected by the variation of the electron-acceptors, whilst the effect on the HOMO was significantly weaker. The impact of the strong molecular dipole moment of the chromophores was examined by analysis of single crystals. These revealed centrosymmetric dimeric packing units in both investigated samples, yielding an extinct dipole moment. As this antiparallel packing motive was determined in all inspected samples, we expect it to exist also in the active layers of the organic solar cells. Hence, the limitations for dyes with large dipole moments according to the Bässler theory are not valid for merocyanine dyes, explaining their efficient application to solar cells. A combination of $PC_{71}BM$ and chromophore **EL86** yielded for example a highly efficient device with a PCE of 4%.

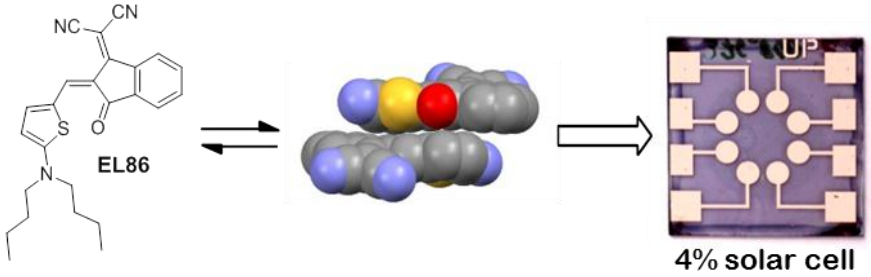

Besides merocyanines for high efficiency solar cells, the exploration of NIR absorbing dyes was envisaged, too (*Chapter 4*). To obtain absorption at long wavelengths, the π-system was extended and a strong acceptor, namely 2-oxo-5-dicyanomethylenepyrrolidine, was applied. The resulting solar cells are indeed transparent and almost colorless, opening up possibilities such as power window applications. However, absorption in the NIR is accompanied by a very low band gap and therefore high-lying HOMO level. Hence, the performance of these dyes will always be restricted by the V_{OC}. In the presented case, a PCE of 1% was achieved in blends with the fullerene $PC_{71}BM$.

A detailed analysis of the solar cell characteristics in correlation with the properties of the molecular materials is described in *Chapter 5* and several rules of actions were established. Concerning the FMO levels a LUMO level of –3.6±0.1 eV seems to be optimal for efficient photoinduced charge transfer from the electron donor to the electron acceptor and concomitantly minimal energy loss, while a HOMO energy of –5.7±0.1 eV enables a large V_{OC}. The determined interval of FMO levels results in an optimal absorption range of 540–650 nm. Moreover, according to our study, merocyanines close to the *cyanine limit* with small reorganization energy[125] appear to be well-suited for organic solar cells. Looking at these rules of action, merocyanine dyes show several benefits: the absorption of the dyes can be easily adjusted by using the appropriate donor and acceptor combinations and they usually display low-lying HOMO levels. However, MC dyes have also some limitation, such as relatively low fill factors, which could originated from suboptimal charge transfer due to energetic disorder caused by the dipolarity.[85] Furthermore, one has to compromise between absorption at long wavelengths and accordingly effective light harvesting and a low-lying HOMO level.

In conclusion, this work comprises the synthesis and molecular characterization of a comprehensive series of merocyanine dyes. Furthermore, the compounds were tested in solution-processed BHJ organic solar cells. Single crystal analyses revealed an antiparallel packing motive for all investigated samples, which comes along with an extinct dipole moment on the supramolecular level. We suggest that the same packing unit prevails in the solar devices, explaining the good performance of merocyanine dyes with PCE of up to 4%. These high efficiencies, which are comparable with the best reported chromophores in this research field, were obtained after carefully adapting the donor and acceptor units to create optimized electronic properties.

Chapter 7 Zusammenfassung

Die Technologie der organischen Photovoltaik eröffnet die Chance, kostengünstige Solarzellen herzustellen, da einfache Produktionstechniken genutzt werden können und nur geringe Materialmengen benötigt werden. Gleichzeitig bietet sie hohe Flexibilität bezüglich des Designs, sowohl was die eingesetzten Substrate als auch die gewünschte Farbpalette betrifft. Aufgrund dieser Vorteile ist der Forschungsbereich der organischen Solarzellen hochaktuell, was sich auch in der stetig wachsenden Zahl an Publikationen widerspiegelt.

Kapitel 1 bietet einen umfassenden Literaturüberblick über den Bereich der lösungsprozessierten organischen BHJ Solarzellen basierend auf niedermolekularen Materialien. In den frühen Jahren dieses Forschungsbereiches (2006-2008) wurden hauptsächlich altbekannte organische Lochleitermaterialien wie triphenylaminbasierte Moleküle, Oligothiophene oder polyaromatische Hydrocarbonverbindungen eingesetzt. Viele dieser Verbindungen zeigten jedoch Defizite betreffend der Absorption, da sie nur bei relativ kurzen Wellenlängen absorbierten und dadurch nur einen Bruchteil des eingestrahlten Sonnenlichts nutzen konnten. Später wurde dieser Nachteil durch sogenannte „low band gap“ Systeme, welche elektronengebenden und elektronenziehenden Einheiten aufweisen, oder durch Kombinationen der klassischen elektronenreichen Lochleiter mit Akzeptoreinheiten überwunden. Zu den vielversprechendsten Verbindungsklassen für die Anwendung in lösungsprozessierten niedermolekularen organischen Solarzellen gehören heute Donor-substituierte Diketopyrrolopyrrole (D-A-D Chromophor), Quadratsäurederivate (D-A-D Chromophor) und Akzeptor-substituierte Oligothiophene (A-D-A Chromophor), deren beste Vertreter Wirkungsgrade von 4-5% erzielen.

Die vorliegende Arbeit basiert auf den Erkenntnissen der Arbeitsgruppen Würthner und Meerholz, die als erste Merocyaninfarbstoffe in organischen BHJ Solarzellen untersuchten.[4] Gemäß der Bässler-Theorie[85] sollte das hohe Grundzustandsdipolmoment dieser Verbindungen den Ladungsträgertransport erheblich behindern. Die erhaltenen, vielversprechenden Wirkungsgrade von 1.7% beim ersten Materialscreenin zeigen jedoch die Eignung dieser Fabstoffklasse für organische Solarzellen. Merocyanine bieten einige Vorteile: sie lassen sich einfach herstellen und aufreinigen, zeigen hohe Farbstärken und sind monodisperse Verbindungen. Zudem lässt sich der elektronische Charakter der Chromophore, also die Absorptions- und elektrochemischen Eigenschaften nahezu beliebig

verändern, indem man die passende Donor-Akzeptor Kombination wählt. Deshalb ist diese Farbstoffklasse für die Applikation der organischen Solarzellen hochinteressant.

Ziel dieser Doktorarbeit war es, ein tieferes Verständnis über das Potential und mögliche Beschränkungen von Merocyaninen in organische Solarzellen zu erlangen. Durch Untersuchung einer Reihe von Donor- und Akzeptoreinheiten wurde ein umfassender Datensatz generiert und analysiert, welcher sowohl die molekularen Materialien als auch die entsprechenden Solarzellen beinhaltet. Die Anordnung der Chromophore im Festkörper wurde bei ausgewählten Farbstoffen mittels Einkristall-Röntgenstrukturanalyse untersucht, um Erkenntnisse über das Packungsverhalten der Moleküle in den Solarzellen und dessen Relevanz für die Leistungsfähigkeit der Zellen zu gewinnen. Anhand von Korrelationen zwischen den molekularen Eigenschaften und den Kennzahlen der entsprechenden Solarzellen wurden mehrere Richtlinien zur Entwicklung von effizienten Chromophoren für organische Solarzellen abgeleitet.

Die in dieser Arbeit eingesetzten Akzeptor- und Donoreinheiten sind im Folgenden abgebildet.

Akzeptoreinheiten A:

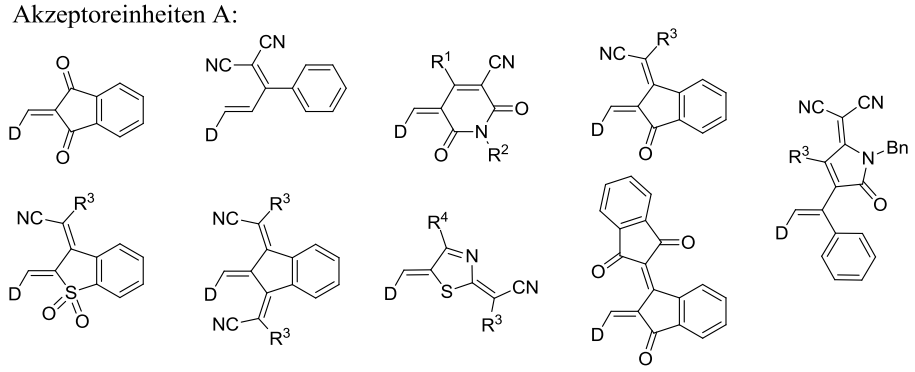

R^1: Me, CF_3; R_2: *n*-Bu, 2-Ethylhexyl; R_3: CN, CO_2Et, CO_2Bn; R_4: Me, *n*-Bu, *t*-Bu, Phenyl

Donoreinheiten D:

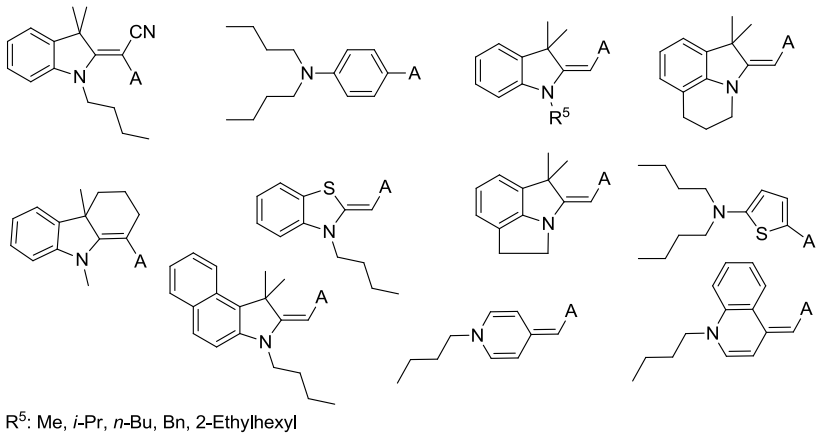

R^5: Me, *i*-Pr, *n*-Bu, Bn, 2-Ethylhexyl

Beide Gruppen sind jeweils nach der Stärke der Akzeptoren beziehungsweise Donoren angeordnet, beginnend mit der schwächsten Einheit. *Kapitel 2-5* beschreiben die Synthese dieser Farbstoffe sowie die Charakterisierung ihrer elektronischen Eigenschaften durch UV-vis Spektroskopie und Cyclovoltammetrie. Das Substitutionsmuster (R^1–R^5) der Donor- und Akzeptoreinheiten wurde variiert, um einerseits den Einfluss von sperrigen Substituenten auf das Packungsverhalten zu untersuchen und andererseits einen Mittelweg zwischen guter Löslichkeit und möglichst geringen Anteilen an nichtabsorbierenden Alkylketten zu finden. Tatsächlich waren lange löslichkeitsfördernde Alkylketten wie 2-Ethylhexyl nur dann von Vorteil, wenn es sich um Chromophore mit sehr schlechter Löslichkeit handelte. Dies war beispielsweise der Fall, wenn die Donoren Pyridin und Chinolin verwendet wurden. Weiterhin wurde entdeckt, dass sperrige Substituenten nur dann einen negativen Einfluss auf die Leistungsfähigkeit der entsprechenden Solarzelle hatten, wenn es sich um einen nahezu planaren Chromophor wie zum Beispiel **MD376** handelte. Bei stark verdrillten Farbstoffen wie **HB094** und dessen Derivaten wurde kein signifikanter Einfluss der Substituenten beobachtet.

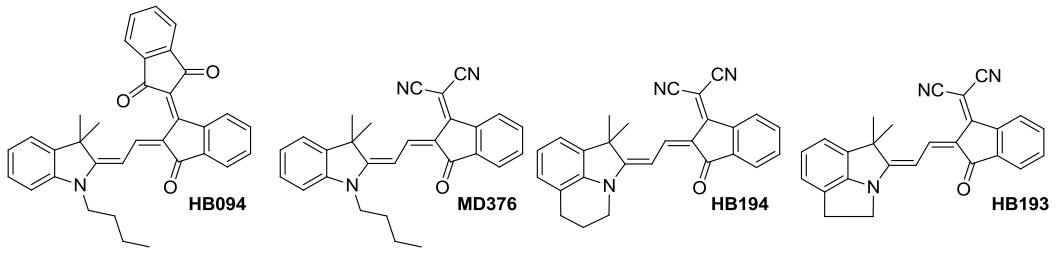

In *Kapitel 2* wird über Chromophore mit Indolenindonor („Fischer Base“) berichtet. Neben einer Akzeptorvariation wurde hier wurde die flexible Butylkette an der Donoreinheit durch eine verbrückende Ethyl bzw. Propyleinheit ersetzt. In allen beschriebenen Beispielen resultierte diese Veränderung in verbesserten Solarzellenkennzahlen, insbesondere in einer höheren Kurzschlussstromdichte. Farbstoffsolarzellen mit dem Chromophor **HB194** erreichten so einen hohen Wirkungsgrad von 2.6%. Anhand einer Chromophorserie, **MD376**, **HB194** und **HB193** wurde dieses Phänomen durch Röntgenbeugung, dynamische Differenzkalorimetrie und Ladungstransportstudien in organischen Feldeffekttransistoren im Detail untersucht. Die Farbstoffe mit der starren Verbückungseinheit, insbesondere **HB194**, zeigten eine höhere Ladungsträgermobilität und eine stärkere Tendenz, im Verbund mit $PC_{61}BM$ kristalline Filme zu bilden. Einkristallanalysen belegten in sechs von sieben untersuchten Beispielen eine antiparallele Anordnung der Moleküle, welche auf supramolekularer Ebene zur Aufhebung der großen molekularen Dipolmomente führt.

Kapitel 3 beschreibt die Synthese und Charakterisierung einer Farbstoffserie mit Aminothiophendonor und verschiedenen Akzeptoreinheiten. Die Absorptionseigenschaften und die Lage des LUMOs wurden signifikant durch die Variation des Akzeptorparts beeinflusst, während die Auswirkungen auf das HOMO deutlich geringer ausfielen. Zudem wurde der Effekt des großen molekularen Dipolmomentes durch Einkristall-Röntgenstrukturanalyse untersucht. Hier wurden zentrosymmetrische Dimere als Packungseinheit gefunden, welche zur Aufhebung der Dipolmomente führen. Da dieses antiparallele Packungsmotiv in allen untersuchten Proben vorlag, gehen wir davon aus, dass es auch in der aktiven Schicht der Solarzelle vorliegt. Folglich ist die Einschränkung für Farbstoffe mit großem Grundzustandsdipolmoment gemäß der Theorie von Bässler für Merocyaninfarbstoffe nicht gültig. Dies erklärt ihren vielversprechenden Einsatz in organischen Solarzellen. Beispielsweise wurde ein hocheffizientes Bauteil mit einer Kombination aus $PC_{71}BM$ und **EL86** gefertigt, welches einen Wirkungsgrad von 4% erreichte.

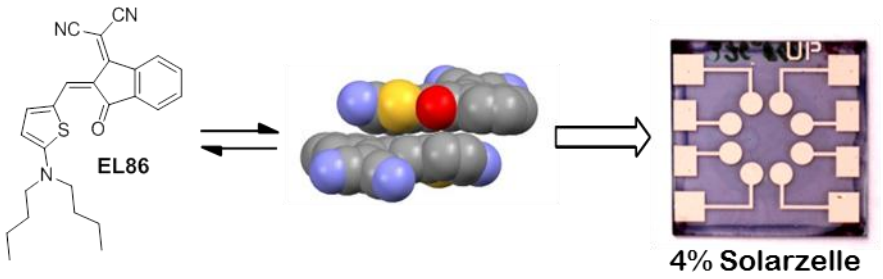

Neben Merocyaninen für Hochleistungszellen wurde auch die Erforschung von NIR absorbierenden Farbstoffen vorgenommen (*Kapitel 4*). Um eine Absorption bei langen Wellenlängen zu erreichen, wurde das π-System verlängert und ein starker Akzeptor, 2-Oxo-5-dicyanomethylenpyrrolidin, eingesetzt. Die daraus resultierenden Solarzellen waren in der Tat transparent und nahezu farblos, was neue Anwendungsmöglichkeiten wie zum Beispiel stromerzeugende Fenster eröffnet. Es ist jedoch zu bedenken, dass Absorption im Nahinfrarotbereich mit einer sehr kleinen Bandlücke und einer dementsprechend hohen HOMO Energie verbunden ist. Deshalb ist die Leistungsfähigkeit dieser Farbstoffe immer durch eine begrenzte Leerlaufspannung eingeschränkt. In vorgestellten Fall wurde in Kombination mit $PC_{71}BM$ ein Wirkungsgrad von maximal 1% erreicht.

Kapitel 5 enthält eine detaillierte Analyse der Solarzellenkennzahlen in Korrelation mit den Eigenschaften der einzelnen Farbstoffe. Auf Basis dieser Korrelationen wurden mehrere Richtlinien erarbeitet. Bezüglich der FMO Niveaus scheint ein LUMO von –3.6±0.1 eV ein optimaler Kompromiss zwischen effizientem photoinduzierten Ladungstransfer vom

Elektronendonor auf den Elektronenakzeptor und gleichzeitigem minimalen Energieverlust zu sein, während ein HOMO von –5.7±0.1 eV eine große Leerlaufspannung ermöglicht. Dieses Intervall der FMO Energien führt zu einer optimalen Absorption von 540–650 nm. Abgesehen davon erscheinen Merocyanine nahe dem *Cyaninlimit* aufgrund ihrer geringen Reorganisationsenergie[125] gut geeignet für die Anwendung in organischen Solarzellen. Betrachtet man nun diese Richtlinien, so treten die Vorzüge der Merocyaninfarbstoffe deutlich hervor: die Absorption dieser Chromophore lässt sich durch geeignete Kombination von Donor und Akzeptor nahezu beliebig einstellen und sie weisen im Allgemeinen niedrigliegende HOMO Niveaus auf. Nichtsdestotrotz unterliegen diese Farbstoffe gewissen Beschränkungen, da sie häufig recht niedrige Füllfaktoren in den Solarzellen aufweisen, die in einem suboptimalen Ladungstransport begründet sein könnten (energetsiche Umordnung wegen Dipolarität[85]). Zudem muss ein Kompromiss zwischen Absorption bei langen Wellenlängen und damit verbundenem effizienten Lichtsammeln und einem niedrigliegenden HOMO eingegangen werden.

Summa summarum beschreibt diese Arbeit die Synthese und Charakterisierung der molekularen Eigenschaften einer umfassenden Serie von Merocyaninfarbstoffen. Außerdem wurden die Verbindungen in lösungsprozessierten organischen BHJ Solarzellen untersucht. Einkristallstrukturanalysen zeigten in jedem untersuchten Fall ein antiparalleles Packungsmuster, welches die Aufhebung des Dipolmoments auf der supramolekularen Ebene bewirkt. Unserer Vorstellung nach dominiert eben dieses Packungsmotiv auch in den Solarzellen, was die gute Leistungsfähigkeit der Farbstoffe in Solarzellen mit Wirkungsgraden von bis zu 4% erklärt. Sorgfältiges Abstimmen der Donor- und Akzeptoreinheiten aufeinander resultierte in optimierten elektronischen Eigenschaften. Diese führten zu hohen Wirkungsgraden, welche mit den aktuellen Rekordwerten in diesem Forschungsgebiet gleichziehen können.

References

(1) Kondratieff, N. D. *Rev. Econom. Statist.* **1935**, *17*, 105.

(2) Green, M. A.; Emery, K.; Hishikawa, Y.; Warta, W. *Prog. Photov. Res. & Appl.* **2011**, *19*, 84.

(3) For reviews on this topic see: a) Cheng, Y.-J.; Yang, S.-H.; Hsu, C.-S. *Chem. Rev.* **2009**, *109*, 5868; b) Hains, A. W.; Liang, Z.; Woodhouse, M. A.; Gregg. B. A. *Chem. Rev.* **2010**, *110*, 6689; c) Walker, B.; Kim, C.; Nguyen, T.-Q. *Chem. Mater.* **2011**, *23*, 470.

(4) Kronenberg, N. M.; Deppisch, M.; Würthner, F.; Lademann, H. W. A.; Deing, K.; Meerholz, K. *Chem. Commun*. **2008**, 6489.

(5) a) Mishra, A.; Behera, R. K.; Behera, P. K.; Mishra, B. K.; Behera, G. B. *Chem. Rev.* **2000**, *100*, 1973; b) Kulinich, A. V.; Ishchenko A. A. *Russ. Chem. Rev.* **2009**, *78*, 141.

(6) Blanchard-Desce, M.; Wortmann, R.; Lebus, S.; Lehn, J.-M.; Krämer, P. *Chem. Phys. Lett.* **1995**, *243*, 526.

(7) a) Würthner, F.; Yao, S.; Wortmann, R. *J. Inf. Rec.* **2000**, *25*, 69; b) Würthner, F.; Wortmann, R.; Meerholz K. *ChemPhysChem* **2002**, *3*, 17.

(8) Shirinian, V. Z.; Shimikin, A. A. *Top. Heterocycl. Chem.* **2008**, *14*, 75.

(9) Mishra, A.; Fischer, M. K. R.; Bäuerle P. *Angew. Chem. Int. Ed.* **2009**, *48*, 2474.

(10) Tang, C. W.; Albrecht A. C. *Nature* **1975**, *254*, 507.

(11) Morel, D. L.; Gosh, A. K.; Feng, T.; Stogryn, E. L.; Purwin, P. E.; Shaw, R. F.; Fishman C. *Appl. Phys. Lett.* **1978**, *32*, 495.

(12) Chamberlain, G. A.; Cooney, P. J.; Dennison S. *Nature* **1981**, *289*, 45.

(13) Chamberlain G. A. *J. Appl. Phys.* **1982**, *53*, 6262.

(14) Walzer, K.; Maennig, B.; Pfeiffer, M.; Leo, K. *Chem. Rev.* **2007**, *107*, 1233.

(15) Gregg, B. *J. Phys. Chem. B* **2003**, *107*, 4688.

(16) a) Peumans, P.; Yakimov, A.; Forrest, S. R. *J. Appl. Phys.* **2003**, *93*, 3693; b) Halls, J. J. M.; Pichler, K.; Friend, R. H.; Moratti, S. C.; Holmes, A. B. *Appl. Phys. Lett.* **1996**, *68*, 3120.

(17) Tang, C. W. *Appl. Phys. Lett*. **1986**, *48*, 183.

(18) a) Halls, J. J. M.; Walsh, C. A.; Greenham, N. C.; Marseglia, E. A.; Friend, R. H.; Moratti, S. C.; Holmes, A. B. *Nature* **1995**, *376*, 498; b) Yu, G.; Gao, J.; Hummelen, J. C.; Wudl, F.; Heeger, A. J. *Science* **1995**, *270*, 1789.

(19) a) Scharber, M. C.; Mühlbacher, D.; Koppe, M.; Denk, P.; Waldauf, C.; Heeger, A. J.; Brabec, C. J. *Adv. Mater.* **2006**, *18*, 789; b) Koster, L. J. A.; Mihailetchi, V. D.; Blom, P. W. M. *Appl. Phys. Lett.* **2006**, *88*, 093511.

(20) a) Shaheen, S. E.; Brabec, C. J.; Sariciftci, N. S.; Padinger, F.; Fromherz, T.; Hummelen, J. C. *Appl. Phys. Lett.* **2001**, *78*, 841; b) Wienk, M. M.; Kroon, J. M.; Verhees W. J. H.; Knol, J.; Hummelen, J. C.; van Hall, P. A.; Janssen, R. A. J. *Angew. Chem., Int. Ed.* **2003**, *42*, 3371.

(21) a) Ma, W.; Yang, C.; Gong, X.; Lee, K.; Heeger, A. J. *Adv. Funct. Mater*. **2005**, *15*, 1617; b) Li, G.; Shrotriya, V.; Huang, J.; Yao, Y.; Moriarty, T.; Emery, K.; Yang, Y. *Nat. Mater*. **2005**, *4*, 864; c) Kim, Y.; Cook, S.; Tuladhar, S. M.; Choulis, S. A.; Nelson, J.; Durrant, J. R.; Bradley, D. D. C.; Giles, M.; McCulloch, I.; Ha, C.-S.; Ree, M. *Nat. Mater.* **2006**, *5*, 197.

(22) For reviews on this topic see: a) Dennler, G.; Scharber, M. C.; Brabec, C. J. *Adv, Mater.* **2009**, *21*, 1323. b) Zhan, X.; Zhu, D. *Polym. Chem.* **2010**, *1*, 409. c) Facchetti, A. *Chem. Mater*. **2011**, *23*, 733.

(23) Chang, J.-F.; Sun, B.; Breiby, D. W.; Nielsen, M. N.; Sölling, T. I.; Giles, M.; McCulloch, I.; Sirringhaus H. *Chem. Mater.* **2004**, *16*, 4772.

(24) Roncali, J.; Frère, P.; Blanchard, P.; de Bettignies, R.; Turbiez, M.; Roquet, S.; Leriche, P.; Nicholas Y. *Thin Solid Films* **2006**, *511–512*, 567.

(25) Sun, X.; Zhou, Y.; Wu, W.; Liu, Y.; Tian, W.; Yu, G.; Qiu, W.; Chen, S.; Zhu D. *J. Phys. Chem. B* **2006**, *110*, 7702.

(26) a) Fitzner, R.; Reinhold, E.; Mishra, A.; Mena-Osteritz, E.; Ziehlke, H.; Körner, C.; Leo, K.; Riede, M.; Weil, M.; Tsaryova, O.; Weiß, A.; Uhrich, C.; Pfeiffer, M.; Bäuerle, P. *Adv Funct. Mater.* **2011**, *21*, 897; b) Liu, Y. S.; Zhou, J. Y.; Wan, X. J.; Chen Y. S. *Tetrahedron* **2009**, *65*, 5209.

(27) a) Liu, Y.; Wan, X.; Yin, B.; Zhou, J.; Long, G.; Yin, S.; Chen Y. *J. Mater. Chem.* **2010**, *20*, 2464; b) Yin, B.; Yang, L.; Liu, Y.; Chen, Y.; Qi, Q.; Zhang, F.; Yin S. *Appl. Phys. Lett.* **2010**, *97*, 023303.

(28) a) Lo, S.-C.; Burn P. L. *Chem. Rev.* **2007**, *107*, 1097; b) Roncali, J.; Leriche, P.; Cravino A. *Adv. Mater.* **2007**, *19*, 2045.

(29) Kopidakis, N.; Mitchell, W. J.; van de Lagemaat, J.; Ginley, D. S.; Rumbles, G.; Shaheen, S. E.; Rance W. L. *Appl. Phys. Lett.* **2006**, *89*, 103524.

(30) Ma, C.-Q.; Fonronda, M.; Schikora, M. C.; Wienk, M. M.; Janssen, R. A. J.; Bäuerle P. *Adv. Funct. Mater.* **2008**, *18*, 3323.

(31) Shirota Y. *J. Mater. Chem.* **2005**, *15*, 75.

(32) Roquet, S.; Cravino, A.; Leriche, P.; Alévêque, O.; Frère, P.; Roncali J. *J. Am. Chem. Soc.* **2006**, *128*, 3459.

(33) a) He, C.; He, Q.; Yi, Y.; Wu, G.; Bai, F.; Shuai, Z.; Li Y. *J. Mater. Chem* **2008**, *18*, 4085; b) Wu, G.; Zhao, G.; He, C.; Zhang, J.; He, Q.; Chen, X.; Li Y. *Sol. Energy Mater. Sol. Cells* **2009**, *93*, 108; c) Zhao, G.; Wu, G.; He, C.; Bai, F.-Q.; Xi, H.; Zhang, H.-X.; Li Y. *J. Phys. Chem. C* **2009**, *113*, 2636; d) Zhang, J.; Yang, Y.; He, C.; He, Y.; Zhao, G.; Li Y. *Macromolecules* **2009**, *42*, 7619; e) Yang, Y.; Zhang, J.; Zhou, Y.; Zhao, G.; He, C.; Li, Y.; Andersson, M.; Inganäs, O.; Zhang F. *J. Phys. Chem. C* **2010**, *114*, 3701; f) Zhang, J.; Deng, D.; He, C.; He, Y.; Zhang, M.; Zhang, Z.-G.; Zhang, Z.; Li Y. *Chem. Mater.* **2011**, *23*, 817; g) Shang, H.; Fan, H.; Liu, Y.; Hu, W.; Li, Y.; Zhan Z. *Adv. Mater.* **2011**, 23, 1554.

(34) Anthony, J. E. *Chem. Rev.* **2006**, *106*, 5028.

(35) Lloyd, M. T.; Mayer, A. C.; Subramanian, S.; Mourey, D. A.; Herman, D. J.; Bapat, A. V.; Anthony, J. E.; Malliaras, G. G. *J. Am. Chem. Soc.* **2007**, *129*, 9144.

(36) Valentini, L.; Bagnis, D.; Marrocchi, A.; Seri, M.; Taticchi, A.; Kenny; J. M. *Chem. Mater.* **2008**, *20*, 32.

(37) a) Marrocchi, A.; Silvestri, F.; Seri, M.; Facchetti, A.; Taticchi, A.; Marks, T. J. *Chem. Commun.* **2009**, 1380. b) Silvestri, F.; Marrocchi, A.; Seri, M.; Kim, C.; Marks, T. J.; Facchetti, A.; Taticchi, A. *J. Am. Chem. Soc.* **2010**, *132*, 6108.

(38) Winzenberg, K. N.; Kemppinen, P.; Fanchini, G.; Bown, M.; Collis, G. E.; Forsyth, C. M.; Hegedus, K.; Singh, T. B.; Watkins, S. E.*Chem. Mater.* **2009**, *21*, 5701.

(39) Wong, W. W. H.; Singh, T. B.; Vak, D.; Pisula, W.; Yan, C.; Feng, X.; Williams, E. L.; Chan, K. L.; Mao, Q.; Jones, D. J.; Ma, C.-Q.; Müllen, K.; Bäuerle, P.; Holmes, A. *Adv. Funct. Mater.* **2010**, *20*, 927.

(40) Pisula, W.; Menon, A.; Stepputat, M.; Lieberwirth, I.; Kolb, U.; Tracz, A.; Sirringhaus, H.; Pakula, T.; Müllen, K. *Adv. Mater.* **2005**, *17*, 684.

(41) Wong, W. W. H.; Ma, C.-Q.; Pisula, W.; Yan, C.; Feng, X.; Jones, D. J.; Müllen, K.; Janssen, R. A. J.; Bäuerle, P.; Holmes; A. B. *Chem. Mater.* **2010**, *22*, 457.

(42) He, C.; He, Q.; He, Y.; Li, Y.; Bai, F.; Yang, C.; Ding, Y.; Wang, L.; Ye; J. *Sol. Energ. Mater. Sol. Cells* **2006**, *90*, 1815.

(43) a) Shang, H.; Fan, H.; Shi, Q.; Li, S.; Li, Y.; Zhan, X. *Sol. Energ. Mater. Sol. Cells* **2010**, *94*, 457; b) Fan, H.; Shang, H.; Li, Y.; Zhan, X. *Appl. Phys. Lett.* **2010**, *97*, 133302.

(44) Li, Y.; Cao, Y.; Gao, J.; Wang, D.; Yu, G.; Heeger, A. J. *Synth. Met.* **1999**, *99*, 243.

(45) Wu, Z.; Fan, B.; Xue, F.; Adachi, C.; Ouyang, J. *Sol. Energ. Mater. Sol. Cells* **2010**, *94*, 2230.

(46) Li, W.; Du, C.; Li, F.; Zhou, Y.; Fahlman, M.; Bo, Z.; Zhang, F. *Chem. Mater.* **2009**, *21*, 5327.

(47) He, C.; He, Q.; Yang, X.; Wu, G.; Yang, C.; Bai, F.; Shuai, Z.; Wang, L.; Li, Y. *J. Phys. Chem. C* **2007**, *111*, 8661.

(48) Xue, L.; He, J.; Gu, X.; Yang, Z.; Xu, B.; Tian, W. *J. Phys. Chem. C* **2009**, *113*, 12911.

(49) Li, Z.; Pei, J.; Li, Y.; Xu, B.; Deng, M.; Liu, Z.; Li, H.; Lu, H.; Li, Q.; Tian, W. *J. Phys. Chem. C* **2010**, *114*, 18270.

(50) Zhang, J.; Wu, G.; He, C.; Deng, D.; Li, Y. *J. Mater. Chem.* **2011**, *21*, 3768.

(51) Tamayo, A. B.; Walker, B.; Nguyen, T.-Q. *J. Phys. Chem. C* **2008**, *112*, 11545.

(52) Tamayo, A. B.; Dang, X.-D.; Walker, B.; Seo, J.; Kent, T.; Nguyen, T.-Q. *Appl. Phys. Lett.* **2009**, *94*, 103301.

(53) Walker, B.; Tamayo, A. B.; Dang, X.-D.; Zalar, P.; Seo, J. H.; Garcia, A.; Tantiwiwat, M.; Nguyen, T.-Q. *Adv. Funct. Mater.* **2009**, *19*, 3063.

(54) Loser, S.; Bruns, C. J.; Miyauchi, H.; Ortiz, R. P.; Facchetti, A.; Stupp, S. I.; Marks, T. *J. J. Am. Chem. Soc.* **2011**, *133*, 8142.

(55) Silvestri, F.; Irwin, M. D.; Beverina, L.; Facchetti, A.; Pagani, G. A.; Marks, T. J. *J. Am. Chem. Soc.* **2008**, *130*, 17640.

(56) Mayerhöffer, U.; Deing, K.; Gruß, K.; Braunschweig, H.; Meerholz, K.; Würthner, F. *Angew. Chem. Int. Ed.* **2009**, *48*, 8776.

(57) Bagnis, D.; Beverina, L.; Huang, H.; Silvestri, F.; Yao, Y.; Yan, H.; Pagani, G. A.; Marks, T. J.; Facchetti, A. *J. Am. Chem. Soc.* **2010**, *132*, 4074.

(58) a) Wei, G.; Wang, S.; Renshaw, K.; Thompson, M. E.; Forrest, S. R. *ACS Nano* **2010**, *4*, 1927; b) Wei, G.; Lunt, R. R.; Sun, K.; Wang, S.; Thompson, M. E.; Forrest, S. R. *Nano Lett.* **2010**, *10*, 3555; c) Wei, G.; Wang, S.; Sun, K.; Thompson, M. E.; Forrest, S. R. *Adv. Energ. Mater.* **2011**, *2*, 184.

(59) Velusamy, M.; Huang, J.-H.; Hsu, Y.-C.; Chou, H.-H.; Ho, K.-C.; Wu, P.-L.; Chang, W.-H.; Lin, J. T.; Chu, C.-W. *Org. Lett.* **2009**, *11*, 4898.

(60) Mei, J.; Graham, K. R.; Stalder, R.; Reynolds; J. R. *Org. Lett.* **2010**, *12*, 660.

(61) Zhang, W.; Tse, S. C.; Lu, J.; Tao, Y.; Wong, M. S. *J. Mater. Chem.* **2010**, *20*, 2182.

(62) Matsuo, Y.; Sato, Y.; Niinomi, T.; Soga, I.; Tanaka, H.; Nakamura, E. *J. Am. Chem. Soc.* **2009**, *131*, 16048.

(63) a) Uchida, S.; Xue, J. G.; Rand, P. B.; Forrest, S. R. *Appl. Phys. Lett.* **2004**, *84*, 4218; b) Xue, J.; Rand, B. P.; Uchida, S.; Forrest, S. R. *Adv. Mater.* **2005**, *17*, 66.

(64) Rousseau, T.; Cravino, A.; Bura, T.; Ulrich, G.; Ziessel, R.; Roncali, J. *Chem. Commun.* **2009**, 1673.

(65) Rousseau, T.; Cravino, A.; Bura, T.; Ulrich, G.; Ziessel, R.; Roncali J. *J. Mater. Chem.* **2009**, *19*, 2298.

(66) Rousseau, T.; Cravino, A.; Ripaud, E.; Leriche, P.; Rihn, S.; De Nicola, A.; Ziessel, R.; Roncali, J. *Chem. Commun.* **2010**, 5082.

(67) Chen, J. J.-A.; Chen, T. L.; Kim, B.; Poulsen, D. A.; Mynar, J. L.; Fréchet, J. M. K.; Ma, B. *Appl. Mater. Interfaces* **2010**, *2*, 2679.

(68) Zhao, X.; Piliego, C.; Kim, B.; Poulsen, D. A.; Ma, B.; Unruh, D. A.; Fréchet, J. M. J. *Chem. Mater.* **2010**, *2*, 2325.

(69) Mikroyannidis, J. A.; Sharma, S. S.; Vijay, Y. K.; Sharma, G. D. *Appl. Mater. Interfaces* **2010**, *2*, 270.

(70) Mikroyannidis, J. A.; Kabanakis, A. N.; Sharma, S. S.; Kumar, A.; Sharma, G. D. *Org. Electron.* **2010**, *11*, 1631.

(71) Mikroyannidis, J. A.; Kabanakis, A. N.; Tsagkournos, D. V.; Balraju, P.; Sharma, G. D. *J. Mater. Chem.* **2010**, *20*, 6464.

(72) Sharma, G. D.; Suresh, P.; Mikroyannidis, J. A.; Stylianakis, M. M. *J. Mater. Chem.* **2010**, *20*, 561.

(73) Mikroyannidis, J. A.; Suresh, P.; Sharma, G. D. *Synth. Met.* **2010**, *160*, 932.

(74) a) Brabec, C. J.; Sariciftci, N. S.; Hummelen, J. C. *Adv. Funct. Mater*. **2001**, *11*, 15; b) Coakley, K. M.; McGehee, M. D. *Chem. Mater*. **2004**, *16*, 4533.

(75) a) Brabec, C. J.; Zerza, G.; Cerullo, G.; De Silvestri, S.; Luzzati, S.; Hummelen, J. C.; Sariciftci, S. *Chem. Phys. Lett*. **2001**, *340*, 232; b) van Hal, P. A.; Meskers, S. C. J.; Janssen, R. A. J. *Appl. Phys. A: Mater. Sci. Process*. **2004**, *79*, 41.

(76) a) Peet, J.; Kim, J. Y.; Coates, N. E.; Ma, W. L.; Moses, D.; Heeger, A. J.; Bazan, G. C. *Nat. Mater*. **2007**, *6*, 497; b) Park, S. H.; Roy, A.; Beaupré, S.; Cho, S.; Coates, N.; Moon, J. S.; Moses, D.; Leclerc, M.; Lee, K.; Heeger, A. J. *Nat. Photon.* **2009**, *3*, 297.

(77) Ehli, C.; Oelsner, C.; Guldi, D. M.; Mateo-Alonso, A.; Prato, M.; Schmidt, C.; Backes, C.; Hauke, F.; Hirsch, A. *Nat. Chem*. **2009**, *1*, 243.

(78) Kraft, A. *ChemPhysChem* **2001**, *2*, 163.

(79) a) Blanchard-Desce, M. *C. R. Phys*. **2002**, *3*, 439; b) Marder, S. R.; Perry, J. W. *Adv. Mater*. **1993**, *5*, 804.

(80) a) Robertson, N. *Angew. Chem., Int. Ed. Engl*. **2006**, *45*, 2338; b) Willinger, K.; Fischer, K.; Kisselev, R.; Thelakkat, M. *J. Mater. Chem*. **2009**, *19*, 5364.

(81) a) Zimmermann, T. *J. Heterocycl. Chem*. **2000**, *37*, 1571; b) Zimmermann, T.; Brede, O. *J. Heterocycl. Chem*. **2004**, *41*, 103.

(82) Shang, Y.; Wen, Y.; Li, S.; Du, S.; He, X.; Cai, L.; Li, Y.; Yang, L.; Gao, H.; Song, Y. *J. Am. Chem. Soc.* **2007**, *129*, 11674.

(83) Würthner, F. *Synthesis* **1999**, *12*, 2103.

(84) The crystal structure of **HB194** reveals a disorder concerning one C-Atom of the propylene bridging unit. Hence, two repetitive units were found in the unit cell, which vary only slightly from each other. The distortion angle of one repetitive unit is slightly larger (7.4°) than the one of the other unit (3.5°). Furthermore, the bond length alternation of the methine bridge is slightly larger for the one repetitive molecule (1.379 Å vs 1.399 Å) compared to the other one (1.385 Å and 1.391 Å).

(85) a) Dieckmann, A.; Bässler, H.; Borsenberger, P. M. *J. Chem. Phys*. **1993**, *99*, 8136; b) Bässler, H. *Phys. Stat. Sol. B.* **1993**, *175*, 15.

(86) Rand, B. P.; Burk, D. P.; Forrest, S. R. *Phys. Rev. B* **2007**, *75*, 115327.

(87) Mihailetchi, V. D.; van Duren, J. K. J.; Blom, P. W. M.; Hummelen, J. C.; Janssen, R. A. J.; Kroon, J. M.; Rispens, M. T.; Verhees, W. J. H.; Wienk, M. M. *Adv. Funct. Mater*. **2003**, *13*, 43.

(88) a) Mihailetchi, V. D.; Wildeman, J.; Blom, P. W. M. *Phys. Rev. Lett*. **2005**, *94*, 126602; b) Koster, L. J. A.; Mihailetchi, V. D.; Blom, P. W. M. *Appl. Phys. Lett*. **2006**, *88*, 52104.

(89) Perrin, D. D.; Amarego, W. L.; Perrin, D. R. *Purification of Laboratory Chemicals;* Pergamon Press Ltd.; Oxford, **1980**.

(90) Fry, A. J. *Laboratory Techniques in Electroanalytical Chemistry* (Eds. P. T. Kessing, W. R. Heineman), Marcel Dekker Ltd, New York, 2nd Ed., **1996**, p. 481.

(91) a) Liptay, W. *Excited States*, Vol. 1 (Eds.: E. C. Lim.), Academic Press, New York, **1974**, 129; b) Beckmann, S.; Etzbach, K.-H.; Krämer, P.; Lukaszuk, K.; Matschiner, R.; Schmidt, A. J.; Schuhmacher, P.; Sens, R.; Seybold, G.; Wortmann, R.; Würthner, F. *Adv. Mater*. **1999**, *11*, 536.

(92) a) Bello, K. A. *Dyes. Pigm.* **1995**, *28*, 83; b) Katritzky, A. R.; Rachwal, S.; Smith, T. J. *Heterocycl. Chem.* **1995**, *32*, 1007.

(93) Allemand, P.-M.; Koch, A.; Wudl, F. *J. Am. Chem. Soc.* **1991**, *113*, 1050.

(94) Singh, T. B.; Marajanovic, N.; Matt, G. J.; Günes, S.; Sariciftci, N. S.; Ramil, A. M.; Andreev, A.; Sitter, H.; Schwödiauer, R.; Bauer, S. *Org. Electron.* **2005**, *6*, 105.

(95) Zhao, G.; He, Y.; Li, Y. *Adv. Mater.* **2010**, *22*, 4355.

(96) Patra, A.; Wijsboom, Y. H.; Leitus, G.; Bendikov, M. *Chem. Mater.* **2011**, *23*, 896.

(97) a) Hou, J.; Chen, H.-Y.; Zhang, S.; Chen, R. I.; Yang, Y.; Wu, Y.; Li, G. *J. Am Chem. Soc.* **2009**, *131*, 15586; b) Liang, Y.; Xu, Z.; Xia, J.; Tsai, S.-T.; Wu, Y.; Li, G.; Ray, C.; Yu, L. *Adv. Mater.* **2010**, *22*, E135; c) Bronstein, H.; Chen, Z.; Ashraf, R. S.; Zhang, W.; Du, J.; Durrant, J. R.; Tuladhar, P. S.; Song, K.; Watkins, S. E.; Geerts, Y.; Wienk, M. W.; Janssen, R. A. J.; Anthopoulos, T.; Sirringhaus, H.; Heeney, M.; McCulloch, I. *J. Am. Chem. Soc.* **2011**, *133*, 3272.

(98) Huang, F.; Chen, K.-S.; Yip, H.-L.; Hau, S. K.; Acton, O.; Zhang, Y.; Luo, J.; Jen, A. K.-Y. *J. Am. Chem. Soc.* **2009**, *131*, 13886.

(99) Bürckstümmer, H.; Kronenberg, N. M.; Meerholz, K.; Würthner, F. *Org. Lett.* **2010**, *12*, 3666 or Chapter 4.

(100) Marder, S, R.; Kippelen, B.; Jen, A. K.-Y.; Peyghambarian, N. *Nature*, **1997**, *388*, 845.

(101) a) Würthner, F.; Yao, S. *Angew. Chem., Int. Ed.* **2000**, *39*, 1978; b) Würthner, F.; Yao, S.; Debardemaeker, T.; Wortmann, R. *J. Am. Chem. Soc.* **2002**, *124*, 9431.

(102) a) Bürckstümmer, H.; Kronenberg, N. M.; Gsänger, M.; Stolte, M.; Meerholz, K.; Würthner, F. *J. Mater. Chem.* **2010**, *20*, 240 or Chapter 2; b) Kronenberg, N. M.; Steinmann, V.; Bürckstümmer, H.; Hwang, J.; Hertel, D.; Würthner, F.; Meerholz, K. *Adv. Mater.* **2010**, *22*, 4193.

(103) Connelly, N. G.; Geiger, W. E. *Chem. Rev.* **1996**, *96*, 877.

(104) Cravino, A. *Appl. Phys. Lett.* **2007**, *91*, 243502.

(105) Details on the device optimization are given in: Lenze, M. Diploma thesis, Universität zu Köln, **2010**.

(106) a) Dalton, L. R.; Harper, A. W.; Robinson, B. H. *Proc. Natl. Acad. Sci. USA* **1997**, *94*, 4842; b) Yitzchaik, S.; Di Bella, S.; Lundquist, P. M.; Wong, G. K.; Marks, T. J. *J. Am. Chem. Soc.* **1997**, *119*, 2995.

(107) Amarego, W. L. F.; Chai, C. L. L. *Purification of Laboratory Chemicals;* Elsevier, Burlington, 5th Ed., **2003**.

(108) Sheldrick, G. M. *Acta. Crystallogr. Sect. A: Found. Crystallogr.* **2008**, *A64*, 112.

(109) Würthner, F.; Yao, S.; Schilling, J.; Wortmann, R.; Redi-Abshiro, M.; Mecher, E.; Gallego-Gomez, F.; Meerholz, K. *J. Am. Chem. Soc.* **2001**, *123*, 2810.

(110) Prim, D.; Kirsch, G.; Nicoud, J. F. *Synlett* **1998**, *4*, 383.

(111) Kato, T.; Sato, M.; Kimura, H. *J. Chem. Soc. Perkin Trans 1* **1979**, *2*, 529.

(112) Seybold, G. (BASF AG), Ger. Offen. DE2801794, **1979**.

(113) Thomas, A. P.; Allott, C. P.; Gibson, K. H.; Major, J. S.; Masek, B. B.; Oldham, A. A.; Ratcliffe, A. H.; Roberts, D. A.; Russell, S. T.; Thomason, D. A. *J. Med. Chem.* **1992**, *35*, 877.

(114) Onsager, L. *J. Am. Chem. Soc.* **1936**, *58*, 1486.

(115) a) Verbiest, T.; Houbrechts, S.; Kauranen, M.; Clays, K.; Persoons, A. *J. Mater. Chem.* **1997**, *7*, 2175; b) Blanchard-Desce, M.; Alain, V.; Bedworth, P. V.; Marder, S. R.; Fort, A.; Runser, C.; Barzoukas, M.; Lebus, S.; Wortmann R. *Chem.–Eur. J.* **1997**, *3*, 1091.

(116) Delgado, J. L.; Bouit, P.-A.; Filippone, S.; Herranz, M. Á.; Martín, N. *Chem. Commun.* **2010**, *46*, 4853.

(117) Fan, B.; de Castro, A.; Chu, B. T.-T.; Heier J.; Opris, D.; Hany, R.; Nüesch, F. *J. Mater. Chem.* **2010**, *20*, 2952.

(118) Thompson, B. C.; Fréchet, J. M. J. *Angew. Chem., Int. Ed.* **2008**, *47*, 58.

(119) For another approach to utilize a broad spectral range, Matile and co-workers have introduced the concept of oriented multicolored antiparallel redox gradients (OMARG) in supramolecular heterojunctions (SHJ): Kishore, R. S. K.; Kel, O.; Banerji, N.; Emery, D.; Bollot, G.; Mareda, J.; Gomez-Casado, A.; Jonkheijm, P.; Huskens, J.; Maroni, P.; Borkovec, M.; Vauthey, E.; Sakai, N.; Matile, S. *J. Am. Chem. Soc.* **2009**, *131*, 11106.

(120) a) Koeppe, R.; Hoeglinger, D.; Troshin, P. A.; Lyubovskaya, R. N.; Razumov, V. F.; Sariciftci, N. S. *ChemSusChem* **2009**, *2*, 309; b) Meiss, J.; Leo, K.; Riede, M. K.; Uhrich, C.; Gnehr, W.-M.; Sonntag, S.; Pfeiffer, M. *Appl. Phys. Lett.* **2009**, *95*, 213306.

(121) Related chromophores have been investigated for nonlinear optics: a) Jang, S. H.; Luo, J. D.; Tucker, N. M.; Leclercq, A.; Zojer, E.; Haller, M. A.; Kim, T. D.; Kang, J. W.; Firestone, K.; Bale, D.; Lao, D.; Benedict, J. B.; Cohen, D.; Kaminsky, W.; Kahr, B.; Bredas, J. L.; Reid, P.; Dalton, L. R.; Jen, A. K. Y. *Chem. Mater.* **2006**, *18*, 2982. b) Willets, K. A.; Nishimura, S. Y.; Schuck, P. J.; Twieg, R. J.; Moerner, W. E. *Acc. Chem. Res.* **2005**, *38*, 549.

(122) Matsumoto, H.; Yono, S.; Imai, H.; Urawa, S.; Tada, S.; Kasukabe, S. DE3716840A1, 1987.

(123) Mittelbach, M.; Junek, H. *Liebigs Ann. Chem.* **1986**, *3*, 533.

(124) Carboni, R. A.; Coffman, D. D.; Howard, E. G. *J. Am. Chem. Soc.* **1958**, *80*, 2838.

(125) Würthner, F.; Sens, R.; Etzbach, K.-H.; Seybold, G. *Angew. Chem., Int. Ed.* **1999**, *38*, 1649.

(126) Hubschwerlen, C.; Fleury, J.-P. *Tetrahedron* **1977**, *33*, 761.

(127) Würthner, F.; Wortmann, R.; Matschiner, R.; Lukaszuk, K.; Meerholz, K.; DeNardin, Y.; Bittner, R.; Bräuchle, C.; Sens, R. *Angew. Chem., Int. Ed. Engl.* **1997**, *36*, 2765.

(128) a) Yao, Y.; Shi, C.; Li, G.; Shrotriya, V.; Pei, Q.; Yang, Y. *Appl. Phys. Lett.* **2006**, *89*, 153507; b) Mühlbacher, D.; Scharber, M.; Morana, M.; Zhu, Z.; Waller, D.; Gaudiana, R.; Brabec, C. *Adv. Mater*. **2006**, *18*, 2884. c) Pfuetzner, S.; Meiss, J.; Petrich, A.; Riede, M.; Leo, K. *Appl. Phys. Lett.* **2009**, *94*, 223307.

(129) Gruda, I.; Leblanc, R. M. *Can. J. Chem.* **1976**, *54*, 576.

(130) Reidlinger, C.; Dwoczak, R.; Fabian, W. M. F.; Junek, H. *Dyes Pigm.* **1994**, *24*, 185.

(131) Würthner, F.; Thalacker, C.; Matschiner, R.; Lukaszuk, K.; Wortmann, R. *Chem. Commun.* **1998**, 1739.

(132) Wortmann, R.; Würthner, F.; Sautter, A.; Lukaszuk, K.; Matschiner, R.; Meerholz, K. *Proc. SPIE-Int. Soc. Opt. Eng.* **1998**, *3471*, 41.

(133) Würthner, F.; Yao, S.; Wortmann, R. *Polym. Mater. Sci. Eng.* **2000**, *83*, 186.

(134) a) Aije, H.; Alvarez, M. M.; Anz, S. J.; Beck, R. D.; Diederich, F.; Fostiropolous, K.; Huffman, D. R.; Krätschmer, W.; Rubin, Y.; Schriver, K. E.; Sensharma, D.; Whetten, R. L. *J. Phys. Chem.* **1990**, *94*, 8630; b) Arbogast, J. W.; Foote, C. S. *J. Am. Chem. Soc.* **1991**, *113*, 8886.

(135) a) Brown, T. M.; Kim, J. S.; Friend, R. H.; Cacialli, F.; Daik, R.; Feast, W. J. *Appl. Phys. Lett.* **1999**, *75*, 1679; b) Hung, L. S.; Tang, C. W.; Mason, M. G. *Appl. Phys. Lett.* **1997**, *70*, 152; c) Peumans, P.; Forrest, S. R. *Appl. Phys. Lett.* **2001**, *79*, 126; d) Gupta, D.; Bag, M.; Naraya, K. S. *Appl. Phys. Lett.* **2008**, *92*, 093301.

(136) Shrotriya, V.; Li, G.; Yao, Y.; Chu, C.-W.; Yang, Y. *Appl. Phys. Lett.* **2006**, *88*, 073508.

(137) a) Brabec, C. J.; Cravino, A.; Meissner, D.; Sariciftci, N. S.; Fromherz, T.; Rispens, M. T.; Sanchez, L.; Hummelen, J. C. *Adv. Funct. Mater.* **2001**, *11*, 374; b) Potscavage, W. J.; Sharma, A.; Kippelen, B. *Acc. Chem. Res.* **2009**, *42*, 1758.

(138) Mihailetchi, V. D.; Blom, P. W. M.; Hummelen, J. C.; Rispens, M. T. *J. Appl. Phys.* **2003**, *94*, 6849.

(139) Snaith, H. J., Greenham, N. C.; Friend, R. H. *Adv. Mater.* **2004**, *16*, 1640.

(140) Würthner, F.; Sens, R.; Schmidt, A.-J.; Etzbach, K.-H.; Beckmann, S. (BASF SE Ludwigshafen), **1999**, DE19920808A1.

(141) Gu, C.; Yao, Z. *Huaxue Yanjiu Yu Yingyong* **2001**, *13(3)*, 315.

(142) Tateoka, Y.; Sagawa, T. (*Nissan Motor*), **1987**, JP62288682A.

(143) Wang, J.; Cao, W.; Su, J.; Tian, H.; Huang, Y.; Sun, Z. *Dyes Pigm.* **2003**, *57(2)*, 171.

(144) Schulze, W.; Jungstand, W.; Gutsche, W.; Wohlrabe, K.; Kramarczyk, K.; Tresselt, D. *Pharmazie* **1977**, *32*, 271.

(145) Keil, D.; Hartmann, H. *Liebigs Ann.* **1995**, *6*, 979.

(146) Bello, K. A.; Cheng, L.; Griffiths, J. *J. Chem. Soc. PT 2* **1987**, *6*, 815.

(147) Metz, H. J.; Steffanut, P.; Winter, M. (Clariant International Ltd.), **2004**, EP1445769A1.

(148) Pardal, A. C.; Ramos, S. S.; Santos, P. F.; Reis, L. V.; Almeida, P. *Molecules* **2002**, *7*, 320.

(149) Kay, A. J.; Woolhouse, A. D.; Gainsford, G. J.; Haskell, T. G.; Barnes, T. H.; McKinnie, I. T.; Wyss, C. P. *J. Mater. Chem.* **2001**, *11*, 996.

Acknowledgement / Danksagung

Zu aller erst danke ich Professor Frank Würthner für die Möglichkeit, das spannende Thema der organischen Solarzellen bearbeiten zu können, und das stete Interesse am Fortgang meiner Arbeit. Die Arbeitsbedingungen waren stets hervorragend, unter anderem auch dank der Syntheseunterstützung durch verschiedene Laboranten. Besonders zu schätzen wusste ich das Vertrauen in meine Arbeit, durch das mir eine selbständige Arbeitsweise möglich war.

Ein wichtiger Partner war Professor Klaus Meerholz, seine Arbeitsgruppe und hier vor allem Herr Dr. Nils Kronenberg. Danke, Nils, für das geduldige Beantworten zahlloser Fragen meinerseits und natürlich für die Untersuchung meiner vielen Merocyanine in den Solarzellen. Von der Kölner Gruppe möchte ich auch Frau Vera Steinmann für die Untersuchung von Aufdampfsolarzellen und Herrn Martin Lenze für die detaillierte Analyse von **EL86** danken.

Wenn auch fachlich meist weit entfernt, war die Arbeitsgruppe Würthner während der Jahre in Würzburg eine stete Unterstützung, vor allem in der stressigen Endphase meiner Arbeit. Die angenehme, freundschaftliche Atmosphäre, die mittwochlichen Treffen und sonstigen Aktivitäten werde ich in guter Erinnerung behalten.

Zudem bin ich für die vielen Beiträge zu meiner Arbeit sehr dankbar.

Für synthetische Unterstützung danke ich herzlich Frau Dr. Elena Tulyakova, Frau Manuela Kaiser (geb. Deppisch), Frau Petra Seufert-Baumbach und Herrn Joachim Bialas.

Herrn Marcel Gsänger für die Messung von Einkristallen und Strukturlösung derselben.

Frau Ana-Maria Krause führte CV- und DSC-Messungen der synthetisierten Farbstoffe aus.

Herr Dr. Matthias Stolte bestimmte die Dipolmomente der Merocyanine mittels elektrooptischer Absorptionsspektroskopie.

Tausend Dank an den gesamten Ak Würthner!

An der Uni Würzburg möchte ich mich noch bei Herrn Dr. Grüne und Frau Ruckdeschel (NMR), Herrn Dr. Büchner und Herrn Dadrich (Massenspektrometrie), Frau Michels (CHN-Analyse), Herrn Brunner (Computerfragen aller Art) und Herrn Braun bedanken.

Ein großer Dank geht an das Team der BASF (Dr. Peter Erk, Dr. Jaehyung Hwang, Dr. Helmut Reichelt und Antti Ojala) für die Projektleitung des BMBF-geförderten OPEG-Programms und viele hilfreiche Diskussionen.

Vielen lieben Dank auch an meine Schwester Dr. Eva Bürckstümmer und Dr. Manuel Bröhmer für das Korrekturlesen der Arbeit.

List of publications

Communications and Articles

- *Improved performance of thermally evaporated small molecule solar cell by multiple donor concept*
  A. Ojala, H. Bürckstümmer, M. Stolte, K. Meerholz, R. Sens, H. Reichelt, P. Erk, J. Hwang, F. Würthner *Adv. Mater.* **2011**, accepted
- *Efficient solution-processed bulk heterojunction solar cells by antiparallel supramolecular arrangement of dipolar D-A dyes*
  H. Bürckstümmer, E. V. Tulyakova, M. Deppisch, M. Lenze, N. M. Kronenberg, M. Gsänger, M. Stolte, K. Meerholz, F. Würthner *Angew. Chem.* **2011**, accepted.
- *Simple, Highly Efficient Vacuum-Processed Bulk Heterojunction Solar Cells Based on Merocyanine Dyes*
  V. Steinmann, N. M. Kronenberg, M. R. Lenze, S. M. Graf, D. Hertel, K. Meerholz, H. Bürckstümmer, E. V. Tulyakova, F. Würthner *Adv. Energy Mater.* **2011**, *1*, 888.
- *Synthesis and Characterization of Optical and Redox Properties of Thiophene-Functionalized Diketopyrrolopyrrol Chromophores*
  H. Bürckstümmer, A. Weißenstein, D. Bialas, F. Würthner *J. Org. Chem.* **2011**, *76*, 2426.
- *Optimized solution-processed merocyanine:PCBM organic bulk heterojunction solar cell*
  N. M. Kronenberg, H. Bürckstümmer, M. Deppisch, F. Würthner, K. Meerholz *J. Photon. Energy* **2011**, *1*, 011101.
- *Near-Infrared Absorbing Merocyanine Dyes for Bulk Heterojunction Solar Cells*
  H. Bürckstümmer, N. M. Kronenberg, K. Meerholz, F. Würthner *Org. Lett.* **2010**, *12*, 3666.
- *Direct Comparison of Highly Efficient Solution- and Vacuum-Processed Organic Solar Cells Based on Merocyanine Dyes*
  N. M. Kronenberg, V. Steinmann, H. Bürckstümmer, J. Hwang, D. Hertel, F. Würthner, K. Meerholz *Adv. Mater.* **2010**, *22*, 4193.
- *Tailored merocyanine dyes for solution-processed BHJ solar cells*
  H. Bürckstümmer, N. M. Kronenberg, M. Gsänger, M. Stolte, K. Meerholz, F. Würthner *J. Mater. Chem.* **2010**, *20*, 240.
- *Synthesis of monodispersed fcc and fct FePt/FePd nanoparticles by microwave irradiation*

H. L. Nguyen, L. E. M. Howard, S. R. Giblin, B. K. Tanner, I. Terry, A. K. Hughes, I. M. Ross, A. Serres, H. Bürckstümmer, J. S. O. Evans *J. Mater. Chem.* **2005**, *15*, 5136.

Own conference contributions

- *Merocyanine dyes for solution-processed bulk heterojunction solar cells (Poster presentation)*
  H. Bürckstümmer, N. M. Kronenberg, M. Deppisch, K. Meerholz, F. Würthner: ChemSystM, Würzburg, 12/2010
- *Merocyanine dyes for solution-processed bulk heterojunction solar cells (Poster presentation)* H. Bürckstümmer, N. M. Kronenberg, M. Deppisch, K. Meerholz, F. Würthner: SPIE Optics and Photonics, San Diego, 08/2010
- *Tailored merocyanine dyes for solution-processed bulk heterojunction solar cells (Poster presentation)*
  H. Bürckstümmer, N. M. Kronenberg, M. Gsänger, K. Meerholz, F. Würthner: Plastic Electronics Europe 2009, Dresden, 10/2009
- *Tailored merocyanine dyes for solution-processed bulk heterojunction solar cells (Poster presentation)*
  H. Bürckstümmer, N. M. Kronenberg, M. Gsänger, K. Meerholz, F. Würthner: IRTG Workshop, Mainz, 08/2009
- *Tailored merocyanine dyes for solution-processed bulk heterojunction solar cells (Poster presentation)*
  H. Bürckstümmer, N. M. Kronenberg, M. Gsänger, K. Meerholz, F. Würthner: ISNA 13, Luxemburg, 07/2009

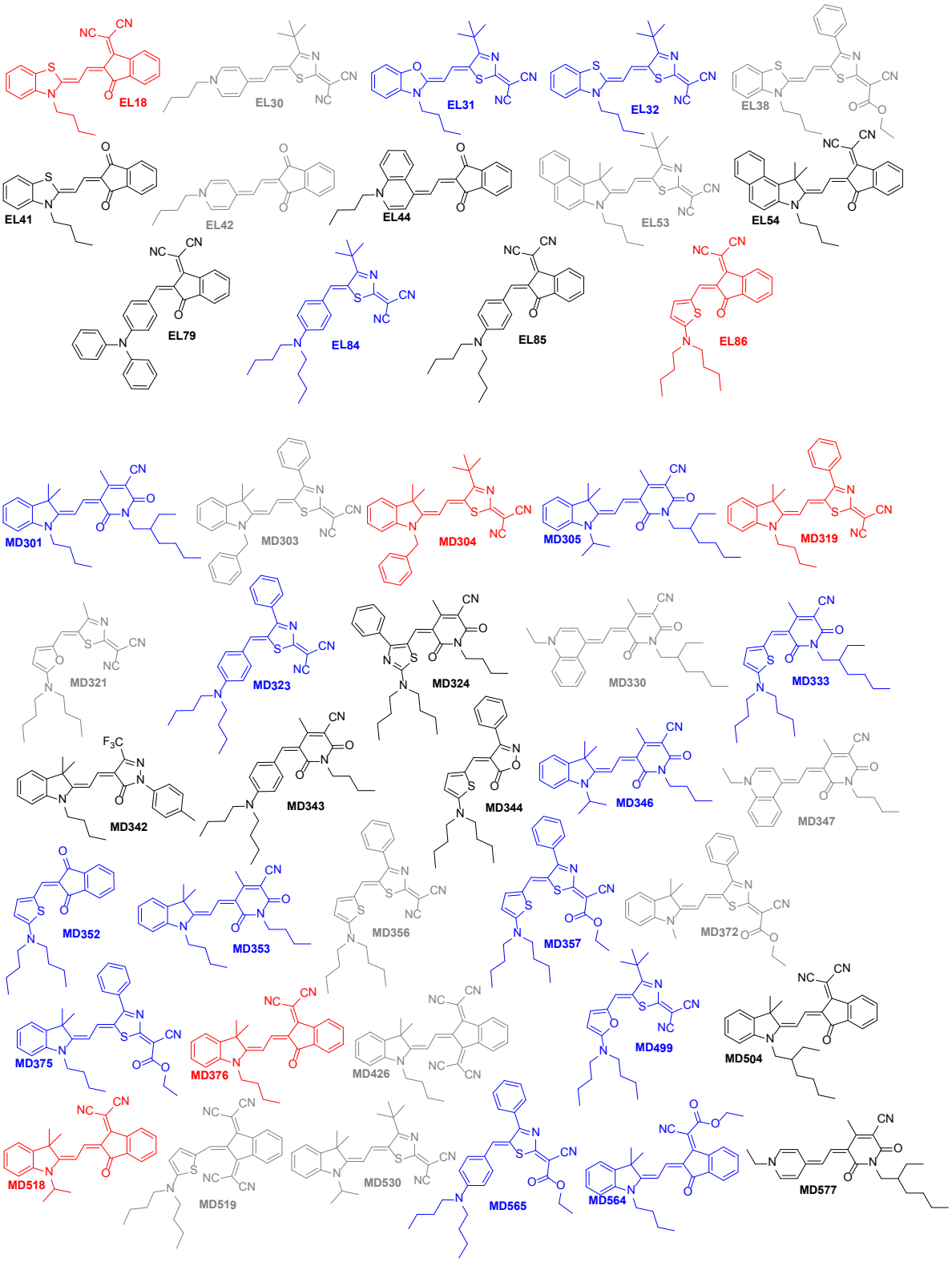
EL18
EL30
EL31
EL32
EL38
EL41
EL42
EL44
EL53
EL54
EL79
EL84
EL85
EL86
MD301
MD303
MD304
MD305
MD319
MD321
MD323
MD324
MD330
MD333
MD342
MD343
MD344
MD346
MD347
MD352
MD353
MD356
MD357
MD372
MD375
MD376
MD426
MD499
MD504
MD518
MD519
MD530
MD565
MD564
MD577

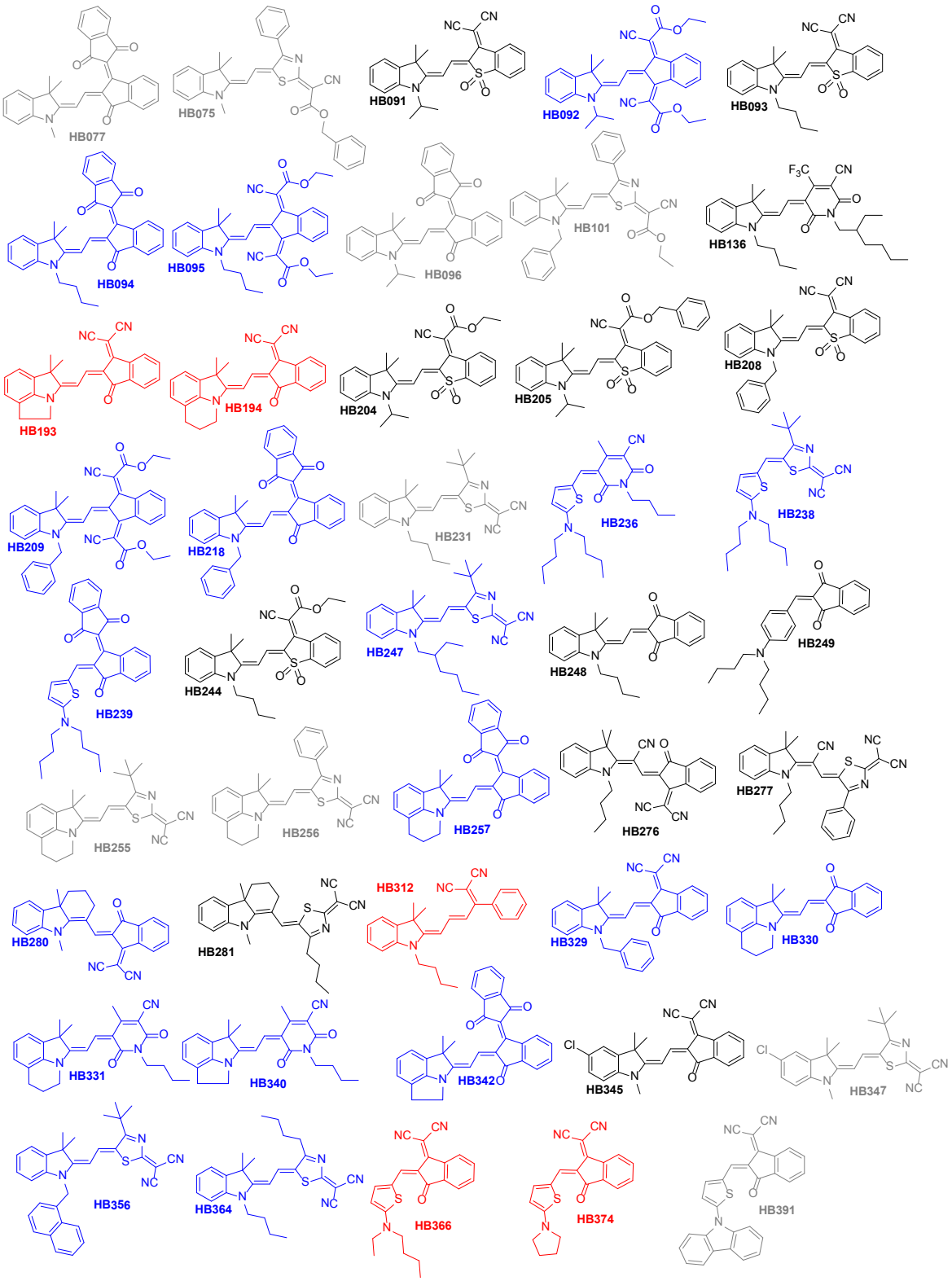
HB077
HB075
HB091
HB092
HB093
HB094
HB095
HB096
HB101
HB136
HB193
HB194
HB204
HB205
HB208
HB209
HB218
HB231
HB236
HB238
HB239
HB244
HB247
HB248
HB249
HB255
HB256
HB257
HB276
HB277
HB280
HB281
HB312
HB329
HB330
HB331
HB340
HB342
HB345
HB347
HB356
HB364
HB366
HB374
HB391